Tomás Monteiro Fernandes

Licenciado em Bioquímica

Characterization of extracellular electron transfer components of *Geobacter* bacteria

Dissertação para obtenção do Grau de Mestre em Bioquímica

Orientador: Doutora Leonor Morgado, Investigadora de Pós-Doutoramento, UCIBIO, Faculdade de Ciências e Tecnologia, Universidade Nova de Lisboa
Co-orientador: Prof. Doutor Carlos A. Salgueiro, Professor Associado com Agregação, Faculdade de Ciências e Tecnologia, Universidade Nova de Lisboa

Júri:

Presidente: Prof. Doutor José Ricardo Ramos Franco Tavares
Arguente: Prof. Doutor Eurico José da Silva Cabrita

FACULDADE DE CIÊNCIAS E TECNOLOGIA
UNIVERSIDADE NOVA DE LISBOA

Outubro 2018

Tomás Monteiro Fernandes

Licenciado em Bioquímica

Characterization of extracellular electron transfer components of *Geobacter* bacteria

Dissertação para obtenção do Grau de Mestre em Bioquímica

Orientador: Doutora Leonor Morgado, Investigadora de Pós-Doutoramento, UCIBIO, Faculdade de Ciências e Tecnologia, Universidade Nova de Lisboa
Co-orientador: Prof. Doutor Carlos A. Salgueiro, Professor Associado com Agregação, Faculdade de Ciências e Tecnologia, Universidade Nova de Lisboa

Júri:

Presidente: Prof. Doutor José Ricardo Ramos Franco Tavares
Arguente: Prof. Doutor Eurico José da Silva Cabrita

FACULDADE DE CIÊNCIAS E TECNOLOGIA
UNIVERSIDADE NOVA DE LISBOA

Outubro 2018

Characterization of extracellular electron transfer components of *Geobacter* bacteria

Characterization of extracellular electron transfer components of *Geobacter* bacteria

The results obtained under the scope of this Thesis were published in the Biochemical Journal[1]. Additionally, the results were presented as poster communication on the VII Ibero-American NMR Meeting[2], 1st Meeting of Young Biophysicists[2] and on the NMR Practical Course on Multidimensional NMR in Structural Biology[2].

[1]T.M Fernandes, L. Morgado, C.A. Salgueiro, Thermodynamic and functional characterization of the periplasmic triheme cytochrome PpcA from *G. metallireducens*, Biochem. J., 475 (2018) 2861-2875 (doi: 10.1042/BCJ20180457)

[2]T.M. Fernandes, L. Morgado, C.A. Salgueiro, Using EXchange SpectroscopY NMR to study the triheme cytochrome PpcA from *Geobacter metallireducens*, 2018

The work developed in this Thesis was supported by Fundação para a Ciência e Tecnologia (FCT) through the grant PTDC/BBB-BQB/3554/2014 (Professor Carlos Salgueiro). This work was also supported by Unidade de Ciências Biomoleculares Aplicadas-UCIBIO, which is financed by national funds from FCT/MEC [UID/Multi/04378/2013] and co-financed by the ERDF under PT2020 Partnership Agreement [POCI-01-0145-FEDER-007728]. The NMR spectrometers are part of the National NMR Network (PTNMR) and are supported by Infrastructure Project Nº022161 (co-financed by FEDER through COMPETE 2020, POCI, and PORL and FCT through PIDDAC).

Ao meu avô Sebastião,
Ao meu amigo Tommy,

Agradecimentos

Este documento é o culminar de dois longos anos de trabalho, nos quais evolui como pessoa, estudante e profissional. Uma Tese não é um trabalho individual, mas sim o resultado de trabalho, esforço e dedicação conjuntos de uma série de pessoas, às quais gostaria de deixar os meus mais profundos agradecimentos.

Primeiramente, gostaria de agradecer ao Professor Doutor Carlos Salgueiro pelo voto de confiança que depositou em mim e no meu trabalho. O seu profissionalismo e dedicação, assim como a sua paciência, disponibilidade e amizade, facilitaram sempre a realização do meu trabalho, mesmo nas horas mais complicadas. Não vou esquecer as discussões científicas, as discussões menos científicas (quase sempre relacionadas com a nossa outra grande paixão para além da ciência, o Sporting) e os muitos bons momentos que passámos. Para além de um extraordinário cientista, é uma extraordinária pessoa. Obrigado por tudo.

De seguida, gostaria de agradecer fortemente à minha orientadora, a Doutora Leonor Morgado. Foi a pessoa que mais tempo passou comigo neste último ano de trabalho. Muitas horas de discussões e frustrações científicas, mas que no fim valeram quase sempre a pena. A Doutora Leonor é um exemplo de trabalho e dedicação. A sua paciência e disponibilidade são inesgotáveis, independentemente das circunstâncias. Com a Doutora Leonor aprendi inúmeras técnicas e aprofundei os meus conhecimentos previamente adquiridos. A facilidade com que explica uma enorme gama de assuntos nunca será esquecida. Uma grande orientadora, com o qual tive e sempre terei o prazer de trabalhar. Uma grande amiga, com a qual tive o prazer de passar muitos bons momentos. Obrigado, Leonor. Por tudo.

Durante o ano de trabalho que passou, tive inúmeros companheiros, colegas e amigos que sempre tornaram mais fácil as minhas tarefas e por esse motivo, deixo-lhes algumas palavras de agradecimento. À Joana Dantas, um forte obrigado por tudo aquilo que já fez por mim e por sempre ter respondido aos meus pedidos de ajuda ao longo do ano. Desejo-lhe muita sorte e sucesso em tudo aquilo que faça. Obrigado, Joana. À Liliana Teixeira, um forte obrigado pelas muitas horas de risada, partilha de frustrações e sucessos, companheirismo, conselhos e ajuda. Liliana, desejo-te muita sorte em tudo aquilo que faças. Obrigado por tudo. À Marisa Ferreira, um agradecimento pela amizade, pelo companheirismo, pelas muitas horas de risada e coscuvilhices. Obrigado por estares sempre disponível a ajudar-me, pela preocupação. Obrigado pela amiga e colega que és. Marisa, espero que continues sempre a ser a pessoa feliz que conheci e conheço. Obrigado por tudo.

À Pilar Portela, à Carlota Conceição, à Ana Almeida, ao João Guerra e ao Bruno Mendes, um forte obrigado por toda e qualquer ajuda que me tenham dado. As pequenas conversas, troca de conhecimento e opiniões, assim como o simples companheirismo, não podem nem serão esquecidos. Por esse motivo, desejo a todos vós um futuro com muito sucesso.

Gostaria de agradecer, também, à Professora Doutora Cristina Cordas. A Doutora Cristina introduziu-me à electroquímica de proteínas e mostrou uma disponibilidade enorme em ajudar-me nos meus problemas com o GSU0105, algo que nunca vou esquecer. Espero ainda vir a aprender muito com a mesma e que este trabalho tenha sido apenas o primeiro de muitos. Um muito obrigado pela constante paciência e simpatia. Professor Doutor David Turner, muito obrigado pela disponibilização do software que permitiu o cálculo dos parâmetros termodinâmicos do PpcA de *G. metallireducens*. Obrigado, também, pelo jantar agradável que tivemos e pela disponibilidade de tirar fotos comigo durante o VII Ibero-American NMR Meeting.

Além das pessoas que trabalharam a meu lado no laboratório este ano, existem algumas outras que colaboraram e muito para que o trabalho corresse da melhor forma. Assim sendo, gostaria de deixar o meu agradecimento à Dona Ermelinda e à Elsa, por garantirem sempre que temos o nosso material lavado e em condições. À Cecília, por estar sempre disponível em ajudar-nos com o funcionamento dos equipamentos do laboratório de análises.

Apesar das muitas horas passadas em laboratório ou na faculdade a trabalhar, uma grande contribuição para este trabalho veio de pessoas fora desses locais. Veio de amigos e família, que em muito contribuíram para que conseguisse ter motivação para terminar este trabalho.

Mãe, obrigado pelos mais de 23 anos de amor, amizade, companheirismo, educação. Por seres a pessoa que me recebe todos os dias em casa com um sorriso. Que me repreende quando devo ser repreendido. Que me elogia quando devo ser elogiado. Que sempre acreditou em mim. Desde o pequeno menino que fazia contas contigo no carro, ao jovem rapaz que determina parâmetros termodinâmicos de proteínas hémicas através de ressonância magnética nuclear. Tudo começou assim. Com as tuas brincadeiras com números. Com as tuas histórias de amor. Com tudo aquilo que me deste. Um obrigado profundo pelas centenas de milhares horas que estiveste a meu lado. Que venham mais umas centenas… e que em elas sejas sempre feliz. Que sejas sempre a minha querida Mãe. Amo-te muito.

Pai. Companheiro, amigo, ídolo, guerreiro, exemplo. Obrigado por sempre teres lutado pelo meu futuro. Sei dos sacrifícios que fizeste e fazes para que possa estudar e ter a vida que tenho.

Uma vida feliz, muito graças a ti. Obrigado por seres o homem que és. Pelos 23 anos de brincadeira, partilha de alegria e tristeza, pela preocupação, por todos os momentos em que estiveste lá para mim. Nunca me falhaste. Espero nunca te ter falhado, nem vir a falhar. Um parágrafo de palavras não chega para agradecer aquilo que fazes e fizeste por mim. Espero um dia poder dar-te metade daquilo que me deste, pois tudo nunca conseguirei. Amo-te, Pai.

Querido Gonçalo, meu grande e mais profundo amigo. O meu grande companheiro. O meu grande colega de desporto e aventuras. O meu grande parceiro nos momentos mais felizes e nos mais tristes. O meu grande irmão. És grande em tudo. É difícil arranjar palavras para descrever aquilo que significas para mim. Obrigado por seres a pessoa que és e por todas as milhares de horas de amizade e amor que me deste. Não deitava fora um segundo passado a teu lado. Espero que sejas a pessoa mais feliz do mundo e que o teu sucesso seja proporcional à enorme pessoa que és. Eras uma criança de chucha na boca e hoje és o homem que és… o tempo passa, mas nós estaremos sempre juntos. Parceiros de vida. Um abraço e obrigado por tudo. Amo-te muito.

Queridos irmão mais novos. Meus lindos. Salvador e Constança. Amo-vos muito. Ainda não têm idade para ler este agradecimento, mas um dia quero que o leiam e consigam perceber o quão importantes foram para este trabalho. O quão importantes são e sempre serão para mim. O mano passa muito menos tempo do que queria com vocês. Mas fá-lo para que um dia tenha um futuro melhor. Luta por isso. E nunca se esquece de vocês… obrigado por serem uma fonte de amor e felicidade na minha vida. Quero que sejam as pessoas mais felizes deste mundo. Que mantenham sempre esses sorrisos lindos e olhos azuis brilhantes. Amo-vos muito e sempre vou amar. Obrigado.

Aos restantes membros da minha família e amigos, um muito obrigado. A família e os amigos são a nossa base e é graças a todos vós que nunca me desequilibro. Obrigado, particularmente, ao meu avô Zé, por ser a pessoa maravilhosa que é. Obrigado às minhas queridas tias Sofia e Fernanda. Por cuidarem de mim como um filho. Por me amarem como a um filho. Obrigado a todos os meus tios, primos e avós. Amo-vos a todos. Um grande e forte obrigado a todos os meus amigos, especialmente ao Marcelo e Renato Domingues.

Sara, obrigado por tudo. Por seres a pessoa maravilhosa que és. Por seres a pessoa que está lá sempre que eu preciso. Por toda a amizade e amor que me deste e dás. Que sejas sempre feliz e que tenhas muito sucesso. Mereces o melhor, pois és uma pessoa extraordinária. Amo-te muito.

Abstract

Geobacter bacteria show an impressive respiratory versatility. They sustain their growth by using different extracellular compounds, in addition to the more frequent respiratory processes, which utilize soluble electron donors and acceptors. These bacteria have the potential to create an impact on biotechnological applications that include the bioremediation of organic and inorganic contaminants, bioenergy production and bioelectronics. In order to optimize these applications, it is crucial to understand how electron transfer between the cell and its exterior occurs, a process designated extracellular electron transfer (EET). The proteins that participate in this process are located at the inner-membrane, periplasm and outer-membrane.

In this Thesis, the periplasmic PpcA cytochrome from *G. metallireducens* was functionally and thermodynamically characterized using NMR and visible spectroscopic techniques. The heme reduction potentials, the redox and redox-Bohr interactions were determined. These parameters revealed unique features compared to other triheme cytochromes from different microorganisms, namely the less negative heme reduction potential values and the concomitant functional working potential ranges. It was also shown that the order of oxidation of the hemes is pH-independent and that the protein is designed to couple e^-/H^+ transfer, exclusively at physiological pH.

Furthermore, the periplasmic cytochrome GSU0105 and the outer-membrane cytochromes OmaV and OmaW of *G. sulfurreducens* were heterologously expressed. The expression and purification protocols for GSU0105 were optimized and a preliminary characterization was obtained by complementary use of NMR, UV-visible and electrochemistry techniques. The results indicate that the cytochrome has three low-spin hemes in the reduced state and a mixture of low- and high-spin hemes in the oxidized state. The electrochemical studies showed that the reduction potential values and the heterogeneous electron transfer constants of the redox centers are different. For OmaV and OmaW, the purification protocols were optimized.

Overall, the results obtained constitute an important contribution to the understanding of the EET mechanisms of *Geobacter* bacteria.

Keywords: *Geobacter*; extracellular electron transfer; multiheme cytochromes; heterologous protein expression; NMR

Resumo

As bactérias *Geobacter* apresentam uma versatilidade respiratória impressionante, sendo capazes de acoplar o seu crescimento à utilização de diversos compostos extracelulares insolúveis em alternativa a doadores e aceitadores de electrões solúveis. Estas bactérias poderão vir a criar impacto em aplicações biotecnológicas, nomeadamente nas áreas de biorremediação de contaminantes orgânicos e inorgânicos, na produção de bioenergia e em bioelectrónica. Para a optimização destas aplicações é fundamental compreender a forma como a transferência electrónica ocorre entre a célula e o seu exterior, um processo designado de transferência electrónica extracelular (TEE). As proteínas que participam neste processo estão localizadas na membrana interna, no periplasma e na membrana externa.

Nesta Tese, o citocromo periplasmático PpcA de *G. metallireducens* foi caracterizado funcionalmente e termodinamicamente, utilizando espectroscopias de RMN e visível. Os potenciais de redução dos hemos, as suas interacções redox e redox-Bohr foram determinados. Estes parâmetros são claramente distintos quando comparados com outros citocromos trihémicos de diferentes microrganismos, em particular os maiores valores de potenciais de redução e concomitantes intervalos funcionais de potencial. Foi também demonstrado que a ordem de oxidação dos hemos é independente do pH e que a proteína acopla a transferência de e^-/H^+ exclusivamente a pH fisiológico.

Além disso, o citocromo periplasmático GSU0105 e os citocromos da membrana externa OmaV e OmaW de *G. sulfurreducens* foram expressos heterologamente. Os protocolos de expressão e purificação do GSU0105 foram optimizados, tendo-se efectuado uma caracterização preliminar através da utilização complementar das técnicas de RMN, UV-visível e electroquímica. Os resultados obtidos indicam que o citocromo contem três hemos de spin-baixo no estado reduzido e uma mistura de hemos de spin-baixo e spin-alto no estado oxidado. Os estudos electroquímicos demonstraram que os potenciais de redução dos hemos, bem como as constantes de transferência electrónica heterogénea dos centros redox, são diferentes. Em relação aos citocromos OmaW e ao OmaV, foram optimizados os seus protocolos de purificação.

Globalmente, os resultados obtidos constituem uma importante contribuição para a compreensão dos mecanismos de TEE em bactérias do género *Geobacter*.

Palavras-chave: *Geobacter*; transferência electrónica extracelular; citocromos multihémicos; expressão heteróloga de proteínas; RMN

Table of contents

List of figures

1 – Introduction

2 – Thermodynamic characterization of PpcA from *G. metallireducens*

3 – Expression, purification and biochemical characterization of GSU0105

4 – Exploring membrane proteins of *G. sulfurreducens*

6 – Appendix

List of tables

1 – Introduction

2 – Thermodynamic characterization of PpcA from *G. metallireducens*

3 – Expression, purification and biochemical characterization of GSU0105

4 – Exploring membrane proteins of *G. sulfurreducens*

5 – Future perspectives

6 – Appendix

Abbreviations, symbols and constants

1D – One dimensional

2D – Two dimensional

2xYT – 2x Yeast extract-tryptone medium

ATP – Adenosine triphosphate

AQDS – Anthraquinone-2,6-disulphonate

BLAST – Basic Local Alignment Search Tool

BMRB – Biological Magnetic Resonance Data Bank

bp – base-pair(s)

BSA – Bovine serum albumin

Ccm – Cytochrome *c* maturation

CD – Circular dichroism

CHAPS – 3-[3-cholamidopropyl)dimethylammonio]-1-propanesulfonate

CHAPSO – 3-([3-cholamidopropyl]dimethylammonio-2-hydroxy-1-propanesulfonate

CMC – Critical micelle concentration

COSY – Correlation spectroscopy

CT – Charge-transfer

CTAB – Cetrimonium bromide

CV – Cyclic voltammetry

Dac_7 – *Desulfuromonas acetoxidans* c_7 cytochrome

DIET – Direct interspecies electron transfer

DNA – Deoxyribonucleic acid

dNTPs – Deoxynucleotides

DSS – 4,4-dimethyl-4-silapentane-1-sulfonic acid

E_{app} – Macroscopic apparent midpoint reduction potential

e_{app} – Microscopic apparent midpoint reduction potential

E. coli – *Escherichia coli*

EDTA – Ethylenediamine tetraacetic acid

EET – Extracellular electron transfer

EGTA – Ethylene glycol-bis(β-aminoethyl ether)-*N,N,N',N'*-tetraacetic acid

EPR – Electron paramagnetic resonance

FID – Free induction decay

Gm/Gmet/G. metallireducens – *Geobacter metallireducens*

Gs/G. sulfurreducens – *Geobacter sulfurreducens*

GuHCl – Guanidine hydrochloride

EXSY – Exchange spectroscopy

Ext – Extracellular

HMQC – Heteronuclear multiple quantum coherence

HSQC – Heteronuclear single quantum coherence

I – Quantum spin number

IM – Inner-membrane

ImcH – Inner-membrane cytochrome H

IPTG – Isopropyl β-D-thiogalactopyranoside

IUB – International Union of Biochemistry

IUPAC – International Union of Pure and Applied Chemistry

J – Coupling constant

kb – kilobase (1000 bp)

k_{sh} – heterogeneous electron transfer constant

LB – Luria-Bertani medium

LDAO – Lauryldimethylamine oxide

m – Magnetic quantum number

MacA – Membrane associated cytochrome A

MFCs – Microbial fuel cells

MQH_2 – Menaquinol

MQ – Menaquinone

Mtr – Metal-reducing

MW – Molecular-weight

MWCO – Molecular-weight cut-off

NAD^+ – Nicotinamide adenine dinucleotide (oxidized form)

NADH – Nicotinamide adenine dinucleotide (reduced form)

NHE – Normal hydrogen electrode

NMR – Nuclear magnetic resonance

NOE – Nuclear Overhauser effect

NOESY – Nuclear Overhauser effect spectroscopy

OD_{600} – Optical density at 600 nm

OM – Outer-membrane

Oma – Outer-membrane associated

Omb – Outer-membrane barrel

Omc – Outer-membrane cytochrome

PBS – Phosphate-buffered saline

PCR – Polymerase Chain Reaction

PDB – Protein Data Bank

PMSF – Phenylmethylsulphonyl fluoride

Ppc – Periplasmic cytochrome

ppm – Parts per million

PSA – Ammonium persulfate

RF – Restriction-free

SDS – Sodium dodecyl sulfate

SDS-PAGE – Sodium dodecyl sulfate – polyacrylamide gel electrophoresis

T_1 – Longitudinal relaxation

T_2 – Transverse relaxation

TAE – Tris-acetate-EDTA buffer

TCI – Triple-resonance cryoprobe

TEMED – Tetramethylethylenediamine

TEV – Tobacco Etch Virus

T_m – Melting temperature

TM – Transmembrane

TMBZ – Tetramethylbenzidine

TMS - Tetramethylsilane

TOCSY – Total correlation spectroscopy

Tris – tris(hydroxymethyl)aminomethane

UV – Ultraviolet

γ – Gyromagnetic ratio

ω_o – Larmor frequency

τ_c – Correlation time

δ – Chemical-shift

ε – Molar extinction coefficient

$\vec{\mu}$ – Magnetic moment of a nuclear spin

F – Faraday constant (96485 C mol^{-1})

h – Planck constant (6.63×10^{-34} m^2 kg s^{-1})

k – Boltzmann constant (1.38×10^{-23} m^2 kg s^{-2} K^{-1})

R – Molar gas constant (8.314 J K^{-1} mol^{-1})

Amino acid abbreviations		
Alanine	Ala	A
Arginine	Arg	R
Asparagine	Asn	N
Aspartate	Asp	D
Cysteine	Cys	C
Glutamate	Glu	E
Glutamine	Gln	Q
Glycine	Gly	G
Histidine	His	H
Isoleucine	Ile	I
Leucine	Leu	L
Lysine	Lys	K
Methionine	Met	M
Phenylalanine	Phe	F
Proline	Pro	P
Serine	Ser	S
Threonine	Thr	T
Tryptophan	Trp	W
Tyrosine	Tyr	Y
Valine	Val	V

1 Introduction

"When the last tree is cut, the last river poisoned, and the last fish dead, we will discover that we can't eat money…"

Greenpeace, 1981

1 – Introduction

Throughout history, humans have both affected and been affected by the natural world. Environmental problems are becoming more complex, especially as issues arise on a more global level, such as that of aquatic and atmospheric pollution, global warming or equitable access to safe and affordable drinking water. The interactions between human society and the environment are constantly changing. The environment is used and altered by a wide variety of people with many different interests and the challenge is to find approaches to environmental management that give people the quality of life they seek, while protecting the environmental systems that are also the foundations of their well-being. An adequate mindset, implemented by schools and families, is a strong first step towards this goal. A multidisciplinary learning approach can be established by the contributions of a wide range of fields, providing a deeper understanding of the technological, political, and social options, as well as strategies for studying and managing the relationship between our society and the environment.

In 2015, the United Nations set the Sustainable Development Goals, which comprise 17 global goals that cover a broad range of environmental, social and economic development issues [1]. These include poverty, hunger, health, education, climate change, gender equality, water sanitation, energy, environment and social justice. Among these goals, the insurance of access to affordable, reliable, sustainable and modern energy for all, as well as the need to guarantee availability and sustainable management of clean water, stand out as the ones that can be achieved with biotechnological applications based on Geobacter bacteria.

The first report that bacteria can generate electricity appeared almost a hundred years ago, by Potter [2]. Some microorganisms, such as Geobacter, can convert chemical energy from a wide range of organic and inorganic substances into electric current. On the other hand, Geobacter species have been shown to play important roles in the bioremediation of groundwater contaminated with petroleum and landfill leachate [3-7]. Since Geobacter's discovery, many studies have been made in order to understand the mechanisms underlying these unique characteristics which make Geobacter an excellent target to develop Microbial Fuel Cells (MFCs) based technologies and for application in bioremediation strategies (Figure 1.1).

Figure 1.1 – In situ test plot for U(VI) bioremediation station – This site, which was part of the Uranium Mill Tailings Remedial Action program from the U.S Department of Energy, was constructed on the grounds of a former uranium ore processing facility in Rifle, Colorado, USA. Geobacter sulfurreducens performs microbial reduction of soluble U(VI) – existing in contaminated groundwaters – to insoluble U(IV), facilitating the immobilization of the heavy metal. This strategy is then coupled with a soil washing technique, allowing the concentration of uranium from contaminated soils. Anderson and co-workers [8], responsible for the implementation of this station, discovered that Geobacter species can be simply and effectively stimulated for U(VI) reduction with the addition of an acetate solution to the contaminated groundwaters. They also verified that U(VI) concentrations decreased in as little as 9 days after acetate injection and that within 50 days, uranium concentration had declined below the prescribed treatment level of 0.18 μM [8] (photo taken from http://www.geobacter.org/bioremediation).

The work developed and presented in this Thesis focuses on the functional, thermodynamic, and biochemical characterization of electron transfer components from Geobacter bacteria.

1.1 – Geobacter bacteria

The family Geobacteraceae is part of the order Desulfuromonadales in the δ-subclass of the Proteobacteria. The order branches phylogenetically between the orders Desulfovibrionales and Desulfobacterales and consists of the genus Geobacter and the sole species Pelobacter propionicus [9].

Geobacter species are Gram-negative bacteria who play an important biogeochemical role in a diversity of natural environments. Geobacter species are mostly known for their capability of making electrical contacts with extracellular electron acceptors and other microorganisms [10]. This remarkable versatility permits Geobacter species to fill important niches in a variety of anaerobic environments [11]. These bacteria can also accept and donate electrons from

electrodes, in current consuming biofilms, a process that is currently explored in microbial electrosynthesis systems.

Geobacter species show an impressive respiratory adaptability, since they are capable of sustaining their growth by using extracellular compounds, such as Fe(III), U(VI) or Mn(IV) oxides, as terminal electron acceptors, in addition to the more frequent respiratory processes, which use soluble electron donors (e.g. acetate) and acceptors (e.g. fumarate) [12]. Some of these compounds are toxic or radioactive, making this organism a potential target for bioremediation and biotechnological applications [12, 13].

Geobacter bacteria were firstly classified as strict anaerobes that are naturally found in a variety of soils and sediments. However, data obtained for Geobacter sulfurreducens (G. sulfurreducens) indicates that Geobacter species can also grow at low levels of molecular oxygen, providing an explanation for their abundance in oxic subsurface environments [14] and for the existence of genes predicted to code for proteins involved in response to oxidative stress, such as rubredoxin, catalase, superoxide dismutase and superoxide reductase, as well as for a terminal cytochrome c oxidase [15].

These bacteria can be easily cultured and genetically manipulated for physiological studies. G. sulfurreducens was the first Geobacter for which methods for genetic manipulation were developed and, therefore, it has served as model for functional genomic studies designed to understand the bacteria's metabolism, gene regulation and extracellular electron transfer (EET) mechanisms [16-22].

1.2 – Geobacter sulfurreducens electron transfer pathways

The bacterium G. sulfurreducens was described for the first time in 1994, after being isolated from surface sediments of a hydrocarbon-contaminated ditch near Norman, Oklahoma, USA [23]. G. sulfurreducens has a versatile approach to capturing energy and carbon, having three enzyme systems capable of converting pyruvate to acetyl-CoA. These systems include a pyruvate-ferredoxin oxidoreductase and a pyruvate-formate lyase, both used by anaerobes, and a putative pyruvate dehydrogenase complex, found largely in aerobic organisms [24].

The genome of G. sulfurreducens has an unprecedented number of putative c-type cytochromes, with 111 coding sequences containing at least one match to the c-type cytochrome motif that identifies heme groups (CXXCH, where X corresponds to any amino acid). Out of these, 73 contain two or more heme groups. The abundance of cytochromes

highlights the importance of electron transport to this microorganism and suggests that this bacterium possesses electron transfer networks with high flexibility and redundancy, allowing the reduction of diverse metal ions in natural environments [15]. In fact, several studies revealed a complex transcriptional response by G. sulfurreducens to different electron acceptors. Currently, no single gene deletion on the G. sulfurreducens genome was found to eliminate electron transfer to all electron acceptors, thus confirming the complexity of the electron transfer networks in G. sulfurreducens [21, 25-34].

The cytochromes from G. sulfurreducens are strategically localized at the bacterial inner membrane (IM), periplasm or outer membrane (OM), allowing the transfer of electrons from intracellular carriers, such as NADH, to extracellular acceptors.

The main IM electron transfer components studied in recent years have been the IM-associated peroxidase MacA (GSU0466 – the nomenclature of the genome of G. sulfurreducens is in agreement with http://www.genome.jp/kegg/genome.html), CbcL (GSU0274) and ImcH (GSU3259) cytochromes. MacA is a dihemic, 35 kDa protein, thought to be involved in the electron transfer from the IM to the periplasmic components of the EET network [35, 36]. This cytochrome was identified as a peroxidase and is also capable of exchanging electrons with the periplasmic c-type cytochrome PpcA [37]. The CbcL protein contains a HydC/FdnI diheme b-type cytochrome linked to a 9-heme periplasmic cytochrome c domain [38]. On the other hand, the cytochrome ImcH was predicted to contain up to three transmembrane helices (depending on processing of a putative signal anchor), a region of NapC/NirT homology, and up to 7 heme c-type heme binding motifs [39].

Amongst all the proteins involved in the EET processes of G. sulfurreducens, the most studied is the periplasmic cytochrome PpcA (GSU0612), that belongs to a family composed by five low molecular weight (10 kDa) triheme cytochromes with approximately 70 residues each. The other four cytochromes of this family are designated PpcB (GSU0364), PpcC (GSU0365), PpcD (GSU0124), PpcE (GSU1760) and share 77% (PpcB), 62% (PpcC), 57% (PpcD) and 65% (PpcE) amino acid sequence identity with PpcA. Due to the cellular location of these five cytochromes, it was proposed that they are likely reservoirs of electrons, destined for the cell outer surface, bridging the electron transfer between the cytoplasm and the cell exterior [19, 27].

Also located in the periplasm of G. sulfurreducens, there are other relevant cytochromes, such as the dodecaheme cytochrome GSU1996 (42 kDa), the monoheme cytochrome PccH (GSU3274, 15 kDa) and the triheme cytochrome GSU0105 (10 kDa). GSU1996 is composed by

four similar triheme domains, designated A, B, C, D and the cytochrome is thought to act as a periplasmic electron capacitor [40, 41]. PccH was unequivocally identified as crucial for G. sulfurreducens cells to be able to accept electrons from electrodes [42]. GSU0105, together with two other uncharacterized cytochromes (GSU0701 and GSU2515), is highly expressed in Fe(III) reducing conditions but is not expressed at all in cultures grown on fumarate [27].

G. sulfurreducens is said to have a similar OM architecture compared to Shewanella oneidensis (S. oneidensis), meaning that the electrons reach the cellular exterior through porin-cytochrome trans-outer membrane complexes [43]. The OM complexes OmaB(GSU2738)-OmbB(GSU2739)-OmcB(GSU2737)/OmaC(GSU2732)-OmbC(GSU2733)-OmcC(GSU2731) in G. sulfurreducens may have similar functions to the ones described for the MtrA-MtrB-MtrC complex in S. oneidensis [44]. These complexes consist of a porin-like OM protein (OmbB or OmbC), a periplasmic octaheme cytochrome c (OmaB or OmaC) and an OM dodecaheme cytochrome c (OmcB or OmcC). Recently, other OM complexes, presenting a similar complex organization, OmaW(GSU2643)-OmbW(GSU2644)-OmcW(GSU2642) and OmaV(GSU2725)-OmbV(GSU2726)-OmcV(GSU2724), were shown to be involved in EET to Fe(III) and Mn(IV) oxides [45]. Shi and co-workers [46] suggested that the OmaW-OmbW-OmcW complex has an extra periplasmic component, the GSU2645 cytochrome. Otero and co-workers [47] identified a five-component OM complex and named it ExtHIJKL (ExtH(GSU2940)-ExtI(GSU2939)-ExtJ(GSU2938)-ExtK(GSU2937)-ExtL(GSU2936)). This complex was found to be important in Fe(III) citrate reduction [47].

Other OM cytochromes have been studied in G. sulfurreducens, namely OmcE, OmcF, OmcS and OmcZ. The 26 kDa tetraheme c-type cytochrome OmcE (GSU0618) is located in the exterior of the OM of the bacterium and was shown to have an important role in Fe(III) oxide reduction [30]. OmcF (GSU2432) is a monoheme cytochrome c predicted to be localized at the OM of G. sulfurreducens, having a crucial role in Fe(III) citrate reduction [29]. Finally, OmcS (GSU2504, 47 kDa) and OmcZ (GSU2076, 30 kDa) are extracellular c-type cytochromes, containing six and eight heme groups, respectively [48, 49]. OmcS is usually associated with conductive pili [49], whereas OmcZ is responsible for promoting electron transfer in current-producing G. sulfurreducens biofilms [50].

As mentioned above, G. sulfurreducens also possesses electrically conductive pili that enable the bacterium's long-range electron transfer to insoluble minerals [51], to other cells [52-54] and through electrically conductive biofilms [55, 56]. Many findings have been supporting the concept of long-range electron transport along the pili of G. sulfurreducens [57], including: (i)

the inhibition of the electron transport to Fe(III) oxides, interspecies electron exchange and the development of thick electrically conductive biofilms in strains with deletion of the PilA (GSU1496), the pilus monomer [31, 51, 53, 55]; (ii) the inhibition of Fe(III) oxide reduction and reduced biofilm conductivity, in strains with genetically modified pilA, specially designed to yield poor conductivity [58]; (iii) infective Fe(III) oxide reduction and current production, in a strain of G. sulfurreducens expressing the poorly conductive pili of Pseudomonas aeruginosa [59]; (iv) the individual pilin filaments are electrically conductive [51, 55, 60]; and (v) the pili propagate charge similarly to carbon nanotubes [61].

Although many EET components of G. sulfurreducens are known, these mechanisms and the proteins implicated in each electron transfer pathway are still under investigation. The initial model presented by Lovley in 2006 [36] suggested that the electrons coming from the menaquinone pool were transferred to the periplasmic components of the bacterium through the IM associated cytochrome MacA (Figure 1.2).

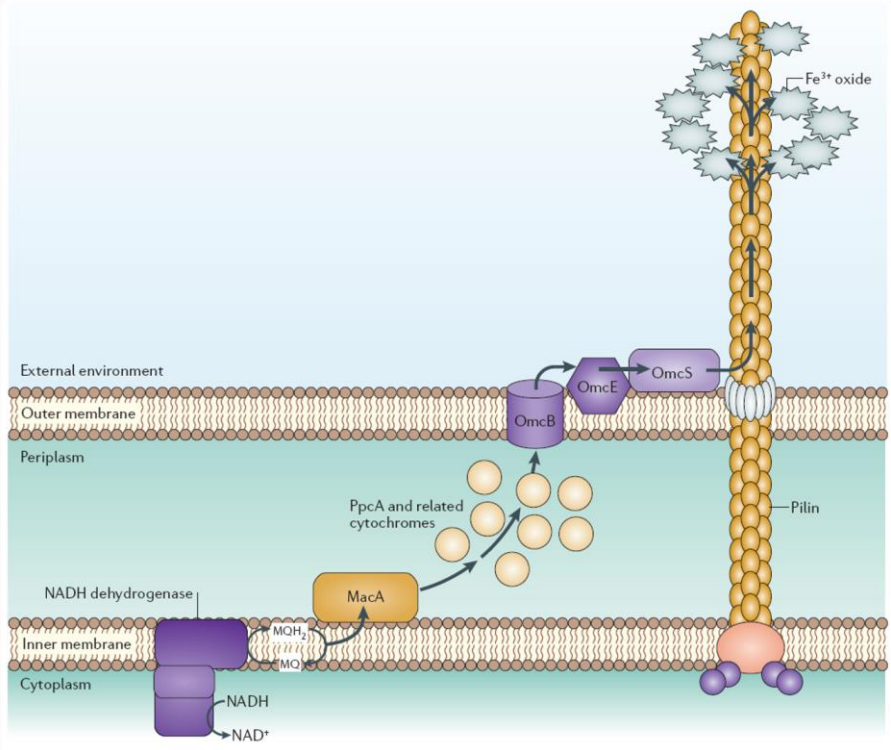

Figure 1.2 – Initial model suggested for EET in G. sulfurreducens by Lovley [36], with iron oxides serving as final electron acceptors – The electrons are transferred from the menaquinone pool to the IM associated cytochrome MacA, who then shuttles them to the periplasmic components of the bacterium. The route continues through the OmcB cytochrome, followed by OmcE and OmcS. Finally, the electrons reach the iron oxides attached to the bacterium's pili. This figure was adapted from [36].

Electrons were then shuttled via PpcA and related cytochromes to the outside of the cell through the OmcB multiheme cytochrome, followed by electron transfer reactions with other OM components and pili. Although the idea for the routes of EET remained the same, in 2014, a slightly different model was presented, since OmcB was found to actually be part of a three-component OM complex (OmaB-OmbB-OmcB) [11, 44]. More recently, a series of findings about important EET components led to a redesign of the EET routes of electron transfer in G. sulfurreducens (Figure 1.3).

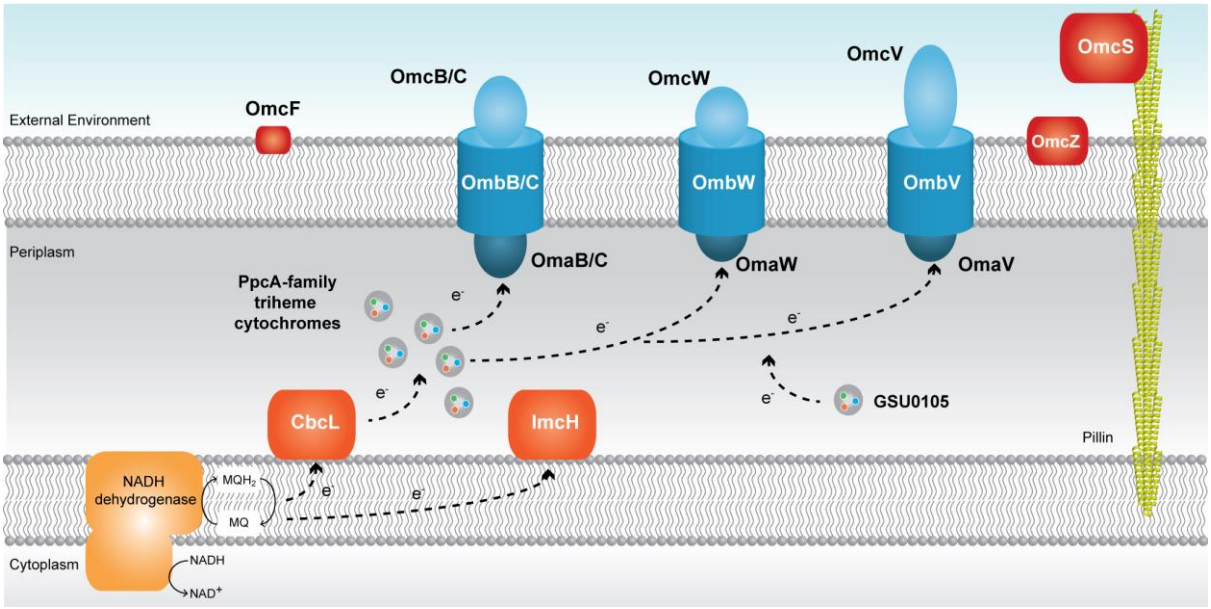

Figure 1.3 – Current proposed model for the extracellular electron transfer pathways in G. sulfurreducens – The black arrows represent the proposed electron transfer pathway. Either CbcL or ImcH (both in dark orange) receive electrons from the menaquinol (MQH_2)/ menaquinone (MQ) pool, at the IM, depending on the final electron acceptor redox potential. The periplasmic components, namely the PpcA-family of triheme cytochromes (PpcA-E) are reduced by the electrons received from either CbcL or ImcH. These cytochromes mediate the electron transfer from the periplasm to the OM complexes (in blue), that are likely directly involved in insoluble Fe(III) oxides reduction, which are not represented in the figure. Other components that participate in electron transfer mechanisms in G. sulfurreducens are also represented (GSU0105 and other OM cytochromes – OmcF, OmcS and OmcZ – which are represented in red).

The current model for EET maintains the theory that electrons are transferred to the menaquinone pool via the NADH dehydrogenase located in the IM [62]. Then, depending on the redox potential of the final electron acceptor, different proteins are involved in the quinone regeneration: the CbcL-dependent pathway operates with acceptors at or below redox potentials of –100 mV (versus the normal hydrogen electrode, NHE), whereas the ImcH-dependent pathway operates above this redox potential [38, 39]. In either case, electrons are

putatively supplied from these two IM associated proteins to periplasmic triheme cytochromes. In order to reduce extracellular compounds, the electrons are transferred from the periplasmic cytochromes to OM associated cytochromes, through porin-cytochrome trans-outer membrane complexes [63].

1.3 – Gene knockout and proteomic studies in Geobacter sulfurreducens

Several studies have been made in order to identify the proteins involved in the different reduction pathways used by G. sulfurreducens. Proteomic analysis under different growth conditions and gene deletion studies were performed, with special focus on the c-type cytochromes who may play important roles in electron transfer to extracellular electron acceptors. In this section, the main conclusions taken from those studies are summarized.

The IM associated cytochrome MacA is more abundant during growth with Fe(III) oxides versus Fe(III) citrate [26] and the deletion of its gene was shown to result in the inhibition of the expression of the omcB gene [64]. However, the expression of the OM cytochrome OmcB in the macA deficient mutant restored the capacity for Fe(III) reduction [64]. In addition to this, a high similarity in the expression patterns and mutant phenotypes between MacA and OmcB, suggests that these two cytochromes may function in the same or similar routes of electron transfer [45]. The deletion of the genes encoding for the IM cytochromes CbcL and ImcH inhibited reduction of Fe(III) oxides and Fe(III) citrate , respectively [38, 39].

Regarding the periplasmic cytochromes, it was shown that the deletion of the gene coding for PpcA affects the ability of G. sulfurreducens to reduce Fe(III) oxides and U(VI) [19, 33]. Also, PpcA was detected in G. sulfurreducens cultures that grow in presence of Fe(III) citrate and Fe(III) oxide [26]. Similarly, PpcB and PpcC were also detected in Fe(III) citrate and Fe(III) oxide cultures [26]. The deletion of the genes encoding for these two cytochromes, which are part of the same locus, was shown to affect U(VI) reduction [33]. The deletion of the gene encoding for PpcD affects the reduction of U(VI) and the cytochrome was shown to be more abundant during growth with Fe(III) oxide versus Fe(III) citrate [27, 33]. PpcE was only detected in cultures with Fe(III) citrate and its gene deletion also affected U(VI) reduction [27, 33]. Finally, PccH is crucial for fumarate reduction in current-consuming biofilms [42].

Several OM cytochromes have been proven to play relevant roles in EET pathways and on the overall regulation of energy transduction in G. sulfurreducens. OmcE, for example, is more abundant in Geobacter cells during growth with Fe(III) oxides than in cells grown in Fe(III) citrate [45]. Other studies revealed that an omcE-deficient mutant strain did slowly adapt to

reduce Fe(III) oxides, suggesting that other EET components can partially compensate for the absence of OmcE [30]. The deletion of the omcF gene affects the expression of other OM cytochromes, namely OmcB, OmcC and OmcS [18]. Specifically, the deletion of omcF resulted in a loss of expression of omcB and omcC, as well as an overexpression of omcS, during growth on Fe(III) citrate [29]. Recently, different studies revealed that a omcF-deficient strain was unable to grow in presence of Fe(III) oxide and presented a significant decrease in current production [29, 45]. On the other hand, the deletion of omcS affects Geobacter's growth in the presence of Fe(III) oxides [30, 45]. The OmcS cytochrome was shown to be more abundant during growth with Fe(III) oxides versus Fe(III) citrate [30, 31], whereas OmcZ is more abundant in the opposite conditions [26].

Other studies performed in vitro demonstrated that OmcZ transfers electrons to a diversity of potential extracellular electron acceptors, such as Fe(III) citrate, U(VI), Cr(VI), Au(III), Mn(IV) oxide and AQDS [26, 48]. These studies also demonstrated that OmcZ does not transfer electrons to Fe(III) oxides, justifying its higher abundance during growth with Fe(III) citrate versus Fe(III) oxides. The OM complexes OmaB-OmbB-OmcB and OmaC-OmbC-OmcC were found to be important in Mn(IV) oxide reduction [25].

Finally, the OmaW-OmbW-OmcW and OmaV-OmbV-OmcV complexes were found to be overexpressed during growth with Mn(IV) oxide versus Fe(III) citrate and with Fe(III) oxide versus Fe(III) citrate [25, 47].

1.4 – Geobacter metallireducens

G. metallireducens is a rod shaped, Gram-negative, anaerobic bacterium and was first isolated from freshwater sediments in 1987. It was the first Geobacter ever to be isolated [65]. This bacterium was also the first organism found to completely oxidize organic compounds to carbon dioxide with Fe(III) oxide serving as the electron acceptor [65-67].

Initially, G. metallireducens was reported to be a non-motile bacterium [68]. However, in 2002, motility was observed for G. metallireducens cells grown in insoluble Fe(III) by phase-contrast microscopy [69]. This bacterium is capable of storing energy through dissimilatory reduction of iron, manganese, uranium and other metals [65].

Besides, this bacterium can also oxidize short chain fatty acids, alcohols and monoaromatic compounds, such as toluene and phenol, using iron as its electron acceptor [68, 70]. Several studies also suggested a core benzoyl-CoA degradation pathway in the utilization of these

aromatic compounds [71-74]. Furthermore, G. metallireducens can also use nitrate as electron acceptor, having a functional enzyme complex (which includes a multiheme cytochrome c) that exhibits both nitrate and nitrite reductase activities [68, 75].

In 2006, studies revealed that G. metallireducens can reduce even very stable iron complexes, such as Prussian Blue (cyanide-metal complex, $Fe_4[Fe(CN)_6]_3$, typically found in soils and aquifers of industrial sites, usually released or spread by outgassing or transport with the groundwater), using it as a primary electron acceptor [76].

G. metallireducens is also capable of reducing ionic mercury (Hg^{2+}) to elemental mercury (Hg) without having to use a mercury reductase [77]. This feature of G. metallireducens can be explored in order to mobilize mercury from contaminated groundwaters and produce methylmercury in anoxic environments [77]. Also, G. metallireducens is able to use vanadium as a final electron acceptor, as proven by Aklujkar and co-workers [78].

In 2008, Tremblay and co-workers [79] developed a genetic system for G. metallireducens and identified a very important role for pili in Fe(III) reduction and electron transfer to electrodes. G. metallireducens unique motility is one of the reasons why this bacterium is more efficient in the reduction of Fe(III) oxides, compared to G. sulfurreducens [79]. As mentioned, in G. sulfurreducens it has been proven that in addition to pili, OM c-type cytochromes are important for extracellular electron exchange with Fe(III) oxide [30, 80], U(VI) [33], humic substances [81], electrodes [28, 31] and other cells [53]. However, there is poor conservation of OM cytochromes between G. sulfurreducens and G. metallireducens. Further studies of the functional homologues in G. metallireducens are likely to provide important insights into the features that c-type cytochromes may share to permit similar function in the absence of sequence homology [79].

In the recent years, a few proteomic and gene knockout studies have been published for G. metallireducens [73, 74, 82, 83]. These studies revealed that there are some EET components that are conserved in G. metallireducens when compared with G. sulfurreducens, namely the PpcA-family of cytochromes and some IM and OM cytochromes. However, there is not much information about the functional properties of these components, in contrast with G. sulfurreducens (as demonstrated in the previous section).

For the family of periplasmic cytochromes existing in G. metallireducens (composed by PpcA (Gmet_2902), PpcB (Gmet_3166), PpcC (Gmet_3165), PpcE (Gmet_1846) and PpcF (Gmet_0335) – the nomenclature of the genome of G. metallireducens is in agreement with

http://www.genome.jp/kegg/genome.html), one can infer that their functions will be very similar to the ones of the PpcA-family from G. sulfurreducens, due to the high homology between both families. This means that in G. metallireducens, this family of cytochromes is probably responsible for controlling the electron flow from the IM to the OM electron transfer components (Figure 1.4). This subject will be addressed in more detail in Chapter 2.

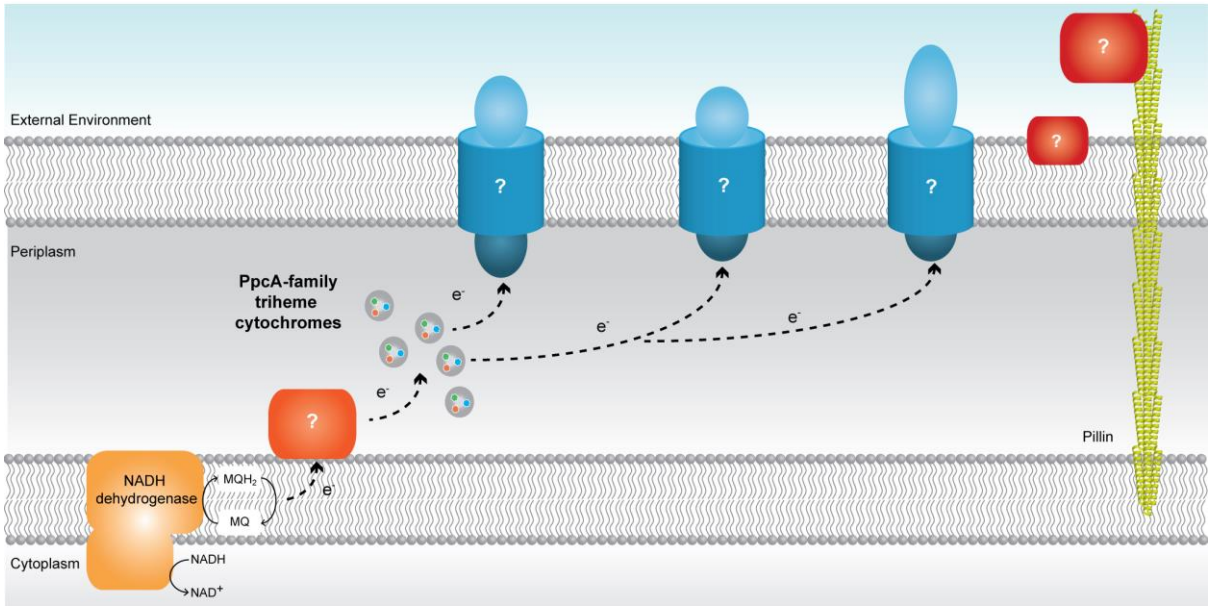

Figure 1.4 – Current extracellular electron transfer pathways model in G. metallireducens – The black arrows represent the proposed electron transfer pathway. The periplasmic PpcA-family triheme cytochromes (PpcA, PpcB, PpcC, PpcE and PpcF) mediate the electron transfer between the IM associated cytochromes (in orange) to the porin-cytochrome complexes in the OM (in blue).

1.5 – Geobacter sulfurreducens versus Geobacter metallireducens

Globally, G. sulfurreducens and G. metallireducens share several metabolic features, including the ability to reduce U(VI) [84], high current production [85], as well as the capability to transfer electrons to different species without the involvement of electron carrier molecules, a process designated direct interspecies electron transfer (DIET) [54, 86, 87].

Although there are several metabolic characteristics shared between the two bacteria, a marked difference relates to their ability to oxidize organic compounds. While G. sulfurreducens can only oxidize acetate, formate, lactate and pyruvate, G. metallireducens can oxidize all the above mentioned, as well as benzaldehyde, butanol, ethanol, phenol, propionate and propanol [78]. Furthermore, G. metallireducens is able to use more inorganic compounds as final electron acceptors, such as vanadium, in contrast with G. sulfurreducens [10, 78]. G. metallireducens can also be considered an organism of interest in the bioremediation field, for

application in several systems, such as: (i) bioremediation of waters contaminated with organic wastes, particularly important for the removal of azo compounds produced by textile industries [88]; (ii) bioremediation of contaminated waters with vanadium [89] and (iii) full degradation of several compounds to methane via DIET mechanisms with methanogenic bacteria [87]. This feature can be applied to the treatment of wastewaters where methanogenic microorganisms tend to degrade organic matter, with concomitant methane production [86].

Considering all the above mentioned, to optimize these processes, it is first necessary to understand the mechanisms underlying EET in these bacteria. The recent development of a genetic system for G. metallireducens is likely to refocus attention on this organism and it will allow the unravelling of the above mentioned physiological mechanisms, as well as other relevant novel properties, such as anaerobic benzene degradation, Fe(III) reduction or the use of cytochromes as capacitors to permit respiration in the absence of exogenous electron acceptors, among other remarkable features [78, 79].

1.6 – Functional diversity of cytochromes

Heme-containing proteins display a diversity of biological functions, including (i) simple electron transfer reactions, such as those catalyzed by b- and c-type cytochromes [90]; (ii) oxygen transport and storage via hemoglobin and myoglobin [91]; (iii) oxygen reduction to the level of water by cytochrome oxidase [92]; (iv) oxygenation of organic substrates, as facilitated by the cytochromes P-450 [93] and (v) the reduction of peroxides by catalases and peroxidases [94]. By combining heme groups with other cofactors, such as flavins and/or metal ions (molybdenum or copper), these proteins can have an even higher range of functions, extending them to a large range of enzymatic processes, which include dehydrogenations [95] and the reduction of numerous small molecules [96].

In the particular case of cytochromes, their functional versatility is mainly related with the type of heme groups (Figure 1.5) and neighbor amino acids.

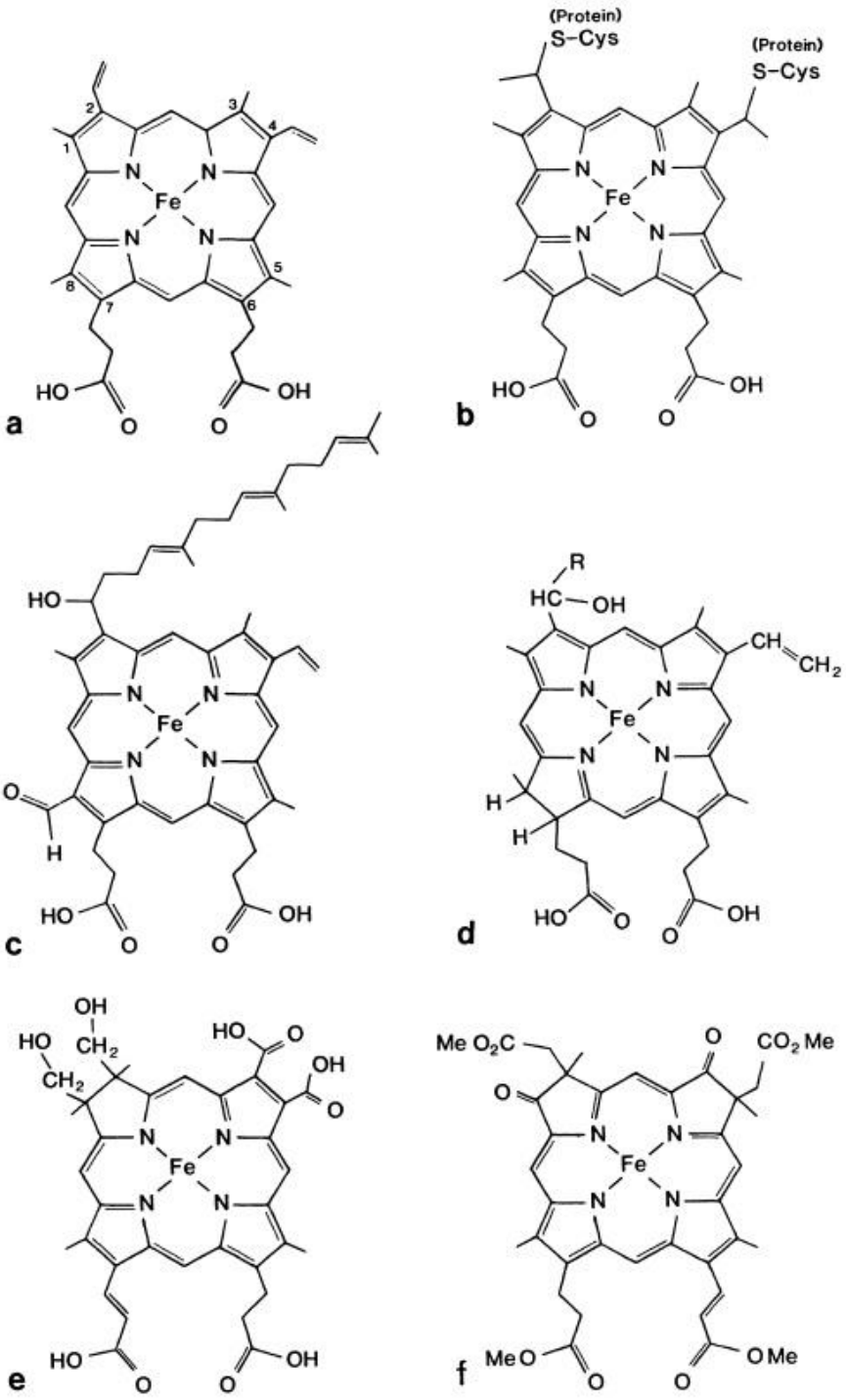

Figure 1.5 – Different types of hemes found in cytochromes – The classification of the heme groups is based on the differences between the porphyrin molecules and types of polypeptide covalent attachments. a) b-type – protoheme IX; b) c-type – substituted protoheme IX; c) a-type, d) d-type; e) and f) d_1-type. This figure was taken from [97].

Of the many factors capable of tuning cytochromes activity, (i) the ability of the protein environment to modulate heme reactivity; (ii) the number and nature of protein donated axial

ligands to iron; (iii) the heme solvent exposure; (iv) the heme accessibility to exogenous ligands; (v) the distribution of polar and charged groups in the heme neighborhood and (vi) the specific properties of the heme-binding site in the protein, stand out as the most crucial ones [95, 98].

The term "cytochrome" dates back to 1925, when Keilin introduced it to describe a group of heme proteins undergoing oxidation/reduction reactions, characterized in the reduced form by intense absorption bands in the 510-615 nm range [99]. Cytochromes are named accordingly to their heme type letter (in italic) and a number in subscript, depending on some intrinsic characteristics related to the protein axial ligands coordination, number of heme groups, optical or functional properties [100].

Cytochromes c, specifically, are heme proteins containing a c-type heme and often function as electron carriers in biological systems. The polypeptide chain of these proteins is covalently bound to one or several c-type heme groups through thioether linkages established with the sulfhydryl groups of two cysteine residues in a conserved binding motif sequence CXXCH [98, 101]. The heme group displays a central role in the functional modulation of these proteins. It is constituted by four pyrrole subunits connected by methane bridges (protoporphyrin IX) and in the center, the iron ion is equatorially coordinated by four nitrogen atoms (Figure 1.5b).

Iron (0) has an electronic structure $1s^2 2s^2 2p^6 3s^2 3p^6 3d^6 4s^2$ (where the first numbers corresponds to the principal quantum number; the letters correspond to the orbital quantum number; and the superscripts correspond to the electron occupancies). The electronic structure of iron is sometimes described as $[Ar]3d^6 4s^2$ to emphasize that the electron occupancies of the higher energy orbitals (3d and 4s), superimposed on an argon core, are responsible for the electronic properties and, ultimately, for the chemical behavior of iron [101]. In heme proteins, iron usually exists in two more common oxidation states: the ferrous state (Fe(II): $[Ar]3d^6 4s^0$) and the ferric state (Fe(III): $[Ar]3d^5 4s^0$).

In an iron atom there are five 3d-orbitals – two orbitals of higher energy ($d_{x^2-y^2}$ and d_{z^2}, also known as the e_g set of orbitals) and three of lower energy (d_{xy}, d_{xz} and d_{yz}, also known as the t_{2g} set of orbitals). Each orbital can be occupied by two electrons, and the distribution of electrons within these orbitals determines the electronic properties of iron. Besides, the electronic distribution of iron is governed by its coordinated ligands [101]. The Crystal Field Theory considers that the bonding between the iron and the ligands is entirely electrostatic [102]. There are two major energy terms that govern the distribution of electrons in the d-orbitals: the strength of the d-orbital splitting (represented by the symbol Δ_0), which depends upon the

electrostatic field created by the ligands and the energy required to pair electrons in the same orbital (pairing energy - P) [101].

The pairing energy is always unfavorable, but what is relevant is whether it requires less energy to pair electrons in the t_{2g} orbitals than it does to keep them unpaired in the e_g orbitals. In a weak crystal field, the d-orbital splitting is smaller than the pairing energy ($\Delta_0 < P$) and the electrons remain unpaired in separate orbitals (Figure 1.6). This electron distribution is the high-spin configuration. On the other hand, in a strong crystal field, the electrons enter the t_{2g} orbitals and pair to produce the low-spin configuration (Figure 1.6).

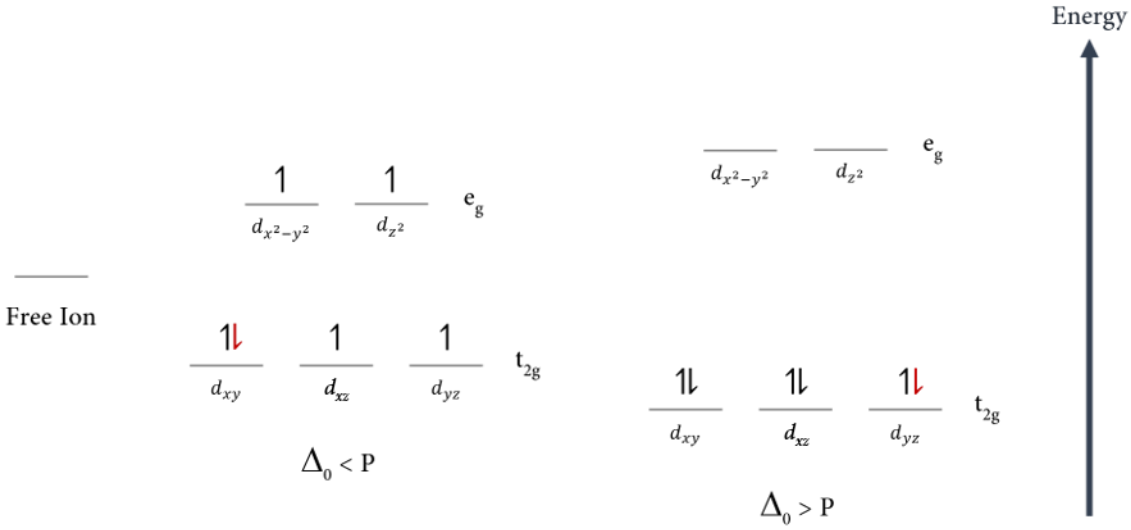

Figure 1.6 – Spin-states of octahedral Fe(III) and Fe(II) – The free iron ion has five 3d-orbitals of the same energy. In the figure, these orbitals are represented as a single one, for simplicity. When placed in an octahedral field, the d-orbitals of the iron atom are rearranged in two sets – the t_{2g} set (of lower energy, composed by the d_{xy}, d_{xz} and d_{yz} orbitals) and the e_g set (composed by the $d_{x^2-y^2}$ and d_{z^2} orbitals). For Fe(III), whose electrons are represented by black arrows, a weak crystal field ($\Delta_0 < P$) leads to a total spin of 5/2 (high-spin configuration), whereas a strong crystal field ($\Delta_0 > P$) results in a total spin of 1/2 (low-spin configuration). On the other hand, for Fe(II), whose extra electron is represented by a red arrow, a weak crystal field ($\Delta_0 < P$) leads to a total spin of 2 (high-spin configuration), whereas a strong crystal field ($\Delta_0 > P$) results in a total spin of 0 (low-spin configuration).

The porphyrin is a strong ligand that places the iron ion close to a state where small energy differences between the axial ligand components of the field can cause the change of spin state. Considering this, important information about the heme axial ligands and their stereochemistry can be accessed after the spin state of a heme protein is determined. The heme

spin state can be determined by a variety of spectroscopic techniques, namely Nuclear Magnetic Resonance (NMR), UV-visible and Electron Paramagnetic Resonance (EPR) [103].

In cytochromes c, one of the two axial coordination positions is occupied by the side chain of a histidine (designated as proximal ligand, see Figure 1.7). On the other hand, the distal ligand is more variable and can be the side chain of a (i) methionine, which predominates in monoheme cytochromes c, (ii) histidine, particularly predominant in multiheme cytochromes c or (iii) asparagine, lysine or tyrosine, although with less frequency. In certain conditions, the distal position of the heme can also be transiently vacant, as observed for various cytochromes with enzymatic activity [62, 100, 104].

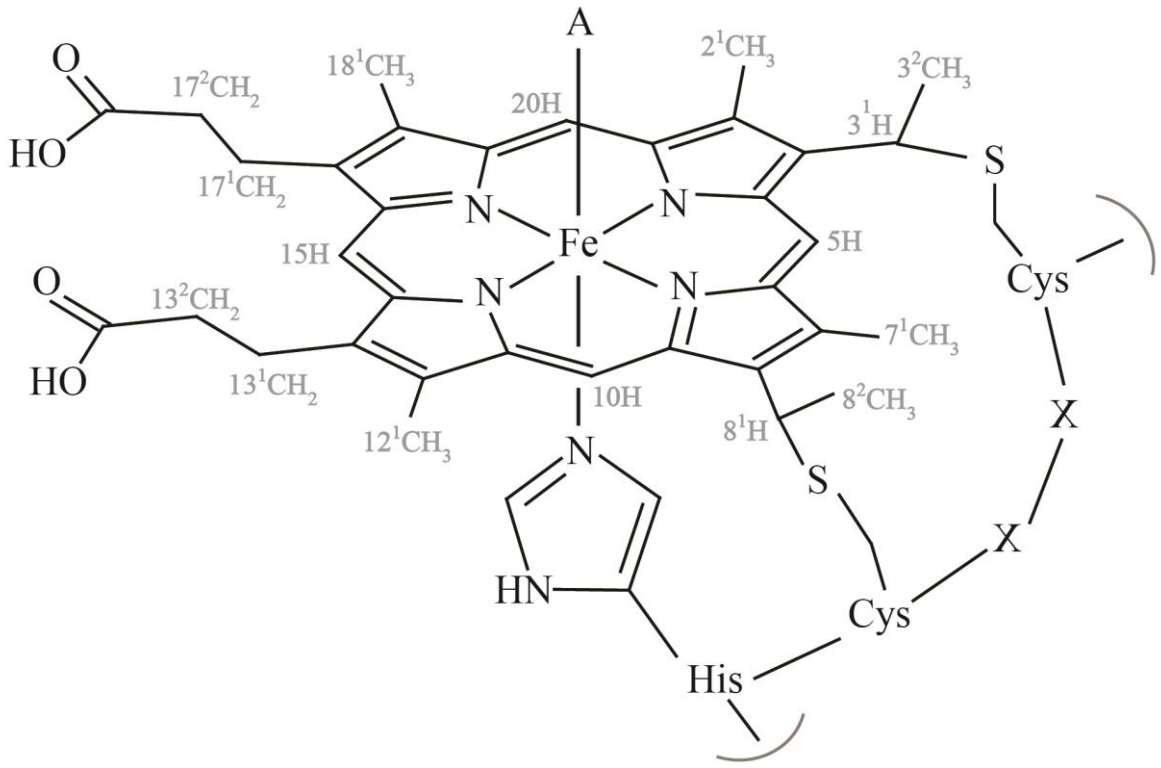

Figure 1.7 – Schematic representation of a c-type heme and the correspondent polypeptide binding motif (CXXCH) – The distal coordination position, labeled with A, can be free or occupied by different amino acids side chains. The IUPAC-IUB nomenclature for tetrapyrroles is illustrated in gray [105]. This figure was taken from [62].

Therefore, in hemes c with histidine or methionine as distal ligands, the d-orbital splitting is larger than the pairing energy, meaning that these hemes will be in a low-spin state (see Figure 1.6). In contrast, if the heme iron distal position is bond to the side chain of an asparagine, lysine, tyrosine or to a water molecule, the d-orbital splitting is smaller than the pairing energy, and the heme will be in a high-spin state. Heme proteins involved in electron transfer

reactions usually have both axial positions occupied and hold histidine or methionine residues as distal ligands [62, 101].

Furthermore, the heme redox potential is also strongly dependent on the nature of the axial ligands. The side chain methionine sulfur is a good electron acceptor and favors the electron-rich reduced state, resulting in a more positive redox potential compared to bis-histidinyl coordinated heme groups [97, 106].

1.7 – Multiheme cytochromes

Multiheme cytochromes are crucial components of several biological processes and are involved in electron transfer [107, 108], enzymatic reactions [108-110] and on signal transduction events [111]. They were also shown to work as electron biocapacitors (e.g. GSU1996, Figure 1.8), thus contributing for the enhancement of the electron-storage capacity of several bacteria [40, 41, 112].

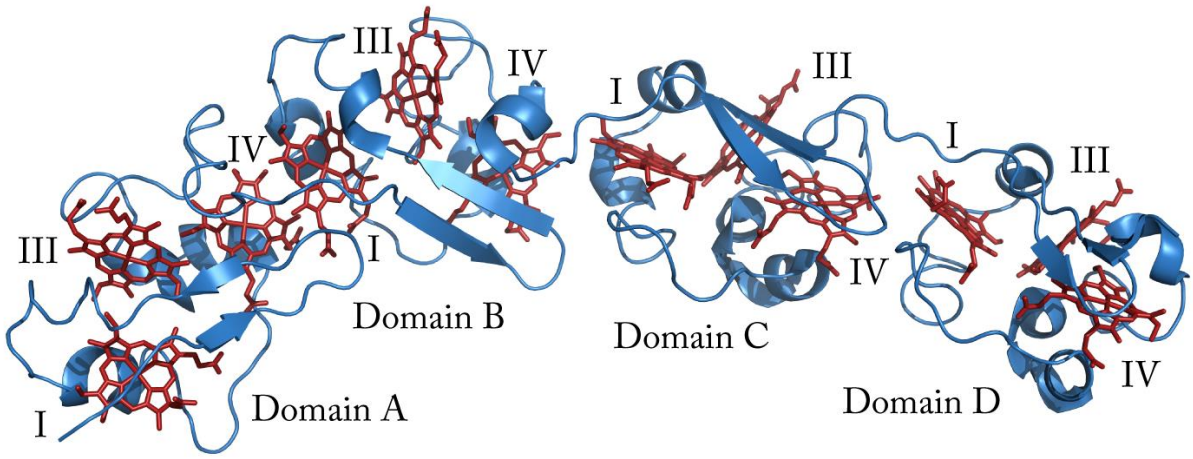

Figure 1.8 – Crystal structure of the dodecaheme cytochrome GSU1996 from G. sulfurreducens, obtained in the oxidized state – The cytochrome (PDB ID: 3OV0 [41]) is organized in four similar domains (A-D), each containing three hemes, connected by a flexible linker. Each domain has structural homology to the triheme cytochromes of the PpcA-family from G. sulfurreducens, except for the heme IV, which contains His-Met axial coordination. In the figure, the backbone is represented in blue, whereas the hemes are represented in red. Roman numerals indicate the hemes in their order of attachment to the CXXCH motif in the polypeptide chain. The structure was drawn using the PyMOL molecular graphics system [113].

Multiheme cytochromes generally have a set of the same type of heme groups, as seen for the PpcA-family from G. sulfurreducens (in which all the hemes are from the c-type). However, some specific multiheme cytochromes can contain two different types of hemes,

namely the cytochrome cd_1-nitrite reductase (hemes c and d_1) [108, 114] and the IM CbcL cytochrome from Geobacter sulfurreducens, which contains a HydC/FdnI diheme b-type cytochrome linked to a 9-heme periplasmic cytochrome c domain [38].

These proteins are able to receive or donate multiple electrons in a cooperative way, depending on the intrinsic properties of the neighboring hemes (redox interactions) or heme surrounding protonable centers (redox-Bohr effect) [115-117]. The several heme groups extend the protein's global working redox potential ranges, as a consequence of the contribution of each individual heme redox potential. Typically, the heme iron-iron distances between adjacent hemes do not exceed 15 Å, allowing a fast electronic exchange between the redox centers and assuring efficient redox reactions [104, 118, 119].

The redox potential of hemes in multiheme cytochromes is affected by several factors, namely (i) the differences in the free energy between the oxidized and reduced sates, resulting from molecular interactions; (ii) the modulation of the electrostatic interactions within the protein or with the solvent; (iii) the heme solvent accessibility; (iv) the extent to which the heme group is distorted from planarity; (v) the protonation state of the heme propionate groups and (vi) the type of axial ligands and heme iron coordination, as stated previously [101, 120-126]. Furthermore, multiheme cytochromes have a lower amino acid residue to heme ratio compared to monoheme cytochromes, meaning that the heme groups are more solvent exposed. The high heme solvent exposure and the typical His-His heme coordination strongly contributes to the lower redox potential values generally observed in multiheme cytochromes.

1.8 – Structural and thermodynamic characterization of cytochromes c

The determination of multiheme cytochromes structures is crucial to understand their functional mechanisms. Three-dimensional structures of biological macromolecules can be determined by X-ray crystallography and NMR at atomic resolution. These techniques are well established complementary high-resolution methods to analyze protein structure-function relationships.

NMR spectroscopy enables the determination of protein structures in conditions similar to their physiological environment, providing information about the protein's internal motions and interactions with its redox partners in solution (this technique is discussed in depth in Chapter 2). However, the numerous proton-containing groups of the hemes in cytochromes, as well as the magnetic properties of the heme iron (particularly in the oxidized state), further complicate the assignment of the NMR signals of these proteins [127-129].

Advances in protein expression protocols have contributed to increase the expression yields for mature multiheme cytochromes. Higher yields of protein expression allowed the overcome of traditional difficulties associated with the determination of solution structures using natural abundance samples [130-134]. This rendered the isotopic labelling of multiheme cytochromes much more cost-effective, facilitated the NMR signal assignment procedure and provided the foundations for the identification of redox partners and mapping of their interacting regions [135-137].

The isotopic labeling protocol developed by Fernandes and co-workers [138] was used to produce ^{15}N and ^{13}C-^{15}N labeled cytochromes and allowed to obtain proteins uniformly labeled, with the correct folding and post-translational incorporation of heme groups [139-141]. Taking advantage of these methodologies, the NMR solution structures of two different cytochromes from Geobacter sulfurreducens have been determined. Currently, there are solution structures available for the periplasmic triheme cytochrome PpcA, in both oxidized [142] and reduced states [143], and for the OM monoheme cytochrome OmcF, in the reduced state [144]. Crystal structures of Geobacter sulfurreducens cytochromes are available in the oxidized state, namely those of PpcA [145], PpcB [146], PpcC [147], PpcD [147], PpcE [147], OmcF [148, 149], GSU1996 [41], PccH [150] and MacA [37]. The structures of some of the referred cytochromes are presented in Figure 1.9. In the GSU1996 cytochrome and in the PpcA-family cytochromes (Figures 1.8 and 1.9, respectively), the hemes are numbered I, III and IV. This designation derives from the superimposition of the hemes in cytochromes c_7 with those of the structurally homologous tetraheme cytochromes c_3 [151]. On the other hand, in MacA, the hemes are named as high potential (HP) and low potential (LP), because of the electric potential difference between them [37] (Figure 1.9).

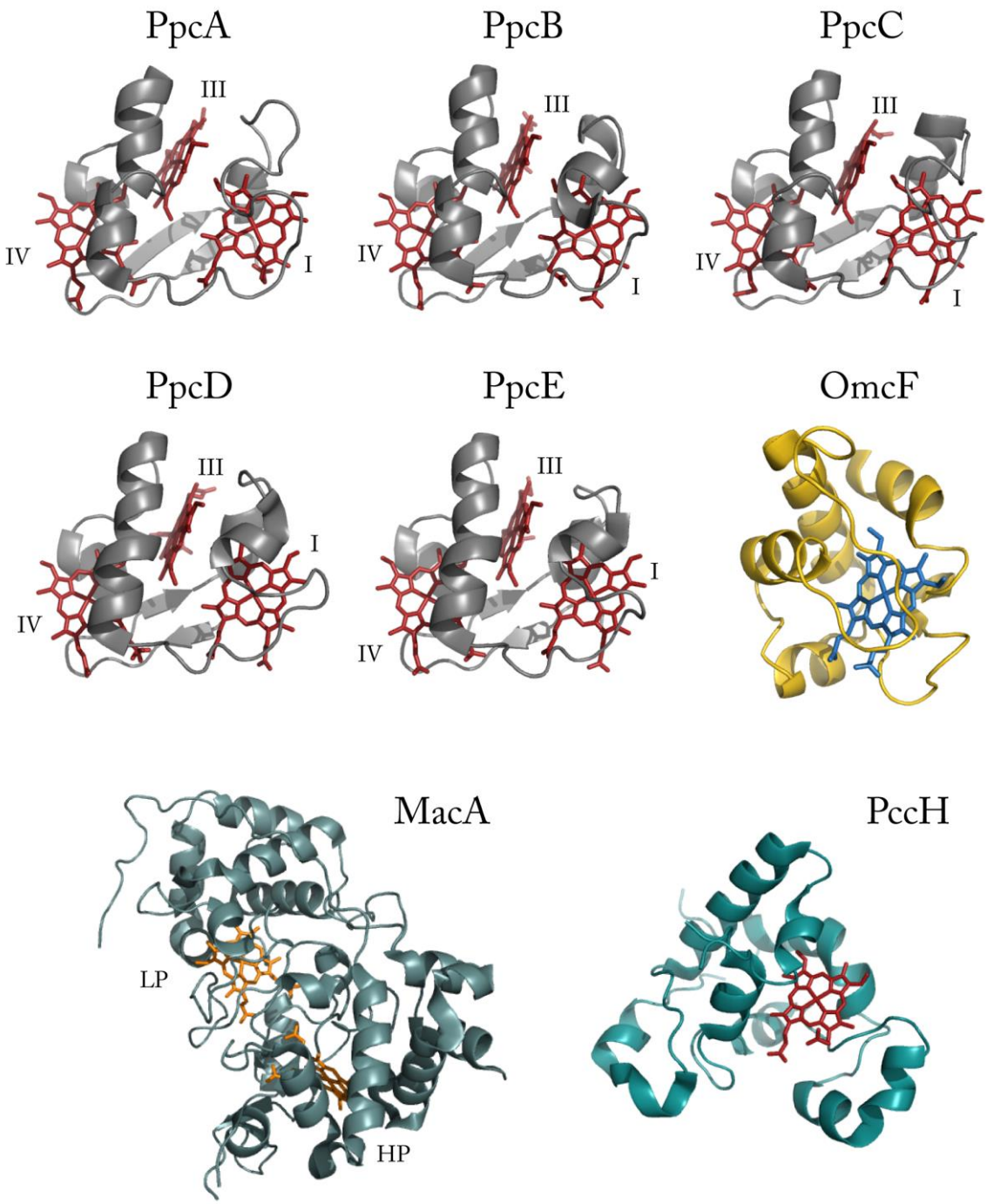

Figure 1.9 – Structures of several cytochromes from G. sulfurreducens, obtained in the oxidized state – The solution structure of PpcA (lowest energy, PDB ID: 2MZ9 [142]) and the crystal structures of PpcB (chain A, PDB ID: 3BXU [146]), PpcC (PDB ID: 3H33 [147]), PpcD (chain A, PDB ID: 3H4N [147]) and PpcE (PDB ID: 3H34 [147]) are represented in gray. The crystal structures of OmcF (PDB ID: 3CU4 [149]), MacA (PDB ID: 4AAL [37]) and PccH (PDB ID: 4RLR [150]) are represented in yellow, blue-gray and cyan, respectively. Roman numerals indicate the hemes (red for the PpcA-E cytochromes and for PccH; blue for OmcF) in their order of attachment to the CXXCH motif in the polypeptide chain. The high (HP) and low potential (LP) hemes (in gold) of MacA are also labelled. The structures were drawn using the PyMOL molecular graphics system [113].

In monoheme cytochromes only the reduced and oxidized states may coexist in solution, whereas for multiheme cytochromes, several one-electron reversible transfer steps convert the fully reduced state (stage 0, S_0) into the fully oxidized state (stage X, S_x). In addition, in each stage, the group responsible for the redox-Bohr effect may be protonated or deprotonated, which further increases the number of microstates in solution. For example, in a triheme cytochrome there are 16 different microstates in solution (Figure 1.10).

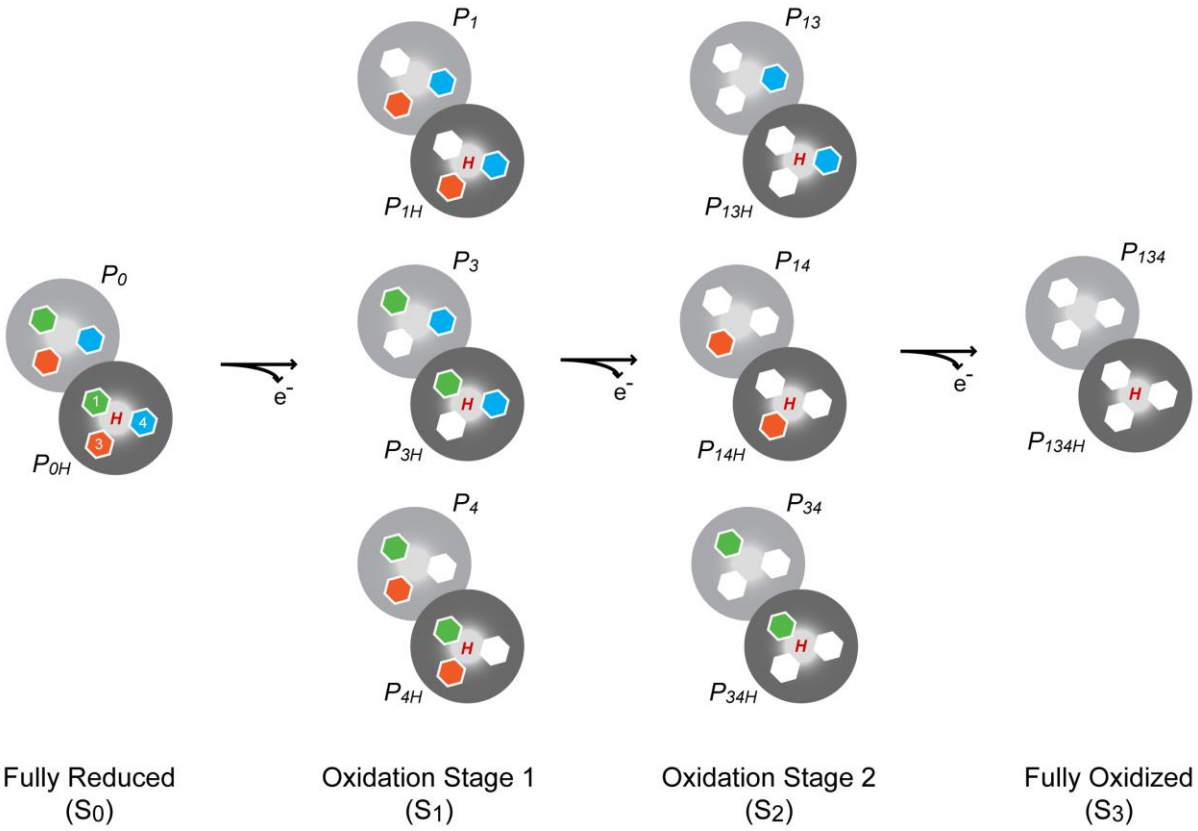

Figure 1.10 – Electronic distribution scheme for a triheme cytochrome with a proton-linked equilibrium, showing the 16 possible microstates – The light gray and dark gray circles correspond to the protonated and deprotonated microstates, respectively. The protonated microstates are also identified with a red "H", which mimics the protonable redox-Bohr center. Inner hexagons represent heme groups. The reduced hemes I, III, and IV are colored green, orange and blue, respectively. The oxidized hemes are colored white. The microstates are grouped, according to the number of oxidized hemes, in four oxidation stages connected by three one-electron redox steps. P_{0H} and P_0 represent the reduced protonated and deprotonated microstates, respectively. P_{ijkH} and P_{ijk} indicate, respectively, the protonated and deprotonated microstates, where i, j and k represent the heme(s) that are oxidized in that particular microstate.

Therefore, on one hand, in a monoheme cytochrome the heme reduction potential value can be directly obtained of the Nernst equation, at the point at which the oxidized and reduced fractions are equal (E_{app}). On the other hand, in multiheme cytochromes, redox

titrations describe the whole-protein macroscopic redox behavior (macroscopic redox potentials), without deconvoluting the reduction potentials of the individual redox centers (microscopic redox potentials) [50, 149, 152, 153]. For multiheme cytochromes, the detailed thermodynamic characterization involves the determination of several parameters, namely the redox potentials, redox interactions, redox-Bohr interactions and pK_a value(s) of the redox-Bohr center(s). To calculate these thermodynamic parameters, it is necessary to monitor the stepwise oxidation of each heme oxidation at several pH values. This information can be achieved by NMR spectroscopy, which allows the determination of the individual heme oxidation profiles, due to the different spectral signatures of the NMR spectra of low-spin multihemes, in the reduced and oxidized states. This topic is explained in more detail in Chapter 2, where a full thermodynamic characterization of the triheme cytochrome PpcA from Geobacter metallireducens is presented.

In the last few years, several thermodynamic parameters of G. sulfurreducens and G. metallireducens cytochromes have been published, namely the (i) heme redox potentials, redox interactions, redox-Bohr interactions (Table 1.1) and the macroscopic pK_a values of the redox-Bohr center of several periplasmic cytochromes (Table 1.2), as well as the (ii) E_{app} values of several periplasmic, inner- and outer-membrane cytochromes (Table 1.3).

Table 1.1 – Heme reduction potentials and pairwise interactions (mV) of the fully reduced and protonated forms of several priplasmic cytochromes from G. sulfurreducens [129, 154] – The values were determined at 288 K . DC stands for Domain C of the GSU1996 cytochrome.

	Heme redox potentials			Redox interactions			Redox-Bohr interactions		
	I	III	IV	I-III	I-IV	III-IV	I-H	III-H	IV-H
PpcA	-154	-138	-125	27	16	41	-32	-31	-58
PpcB	-150	-166	-125	17	8	32	-16	-9	-38
PpcD	-156	-139	-149	46	3	14	-28	-23	-53
PpcE	-167	-175	-116	27	5	22	-12	2	-13
DC	-106	-136	-125	44	7	40	-4	-25	-13

Table 1.2 – Macroscopic pK_a values of the redox-Bohr center of several periplasmic cytochromes from G. sulfurreducens at each stage of oxidation [129, 154] – The values were determined at 288 K. DC stands for Domain C of the GSU1996 cytochrome.

	pK_a				
Oxidation stage	PpcA	PpcB	PpcD	PpcE	DC
0	8.6	7.4	8.7	7.7	6.0
1	8.0	7.1	8.1	7.6	5.6
2	7.2	6.8	7.4	7.5	5.4
3	6.5	6.3	6.9	7.4	5.2
ΔpK_a	2.1	1.1	1.8	0.3	0.8

Table 1.3 – Data set of G. sulfurreducens (Gs) and G. metallireducens (Gmet) c-type cytochromes participating in EET pathways – The redox potential values were determined at pH 7.

Protein	Heme axial ligands	E_{app} (mV) vs NHE
MacA Gs	His-Met	-188 [37]
GSU1996	His-His; His-Met	-124 [11]
PpcA Gs	His-His	-117 [146]
PpcB Gs	His-His	-137 [146]
PpcC Gs	His-His	-143 [11]
PpcD Gs	His-His	-132 [129]
PpcE Gs	His-His	-134 [129]
PpcA Gmet	His-His	-78 [155]
PpcF Gmet	His-His	-56 [156]
OmcF Gs	His-Met	+180 [149]
OmcS Gs	His-His	-212 [152]
OmcZ Gs	Not determined	-220 [50]

1.9 – Objectives and thesis outline

The structural and functional characterization of individual electron transfer components is crucial to understand the EET mechanisms of Geobacter. This knowledge can be further used to design optimized Geobacter mutant strains, with increased bacterial respiratory rates.

The goal of this Thesis was to study different electron transfer components from Geobacter bacteria, namely the periplasmic cytochrome PpcA from G. metallireducens, the periplasmic cytochrome GSU0105 from G. sulfurreducens and the OM cytochromes OmaV and OmaW from G. sulfurreducens. The Thesis is divided in five Chapters. A general introduction to Geobacter and cytochromes is presented in Chapter 1. In Chapter 2, the functional and thermodynamic characterization of the properties of the triheme cytochrome PpcA from G. metallireducens and their comparison with those of PpcA from G. sulfurreducens are presented. Chapter 3 describes the optimization of the expression and purification protocols of the periplasmic cytochrome GSU0105 from G. sulfurreducens, as well as preliminary insights on the biochemical and functional properties of the cytochrome. Chapter 4 focuses on initial work made in the expression and purification protocols of OmaW and OmaV cytochromes from G. sulfurreducens. Finally, future perspectives are presented in Chapter 5.

1.10 – References

[1] U. Nations, Transforming our world: The 2030 agenda for sustainable development A/RES/70/1, New York, 2015.

[2] M.C. Potter, Electrical effects accompanying the decomposition of organic compounds, P. Roy. Soc. B - Biol. Sci., 84 (1911) 260-276.

[3] R.T. Anderson, D.R. Lovley, Naphthalene and benzene degradation under Fe(III)-reducing conditions in petroleum-contaminated aquifers, Bioremediat. J., 3 (1999) 121-135.

[4] R.T. Anderson, J.N. Rooney-Varga, C.V. Gaw, D.R. Lovley, Anaerobic benzene oxidation in the Fe(III) reduction zone of petroleum-contaminated aquifers, Envir. Sci. Tech., 32 (1998) 1222-1229.

[5] J.D. Coates, J. Woodward, J. Allen, P. Philp, D.R. Lovley, Anaerobic degradation of polycyclic aromatic hydrocarbons and alkanes in petroleum-contaminated marine harbor sediments, Appl. Environ. Microbiol., 63 (1997) 3589-3593.

[6] J.N. Rooney-Varga, R.T. Anderson, J.L. Fraga, D. Ringelberg, D.R. Lovley, Microbial communities associated with anaerobic benzene degradation in a petroleum-contaminated aquifer, Appl. Environ. Microbiol., 65 (1999) 3056-3063.

[7] J.M. Weiner, D.R. Lovley, Anaerobic benzene degradation in petroleum-contaminated aquifer sediments after inoculation with a benzene-oxidizing enrichment, Appl. Environ. Microbiol., 64 (1998) 775-778.

[8] R.T. Anderson, H.A. Vrionis, I. Ortiz-Bernad, C.T. Resch, P.E. Long, R. Dayvault, K. Karp, S. Marutzky, D.R. Metzler, A. Peacock, D.C. White, M. Lowe, D.R. Lovley, Stimulating the in situ activity of Geobacter species to remove uranium from the groundwater of a uranium-contaminated aquifer, Appl. Environ. Microbiol., 69 (2003) 5884-5891.

[9] E. Rosenberg, The prokaryotes: Deltaproteobacteria and epsilonproteobacteria, Fourth edition, 2014.

[10] D.R. Lovley, T. Ueki, T. Zhang, N.S. Malvankar, P.M. Shrestha, K.A. Flanagan, M. Aklujkar, J.E. Butler, L. Giloteaux, A.E. Rotaru, D.E. Holmes, A.E. Franks, R. Orellana, C. Risso, K.P. Nevin, Geobacter: The microbe electric's physiology, ecology, and practical applications, Adv. Microb. Physiol., 59 (2011) 1-100.

[11] T.C. Santos, M.A. Silva, L. Morgado, J.M. Dantas, C.A. Salgueiro, Diving into the redox properties of Geobacter sulfurreducens cytochromes: A model for extracellular electron transfer, Dalton T., 44 (2015) 9335-9344.

[12] D.R. Lovley, Dissimilatory metal reduction, Annu. Rev. Microbiol., 47 (1993) 263-290.

[13] J.R. Lloyd, D.R. Lovley, Microbial detoxification of metals and radionuclides, Curr. Opin. Biotechnol., 12 (2001) 248-253.

[14] W.C. Lin, M.V. Coppi, D.R. Lovley, Geobacter sulfurreducens can grow with oxygen as a terminal electron acceptor, Appl. Environ. Microbiol., 70 (2004) 2525-2528.

[15] B.A. Methé, K.E. Nelson, J.A. Eisen, I.T. Paulsen, W. Nelson, J.F. Heidelberg, D. Wu, M. Wu, N. Ward, M.J. Beanan, R.J. Dodson, R. Madupu, L.M. Brinkac, S.C. Daugherty, R.T. DeBoy, A.S. Durkin, M. Gwinn, J.F. Kolonay, S.A. Sullivan, D.H. Haft, J. Selengut, T.M. Davidsen, N. Zafar, O. White, B. Tran, C. Romero, H.A. Forberger, J. Weidman, H. Khouri, T.V. Feldblyum, T.R. Utterback, S.E. Van Aken, D.R. Lovley, C.M. Fraser, Genome of Geobacter sulfurreducens: Metal reduction in subsurface environments, Science, 302 (2003) 1967-1969.

[16] M. Aklujkar, N.D. Young, D. Holmes, M. Chavan, C. Risso, H.E. Kiss, C.S. Han, M.L. Land, D.R. Lovley, The genome of Geobacter bemidjiensis, exemplar for the subsurface clade of Geobacter species that predominate in Fe(III)-reducing subsurface environments, BMC Genomics, 11 (2010) 490.

[17] M.V. Coppi, C. Leang, S.J. Sandler, D.R. Lovley, Development of a genetic system for Geobacter sulfurreducens, Appl. Environ. Microbiol., 67 (2001) 3180-3187.

[18] B.C. Kim, C. Leang, Y.H. Ding, R.H. Glaven, M.V. Coppi, D.R. Lovley, OmcF, a putative c-type monoheme outer membrane cytochrome required for the expression of other outer membrane cytochromes in Geobacter sulfurreducens, J. Bacteriol., 187 (2005) 4505-4513.

[19] J.R. Lloyd, C. Leang, A.L. Hodges Myerson, M.V. Coppi, S. Cuifo, B. Methe, S.J. Sandler, D.R. Lovley, Biochemical and genetic characterization of PpcA, a periplasmic c-type cytochrome in Geobacter sulfurreducens, Biochem. J., 369 (2003) 153-161.

[20] I. Park, B.C. Kim, Homologous overexpression of omcZ, a gene for an outer surface c-type cytochrome of Geobacter sulfurreducens by single-step gene replacement, Biotechnol. Lett., 33 (2011) 2043-2048.

[21] J.B. Rollefson, C.E. Levar, D.R. Bond, Identification of genes involved in biofilm formation and respiration via mini-Himar transposon mutagenesis of Geobacter sulfurreducens, J. Bacteriol., 191 (2009) 4207-4217.

[22] T. Ueki, D.R. Lovley, Genome-wide gene regulation of biosynthesis and energy generation by a novel transcriptional repressor in Geobacter species, Nucleic Acids Res., 38 (2010) 810-821.

[23] F. Caccavo, Jr., D.J. Lonergan, D.R. Lovley, M. Davis, J.F. Stolz, M.J. McInerney, Geobacter sulfurreducens sp. nov., a hydrogen- and acetate-oxidizing dissimilatory metal-reducing microorganism, Appl. Environ. Microbiol., 60 (1994) 3752-3759.

[24] K.A. Jolley, D.G. Maddocks, S.L. Gyles, Z. Mullan, S.L. Tang, M.L. Dyall-Smith, D.W. Hough, M.J. Danson, 2-oxoacid dehydrogenase multienzyme complexes in the halophilic Archaea? Gene sequences and protein structural predictions, Microbiology, 146 (Pt 5) (2000) 1061-1069.

[25] M. Aklujkar, M.V. Coppi, C. Leang, B.C. Kim, M.A. Chavan, L.A. Perpetua, L. Giloteaux, A. Liu, D.E. Holmes, Proteins involved in electron transfer to Fe(III) and Mn(IV) oxides by Geobacter sulfurreducens and Geobacter uraniireducens, Microbiology, 159 (2013) 515-535.

[26] Y.H. Ding, K.K. Hixson, M.A. Aklujkar, M.S. Lipton, R.D. Smith, D.R. Lovley, T. Mester, Proteome of Geobacter sulfurreducens grown with Fe(III) oxide or Fe(III) citrate as the electron acceptor, Biochim. Biophys. Acta, 1784 (2008) 1935-1941.

[27] Y.H. Ding, K.K. Hixson, C.S. Giometti, A. Stanley, A. Esteve-Núñez, T. Khare, S.L. Tollaksen, W. Zhu, J.N. Adkins, M.S. Lipton, R.D. Smith, T. Mester, D.R. Lovley, The proteome of dissimilatory metal-reducing microorganism Geobacter sulfurreducens under various growth conditions, Biochim. Biophys. Acta, 1764 (2006) 1198-1206.

[28] D.E. Holmes, S.K. Chaudhuri, K.P. Nevin, T. Mehta, B.A. Methe, A. Liu, J.E. Ward, T.L. Woodard, J. Webster, D.R. Lovley, Microarray and genetic analysis of electron transfer to electrodes in Geobacter sulfurreducens, Environ. Microbiol., 8 (2006) 1805-1815.

[29] B.C. Kim, B.L. Postier, R.J. DiDonato, S.K. Chaudhuri, K.P. Nevin, D.R. Lovley, Insights into genes involved in electricity generation in Geobacter sulfurreducens via whole genome microarray analysis of the OmcF-deficient mutant, Bioelectrochemistry, 73 (2008) 70-75.

[30] T. Mehta, M.V. Coppi, S.E. Childers, D.R. Lovley, Outer membrane c-type cytochromes required for Fe(III) and Mn(IV) oxide reduction in Geobacter sulfurreducens, Appl. Environ. Microbiol., 71 (2005) 8634-8641.

[31] K.P. Nevin, B.C. Kim, R.H. Glaven, J.P. Johnson, T.L. Woodard, B.A. Methe, R.J. Didonato, S.F. Covalla, A.E. Franks, A. Liu, D.R. Lovley, Anode biofilm transcriptomics reveals outer surface components essential for high density current production in Geobacter sulfurreducens fuel cells, PLoS One, 4 (2009) e5628.

[32] R. Orellana, K.K. Hixson, S. Murphy, T. Mester, M.L. Sharma, M.S. Lipton, D.R. Lovley, Proteome of Geobacter sulfurreducens in the presence of U(VI), Microbiology, 160 (2014) 2607-2617.

[33] E.S. Shelobolina, M.V. Coppi, A.A. Korenevsky, L.N. DiDonato, S.A. Sullivan, H. Konishi, H. Xu, C. Leang, J.E. Butler, B.C. Kim, D.R. Lovley, Importance of c-type cytochromes for U(VI) reduction by Geobacter sulfurreducens, BMC Microbiol., 7 (2007) 16.

[34] P.L. Tremblay, Z.M. Summers, R.H. Glaven, K.P. Nevin, K. Zengler, C.L. Barrett, Y. Qiu, B.O. Palsson, D.R. Lovley, A c-type cytochrome and a transcriptional regulator responsible for enhanced extracellular electron transfer in Geobacter sulfurreducens revealed by adaptive evolution, Environ. Microbiol., 13 (2011) 13-23.

[35] J.E. Butler, F. Kaufmann, M.V. Coppi, C. Nunez, D.R. Lovley, MacA, a diheme c-type cytochrome involved in Fe(III) reduction by Geobacter sulfurreducens, J. Bacteriol., 186 (2004) 4042-4045.

[36] D.R. Lovley, Bug juice: Harvesting electricity with microorganisms, Nat. Rev. Microbiol., 4 (2006) 497-508.

[37] J. Seidel, M. Hoffmann, K.E. Ellis, A. Seidel, T. Spatzal, S. Gerhardt, S.J. Elliott, O. Einsle, MacA is a second cytochrome c peroxidase of Geobacter sulfurreducens, Biochemistry, 51 (2012) 2747-2756.

[38] L. Zacharoff, C.H. Chan, D.R. Bond, Reduction of low potential electron acceptors requires the CbcL inner membrane cytochrome of Geobacter sulfurreducens, Bioelectrochemistry, 107 (2016) 7-13.

[39] C.E. Levar, C.H. Chan, M.G. Mehta-Kolte, D.R. Bond, An inner membrane cytochrome required only for reduction of high redox potential extracellular electron acceptors, MBio, 5 (2014) e02034.

[40] A.P. Fernandes, T.C. Nunes, C.M. Paquete, C.A. Salgueiro, Interaction studies between periplasmic cytochromes provide insights into extracellular electron transfer pathways of Geobacter sulfurreducens, Biochem. J., 474 (2017) 797-808.

[41] P.R. Pokkuluri, Y.Y. Londer, N.E. Duke, M. Pessanha, X. Yang, V. Orshonsky, L. Orshonsky, J. Erickson, Y. Zagyansky, C.A. Salgueiro, M. Schiffer, Structure of a novel dodecaheme cytochrome c from Geobacter sulfurreducens reveals an extended 12 nm protein with interacting hemes, J. Struct. Biol., 174 (2011) 223-233.

[42] S.M. Strycharz, R.H. Glaven, M.V. Coppi, S.M. Gannon, L.A. Perpetua, A. Liu, K.P. Nevin, D.R. Lovley, Gene expression and deletion analysis of mechanisms for electron transfer from electrodes to Geobacter sulfurreducens, Bioelectrochemistry, 80 (2011) 142-150.

[43] C. Giometti, Tale of two metal reducers: Comparative proteome analysis of Geobacter sulfurreducens PCA and Shewanella oneidensis MR-1, Methods Biochem. Anal., 49 (2006) 97-111.

[44] Y. Liu, Z. Wang, J. Liu, C. Levar, M.J. Edwards, J.T. Babauta, D.W. Kennedy, Z. Shi, H. Beyenal, D.R. Bond, T.A. Clarke, J.N. Butt, D.J. Richardson, K.M. Rosso, J.M. Zachara, J.K. Fredrickson, L. Shi, A trans-outer membrane porin-cytochrome protein complex for extracellular electron transfer by Geobacter sulfurreducens PCA, Environ. Microbiol. Rep., 6 (2014) 776-785.

[45] M. Aklujkar, M.V. Coppi, C. Leang, B.C. Kim, M.A. Chavan, L.A. Perpetua, L. Giloteaux, A. Liu, D.E. Holmes, Proteins involved in electron transfer to Fe(III) and Mn(IV) oxides by Geobacter sulfurreducens and Geobacter uraniireducens, Microbiol., 159 (2013) 515-535.

[46] L. Shi, J.K. Fredrickson, J.M. Zachara, Genomic analyses of bacterial porin-cytochrome gene clusters, Front. Microbiol., 5 (2014) 657.

[47] F. Jiménez Otero, C.H. Chan, D.R. Bond, Identification of different putative outer membrane electron conduits necessary for Fe(III) citrate, Fe(III) oxide, Mn(IV) oxide, or electrode reduction by Geobacter sulfurreducens, J. Bacteriol., 200 (2018) e00347-00318.

[48] K. Inoue, C. Leang, A.E. Franks, T.L. Woodard, K.P. Nevin, D.R. Lovley, Specific localization of the c-type cytochrome OmcZ at the anode surface in current-producing biofilms of Geobacter sulfurreducens, Environ. Microbiol. Rep., 3 (2011) 211-217.

[49] C. Leang, X. Qian, T. Mester, D.R. Lovley, Alignment of the c-type Cytochrome OmcS along pili of Geobacter sulfurreducens, Appl. Environ. Microbiol., 76 (2010) 4080-4084.

[50] K. Inoue, X. Qian, L. Morgado, B.C. Kim, T. Mester, M. Izallalen, C.A. Salgueiro, D.R. Lovley, Purification and characterization of OmcZ, an outer-surface, octaheme c-type cytochrome essential for optimal current production by Geobacter sulfurreducens, Appl. Environ. Microbiol., 76 (2010) 3999-4007.

[51] G. Reguera, K.D. McCarthy, T. Mehta, J.S. Nicoll, M.T. Tuominen, D.R. Lovley, Extracellular electron transfer via microbial nanowires, Nature, 435 (2005) 1098-1101.

[52] P.M. Shrestha, A.E. Rotaru, M. Aklujkar, F. Liu, M. Shrestha, Z.M. Summers, N. Malvankar, D.C. Flores, D.R. Lovley, Syntrophic growth with direct interspecies electron transfer as the primary mechanism for energy exchange, Environ. Microbiol. Rep., 5 (2013) 904-910.

[53] Z.M. Summers, H.E. Fogarty, C. Leang, A.E. Franks, N.S. Malvankar, D.R. Lovley, Direct exchange of electrons within aggregates of an evolved syntrophic coculture of anaerobic bacteria, Science, 330 (2010) 1413-1415.

[54] A.E. Rotaru, P.M. Shrestha, F.H. Liu, M. Shrestha, D. Shrestha, M. Embree, K. Zengler, C. Wardman, K.P. Nevin, D.R. Lovley, A new model for electron flow during anaerobic digestion: Direct interspecies electron transfer to Methanosaeta for the reduction of carbon dioxide to methane, Energ. Environ. Sci., 7 (2014) 408-415.

[55] N.S. Malvankar, M. Vargas, K.P. Nevin, A.E. Franks, C. Leang, B.C. Kim, K. Inoue, T. Mester, S.F. Covalla, J.P. Johnson, V.M. Rotello, M.T. Tuominen, D.R. Lovley, Tunable metallic-like conductivity in microbial nanowire networks, Nat. Nanotechnol., 6 (2011) 573-579.

[56] G. Reguera, K.P. Nevin, J.S. Nicoll, S.F. Covalla, T.L. Woodard, D.R. Lovley, Biofilm and nanowire production leads to increased current in Geobacter sulfurreducens fuel cells, Appl. Environ. Microbiol., 72 (2006) 7345-7348.

[57] D.E. Holmes, Y. Dang, D.J. Walker, D.R. Lovley, The electrically conductive pili of Geobacter species are a recently evolved feature for extracellular electron transfer, Microb. Genom., 2 (2016) e000072.

[58] M. Vargas, N.S. Malvankar, P.L. Tremblay, C. Leang, J.A. Smith, P. Patel, O. Snoeyenbos-West, K.P. Nevin, D.R. Lovley, Aromatic amino acids required for pili conductivity and long-range extracellular electron transport in Geobacter sulfurreducens, MBio, 4 (2013) e00105-00113.

[59] X. Liu, P.L. Tremblay, N.S. Malvankar, K.P. Nevin, D.R. Lovley, M. Vargas, A Geobacter sulfurreducens strain expressing Pseudomonas aeruginosa type IV pili localizes OmcS on pili but is deficient in Fe(III) oxide reduction and current production, Appl. Environ. Microbiol., 80 (2014) 1219-1224.

[60] M.N.S. Adhikari R. Y., Tuominen M. T., Lovley D. R., Conductivity of individual Geobacter pili, RSC Advances, 6 (2016) 8354-8357.
[61] N.S. Malvankar, S.E. Yalcin, M.T. Tuominen, D.R. Lovley, Visualization of charge propagation along individual pili proteins using ambient electrostatic force microscopy, Nat. Nanotechnol., 9 (2014) 1012-1017.
[62] C.A. Salgueiro, J.M. Dantas, Multiheme cytochromes, Protein folding and structure, Springer-Verlag Berlin Heidelberg, 2017.
[63] Y. Liu, J.K. Fredrickson, J.M. Zachara, L. Shi, Direct involvement of ombB, omaB, and omcB genes in extracellular reduction of Fe(III) by Geobacter sulfurreducens PCA, Front. Microbiol., 6 (2015) 1075.
[64] B.C. Kim, D.R. Lovley, Investigation of direct vs indirect involvement of the c-type cytochrome MacA in Fe(III) reduction by Geobacter sulfurreducens, FEMS Microbiol. Lett., 286 (2008) 39-44.
[65] D.R. Lovley, E.J. Phillips, Novel mode of microbial energy metabolism: Organic carbon oxidation coupled to dissimilatory reduction of iron or manganese, Appl. Environ. Microbiol., 54 (1988) 1472-1480.
[66] D.R. Lovley, J.F. Stolz, G.L. Nord Jr, E.J.P. Phillips, Anaerobic production of magnetite by a dissimilatory iron-reducing microorganism, Nature, 330 (1987) 252-254.
[67] D.R. Lovley, M.J. Baedecker, D.J. Lonergan, I.M. Cozzarelli, E.J.P. Phillips, D.I. Siegel, Oxidation of aromatic contaminants coupled to microbial iron reduction, Nature, 339 (1989) 297-300.
[68] D.R. Lovley, S.J. Giovannoni, D.C. White, J.E. Champine, E.J. Phillips, Y.A. Gorby, S. Goodwin, Geobacter metallireducens gen. nov. sp. nov., a microorganism capable of coupling the complete oxidation of organic compounds to the reduction of iron and other metals, Arch. Microbiol., 159 (1993) 336-344.
[69] S.E. Childers, S. Ciufo, D.R. Lovley, Geobacter metallireducens accesses insoluble Fe(III) oxide by chemotaxis, Nature, 416 (2002) 767-769.
[70] N.B. Tobler, T.B. Hofstetter, R.P. Schwarzenbach, Carbon and hydrogen isotope fractionation during anaerobic toluene oxidation by Geobacter metallireducens with different Fe(III) phases as terminal electron acceptors, Environ. Sci. Technol., 42 (2008) 7786-7792.
[71] J.E. Butler, Q. He, K.P. Nevin, Z. He, J. Zhou, D.R. Lovley, Genomic and microarray analysis of aromatics degradation in Geobacter metallireducens and comparison to a Geobacter isolate from a contaminated field site, BMC Genomics, 8 (2007) 180.
[72] S.R. Kane, H.R. Beller, T.C. Legler, R.T. Anderson, Biochemical and genetic evidence of benzylsuccinate synthase in toluene-degrading, ferric iron-reducing Geobacter metallireducens, Biodegradation, 13 (2002) 149-154.
[73] F. Peters, D. Heintz, J. Johannes, A. van Dorsselaer, M. Boll, Genes, enzymes, and regulation of para-cresol metabolism in Geobacter metallireducens, J. Bacteriol., 189 (2007) 4729-4738.

[74] S. Wischgoll, D. Heintz, F. Peters, A. Erxleben, E. Sarnighausen, R. Reski, A. Van Dorsselaer, M. Boll, Gene clusters involved in anaerobic benzoate degradation of Geobacter metallireducens, Mol. Microbiol., 58 (2005) 1238-1252.
[75] J.M. Senko, J.F. Stolz, Evidence for iron-dependent nitrate respiration in the dissimilatory iron-reducing bacterium Geobacter metallireducens, Appl. Environ. Microbiol., 67 (2001) 3750-3752.
[76] M.K. Jahn, S.B. Haderlein, R.U. Meckenstock, Reduction of Prussian Blue by the two iron-reducing microorganisms Geobacter metallireducens and Shewanella alga, Environ. Microbiol., 8 (2006) 362-367.
[77] H.A. Wiatrowski, P.M. Ward, T. Barkay, Novel reduction of mercury (II) by mercury-sensitive dissimilatory metal reducing bacteria, Environ. Sci. Technol., 40 (2006) 6690-6696.
[78] M. Aklujkar, J. Krushkal, G. DiBartolo, A. Lapidus, M.L. Land, D.R. Lovley, The genome sequence of Geobacter metallireducens: features of metabolism, physiology and regulation common and dissimilar to Geobacter sulfurreducens, BMC Microbiol., 9 (2009) 109.
[79] P.L. Tremblay, M. Aklujkar, C. Leang, K.P. Nevin, D. Lovley, A genetic system for Geobacter metallireducens: Role of the flagellin and pilin in the reduction of Fe(III) oxide, Environ. Microbiol. Rep., 4 (2012) 82-88.
[80] C. Leang, M.V. Coppi, D.R. Lovley, OmcB, a c-type polyheme cytochrome, involved in Fe(III) reduction in Geobacter sulfurreducens, J. Bacteriol., 185 (2003) 2096-2103.
[81] J.W. Voordeckers, B.C. Kim, M. Izallalen, D.R. Lovley, Role of Geobacter sulfurreducens outer surface c-type cytochromes in reduction of soil humic acid and anthraquinone-2,6-disulfonate, Appl. Environ. Microbiol., 76 (2010) 2371-2375.
[82] E. Afkar, Y. Fukumori, Purification and characterization of triheme cytochrome c_7 from the metal-reducing bacterium, Geobacter metallireducens, FEMS Microbiol. Lett., 175 (1999) 205-210.
[83] J.A. Smith, D.R. Lovley, P.L. Tremblay, Outer cell surface components essential for Fe(III) oxide reduction by Geobacter metallireducens, Appl. Environ. Microbiol., 79 (2013) 901-907.
[84] J.E. Butler, N.D. Young, D.R. Lovley, Evolution from a respiratory ancestor to fill syntrophic and fermentative niches: Comparative fenomics of six Geobacteraceae species, BMC Genomics, 10 (2009) 103.
[85] D.R. Bond, D.R. Lovley, Electricity production by Geobacter sulfurreducens attached to electrodes, Appl. Environ. Microbiol., 69 (2003) 1548-1555.
[86] C.D. Dubé, S.R. Guiot, Direct interspecies electron transfer in anaerobic digestion: A review, Adv. Biochem. Eng. Biotechnol., 151 (2015) 101-115.
[87] A.E. Rotaru, P.M. Shrestha, F. Liu, B. Markovaite, S. Chen, K.P. Nevin, D.R. Lovley, Direct interspecies electron transfer between Geobacter metallireducens and Methanosarcina barkeri, Appl. Environ. Microbiol., 80 (2014) 4599-4605.

[88] G. Liu, J. Zhou, C. Chen, J. Wang, R. Jin, H. Lv, Decolorization of azo dyes by Geobacter metallireducens, Appl. Microbiol. Biotechnol., 97 (2013) 7935-7942.
[89] I. Ortiz-Bernad, R.T. Anderson, H.A. Vrionis, D.R. Lovley, Vanadium respiration by Geobacter metallireducens: Novel strategy for in situ removal of vanadium from groundwater, Appl. Environ. Microbiol., 70 (2004) 3091-3095.
[90] G.R. Moore, Hemeproteins, Bios Scientific Publishers, Oxford, 1996.
[91] G.B. Jameson, J.A. Ibers, Biological and synthetic dioxygen carriers, University Science Books, Mill Valley, CA, 1994.
[92] F. Malatesta, G. Antonini, P. Sarti, M. Brunori, Structure and function of a molecular machine: Cytochrome c oxidase, Biophys. Chem., 54 (1995) 1-33.
[93] O.d. Montellano, Cytochrome P450 - Structure, mechanism and biochemistry, Third edition, Springer US, New York, 2005.
[94] J.P. Frew J. E., Structure and functional properties of peroxidases and catalases, Academic Press, London, 1984.
[95] C.G. Mowat, S.K. Chapman, Flavocytochrome b_2, Enzyme-catalyzed electron and radical transfer: Subcellular biochemistry, Springer US, Boston, MA, 2000, 279-295.
[96] S. Ida, Nitrate reductase and nitrite reductase, Elsevier, Amsterdam, 1988.
[97] G.W. Pettigrew, G.R. Moore, Cytochromes c: Biological aspects, London, 1987.
[98] S.E. Bowman, K.L. Bren, The chemistry and biochemistry of heme c: Functional bases for covalent attachment, Nat. Prod. Rep., 25 (2008) 1118-1130.
[99] D. Keilin, On cytochrome, a respiratory pigment, common to animals, yeast, and higher plants, P. R. Soc. Lond. B Conta., 98 (1925) 312.
[100] I. Bertini, G. Cavallaro, A. Rosato, Cytochrome c: Occurrence and functions, Chem. Rev., 106 (2006) 90-115.
[101] G.R. Moore, G.W. Pettigrew, Cytochromes c: Evolutionary, structural and physicochemical aspects, Molecular Biology, Springer-Verlag Heidelberg, Berlin, 1990.
[102] J.H. van Vleck, Theory of the variations in paramagnetic anisotropy among different salts of the iron group, Phys. Rev., 41 (1932) 208-215.
[103] F.A. Walker, Magnetic spectroscopic (EPR, ESEEM, Mössbauer, MCD and NMR) studies of low-spin ferriheme centers and their corresponding heme proteins, Coordin. Chem. Rev., 185-186 (1999) 471-534.
[104] L.J. Smith, A. Kahraman, J.M. Thornton, Heme proteins-diversity in structural characteristics, function, and folding, Proteins, 78 (2010) 2349-2368.
[105] G.P. Moss, Nomenclature of tetrapyrroles. Recommendations 1986 IUPAC-IUB joint commission on biochemical nomenclature (JCBN), Eur. J. Biochem., 178 (1988) 277-328.
[106] L. Banci, I. Bertini, A. Rosato, G. Varani, Mitochondrial cytochromes c: A comparative analysis, J. Biol. Inorg. Chem., 4 (1999) 824-837.
[107] K.D. Bewley, K.E. Ellis, M.A. Firer-Sherwood, S.J. Elliott, Multi-heme proteins: Nature's electronic multi-purpose tool, Biochim. Biophys. Acta, 1827 (2013) 938-948.

[108] C.J. Reedy, B.R. Gibney, Heme protein assemblies, Chem. Rev., 104 (2004) 617-649.
[109] A. Brausemann, J. Seidel, A. Wust, O. Einsle, Chapter 6 - Multiheme peroxidases, Heme peroxidases, Roy. Soc. Chem., 2016, 113-132.
[110] E.H. Gordon, S.L. Pealing, S.K. Chapman, F.B. Ward, G.A. Reid, Physiological function and regulation of flavocytochrome c_3, the soluble fumarate reductase from Shewanella putrefaciens NCIMB 400, Microbiology, 144 (Pt 4) (1998) 937-945.
[111] P.R. Pokkuluri, M. Pessanha, Y.Y. Londer, S.J. Wood, N.E.C. Duke, R. Wilton, T. Catarino, C.A. Salgueiro, M. Schiffer, Structures and solution properties of two novel periplasmic sensor domains with c-type heme from chemotaxis proteins of Geobacter sulfurreducens: Implications for signal transduction, J. Mol. Biol., 377 (2008) 1498-1517.
[112] A. Esteve-Núñez, J. Sosnik, P. Visconti, D.R. Lovley, Fluorescent properties of c-type cytochromes reveal their potential role as an extracytoplasmic electron sink in Geobacter sulfurreducens, Environ. Microbiol., 10 (2008) 497-505.
[113] L.L.C. Schrödinger, The PyMOL molecular graphics system, Version 1.8, 2015.
[114] V. Fulop, J.W. Moir, S.J. Ferguson, J. Hajdu, The anatomy of a bifunctional enzyme: Structural basis for reduction of oxygen to water and synthesis of nitric oxide by cytochrome cd_1, Cell, 81 (1995) 369-377.
[115] F.A. Leitch, G.R. Moore, G.W. Pettigrew, Structural basis for the variation of pH-dependent redox potentials of Pseudomonas cytochromes c-551, Biochemistry, 23 (1984) 1831-1838.
[116] N.K. Rogers, G.R. Moore, On the energetics of conformational changes and pH dependent redox behaviour of electron transfer proteins, FEBS Lett., 228 (1988) 69-73.
[117] A.V. Xavier, Energy transduction coupling mechanisms in multiredox center proteins, J. Inorg. Biochem., 28 (1986) 239-243.
[118] M. Breuer, K.M. Rosso, J. Blumberger, J.N. Butt, Multi-haem cytochromes in Shewanella oneidensis MR-1: Structures, functions and opportunities, J. R. Soc. Interface, 12 (2015) 20141117.
[119] C.C. Page, C.C. Moser, X. Chen, P.L. Dutton, Natural engineering principles of electron tunnelling in biological oxidation-reduction, Nature, 402 (1999) 47-52.
[120] F.A. Armstrong, Evaluations of reduction potential data in relation to coupling, kinetics and function, J. Biol. Inorg. Chem., 2 (1997) 139-142.
[121] D.K. Das, O.K. Medhi, The role of heme propionate in controlling the redox potential of heme: Square wave voltammetry of protoporphyrinato IX iron (III) in aqueous surfactant micelles, J. Inorg. Biochem., 70 (1998) 83-90.
[122] A. de Lacroix de Lavalette, L. Barucq, J. Alric, F. Rappaport, F. Zito, Is the redox state of the c_i heme of the cytochrome b_6f complex dependent on the occupation and structure of the Q_i site and vice-versa?, J. Biol. Chem., 284 (2009) 20822-20829.

[123] M.R. Gunner, E. Alexov, E. Torres, S. Lipovaca, The importance of the protein in controlling the electrochemistry of heme metalloproteins: Methods of calculation and analysis, J. Biol. Inorg. Chem., 2 (1997) 126-134.

[124] Y. Liu, P. Moenne-Loccoz, D.P. Hildebrand, A. Wilks, T.M. Loehr, A.G. Mauk, P.R. Ortiz de Montellano, Replacement of the proximal histidine iron ligand by a cysteine or tyrosine converts heme oxygenase to an oxidase, Biochemistry, 38 (1999) 3733-3743.

[125] J.G. Ma, J. Zhang, R. Franco, S.L. Jia, I. Moura, J.J. Moura, P.M. Kroneck, J.A. Shelnutt, The structural origin of nonplanar heme distortions in tetraheme ferricytochromes c_3, Biochemistry, 37 (1998) 12431-12442.

[126] F.A. Tezcan, J.R. Winkler, H.B. Gray, Effects of ligation and folding on reduction potentials of heme proteins, J. Am. Chem. Soc., 120 (1998) 13383-13388.

[127] V.B. Paixão, H. Vis, D.L. Turner, Redox-linked conformational changes in cytochrome c_3 from Desulfovibrio desulfuricans ATCC 27774, Biochemistry, 49 (2010) 9620-9629.

[128] L. Morgado, A.P. Fernandes, Y.Y. Londer, M. Bruix, C.A. Salgueiro, One simple step in the identification of the cofactors signals, one giant leap for the solution structure determination of multiheme proteins, Biochem. Biophys. Res. Commun., 393 (2010) 466-470.

[129] L. Morgado, M. Bruix, M. Pessanha, Y.Y. Londer, C.A. Salgueiro, Thermodynamic characterization of a triheme cytochrome family from Geobacter sulfurreducens reveals mechanistic and functional diversity, Biophys. J., 99 (2010) 293-301.

[130] Y.Y. Londer, P.R. Pokkuluri, J. Erickson, V. Orshonsky, M. Schiffer, Heterologous expression of hexaheme fragments of a multidomain cytochrome from Geobacter sulfurreducens representing a novel class of cytochromes c, Protein Expr. Purif., 39 (2005) 254-260.

[131] Y.Y. Londer, P.R. Pokkuluri, V. Orshonsky, L. Orshonsky, M. Schiffer, Heterologous expression of dodecaheme "nanowire" cytochromes c from Geobacter sulfurreducens, Protein Expr. Purif., 47 (2006) 241-248.

[132] Y.Y. Londer, P.R. Pokkuluri, D.M. Tiede, M. Schiffer, Production and preliminary characterization of a recombinant triheme cytochrome c_7 from Geobacter sulfurreducens in Escherichia coli, Biochim. Biophys. Acta, 1554 (2002) 202-211.

[133] P.R. Pokkuluri, Y.Y. Londer, N.E. Duke, J. Erickson, M. Pessanha, C.A. Salgueiro, M. Schiffer, Structure of a novel c_7-type three-heme cytochrome domain from a multidomain cytochrome c polymer, Protein Sci., 13 (2004) 1684-1692.

[134] L. Shi, J.T. Lin, L.M. Markillie, T.C. Squier, B.S. Hooker, Overexpression of multi-heme c-type cytochromes, Biotechniques, 38 (2005) 297-299.

[135] J.M. Dantas, O. Kokhan, P.R. Pokkuluri, C.A. Salgueiro, Molecular interaction studies revealed the bifunctional behavior of triheme cytochrome PpcA from Geobacter sulfurreducens toward the redox active analog of humic substances, Biochim. Biophys. Acta., 1847 (2015) 1129-1138.

[136] J.M. Dantas, L. Morgado, T. Catarino, O. Kokhan, P. Raj Pokkuluri, C.A. Salgueiro, Evidence for interaction between the triheme cytochrome PpcA from Geobacter sulfurreducens and anthrahydroquinone-2,6-disulfonate, an analog of the redox active components of humic substances, Biochim. Biophys. Acta, 1837 (2014) 750-760.

[137] M.R. Ferreira, J.M. Dantas, C.A. Salgueiro, Molecular interactions between Geobacter sulfurreducens triheme cytochromes and the electron acceptor Fe(III) citrate studied by NMR, Dalton T., 46 (2017) 2350-2359.

[138] A.P. Fernandes, I. Couto, L. Morgado, Y.Y. Londer, C.A. Salgueiro, Isotopic labeling of c-type multiheme cytochromes overexpressed in E. coli, Prot. Expr. Purif., 59 (2008) 182-188.

[139] J.M. Dantas, C.A. Salgueiro, M. Bruix, Backbone, side chain and heme resonance assignments of the triheme cytochrome PpcD from Geobacter sulfurreducens, Biomol. NMR Assign., 9 (2015) 211-214.

[140] L. Morgado, V.B. Paixão, C.A. Salgueiro, M. Bruix, Backbone, side chain and heme resonance assignments of the triheme cytochrome PpcA from Geobacter sulfurreducens, Biomol. NMR Assign., 5 (2011) 113-116.

[141] J.M. Dantas, M. Sousa e Silva, C.A. Salgueiro, M. Bruix, Backbone, side chain and heme resonance assignments of cytochrome OmcF from Geobacter sulfurreducens, Biomol. NMR Assign., 9 (2015) 365-368.

[142] L. Morgado, M. Bruix, P.R. Pokkuluri, C.A. Salgueiro, D.L. Turner, Redox- and pH-linked conformational changes in triheme cytochrome PpcA from Geobacter sulfurreducens, Biochem. J., 474 (2017) 231-246.

[143] L. Morgado, V.B. Paixão, M. Schiffer, P.R. Pokkuluri, M. Bruix, C.A. Salgueiro, Revealing the structural origin of the redox-Bohr effect: The first solution structure of a cytochrome from Geobacter sulfurreducens, Biochem. J., 441 (2012) 179-187.

[144] J.M. Dantas, M.A. Silva, D. Pantoja-Uceda, D.L. Turner, M. Bruix, C.A. Salgueiro, Solution structure and dynamics of the outer membrane cytochrome OmcF from Geobacter sulfurreducens, Biochim. Biophys. Acta, 1858 (2017) 733-741.

[145] P.R. Pokkuluri, Y.Y. Londer, N.E.C. Duke, W.C. Long, M. Schiffer, Family of cytochrome c_7-type proteins from Geobacter sulfurreducens: Structure of one cytochrome c_7 at 1.45 Å resolution, Biochemistry, 43 (2004) 849-859.

[146] L. Morgado, M. Bruix, V. Orshonsky, Y.Y. Londer, N.E. Duke, X. Yang, P.R. Pokkuluri, M. Schiffer, C.A. Salgueiro, Structural insights into the modulation of the redox properties of two Geobacter sulfurreducens homologous triheme cytochromes, Biochim. Biophys. Acta, 1777 (2008) 1157-1165.

[147] P.R. Pokkuluri, Y.Y. Londer, X. Yang, N.E. Duke, J. Erickson, V. Orshonsky, G. Johnson, M. Schiffer, Structural characterization of a family of cytochromes c_7 involved in Fe(III) respiration by Geobacter sulfurreducens, Biochim. Biophys. Acta, 1797 (2010) 222-232.

[148] P. Lukat, M. Hoffmann, O. Einsle, Crystal packing of the c_6-type cytochrome OmcF from Geobacter sulfurreducens is mediated by an N-terminal Strep-tag II, Acta Crystallogr. D Biol. Crystallogr., 64 (2008) 919-926.

[149] P.R. Pokkuluri, Y.Y. Londer, S.J. Wood, N.E. Duke, L. Morgado, C.A. Salgueiro, M. Schiffer, Outer membrane cytochrome c, OmcF, from Geobacter sulfurreducens: High structural similarity to an algal cytochrome c_6, Proteins, 74 (2009) 266-270.

[150] J.M. Dantas, L. Campelo, N. Duke, C.A. Salgueiro, P.R. Pokkuluri, The structure of PccH from Geobacter sulfurreducens: A novel low reduction potential monoheme cytochrome essential for accepting electrons from an electrode, FEBS Journal, 282 (2015) 2215-2231.

[151] D.L. Turner, H.S. Costa, I.B. Coutinho, J. Legall, A.V. Xavier, Assignment of the ligand geometry and redox potentials of the trihaem ferricytochrome c_3 from Desulfuromonas acetoxidans, Eur. J. Biochem, 243 (1997) 474-481.

[152] X. Qian, T. Mester, L. Morgado, T. Arakawa, M.L. Sharma, K. Inoue, C. Joseph, C.A. Salgueiro, M.J. Maroney, D.R. Lovley, Biochemical characterization of purified OmcS, a c-type cytochrome required for insoluble Fe(III) reduction in Geobacter sulfurreducens, Biochim. Biophys. Acta, 1807 (2011) 404-412.

[153] C.A. Salgueiro, The multifaceted role of cytochromes c_7 in metal reduction - A structural and functional overview, Global J. Biochem., 3 (2012) 5.

[154] L. Morgado, A.P. Fernandes, Y.Y. Londer, P.R. Pokkuluri, M. Schiffer, C.A. Salgueiro, Thermodynamic characterization of the redox centres in a representative domain of a novel c-type multihaem cytochrome, Biochem. J., 420 (2009) 485-492.

[155] P.C. Portela, T.M. Fernandes, J.M. Dantas, M.R. Ferreira, C.A. Salgueiro, Biochemical and functional insights on the triheme cytochrome PpcA from Geobacter metallireducens, Arch. Biochem. Biophys., 644 (2018) 8-16.

[156] M.R. Ferreira, J.M. Dantas, C.A. Salgueiro, The triheme cytochrome PpcF from Geobacter metallireducens exhibits distinct redox properties, FEBS Open Bio, In press (2018).

2

Thermodynamic characterization of PpcA from G. metallireducens [1]

"Many of life's failures are people who did not realize how close they were to success when they gave up."

Thomas A. Edison

[1] This Chapter was partially reproduced from T.M. Fernandes, L. Morgado, C.A. Salgueiro, Thermodynamic and functional characterization of the periplasmic triheme cytochrome PpcA from G. metallireducens, Biochem. J., 475 (2018) 2861-2875 (doi: 10.1042/BCJ20180457), in accordance with the Editors' Copyright Policy.

2 – Thermodynamic characterization of PpcA from G. metallireducens

The PpcA-family of triheme periplasmic cytochromes is well conserved among the Geobacter species and its members are known to occupy a strategic position in the cell to function as capacitors and control electron flow towards OM components (see Figures 1.3 and 1.4) [1, 2]. The cytochromes belonging to this family are in the frontline as potential targets to develop rational Geobacter mutated strains with increased respiratory rates and concomitant higher current densities. In order to achieve this goal, it is first necessary to obtain detailed structural and functional data for the targeted electron transfer components [3].

The PpcA-family from G. sulfurreducens has been deeply studied over the years [4-13]. Although there is not much information coming from genomic and proteomic studies about the role of this family of cytochromes in G. metallireducens, it is known that PpcA is involved in the Fe(III) reduction pathways of G. metallireducens [14, 15]. Furthermore, the high sequence identity between the cytochromes of the two bacteria (Table 1.1) suggests that their functions in the EET pathways are going to be very similar.

Table 1.1 – Amino acid sequence identity percentages within and between the PpcA-families from G. metallireducens and G. sulfurreducens – The sequence identity percentage values between the homologous cytochromes of the two bacteria are highlighted in red. Notice that in G. metallireducens there is no PpcD, but there is a PpcF cytochrome and that for that reason, the highlighted values do not follow a diagonal. The values were determined using the BLAST tool from the database Uniprot [16].

		Geobacter metallireducens				
		PpcA	PpcB	PpcC	PpcE	PpcF
Geobacter sulfurreducens	PpcA	80%	68%	59%	54%	62%
	PpcB	73%	72%	56%	61%	58%
	PpcC	64%	57%	79%	52%	57%
	PpcD	68%	68%	42%	55%	55%
	PpcE	62%	63%	51%	69%	57%
Geobacter metallireducens	PpcA	–	81%	59%	59%	69%
	PpcB	81%	–	56%	61%	58%
	PpcC	59%	56%	–	49%	53%
	PpcE	59%	61%	49%	–	56%
	PpcF	69%	58%	53%	56%	–

The PpcA cytochrome is the most studied among all the cytochromes of G. sulfurreducens [4, 6, 7, 10, 12, 13, 17, 18] and for that reason, it was thought that the PpcA from G. metallireducens would be the perfect target for preliminary studies on the EET components of this bacterium, whose advantages over G. sulfurreducens were highlighted in Chapter 1.

Considering the above mentioned, an initial characterization of PpcA from G. metallireducens was recently published [19]. This cytochrome is a 9.7 kDa protein with 70 amino acids (Figure 2.1A), having 80% amino acid sequence identity with PpcA from G. sulfurreducens.

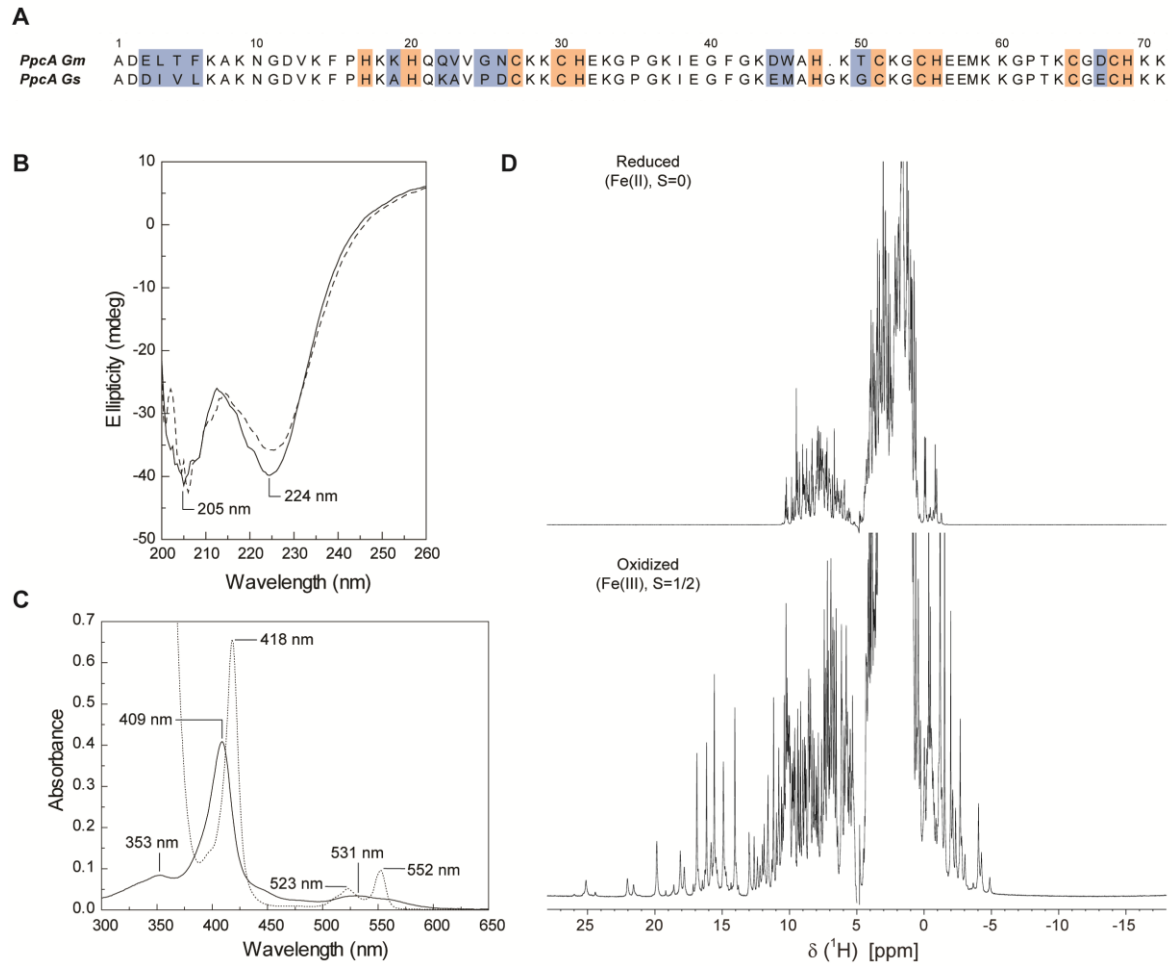

Figure 2.1 – Amino acid sequence and spectroscopic properties of PpcA from G. metallireducens – (A) Amino acid sequence alignment of PpcA cytochromes from G. metallireducens (PpcA Gm) and G. sulfurreducens (PpcA Gs). The heme binding motifs and axial ligands are highlighted in orange and non-conserved residues are highlighted in blue. (B) Far-UV CD spectrum in the native state at 25 ºC (solid line) and upon heating to 95 ºC (dashed line). The more intense negative bands, typical of α-helix, are labeled. (C) UV-visible spectra of the fully oxidized (solid line) and fully reduced (dashed line) forms. The optical absorption spectrum of the oxidized cytochrome has maxima at 353, 409 and 531 nm. Upon reduction, the protein shows the Soret, β and α bands at 418, 523 and 552 nm, respectively. (D) 1D ^{1}H-NMR spectra of the reduced (upper) and oxidized (lower) forms (25 ºC and pH 7). This figure was taken from [19].

PpcA contains three low-spin c-type heme groups with His-His axial coordination, a feature also observed for its homologue in G. sulfurreducens [3, 5, 19].

The native far-UV circular dichroism (CD) spectra (Figure 2.1B) of the cytochrome revealed a high α-helix content, featuring intense negative bands with slightly uncommon wavelengths (205 and 224 nm, instead of the typical 208 and 222 nm), probably resulting from substantial contributions from the protein's heme groups [19]. The thermal stability of the protein was also accessed by CD spectroscopy and revealed that the protein is stable, even at high temperatures [19].

The 1D ^{1}H-NMR signals of PpcA cover the regions -5 to 27 ppm in the oxidized paramagnetic state (Fe(III), S = 1/2) and -5 to 10 ppm in the reduced diamagnetic state (Fe(II), S = 0), which are typical of low-spin heme groups (Figure 2.1D) [19]. The heme-spin state features observed for the protein were additionally corroborated by UV-visible spectroscopy (Figure 2.1C). The assignment of the backbone, side chain and heme substituents in the reduced state (BMRB accession number 27363) allowed a comparative structural analysis with the PpcA from G. sulfurreducens and revealed marked differences in the relative orientation of the hemes I and III, between the cytochromes [19].

Finally, redox titrations followed by visible spectroscopy showed that the redox potential values for PpcA from G. metallireducens (-78 and -93 mV at pH 7 and 8, respectively) are considerably less negative, when compared with its homologous from G. sulfurreducens, and that the redox-Bohr effect (which will be further explained) is less evident [19].

The results detailed above raised interest on the full thermodynamic characterization of the PpcA cytochrome from G. metallireducens, since the characterization of the redox centers of this multiheme protein is crucial to assist in the elucidation of its physiological function and interactions with redox partners. In this Thesis, NMR redox titrations were performed at different pH values and the results obtained allowed the calculation of the microscopic parameters that fully characterize the thermodynamic behavior of the protein. Furthermore, the results obtained were compared with the ones previously obtained for the PpcA from G. sulfurreducens [13].

2.1 – Materials and methods

2.1.1 – Nuclear magnetic resonance fundamentals

NMR spectroscopy is a very powerful tool in the field of structural biology and has been used in the study of protein structure and dynamics, as well as in protein-ligand and protein-protein interaction studies. Historically, the first published work using NMR to study a biological molecule dates back to 1954 [20]. Furthermore, ribonuclease was the first intact protein studied by NMR, in 1957 [21], whereas the first protein structure was determined in 1985 [22].

This technique studies the selective absorption of electromagnetic radiation (radiofrequencies region) by nucleus in the presence of an external magnetic field. Nuclei are characterized by a quantum spin number (I), which can be determined from the atomic mass (number of protons and neutrons) and the atomic number (number of protons). When the atomic number and the atomic mass are even, nuclei have a quantum spin number of 0 (absence of magnetic properties, NMR silent nuclei). Then, when the atomic mass is odd (semi-integer quantum spin number) or when the atomic mass is even and the atomic number is odd (integer quantum spin number), nuclei have a quantum spin number different from 0 and present magnetic properties (NMR active nuclei) [23].

Spectra of several nuclei can be readily obtained (^{1}H, ^{13}C, ^{15}N, ^{19}F, ^{31}P), since they have quantum spin numbers different from 0 and a uniform spherical charge distribution (Table 2.2).

Table 2.2 – Properties of some NMR active nuclei – Some important NMR active nuclei in the study of biomolecules with the corresponding gyromagnetic constant (see below), nuclear spin quantum number and natural abundance. The data was taken from [23].

Nuclei	γ (10^6 rad s^{-1} T^{-1})	I	Natural abundance (%)
^{1}H	267.513	1/2	99.980
^{13}C	67.262	1/2	1.108
^{15}N	-27.116	1/2	0.370
^{19}F	251.815	1/2	100.000
^{31}P	108.291	1/2	100.000

The most widely observed in NMR spectroscopy are the ^{1}H and ^{13}C nuclei. Other nuclei, with quantum spin number of 1 or higher, may have non-spherical charge distribution. This particular asymmetry affects the relaxation times of these nuclei and, consequently, the linewidth

and coupling (with neighboring nuclei) of these nuclei signals, making it harder to obtain resolved NMR spectra.

The magnetic moment of a nuclear spin ($\vec{\mu}$) is related to its quantum spin number (I) and gyromagnetic ratio (γ), as shown in Equation 1.

$$\vec{\mu} = \gamma I \tag{1}$$

The gyromagnetic ratio (γ) is a constant number, characteristic for each nucleus, and indicates the frequency at which they will precess in a fixed external magnetic field [23].

In the absence of an external magnetic field (B_0), all nuclei of the same isotope have the same energy (degenerated states of energy). However, when an external magnetic field is applied, a splitting of nuclei spin energies occurs. For example, if a nucleus of I = 1/2 is considered, two linearly independent spin states (m = 1/2 and m = –1/2, with m being the magnetic quantum number) exist for the z-component of spin. On one hand, in the absence of a magnetic field, these states have the same energy and are in "thermal equilibrium". On the other hand, in the presence of an external magnetic field, two different levels of energy are defined (Figure 2.2).

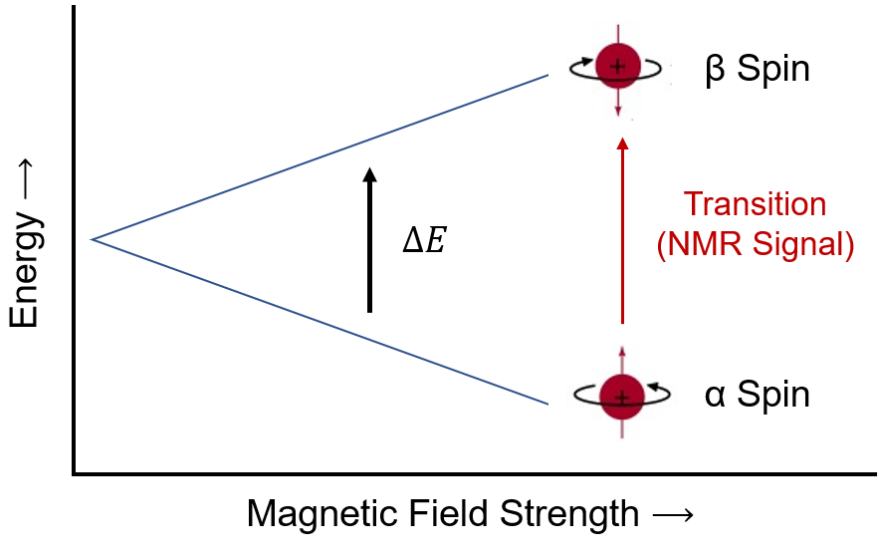

Figure 2.2 – Energy diagram of a nucleus with increasing magnetic field strength – In the absence of a magnetic field, the α and β states are degenerated. When a magnetic field is applied, there is an energy splitting and, the low and high energy levels get populated with the nucleus whose spins have the same (α-state) or opposite (β-state) direction to the external magnetic field, respectively.

The energy splitting is determined by the applied field (B_0) and gyromagnetic ratio of the nucleus (γ, rad s^{-1} T^{-1}), according to Equation 2. In this equation, h is the Planck constant.

$$\Delta E = h\gamma B_0/2\pi \quad (2)$$

In the state of lower energy (α), the nuclear magnetic moment is aligned with B_0 (m = 1/2), whereas in the state of higher energy (β), the nuclear magnetic moment is opposed to B_0 (m = –1/2). In reality, the nuclear magnetic moments are not aligned or opposed to B_0 but are precessing along the z-axis (Figure 2.3). This precession frequency, intrinsic for each nucleus in the presence of an external magnetic field, is called Larmor frequency (ω_o) [24].

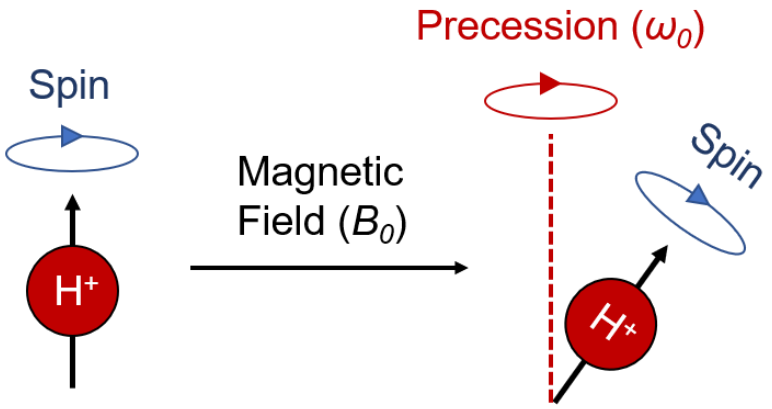

Figure 2.3 – Nuclei precess in the presence of a magnetic field – Nuclei spin naturally around their own axis and when a magnetic field is applied, they will also rotate about the axis of the applied magnetic field (precession).

The distribution of spin populations between the referred energy states (α and β) occurs according to Equation 3, where N_α and N_β are the populations of the α and β states, k is the Boltzmann constant and T is the absolute temperature (K).

$$N_\beta/N_\alpha = e^{-\Delta E/kT} \quad (3)$$

At room temperature, the population difference between the two energy states is very small. For example, the population ratio for protons at 800 MHz field strength is 0.99987. Therefore, only a small fraction of the spins contributes to the signal intensity of the NMR spectrum. For this reason, the use of stronger magnetic fields favors the NMR spectral resolution, since higher magnetic fields increase the population ratio between the ground and excited NMR energy states.

An NMR signal is produced when a nuclear transition between the two energy states occurs (resonance condition). This transition will occur if the energy of the electromagnetic radiation applied is equal to the energy difference between the two states. Theoretically, in a molecule, all protons have the same Larmor frequency. However, due to the effect of the electron density surrounding each individual proton, different Larmor frequencies will be detected for different

protons. This phenomenon is what makes NMR a powerful technique, since it gives information about the nuclei and their interactions and/or surroundings.

These frequencies are expressed in terms of an empirical quantity called chemical shift (δ), which is related to the difference between the resonance frequency of a certain nucleus (ν) and that of a reference standard (ν_{ref}), as depicted in Equation 4.

$$\delta = \frac{\nu - \nu_{ref}}{\nu_{ref}} \times 10^6 \quad (4)$$

The detected frequencies are usually referenced against TMS or DSS, which by the equation above have a chemical shift of zero if chosen as the reference and are expressed in ppm (parts per million). The NMR spectra, by convention, are plotted with chemical shift values increasing from the right to the left.

The magnetic field of a nucleus is not only affected by the magnetic fields created by its own electrons, but also from the magnetic moments of the neighboring nuclei. This interaction between different nuclei results in signal splitting for each of the nucleus involved. The separation between the resulted peaks is called coupling constant (J), which is independent of the applied magnetic field and is measured in frequency units (Hz).

In NMR, the approach to any structural or mechanistic problem will invariably start with the acquisition of one dimensional (1D) spectra, since these provide information about the preliminary stage of the sample in study, as well as foundations to design further experiments.

In the simplest 1D experiment, a two building block (preparation and detection) pulse sequence is applied (Figure 2.4). In the preparation, there is a delay time of relaxation that allows the magnetization to return to equilibrium. After that, a 90º radiofrequency pulse is applied during a certain time period (intrinsic of the sample), which rotates the equilibrium magnetization from the z-axis to the xy-plane. The recovery of the magnetization back to equilibrium is then detected in the form of a FID (free induction decay), during the detection period.

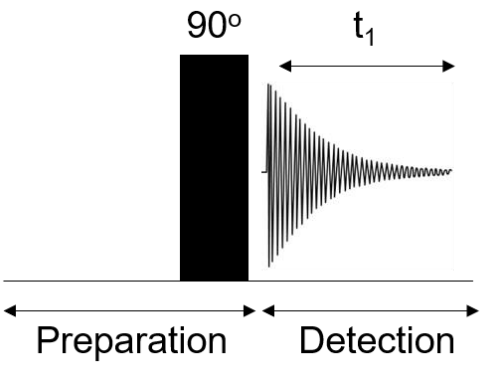

Figure 2.4 – Simplest 1D pulse sequence – During preparation, the spin-systems are set to a defined state. During detection, the resulting signal is recorded. The 90º pulse rotates the equilibrium magnetization from the z-axis onto the xy-plane. After this pulse, each spin precesses with its own Larmor frequency around the z-axis and induces voltage in the receiver coil. This signal is called FID.

In the case of small molecules, 1D spectra can contain valuable information (Figure 2.5). However, for complex macromolecules, such as proteins, 1D spectra become much more complex and crowded due to signal overlapping (Figure 2.6). In the last decades, in order to solve this problem and improve the NMR spectra resolution and the concomitant assignment of the signals, multidimensional NMR has been developed.

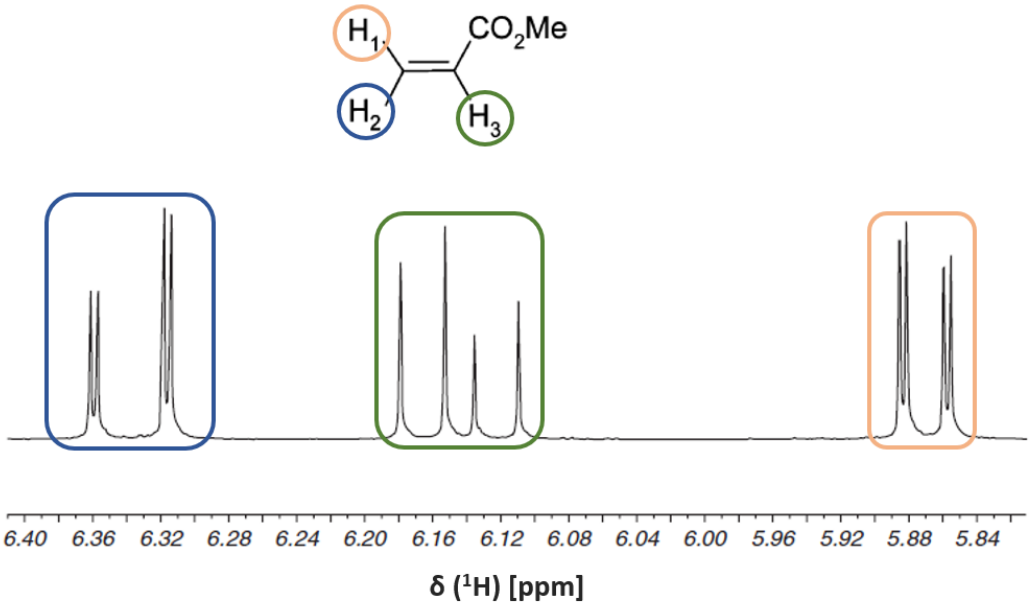

Figure 2.5 – Expansion of the 1D ^{1}H-NMR spectrum of methyl acrylate, in acetone solution – The spectra of small organic molecules, such as methyl acrylate, are simple and contain very few signals. These signals, however, are enough to assign and distinguish the different protons in the molecule. The methyl acrylate molecule is represented and the different signals of the molecule are labeled. This figure was adapted from [25].

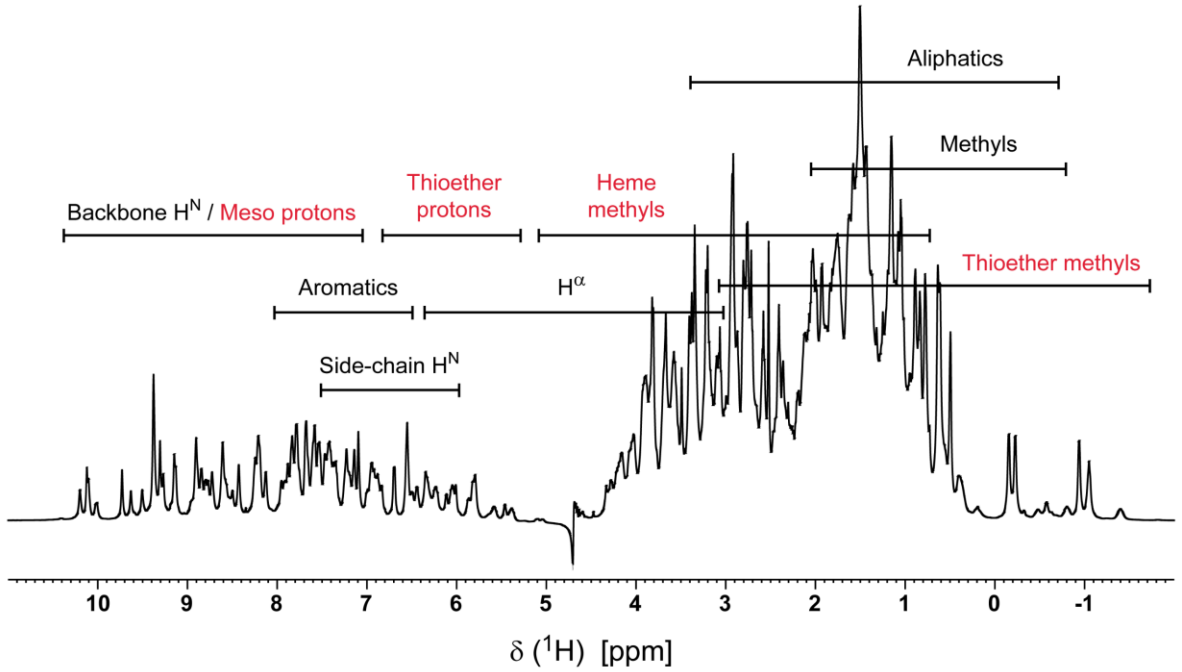

Figure 2.6 – 1D ^{1}H-NMR spectrum of the triheme cytochrome PpcA from G. metallireducens in the reduced state – The NMR spectra of proteins are much more complex, with spectral crowded regions arising from the amino acid backbone and side chains signals (black labels). Furthermore, in this particular protein, the three hemes substituents signals (red labels) add further complexity to the spectrum.

In the case of two-dimensional (2D) NMR spectra, the signals are dispersed over two frequency dimensions, yielding a 2D spectrum. In these experiments, one additional period, called the evolution time (which contains a variable time delay t_1), is inserted between the preparation and detection periods (Figure 2.7).

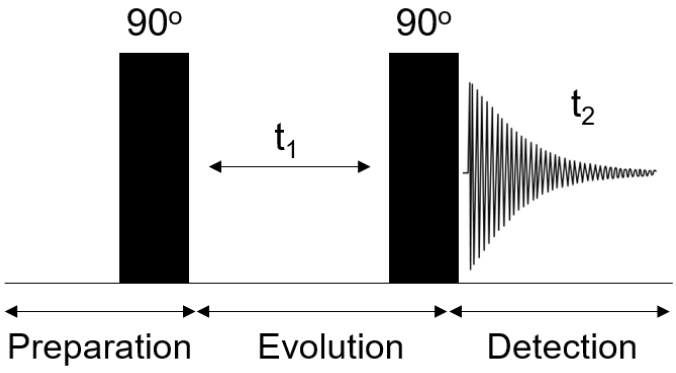

Figure 2.7 – Pulse sequence of the 2D ^{1}H-COrrelation SpectroscopY (COSY) experiment – In this experiment, the preparation begins with a relaxation delay that allows the magnetization to come back to its equilibrium, followed by a 90º pulse. Then, the t_1 period occurs with a stepwise increase in time and after a second 90º pulse, the signal is detected during the detection time (t_2).

The evolution delay increases systematically for each increment of the 2D experiment. After all the scans, the different FIDs obtained are transformed with the same phase parameters and the use of two Fourier transformations results in a two-dimensional NMR spectrum. These types of experiments can be homonuclear (usually ^{1}H-^{1}H experiments), giving rise to squared spectra with diagonal peaks, or heteronuclear (^{1}H-^{13}C, ^{1}H-^{15}N, among others), resulting in asymmetric spectra. 2D experiments may also contain other additional periods, such as the mixing period (t_m), that further complicate the pulse sequences (see below).

In this Thesis, a series of 2D-NMR experiments were used, namely homonuclear (2D ^{1}H-TOCSY, 2D ^{1}H-NOESY, 2D ^{1}H-EXSY) and heteronuclear (2D ^{1}H,^{13}C-HMQC) ones. The principles of these techniques are summarized below.

Total Correlation SpectroscopY (TOCSY) uses scalar coupling (through bond nuclear interactions) to correlate the spins within a spin system. This experiment provides geometric information about molecules via J-coupling and correlates the coupled homonuclear spins and those that reside within the same spin system, but which may not share mutual couplings (a propagation of magnetization along a continuous chain of spins occurs) [23]. Usually, in this experiment, the magnetization is transferred successively over up to five or six bonds, as long as successive protons are coupled. This magnetization transfer may be interrupted by small or zero proton-proton couplings, or either by the presence of hetero-atoms, such as oxygen. The number of magnetization transfer steps can be adjusted by adjustment of the spin-lock time. Short spin-lock times (around 20 ms) will result in one-bond transfers, whereas longer spin-lock times (80 – 120 ms) will result in five- or six-bond transfers [23]. The pulse sequence of the 2D ^{1}H-TOCSY experiment is presented below (Figure 2.8).

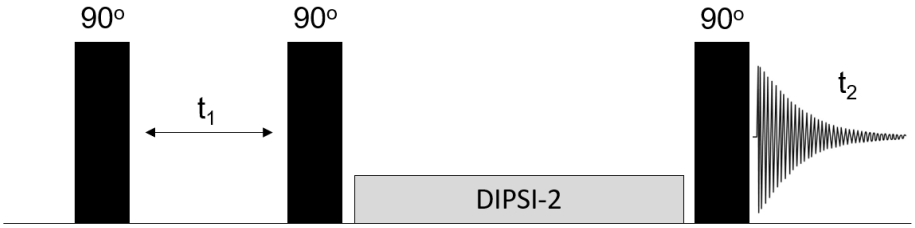

Figure 2.8 – Pulse sequence of the 2D ^{1}H-TOCSY experiment – In this pulse sequence, t_1 and t_2 stand for the evolution and detection period, respectively. After the first 90º pulse, transverse magnetization evolves during a free variable t_1 period. After the second 90º pulse, the TOCSY experiment uses an isotropic mixing sequence (in this case, DIPSI-2 (Decoupling In the Presence of Scalar Interactions)) to transfer magnetization via scalar coupling. The signal detection is performed as in the 2D ^{1}H-COSY experiment, during the t_2 period.

Nuclear Overhauser Effect SpectroscopY (NOESY) uses the Nuclear Overhauser Effect (NOE) to exchange magnetization between protons that have spatial proximity (up to 5 Å). The NOE is defined as the change in intensity of one NMR resonance as a consequence of the saturation of another close by resonance. This effect results from dipole-dipole cross-relaxation between nuclei and is proportional to their inter-nuclear distance (r) by a factor of $1/r^6$ [23]. For small molecules in solution, the effect is positive (affected resonances increase in intensity), whereas for larger molecules, the effect is negative (affected resonances decrease in intensity). This experiment can therefore be used to get structural restraints for solution structure calculations, but it is also useful for specific assignments [23]. The pulse sequence of the 2D ^{1}H-NOESY experiment is presented below (Figure 2.9).

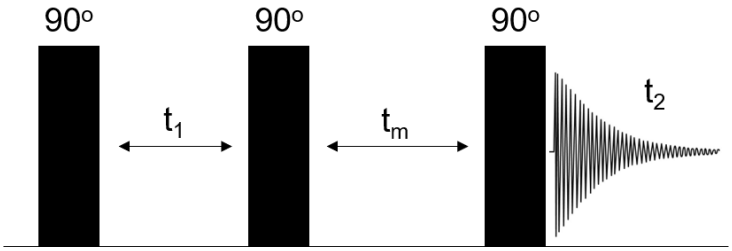

Figure 2.9 – Pulse sequence of the 2D ^{1}H-NOESY experiment – In this pulse sequence, t_1, t_m and t_2 stand for the evolution, mixing and detection period, respectively. After the first 90º pulse, transverse magnetization evolves during a free variable t_1 period. Another 90º pulse is applied to create longitudinal magnetization and during the t_m, magnetization is transferred via cross-relaxation. The final 90º pulse creates transverse magnetization, which is detected during t_2.

The 2D ^{1}H-EXSY experiment is very similar to the 2D ^{1}H-NOESY experiment. This particular technique is discussed in more detail in the next section.

The Heteronuclear Multiple Quantum Coherence (HMQC) experiment correlates the chemical shift of coupled heteronuclear spins, via the J-coupling existing between them. This experiment is very similar to the Heteronuclear Single Quantum Coherence (HSQC) experiment, with the only difference being the fact that in a HMQC, both proton (^{1}H) and the heteronucleus (for example, ^{13}C) are allowed to evolve during the evolution time, whereas in a HSQC, only the heteronucleus magnetization is allowed to evolve. In simple words, the HMQC experiment is affected by homonuclear proton J-coupling during the evolution time, whereas the HSQC experiment is not. The pulse sequence of the 2D ^{1}H,^{13}C-HMQC experiment is presented below (Figure 2.10).

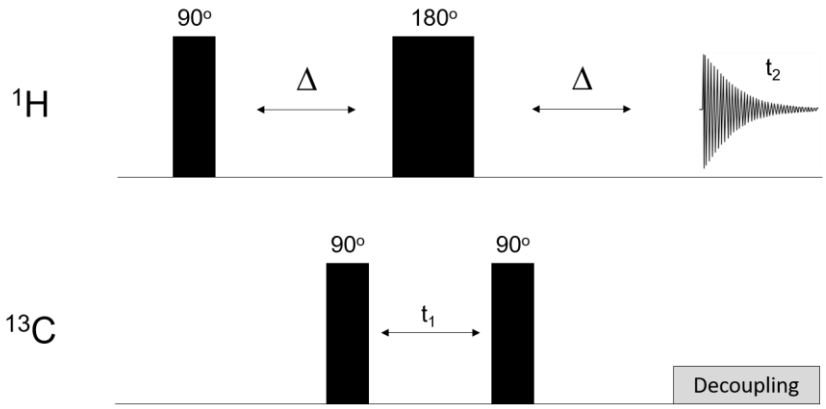

Figure 2.10 – Pulse sequence of the 2D ^{1}H,^{13}C-HMQC experiment – The first 90º pulse is applied on the ^{1}H-channel, creating transverse magnetization that evolves under the effect of heteronuclear coupling, during a time period (Δ) that usually corresponds to 1/2 J_{CH} (carbon-proton coupling constant). The second 90º pulse is applied on the ^{13}C-channel, creating heteronuclear multiple-quantum coherences, that evolve during the variable evolution period t_1. The 180º pulse applied on the ^{1}H-channel, which is inserted at middle of t_1, removes the evolution of heteronuclear couplings and ^{1}H chemical shifts. The third and final 90º pulse, applied on the ^{13}C-channel, creates antiphase single-quantum coherence in ^{1}H, which is then refocused after a second Δ. Finally, the signal is detected during t_2 on the ^{1}H dimension, with ^{13}C decoupling.

Although 2D-NMR experiments are already very useful and informative to study a broad range of proteins, in more complex cases, three and four dimension experiments are necessary [26]. For the purpose of this Thesis, these multidimensional experiments will not be discussed.

Finally, it is important to highlight the relaxation processes in NMR, that are not only important for the existence of the NMR signal itself, but also for the study of biomolecules dynamics. In NMR, there are two relaxation parameters: the spin-lattice or longitudinal relaxation time (T_1) and the spin-spin or transverse relaxation time (T_2). The parameter T_1 measures the efficiency with which excited nuclear spins return to their ground state by exchanging energy with their surroundings. T_2 is a measurement of the efficiency with which spins exchange energy with each other. The more efficient this exchange, the shorter the relaxation time. In a single NMR experiment, one of two relaxation times can be studied to understand biomolecule's dynamics, in a timescale of milliseconds (transverse relaxation, T_2) to seconds (longitudinal relaxation, T_1). In solution, the resonance linewidths are inversely proportional to the T_2 relaxation time, which decreases with the increase in molecular size and tumbling time (Figure 2.11) [27].

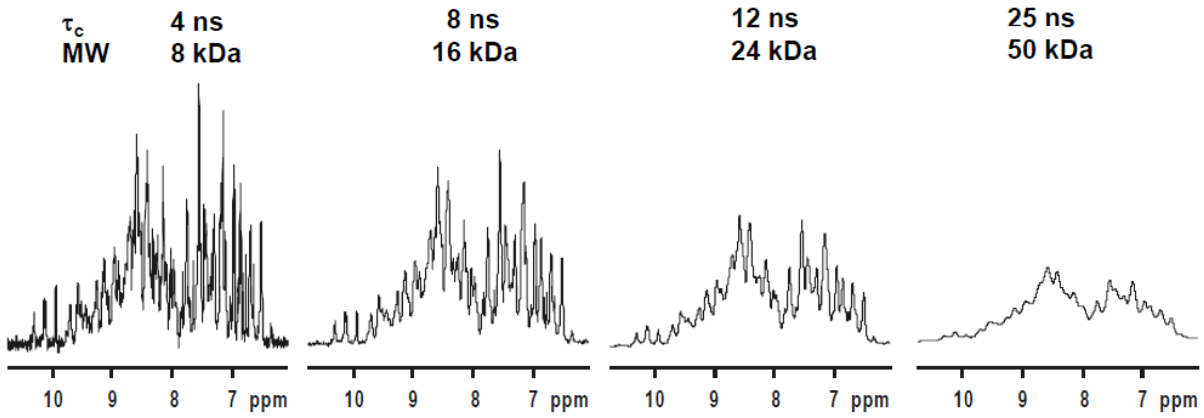

Figure 2.11 – Size limitation of the NMR technique – The increase in molecular weight (MW) and, consequently, on the correlation time of the molecule (τ_c, see below), leads to shorter T_2 relaxation times and concomitant broadening of the NMR signals.

Dipole-dipole interaction is probably the most important mechanism of relaxation pathway for protons in molecules containing contiguous protons and for carbons with directly attached protons.

The relaxation consequent of these interactions is dependent on the correlation time of the molecule, τ_c. Small molecules tumble very fast and have short τ_c, usually in the order of picoseconds. Large molecules, such as proteins, usually move slowly in solution and have longer τ_c (in the order of the nanoseconds). The relationship between relaxation (T_1 and T_2) and correlation (τ_c) times for small- and macromolecules is represented below (Figure 2.12).

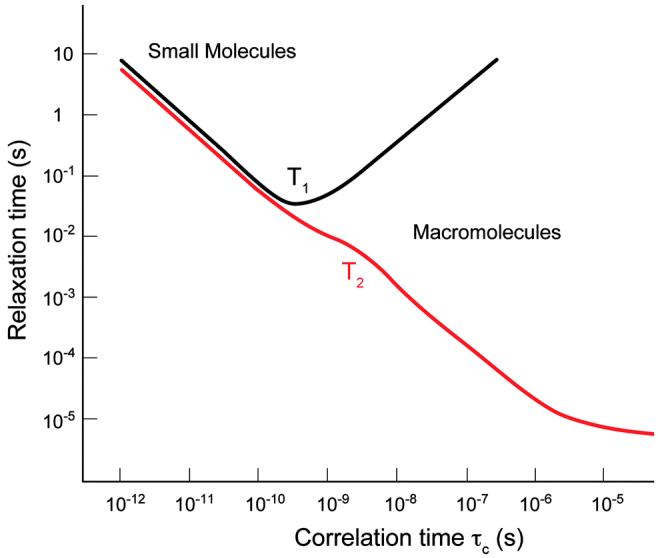

Figure 2.12 – Plot of relaxation time versus correlation time (τ_c) – The expected changes in the T_1 (black line) and T_2 (red line) relaxation times with respect to the molecular size are represented. Small molecules have shorter correlation times and relax slower, whereas macromolecules (such as proteins) have longer correlation times and relax faster. This figure was taken from [28].

2.1.2 – Exchange spectroscopy and its importance for cytochromes characterization

NMR parameters are influenced by a number of rate processes, the most dominant ones being molecular relaxation, molecular diffusion and chemical exchange processes. The use of 2D-NMR for studying chemical kinetics was first proposed by Jeener, Meier, Bachmann and Ernst, in 1979 [29]. They developed a three-pulse technique for 2D-EXchange SpectroscopY (2D-EXSY) and comprised a study of chemical exchange, magnetization transfer by inter- and intramolecular relaxation in liquids, and of spin diffusion and cross-relaxation processes in solids [29].

Dynamic NMR involves the study of samples that undergo chemical or physical changes with time. The timescale of motions that can be observed in NMR ranges from nanoseconds to minutes, depending on the sampled experimental observed, such as chemical shift, relaxation rate or coupling constant [30]. EXSY experiments can be used to study molecular motions and molecular exchanges that occur within a timescale of 1 to 10^{-3} seconds. Many parameters can be measured to access the exchange between two different environments, namely the chemical shift. The exchange between two environments (A and B) is considered slow if $k << |\nu_A - \nu_B|$ (with k being an exchange rate constant), intermediate if $k \approx |\nu_A - \nu_B|$ and fast if $k >> |\nu_A - \nu_B|$, where the resonance frequencies of the two environments are ν_A and ν_B. Since chemical shift differences are magnetic field dependent, a system that is in the fast exchange regime on a low field instrument, may enter the slow exchange regime when studied at a higher field. Under slow exchange, each chemical shift is observed distinctly (Figure 2.13). In contrast, under fast exchange, only a single chemical shift is observed at the population-weighted average position [30]. Therefore:

$$\delta_{obs} = p_A \delta_A + (1 - p_A)\delta_B \quad (5)$$

In Equation 5, p_A is the fractional population of A. Figure 2.13 shows the features of 1D NMR spectra under slow, intermediate and fast exchange conditions.

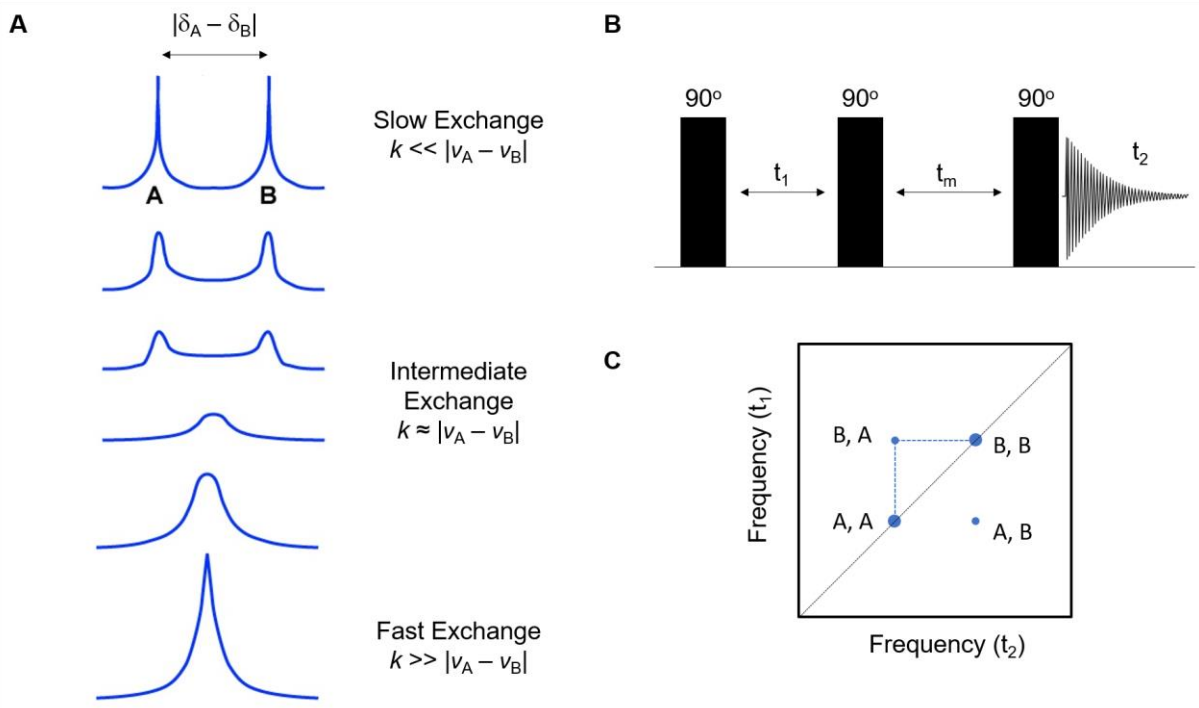

Figure 2.13 – Exchange spectroscopy basics – (A) Variation of the NMR spectra for two molecular environments (A and B) as a function of the reaction exchange constant (slow, intermediate and fast exchange) and resonance frequencies. (B) Pulse sequence of a 2D-EXSY experiment – the pulse sequence has exactly the same features of the pulse sequence used in 2D-NOESY, but in this case, it is used to investigate chemical exchange. (C) Schematic 2D exchange spectrum in the slow exchange regime – the off-diagonal peaks correspond to peaks that undergo exchange during the experiment.

The EXSY experiment is based on the pulse sequence of the NOESY experiment, which is used to investigate cross-relaxation due to dipolar coupling. In the case of EXSY, the pulse sequence is used to investigate cross-relaxation due to chemical exchange. In an EXSY experiment, transverse magnetization is created by a 90° pulse, and all components are "frequency labeled" since they process at their characteristic frequencies during the evolution period t_1. The magnetization is stored along the z-axis with another 90° pulse, for a mixing time t_m. During this time, chemical exchange may or may not occur, depending on the sample conditions. The magnetization is detected during time t_2, with a final 90° pulse. Nuclei that have not undergone exchange will resonate at the same characteristic frequency during t_1 and t_2 (the peaks lie along the diagonal of the 2D spectrum). Nuclei that have undergone exchange will have different frequencies in t_1 and t_2 (the peaks lie off-diagonal). The magnitude of these cross-peaks is directly related to the exchange rate [30].

In EXSY experiments, the cross-peaks and diagonal peaks are all positive. Moreover, the magnitude of these cross-peaks is generally large compared to NOESY cross-peaks. Furthermore, NOESY cross-peaks are positive in the slow tumbling regime and negative in the

extreme narrowing limit. So, for small molecules, cross-peaks due to exchange and NOE are easily distinguished. For bigger molecules, such as proteins, the distinction between cross-peaks due to exchange (EXSY cross-peaks) and NOE is not straightforward.

There are several experimental conditions that must be varied and optimized to obtain exchange rates that fit into the EXSY timescale (1 to 10^{-3} seconds), namely the magnetic field strength, temperature and ionic-strength [6, 30-33].

The biological role of electron-transfer proteins, such as cytochromes, has been thoroughly investigated during the last decades. In order to study and understand these proteins, namely the specific way the electron transfer is mediated, suitable techniques, that provide specific information about each redox center and its interactions at different stages of oxidation, must be used.

Until 1984, several physico-chemical techniques, mainly Mössbauer spectroscopy [34], circular dichroism [35], EPR [36-39], NMR (mostly 1D ^{1}H-NMR and saturation transfer experiments) [40-44], cyclic voltammetry, differential pulse polarography [45-49] and pulse radiolysis [50] had been used to elucidate the mechanisms of electron transfer in cytochromes.

In 1984, Santos and co-workers suggested the application of 2D exchange NMR to obtain the cross-assignments of the resonances in a multisite electron transfer system [51], important for the understanding of the intramolecular and intermolecular electron transfer mechanisms of cytochromes. Since then, over 50 cytochromes (including wild-type and mutants) have been functionally characterized using this approach, including proteins from Geobacter [6, 8, 9, 13, 52, 53], Shewanella [54-59], Desulfuromonas [60], Desulfomicrobium [61] and Desulfovibrio [51, 62-71] bacteria. In this Thesis, 2D-EXSY experiments were also used to study the triheme cytochrome PpcA from G. metallireducens, as described in the next sections.

2.1.3 – Expression and purification of PpcA from G. metallireducens

PpcA from G. metallireducens was produced and purified as previously described [19]. Briefly, Escherichia coli (E. coli) BL21 (DE3) cells, containing the plasmid pEC86 (encoding for cytochrome c maturation gene cluster ccmABCDEFGH and a chloramphenicol resistance gene), were transformed with the plasmid pCSGmet2902 (containing the gene Gmet_2902, encoding for G. metallireducens PpcA and carrying and ampicillin resistance gene) and grown in 2xYT media supplemented with 34 μg/mL chloramphenicol and 100 μg/mL ampicillin, to an OD_{600} of approximately 1.5 at 30 ^{o}C. The protein expression was then induced with 10 μM of isopropyl

β-D-thiogalactoside (IPTG) and the cell cultures grown overnight at 30 ºC. Following overnight incubation, cells were harvested by centrifugation at 4000 xg for 20 minutes and the periplasmic fraction was isolated using lysis buffer (100 mM Tris-HCl pH 8.0, 0.5 mM EDTA, 20% sucrose and 0.5 mg/mL lysozyme). The periplasmic fraction was recovered by centrifugation at 14700 xg, at 4 ºC for 20 minutes and further ultracentrifugated at 150000 xg, at 4 ºC for 1 hour. The final supernatant obtained was dialyzed against 2 x 4.5 L of 10 mM Tris-HCl pH 8.0 and loaded onto 2 x 5 mL Bio-Scale™ Mini UNOsphere™ S cartridges (Bio-Rad), equilibrated with the same buffer. The protein was eluted with a sodium chloride gradient (0-300 mM) and the obtained fraction was concentrated to 1 mL and injected in a XK 16/70 Superdex 75 molecular exclusion column (GE Healthcare), equilibrated with 100 mM sodium phosphate buffer (pH 8.0). Both chromatography steps were performed on an ÄKTA Pure (GE Healthcare) system. Protein purity was evaluated by BlueSafe stained SDS-PAGE. The concentration of the cytochrome was determined by measuring the absorbance of the reduced form at 552 nm, using the extinction coefficient of 118 mM^{-1} cm^{-1} [19].

2.1.4 – NMR studies

2.1.4.1 – Sample preparation

Protein samples for NMR studies at intermediate levels of oxidation were prepared with approximately 80 μM concentration, in 80 mM phosphate buffer prepared in pure $^{2}H_{2}O$ (CIL isotopes), at different pH values, with NaCl (250 mM of final ionic strength), after lyophilization. The protein samples used on the NMR pH titration in the fully oxidized state were prepared in the same conditions. The protein samples used to assign the heme methyl chemical shifts, both in the fully reduced and fully oxidized states, were prepared with approximately 750 μM concentration, in the same buffer at pH 5.8 and 8.1. The pH values of the samples were checked with a glass micro electrode and were not corrected for isotope effects. For sample reduction, the NMR tubes were sealed with a gas-tight serum cap and the air was flushed out from the sample, to avoid possible oxidation of the samples. Then, the samples were reduced directly in the NMR tube with gaseous hydrogen (Air Liquide) in the presence of catalytic amounts of hydrogenase from Desulfovibrio vulgaris (Hildenborough). The partially oxidized samples, used for the NMR redox titrations, were obtained by first removing the hydrogen from the reduced sample with argon (Gasin) and then adding controlled amounts of air into the NMR tube with a Hamilton syringe.

2.1.4.2 – NMR experiments

All the NMR experiments were acquired in a Bruker Avance III 600 MHz spectrometer equipped with a triple-resonance cryoprobe (TCI). The ^{1}H chemical shifts were calibrated using the water signal as internal reference. All the different spectra obtained were processed using TopSpin3.5.7^{TM} (Bruker BioSpin, Karlsruhe, Germany).

2.1.4.2.1 – Redox titrations

The oxidation patterns of PpcA from G. metallireducens were monitored by 2D-EXSY spectroscopy, at different pH values. All the 2D-EXSY spectra were accumulated with a mixing time of 25 ms and were acquired at 288 K, collecting 2048 (t_2) x 256 (t_1) data points to cover a sweep width of 27.5 kHz, with 256 scans per increment. 1D ^{1}H-NMR spectra were obtained before and after each 2D-NMR spectrum to check for any changes in the oxidation state of the sample during the 2D-NMR experiment. The 1D-NMR spectra were acquired at 288 K, with water pre-saturation, collecting 32k data points to cover a spectral width of 33 kHz.

2.1.4.2.2 – Fully reduced state experiments

For the assignment of the heme methyl substituents in the fully reduced state, 2D ^{1}H-NOESY and 2D ^{1}H-TOCSY experiments were acquired using pulse sequences with water pre-saturation. The 2D ^{1}H-NOESY spectra were acquired with a mixing time of 80 ms, collecting 2048 (t_2) x 256 (t_1) data points to cover a sweep width of 8.4 kHz, with 160 scans per increment. The 2D ^{1}H-TOCSY spectra were acquired with a mixing time of 60 ms, 128 scans and with the same number of data points and spectral width.

2.1.4.2.3 – Fully oxidized state experiments

For the assignment of the heme methyl substituents of the protein in the fully oxidized state, the following set of 2D-NMR experiments was acquired: 2D ^{1}H,^{13}C-HMQC, 2D ^{1}H-NOESY and 2D ^{1}H-TOCSY. The 2D ^{1}H,^{13}C-HMQC spectra were acquired collecting 4096 (t_2) x 256 (t_1) data points to cover a sweep width of 28.8 kHz in the ^{1}H dimension and 52.8 kHz in the ^{13}C dimension, with 360 scans per increment. The 2D ^{1}H-NOESY spectra were acquired with a mixing time of 80 ms, collecting 4096 (t_2) x 512 (t_1) data points, to cover a sweep width of 28.8 kHz, with 200 scans per increment. The 2D ^{1}H-TOCSY spectra were acquired with a mixing time of 45 ms, collecting 2048 (t_2) x 512 (t_1) data points to cover a sweep width of 28.8 kHz, with 160 scans per increment.

2.1.4.2.4 – NMR pH titration in the fully oxidized state

1D ^{1}H-NMR spectra were used to monitor the effect of pH on the chemical shifts of the heme methyl substituents, in the fully oxidized state at 288 K. The spectra were acquired in the pH range 5.5 to 9.5, with 32k data points, a spectral width of 30 kHz, with a total of 256 transients and water pre-saturation. The sample pH was adjusted by addition of small amounts of $NaO^{2}H$ or ^{2}HCl (both from Sigma-Aldrich). The pH values of the samples were checked with a glass micro electrode and were not corrected for isotope effects.

2.1.5 – Assignment of the heme substituents signals in the reduced state

The PpcA cytochrome is diamagnetic when reduced (Fe(II), S = 0) and paramagnetic when oxidized (Fe(III), S = 1/2), as said previously. In the diamagnetic reduced form, the proton chemical shifts of the heme substituents are essentially affected by the heme ring-current effects [72-77]. Therefore, for the fully reduced cytochrome, typical regions for the signals of the heme substituents can be easily identified in 2D ^{1}H-NOESY spectra: 8 to 10 ppm – meso protons (5H, 10H, 15H and 20H); 6 to 8 ppm – thioether methines (3^{1}H and 8^{1}H); 2.5 to 5 ppm – methyl groups ($2^{1}CH_3$, $7^{1}CH_3$, $12^{1}CH_3$ and $18^{1}CH_3$); and -1 to 3 pm – thioether methyls ($3^{2}CH_3$ and $8^{2}CH_3$). In the reduced state, the first step of the assignment is the analysis of the 2D ^{1}H-TOCSY spectra, in which the connectivities between the thioether methines (3^{1}H or 8^{1}H) and the thioether methyl groups ($3^{2}CH_3$ and $8^{2}CH_3$) are identified. Indeed, these are the only heme protons that are in the same spin system (except for the propionates αCH_2 ($17^{1}CH_2$ and $13^{1}CH_2$) and βCH_2 ($17^{2}CH_2$ and $13^{2}CH_2$) protons) and that can be easily identified in the 2D ^{1}H-TOCSY spectra (Figure 2.14). The heme nomenclature is represented in Figure 2.14.

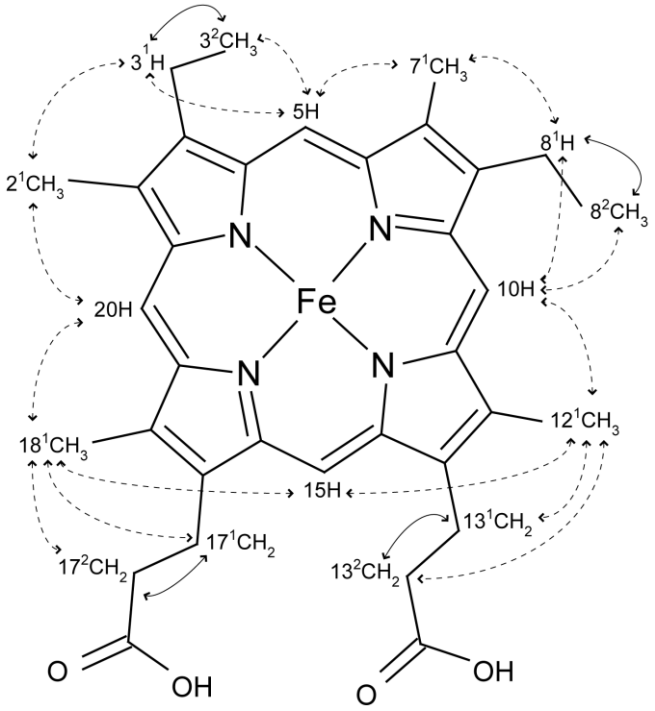

Figure 2.14 – Diagram of heme c, numbered according to the IUPAC-IUB nomenclature [78] – Dashed and solid lines indicate the connectivities observed in NOESY and TOCSY spectra, respectively.

As previously said, 2D ^{1}H-NOESY experiments allow the detection of spatial correlation between nuclei that are typically closer than 5 Å [23]. Meso protons have some short-range intraheme connectivities and thus present a characteristic pattern in the 2D ^{1}H-NOESY spectra. Protons 15H are not connected to either methyl groups or thioether substituents and are the most difficult meso protons to assign. Protons 20H are connected to two heme methyls ($2^{1}CH_3$ and $18^{1}CH_3$) and can be easily assigned. Finally, the most ambiguous assignment arises with the 5H and 10H protons, since they both present connectivities with a thioether methine ($3^{1}H$ or $8^{1}H$, respectively), a thioether methyl ($3^{2}CH_3$ or $8^{2}CH_3$, respectively) and one heme methyl group ($7^{1}CH_3$ or $12^{1}CH_3$, respectively). This ambiguity is solved by observing the connectivities between the heme methyls near the 20H protons ($2^{1}CH_3$) with the closest thioether groups ($3^{1}H$ or $3^{2}CH_3$), which are unequivocally assigned in the 2D ^{1}H-TOCSY spectrum. This allows the connection between the 20H and 5H faces of each heme. The heme methyls $7^{1}CH_3$ are part of the 5H faces of the heme and also show connectivities with thioether groups ($8^{1}H$ and $8^{2}CH_3$), which are in 10H faces. After the identification of these three heme faces, 15H protons can be identified by observing the connectivities between cross-peaks that connect 15H and $12^{1}CH_3$ or $18^{1}CH_3$ protons. This strategy of assignment was initially described by Keller and Wüthrich [79] for the horse heart ferrocytochrome and later applied to multiheme ferrocytochromes by Turner et al. [80].

The NOE connectivities observed for PpcA from G. metallireducens in the reduced state (Figure 2.15) were previously assigned (pH 7.1, 100 mM ionic strength and 298 K) [19] and were used as a guide to distinguish the different heme faces and unequivocally assign the heme substituents at the new experimental conditions (pH 5.8, 250 mM ionic strength and 288 K).

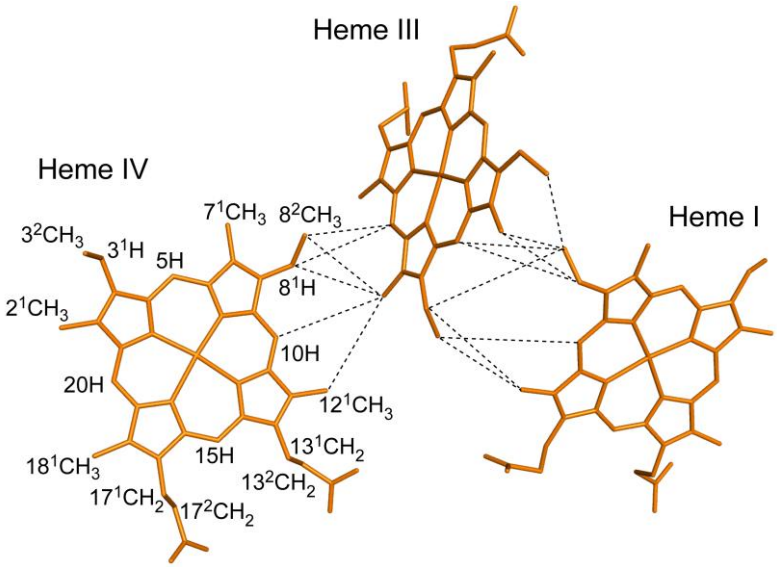

Figure 2.15 – Interheme NOE connectivities observed in the 2D ^{1}H-NOESY spectra of PpcA from G. metallireducens – The indicated NOE connectivities were observed at pH 7, 100 mM ionic strength, 298 K. The heme core of PpcA from G. sulfurreducens (PDB ID: 2LDO [10]) is used as model and the IUPAC-IUB nomenclature for tetrapyrroles [78] is shown on heme IV.

2.1.6 – Assignment of the heme substituents signals in the oxidized state

In the oxidized state, in addition to the ring-current effect, the intrinsic (from own heme) and the extrinsic (from neighbor hemes) paramagnetic contributions due to the presence of unpaired electrons, strongly contribute to the final observed chemical shift of the heme substituents. The intrinsic and extrinsic paramagnetic contributions of a heme substituent usually have two components: (i) the scalar contact shift (or Fermi contact shift), which is a through-bond effect and depends on the heme unpaired electronic distribution; and (ii) the dipolar pseudocontact shift, which is a spatial effect [81]. The magnitude of the observed paramagnetic shifts is mostly dominated by the contact contribution.

In the oxidized form, the same type of signals are (i) differently affected by the paramagnetic centers, (ii) show different levels of broadness and (iii) are spread over the entire NMR spectral width, making their assignment more complex than for the diamagnetic reduced state.

The acquisition of 2D $^{1}H,^{13}C$-HMQC spectra is usually used to assist the assignment of the heme substituents signals, since the dipolar shifts of the carbon nuclei attached to the pyrrole β-carbons are very small and unlike the protons bonded to them, their Fermi contact shits are directly proportional to the spin density on the pyrrole β-carbons [82]. In 2D $^{1}H,^{13}C$-HMQC spectra, there is overlap between the heme signals with those of the polypeptide chain, which are also displaced from their typical positions in paramagnetic proteins, making their assignment extremely complex as well. Although the assignment of the heme substituents is complex in the oxidized paramagnetic state, there are typical ^{1}H-^{13}C regions for some of the heme substituents (Figure 2.16).

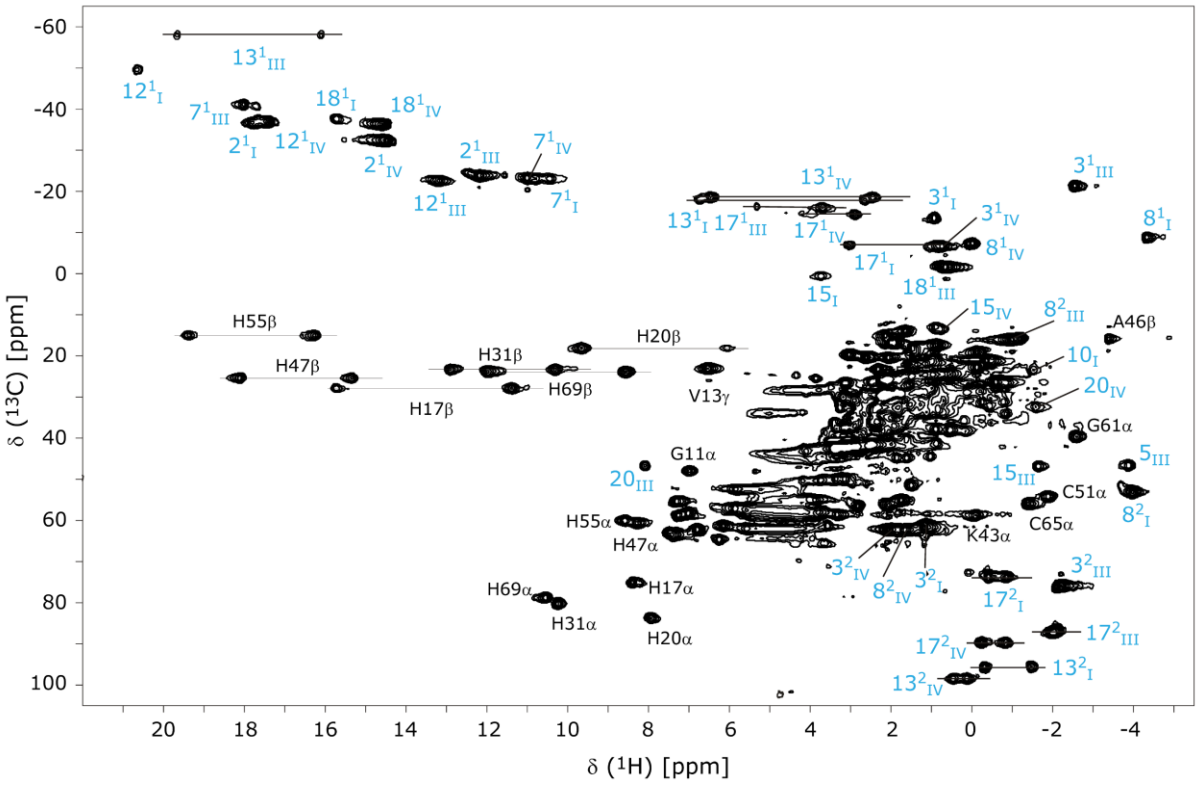

Figure 2.16 – 2D $^{1}H,^{13}C$-HMQC spectra of PpcA from G. sulfurreducens at pH 5.5 and 298 K – The blue and black labels indicate the heme substituents and the polypeptide resonances, respectively. The peaks of the protons connected to the same carbon atom (CH_2 groups) are linked by a straight line. This figure was adapted from [83].

The propionates αCH_2 protons ($17^{1}CH_2$ and $13^{1}CH_2$) are identified in the 2D $^{1}H,^{13}C$-HMQC spectrum, whereas the intraheme connectivities with the propionates βCH_2 ($17^{2}CH_2$ and $13^{2}CH_2$) are obtained from the analysis of a 2D ^{1}H-TOCSY spectrum. This intraheme connectivities are then confirmed in the 2D $^{1}H,^{13}C$-HMQC spectrum, at the typical region of propionates βCH_2.

Finally, a 2D ^{1}H-NOESY spectrum is used to identify the cross-peaks of each propionate proton with those of the closest heme methyl ($18^{1}CH_3$ and $12^{1}CH_3$), as well as to identify the remaining cross-peaks existing between the different heme substituents, for each heme. Since the interheme NOE connectivities for the PpcA from G. metallireducens were previously identified [19], it is possible to distinguish the different hemes and complete the assignment in the paramagnetic form.

This strategy of assignment, which gathers the analysis of 2D ^{1}H,^{13}C-HMQC, 2D ^{1}H-TOCSY and 2D ^{1}H-NOESY spectra, was previously described [11, 81, 84]. In this Thesis, the assignment of the hemes methyls and propionates ^{13}C and ^{1}H chemical shifts, in the oxidized state, was performed at pH 5.8 (288 K) and pH 8.1 (288 and 298 K).

2.1.7 – Thermodynamic model

In multiheme cytochromes, the coexistence of several microstates in solution makes the study of the properties of the redox centers particularly complex. In the particular case of a triheme cytochrome, three consecutive reversible steps of one-electron transfer convert the fully reduced state (stage 0, S_0) in the fully oxidized state (stage 3, S_3) and, therefore, four different redox stages can be defined (Figure 2.17). At each stage, microstates are grouped with the same number of oxidized hemes. Additionally, within each microstate, the group responsible for the redox-Bohr effect may be protonated or deprotonated, leading to a total of 16 possible microstates.

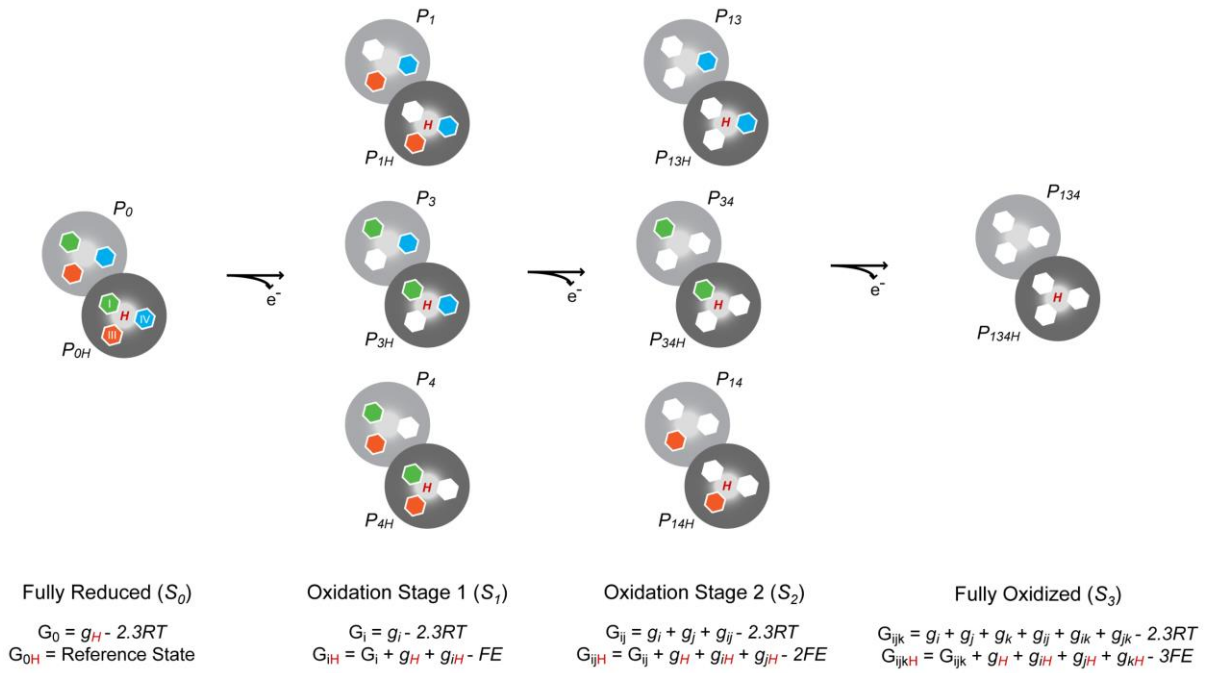

Figure 2.17 – Thermodynamic model of a triheme cytochrome – This figure is presented with the same features of Figure 1.10. Furthermore, the presented equations describe the energy parameters that allow the calculation of the global energy of each microstate. In these equations, G_{0H} and G_0 represent the energies of the reduced protonated and deprotonated microstates, respectively. G_{ijkH} and G_{ijk} represent the energies of the protonated and deprotonated microstates, respectively. For more details, see Equations 6 and 7, presented below.

As a consequence of the close spatial disposition of the heme groups in small multiheme cytochromes, the redox potential of one heme is modulated by the oxidation state of its neighbors (redox interactions, g_{ij}, Figure 2.18). Moreover, the redox potential of the hemes can also be modulated by the pH (redox-Bohr effect). The magnitude of this effected is determined by the so-called redox-Bohr interactions (g_{iH}, Figure 2.18), which measure the effect of the protonation state of the redox-Bohr center (a protonable center, located in the vicinity of the hemes [85-88]) on the heme redox potentials.

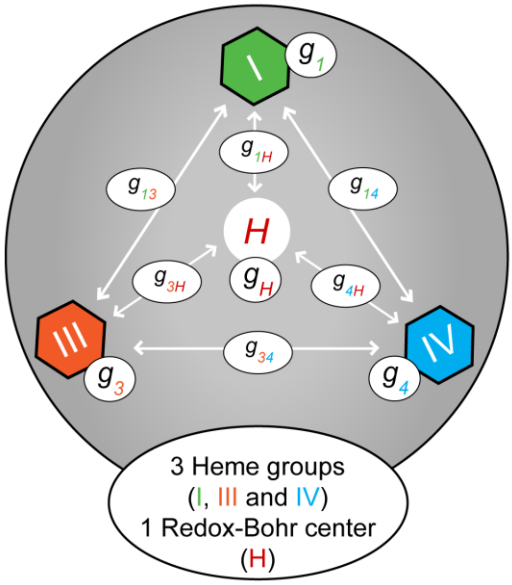

3 Heme oxidation energies (g_1, g_3 and g_4)
1 Redox-Bohr center deprotonation energy (g_H)
3 Redox interaction energies (g_{13}, g_{14}, g_{34})
3 Redox-Bohr interaction energies (g_{1H}, g_{3H}, g_{4H})

$$G_{iH} = \Sigma g_i + \Sigma g_{ij} - SFE$$
$$G_i = G_{iH} + g_H + \Sigma g_{iH} - 2.3RTpH$$

Figure 2.18 – Energy interactions in a triheme cytochrome with one redox-Bohr center – Schematic representation of the interaction network of a multiheme cytochrome with three hemes (numbered I (green), III (orange) and IV (blue)) and one redox-Bohr center (red "H"). The terms g_{ij} and g_{iH} represent the interaction energies between the hemes (ij) and between the hemes and the redox-Bohr center (H), respectively. The individual heme oxidation energies are represented as g_1, g_3 and g_4, for hemes I, III and IV, respectively. The 10 energy parameters that describe the full interaction network and the global equations that describe the energy of each possible microstate are listed next to the figure.

The fractional contribution of the 16 microstates, across the full range of pH and solution potential can be defined by 10 thermodynamic parameters: the three heme oxidation energies (reduction potentials), the pK_a of the redox-Bohr center, the three interaction energies between each pair of hemes (redox interactions) and the three interaction energies between each heme and the redox-Bohr center (redox-Bohr interactions).

The energy of each microstate relative to the reference microstate (fully reduced and protonated, P_{0H}) is then given by a simple sum of the appropriate energy terms amongst the four independent centers, the six possible two-center interactions and one term that accounts for the effect of the solution potential (SFE) in the oxidation stage S (Equation 6), and another for the proton chemical potential (2.3RTpH) added for the deprotonated forms (Equation 7):

$$G_{iH} = \Sigma g_i + \Sigma g_{ij} - SFE \quad (6)$$

$$G_i = G_{iH} + g_H + \Sigma g_{iH} - 2.3RTpH \quad (7)$$

In these equations, iH designates a particular protonated microstate with oxidized heme(s) group(s) i (i = 1-3); g_i the energy of oxidation of heme i; g_{ij} the interaction energy between each

pair of hemes i and j; g_H the deprotonation energy of the fully reduced protein; g_{iH} the energy of interaction between the hemes and the redox-Bohr center; S the oxidation stage (that corresponds to the number of oxidized hemes); F the Faraday constant; E the redox potential of the solution; R the molar gas constant and T the absolute temperature.

The referred energy values can be converted to reduction potentials, which further facilitates data interpretation, using the Nernst equation (Equation 8):

$$\Delta G = -nF\Delta E \tag{8}$$

Finally, the fractional contribution of each microstate (P_i) can be determined by the Boltzmann equation (Equation 9):

$$P_i = e^{-G_i/RT} \tag{9}$$

In experimental terms, the thermodynamic parameters can be determined by combining data obtained from NMR and visible redox titrations. In order to obtain information about each microstate, it is necessary to monitor the stepwise oxidation of each individual heme at different pH values, which for the particular case of heme groups displaying identical optical properties (as in PpcA from G. metallireducens, which contains three low-spin c-type hemes) can be obtained with EXSY spectroscopy [89].

When the interconversion between microstates within the same oxidation stage (intramolecular electron exchange) is fast on the NMR time scale and the interconversion between microstates belonging to different oxidation stages (intermolecular electron exchange) is slow, the individual heme NMR signals can be discriminated. This allows for the separation of the peaks belonging to the same heme substituent at different stages of oxidation. On the other hand, the intermolecular electron exchange has to be fast enough for significant transfer to occur before the magnetization has decayed, so that exchange cross-peaks can be observed in the EXSY spectra [71].

This is only possible because the distribution of the paramagnetic shifts observed for each oxidation stage is governed by the relative microscopic reduction potentials of the heme groups, and thus provides information on the relative order of oxidation of the hemes [70, 89]. The substituents of each heme have different chemical shifts in the four macroscopic oxidation stages, and since these paramagnetic shifts are proportional to the degree of oxidation of that particular heme group, they can be used to monitor the oxidation of each heme throughout a redox titration. As the reoxidation of a multiheme protein proceeds, the heme methyl signals

become much shifted from the diamagnetic region of the spectra. Furthermore, the three-proton intensity of these signals facilitates their assignment. Therefore, these are the most adequate heme substituents to monitor the protein reoxidation process. However, this is only valid if the extrinsic paramagnetic shifts (the contributions of the paramagnetic interactions with the other heme groups in the protein) are negligible.

Considering the above mentioned, at each pH, a methyl group of any heme, in the oxidation stage S, has a single peak with a determined chemical shift ($\delta_{obs}^{i,S}$). This shift depends on the populations of the microstates in which that heme is oxidized, weight-averaged according to the deprotonated and protonated populations (Equation 10 – also see section 6.9):

$$\delta_{obs}^{i,S} = \frac{(\delta^{i,3} - \delta^{i,0}) \sum p_{i,S} + \left(\delta_H^{i,3} - \delta^{i,0}\right) \sum p_{i,S}^H}{\sum p_S} + \delta^{i,0} \quad (10)$$

In this equation, $\delta^{i,0}$ is the observed chemical shift of the methyl i in the fully reduced protein and $\delta^{i,3}$ and $\delta_H^{i,3}$ are those observed in the fully oxidized deprotonated and protonated protein, respectively. The chemical shift of the heme methyl in the fully reduced form is assumed to be independent of pH. $\sum p_{i,S}$ and $\sum p_{i,S}^H$ are the sums over all the populations with heme i oxidized in stage S, with the redox-Bohr center being deprotonated and protonated, respectively; whereas $\sum p_S$ is the sum over all the populations (either protonated or deprotonated), for each stage S (see Figure 2.17 and 2.18).

It is also possible to represent the averaged oxidation fraction for each heme (m), in each stage of oxidation (S), using a simple equation (Equation 11). This equation considers that at each pH, the paramagnetic shifts of one methyl group of each heme in oxidation stages 1 or 2, relative to the fully oxidized form (stage 3) follow the presented relationship:

$$\Sigma_{m=1}^{3} \frac{(\delta_{obs}^{m,S} - \delta_{obs}^{m,0})}{(\delta_{obs}^{m,3} - \delta_{obs}^{m,0})} = S \quad (11)$$

However, the NMR data obtained with redox titrations only defines the relative heme reduction potentials and heme redox interactions. To determine the absolute potentials, the total reduced protein fractions need to be measured through redox titrations followed by UV-visible

spectroscopy. The total reduced fraction (Equation 12) as a function of the solution potential for each pH value, can be represented by accounting the relative populations weighted by the number of reduced hemes:

$$Reduced\ fraction = \frac{3\sum P_{S,0} + 2\sum P_{S,1} + \sum P_{S,2}}{3\sum p_S} \quad (12)$$

In this equation, $\sum P_{S,0}$, $\sum P_{S,1}$ and $\sum P_{S,2}$ are the sums over all the populations in stages 0, 1 and 2, respectively.

In this Thesis, the chemical shifts of the different heme methyl groups at different stages of oxidation were assigned through redox titrations followed by NMR. Then, together with the data previously obtained from the UV-visible spectroscopy redox titrations [19], the experimental data were fitted to the presented thermodynamic model using a software developed by Turner et al. [71]. This software uses the Marquardt method [90] to simultaneously fit the NMR and UV-visible data in an iterative approach, targeting a minimization in the differences between the target function and the experimental data. The experimental uncertainty of the NMR data was evaluated from the line width of each NMR signal at half height and taken into account in the data fitting. Finally, the UV-visible data points were estimated to have an uncertainty of 3% of the total optical signal.

2.2 – Results and discussion

2.2.1 – Order of oxidation of the heme groups

As described above, the individual heme oxidation profiles can be monitored by 2D ^{1}H-EXSY NMR experiments, if the intra- and intermolecular electron exchange rates are fast and slow on the NMR time scale, respectively. The 2D ^{1}H-EXSY NMR spectra obtained for the samples at intermediate levels of oxidation show that the cytochrome PpcA from G. metallireducens meets these requirements in the experimental conditions used, since the heme methyl signals can be followed throughout the different oxidation stages (Figure 2.19).

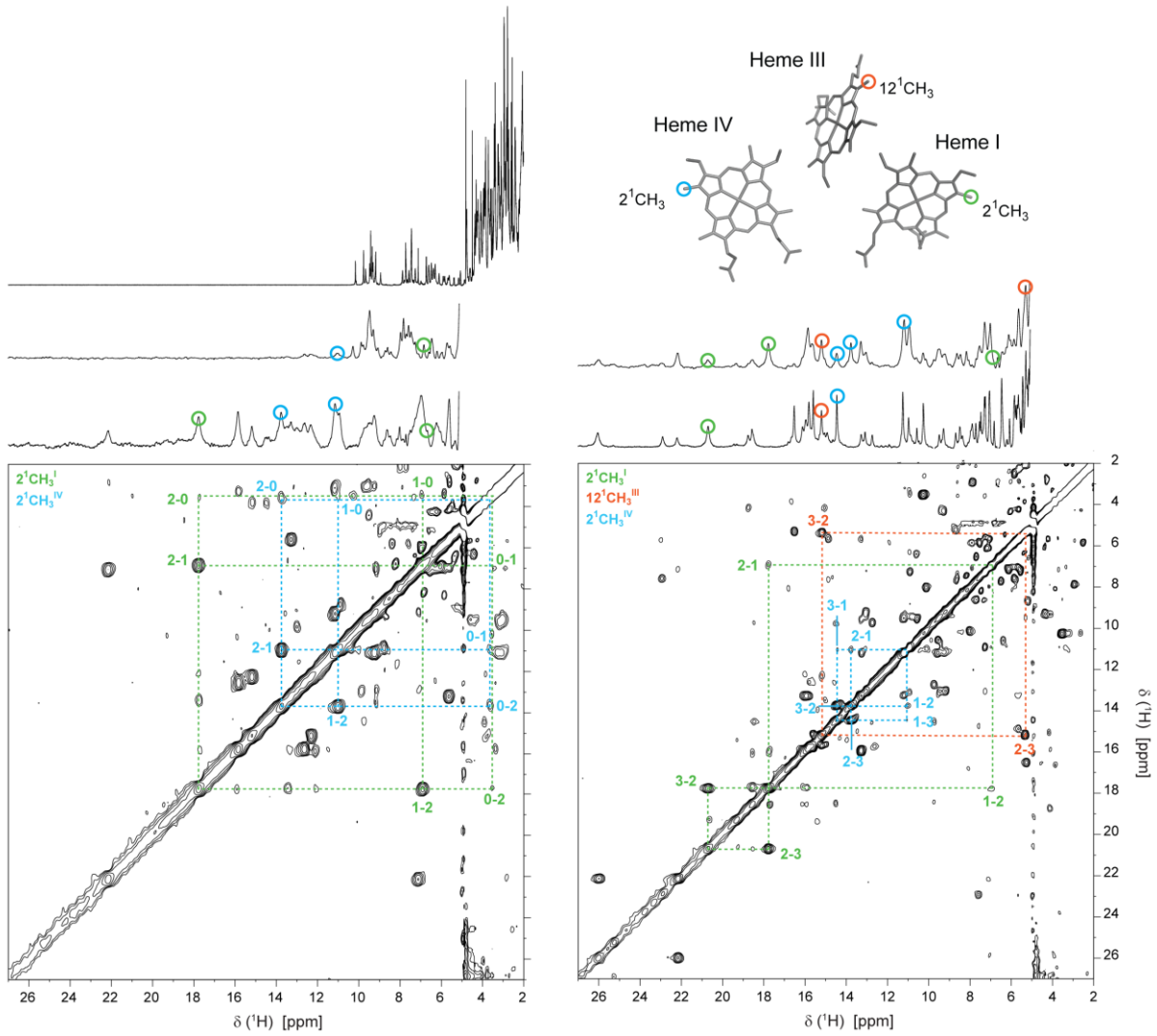

Figure 2.19 – Illustration of the heme oxidation profiles for PpcA from G. metallireducens (pH 5.8, 288 K) – The 1D ^{1}H-NMR spectra, acquired at different stages of oxidation, illustrate the redox titration of the cytochrome. The peaks corresponding to the heme methyls $2^{1}CH_3^{I}$, $12^{1}CH_3^{III}$ and $2^{1}CH_3^{IV}$ (labelled according to the IUPAC-IUB nomenclature for tetrapyrroles [78]) are marked by green, orange and blue circles, respectively. These heme methyls are also highlighted with the same color code in the heme core of PpcA from G. sulfurreducens (PDB ID: 2MZ9 [7]). In the expansions of the 2D ^{1}H-EXSY NMR spectra, the cross-peaks resulting from intermolecular electron transfer between the different oxidation stages (0-3) are indicated by dashed lines for heme methyls $2^{1}CH_3^{I}$ (green), $12^{1}CH_3^{III}$ (orange) and $2^{1}CH_3^{IV}$ (blue).

The chemical shifts of the heme methyls in the reduced state constitute excellent starting points to monitor their variation up to their final position in the fully oxidized state. The assignment of the heme methyls signals in the reduced form was previously obtained at pH 7.1 and 298 K [19]. In this Thesis, the assignment was redone at the experimental conditions used to monitor the heme oxidation profiles of PpcA from G. metallireducens (see Table 6.8).

However, when the hemes show a very small percentage of oxidation in the first oxidation steps, the variation in their chemical shifts is also very small, leading to exchange connectivities that are placed at or near the diagonal of the spectra. This is exactly the case for one of the heme groups in PpcA, as illustrated by the 2D ^{1}H-EXSY NMR spectrum obtained at early stages of oxidation, in Figure 2.19. In fact, only connectivities between oxidation stages 0 and 1 for hemes I and IV could be observed. As discussed below, the first oxidation step is essentially dominated by the oxidation of heme IV, followed by heme I, which prevents the observation of connectivities between stages 0 and 1 for heme III. Consequently, it was not possible to monitor the stepwise oxidation of heme III, starting from the fully reduced state.

In order to overcome this, the assignment of the heme methyls was also carried out in the fully oxidized state (as described in section 2.1.6). The assignment of the hemes methyls and propionates was carried at three different experimental conditions – (i) pH 8.1, 288 K (Figure 6.3 and Table 6.5), (ii) pH 8.1, 298 K (Figure 6.4 and Table 6.6) and (iii) pH 5.8, 288 K (Figure 2.20 and Table 6.7).

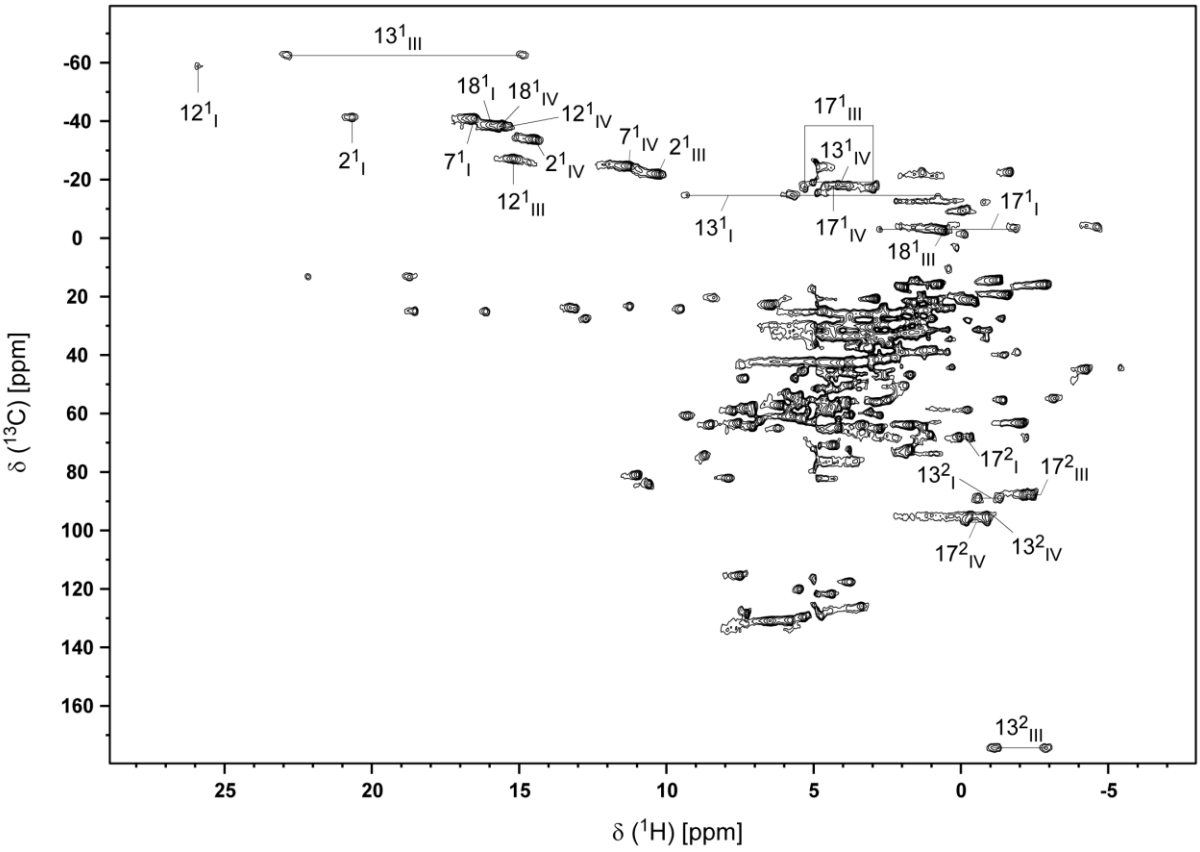

Figure 2.20 – 2D ^{1}H,^{13}C-HMQC spectrum of PpcA from G. metallireducens at pH 5.8, 288 K – The heme methyls and propionates signals are identified in the spectrum, according to the IUPAC-IUB nomenclature for tetrapyrroles [78]. The peaks of the protons connected to the same carbon atom (CH_2 groups) are linked by a straight line. The assignment table can be found in section 6.4.

The chemical shifts of the heme methyls in the oxidized state were then used to follow signals backwards to their position at intermediate oxidation states. This strategy allowed the monitorization of the stepwise oxidation of each heme in the pH range 5.8 – 8.9. As an example, the heme oxidation profiles of the cytochrome, at pH 5.8, are illustrated by the heme methyls $2^1CH_3^I$, $12^1CH_3^{III}$ and $2^1CH_3^{IV}$ in Figure 2.19. The correspondent oxidation fractions were calculated using Equation 11 and the values are listed in Table 2.3 (also see section 6.6).

Table 2.3 – Redox-dependent heme methyl chemical shifts of PpcA from G. metallireducens at pH 5.8, 288 K – The heme methyls $2^1CH_3^I$, $12^1CH_3^{III}$ and $2^1CH_3^{IV}$ were chosen to monitor each heme oxidation through the four oxidation stages (see text). The heme oxidation fractions, x_i, in each stage of oxidation, were calculated according to the equation $x_i = (\delta_i-\delta_0)/(\delta_3-\delta_0)$, where δ_i, δ_0 and δ_3 are the observed chemical shifts of the heme methyl in stage i, 0 (fully reduced) and 3 (fully oxidized), respectively. The value indicated in parenthesis was obtained from the fitting of the thermodynamic model.

pH 5.8	Chemical shift (ppm)			x_i			
Oxidation stage	$2^1CH_3^I$	$12^1CH_3^{III}$	$2^1CH_3^{IV}$	$2^1CH_3^I$	$12^1CH_3^{III}$	$2^1CH_3^{IV}$	$\sum x_i$
0	3.55	3.51	3.64	0.00	0.00	0.00	0
1	6.91	(4.83)	11.02	0.20	0.11	0.68	0.99
2	17.77	5.34	13.76	0.83	0.16	0.94	1.93
3	20.70	15.18	14.45	1.00	1.00	1.00	3.00

In the typical arrangement of the heme core of a triheme cytochrome (Figure 2.19), the selected methyl groups for each heme point away from neighboring hemes and, consequently, the extrinsic contribution to their chemical shifts from the oxidation of neighboring hemes is minimized. The analysis of Table 2.3 confirms that the extrinsic shifts for the selected heme methyls are not significant, since the sums of the oxidation fractions at each oxidation stage are close to integers and, therefore, each methyl reflects the oxidation state of its own heme [71, 89, 91]. The heme oxidation fractions obtained at pH 5.8 show that heme IV clearly dominates the first oxidation step (68%). The largest fractional oxidation of heme I is obtained in the second step (63%), followed by heme III in the last step (84%).

2.2.2 – Thermodynamic properties of PpcA from G. metallireducens

To determine the thermodynamic parameters of PpcA, the pH dependence of the heme methyl chemical shifts, in the pH range 5.8 – 8.9, together with the data from visible redox

titrations obtained at pH 7 and 8 [19], was fitted to the model summarized previously (Figure 2.21).

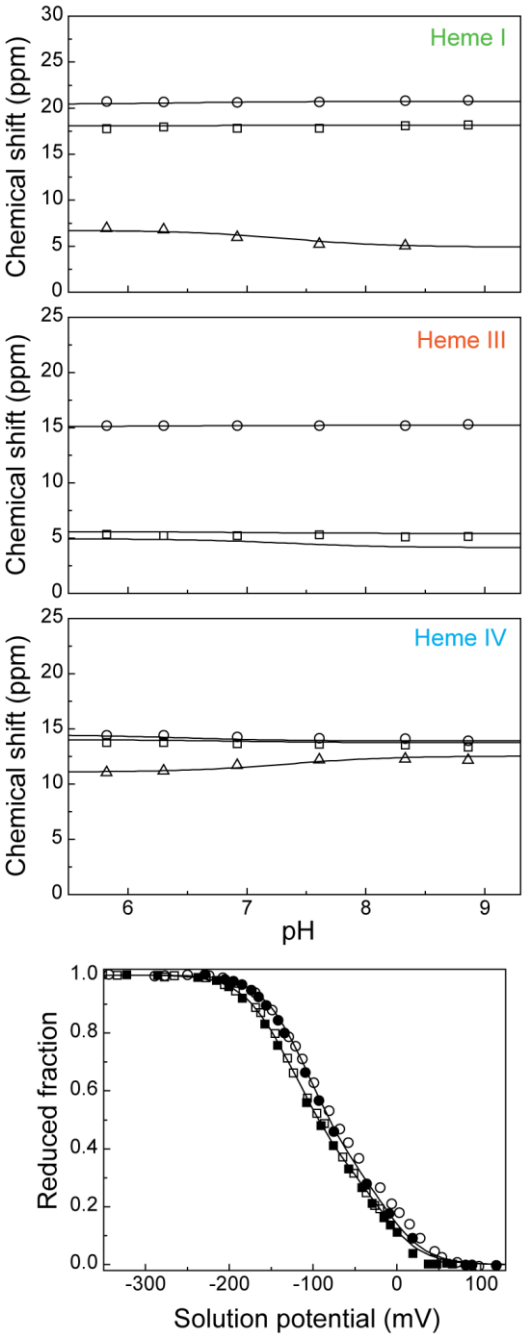

Figure 2.21 – Fitting of the thermodynamic model to the experimental data for PpcA from G. metallireducens - The solid lines are the result of the simultaneous fitting of the NMR and visible data. The upper figures show the pH dependence of heme methyl chemical shifts at oxidation stages one (triangles), two (squares) and three (circles). The chemical shift of the heme methyls in the fully reduced stage (stage 0) are not plotted since they are unaffected by the pH. The bottom figure corresponds to the reduced fraction of the cytochrome, determined by visible spectroscopy at pH 7 (circles) and pH 8 (squares). The open and filled symbols represent the data points in the reductive and oxidative titrations, respectively.

The quality of the fitting obtained clearly shows that the thermodynamic properties of PpcA are well described by the model. The thermodynamic parameters and the macroscopic pK_a values associated with the four stages of oxidation are indicated in Table 2.4.

Table 2.4 – Thermodynamic parameters (mV) of the fully reduced and protonated form of PpcA, obtained at 288 K and 250 mM ionic strength – Diagonal terms (in bold) represent the redox potentials of the three hemes and the redox potential of the redox-Bohr center, in the fully reduced and protonated protein. Off-diagonal values are the redox (heme-heme) and redox-Bohr (heme-proton) interaction redox potentials. The standard errors are given in parenthesis. All the redox potentials presented are relative to NHE. The pK_a values of the redox-Bohr center, at the different oxidation stages, are also indicated.

	Redox potential (mV)			
	Heme I	Heme III	Heme IV	Redox-Bohr center
Heme I	-80 (6)	35 (4)	2 (5)	-22 (6)
Heme III		-70 (7)	33 (7)	-23 (7)
Heme IV			-113 (6)	-49 (6)
Redox-Bohr center				477 (13)

pK_a	Stage 0	Stage 1	Stage 2	Stage 3
	8.1	7.3	6.9	6.5

The macroscopic pK_a values of the fully reduced and oxidized states of the protein are given by Equations 13 and 14, respectively (see section 2.1.7):

$$pK_a\ (Stage\ 0) = \ g_H F/(2.3RT) \tag{13}$$

$$pK_a\ (Stage\ 1-3) = (g_H + \Sigma_{i=1}^{3} g_{iH})F/(2.3RT) \tag{14}$$

The parameters show that the microscopic reduction potentials of the hemes are different and negative: -80, -70 and -113 for hemes I, III and IV, respectively. Compared with the data available for homologous cytochromes, the reduction potentials of the hemes in PpcA from G. metallireducens are considerably less negative, though at a smaller extent for heme IV (Table 2.5).

Table 2.5 – Heme reduction potentials of triheme cytochromes from G. metallireducens (Gm), G. sulfurreducens (Gs) and Desulfuromonas acetoxidans (Da) in the fully reduced and protonated state – The presented values are relative to NHE and were calculated at 288 K.

Cytochrome	Heme reduction potentials (mV)		
	Heme I	Heme III	Heme IV
GmPpcA (this Thesis)	-80	-70	-113
GsPpcA [6]	-154	-138	-125
GsPpcB [6]	-150	-166	-125
GsPpcD [6]	-156	-139	-149
GsPpcE [6]	-167	-175	-116
Dac_7 [60]	-201	-200	-142

The structural analysis carried out by the comparison of the heme substituents and backbone NMR chemical shifts of PpcA from G. metallireducens, with those obtained for the homologous cytochrome from G. sulfurreducens in a previous study, showed that the non-conserved residues are responsible for important local conformational changes in the vicinity of hemes I and III [19], which might explain the differences observed in the reduction potential values of the hemes.

The thermodynamic parameters of PpcA from G. metallireducens also showed that the redox interactions for each pair of hemes are positive, indicating that the oxidation of one heme makes difficult the oxidation of its neighbor. As expected from the heme core architecture (Figure 2.19), the higher redox interaction values are of the same magnitude and are observed for the closest pairs of hemes: I-III (35 mV) and III-IV (37 mV). Furthermore, the redox-Bohr interactions are negative, which indicates that the removal of proton(s), upon deprotonation of the redox-Bohr center, lowers the affinity for electrons by the heme groups (lower reduction potential values) and vice-versa. Heme IV shows the highest redox-Bohr interaction (-49 mV), which suggests that the redox-Bohr center is located in its vicinity. This was independently confirmed by the analysis of the pH dependence of all heme methyl chemical shifts, which showed that methyl $12^1CH_3^{IV}$ is clearly the most affected one (Figure 2.22). The full pH titration of the cytochrome, in the oxidized state, is presented in section 6.5 (Figures 6.5-6.7). The pH dependence analysis was carried out by comparing the values of the heme methyls chemical shifts at pH 5.8 and pH 8.1.

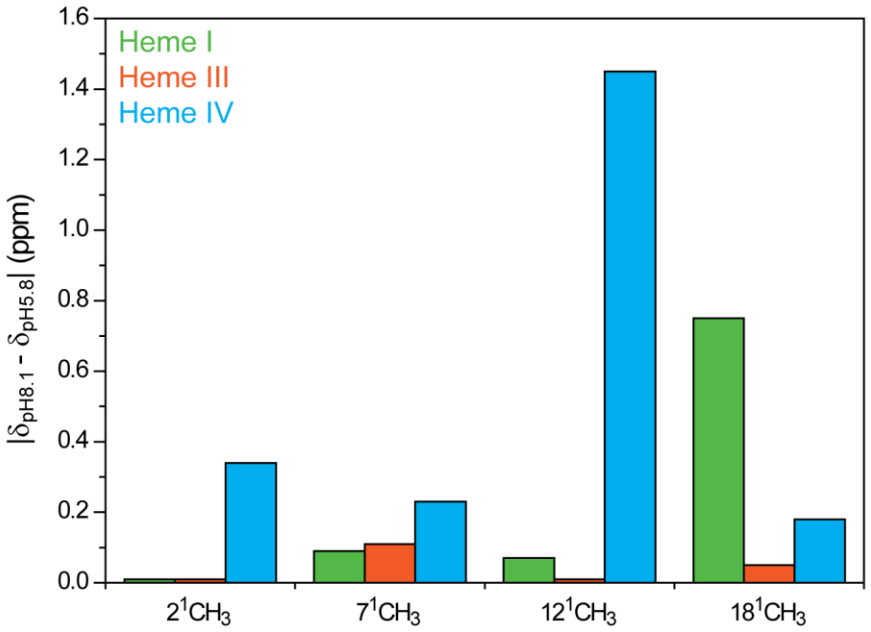

Figure 2.22 – pH dependence of the heme methyl proton chemical shifts of PpcA from G. metallireducens in the oxidized state – The chemical shift variations were calculated between pH 8.1 and 5.8. The green, orange and blue bars represent the variations observed for the hemes I, III and IV methyls, respectively. The complete lists of the assigned heme methyls are provided in section 6.4.

2.2.3 – The effect of pH on the heme oxidation profiles

Previously, it was shown that the cytochrome PpcA from G. metallireducens has visible redox titration curves that are pH dependent (redox-Bohr effect) [19]. The data obtained in this Thesis clearly confirms this observation, since the macroscopic pK_a values of the redox-Bohr center are significantly different in the reduced and oxidized states (8.1 and 6.5, respectively – Table 2.4). From the thermodynamic parameters (Table 2.4), it is possible to establish the order of oxidation of the hemes for the fully reduced and protonated protein, which is IV-I-III (-113, -80 and -70 mV, respectively). As mentioned before, the negative redox-Bohr interactions decrease the affinity of the hemes for electrons. This is, in fact, reflected in the heme reduction potentials of the fully reduced and deprotonated protein, which can be obtained by the simple sum of the heme reduction potentials of the fully reduced and protonated state with their respective redox-Bohr interactions: -162, -102 and -93 mV for hemes IV, I and III, respectively (Table 2.4).

Since the solution pH modulates the affinity of the hemes for electrons in PpcA, the individual heme oxidation profiles were analyzed, inside and outside the physiological pH range (Figure 2.23).

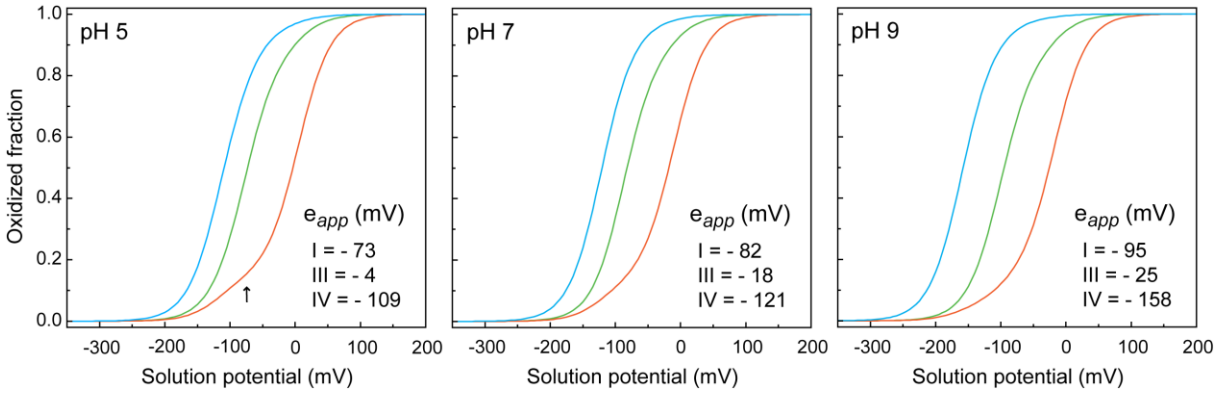

Figure 2.23 – Redox dependence of the heme oxidation fractions of PpcA from G. metallireducens at different pH values – The curves (green, orange and blue for hemes I, III and IV, respectively) were calculated as a function of the solution reduction potential (relative to NHE) using the parameters listed in Table 2.4. The midpoint reduction potentials of the hemes (e_{app}) are also indicated. The arrow highlights the deviation from a pure Nernst curve.

The shape of the heme redox curves differs from a pure Nernst curve, which indicates that the heme electron affinity is also modulated by the heme-heme redox interactions. This is particularly notorious for heme III at pH 5 (see arrow in Figure 2.23). In fact, at low pH, the e_{app} values (i.e. the point at which the oxidized and reduced fractions of each heme group are equally populated) of the first two hemes to oxidize (hemes I and IV) are close to each other. Consequently, as their oxidation progresses, the oxidation curve of heme III shifts to higher reduction potential values, as a result of the large redox interactions with hemes I and IV (35 and 37 mV, respectively).

Overall, the individual heme oxidation profiles in the pH range 5 to 9 show that the relative order of oxidation remains unaltered (Figure 2.23). This is explained by the largest redox-Bohr interaction showed by heme IV (-49 mV), the first heme to oxidize, compared to the nearly identical redox-Bohr interactions of hemes I and III (-22 and -23 mV, respectively). Although the order of oxidation of the heme groups is independent from the pH, the redox-Bohr center still plays a role in the modulation of the e_{app} values, as they decrease with the solution pH (Figure 2.23). Due to the higher redox-Bohr interaction, this is particularly notorious for the heme IV curve, which progressively deviates from those of the other hemes, with the increase of pH (Figure 2.23).

2.2.4 – Functional mechanism of PpcA at physiological pH

The redox-Bohr effect is functionally relevant if observed at the physiological pH range for cellular growth. The optimal growth for G. metallireducens cells occurs between pH 7 and 8 [92,

93]. Therefore, to further rationalize the effect of the protonation/deprotonation of the redox-Bohr center in the functional mechanism of the cytochrome PpcA, the fractional contributions of the 16 microstates were determined at pH 5, 7 and 9, in order to obtain functional mechanistic insights on the electron transfer pathways of the protein (Figure 2.24A).

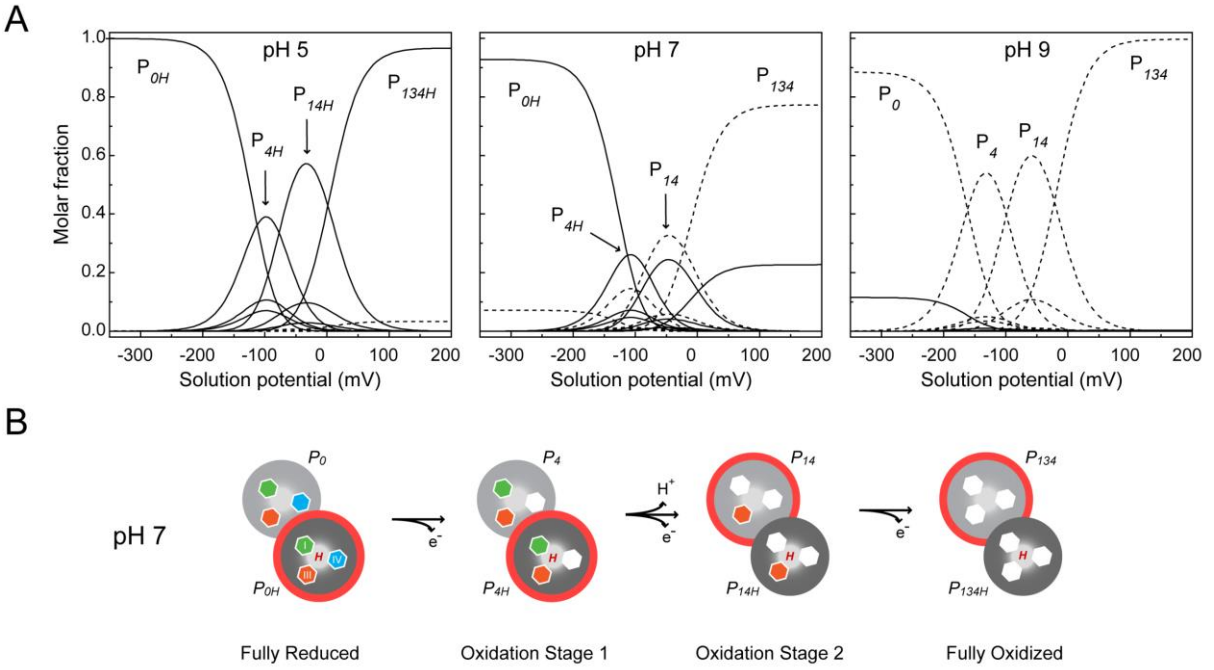

Figure 2.24 – Electron/proton transfer pathways of PpcA from G. metallireducens – (A) Redox dependence of the molar fractions of the 16 microstates of the cytochrome, at different pH values. The curves were calculated as a function of the solution reduction potential (relative to NHE) using the parameters listed in Table 2.4. Solid and dashed lines indicate the protonated and deprotonated microstates, respectively. For clarity, only the dominant microstates are labelled. (B) Preferential electron/proton coupled transfer pathway of PpcA from G. metallireducens, at physiological pH. The figure is represented with the same features of Figure 2.17, although in a simpler extend, for clarity. The dominant microstates are highlighted by red circles.

The analysis of Figure 2.24A shows that the relevant microstates are quite distinct at different pH values. At values outside the physiological pH range, the dominant microstates are all protonated (pH 5) or deprotonated (pH 9). However, at pH 7, stage 0 is dominated by the protonated form P_{0H} and stage 1 is dominated by the oxidation of heme IV (P_{4H}), while keeping the redox-Bohr protonated. Stage 2 is then dominated by the oxidation of heme I and deprotonation of the acid-base center (P_{14}), which remains deprotonated in stage 3 (P_{134}). Therefore, at pH 7, the following route is defined for the electrons: $P_{0H} \rightarrow P_{4H} \rightarrow P_{14} \rightarrow P_{134}$ (Figure 2.24B). This clearly indicates that at physiological pH, a concerted e^-/H^+ transfer occurs between oxidation stages 1 and 2.

2.2.5 – Functional comparison with the homologous PpcA from G. sulfurreducens

The optimal growth of Geobacter bacteria occurs at pH values between 7 and 8 [92, 93]. G. metallireducens and G. sulfurreducens have similar optimal growth conditions and there are evidences that the bacterial growth is severely affected with slight pH changes (down to one pH unit) [94]. Direct measurements of the periplasmic pH in the Gram-negative bacterium E. coli showed that the periplasmic pH remains at or near the pH of the external medium [95]. Therefore, it is reasonable to assume that in Gram-negative Geobacter bacteria, the periplasmic pH would also be close to that of the external medium.

In this section, the functional properties of the homologous PpcA cytochromes from G. metallireducens and G. sulfurreducens are analyzed and compared at pH 7. In Table 2.6, some of the main thermodynamic features of these two cytochromes are presented.

Table 2.6 – Thermodynamic parameters of the fully reduced and protonated forms of PpcA from G. metallireducens (Gm) and PpcA from G. sulfurreducens (Gs), obtained at 288 K and 250 mM ionic strength – Redox potentials are relative to NHE. Standard errors are given in parenthesis. The pK_a values of the different oxidation stages were obtained from Equations 13 and 14.

	Redox centers	PpcA Gm	PpcA Gs [96]
Heme redox potentials (mV)	I	-80 (6)	-154 (5)
	III	-70 (7)	-138 (5)
	IV	-113 (6)	-125 (5)
Heme-heme redox interactions (mV)	I-III	35 (4)	27 (2)
	I-IV	3 (5)	16 (3)
	III-IV	37 (7)	41 (3)
Redox-Bohr interactions (mV)	I-H	-22 (6)	-32 (4)
	III-H	-23 (7)	-31 (4)
	IV-H	-49 (6)	-58 (4)
pK_a	Stage 0	8.1 (0.1)	8.6 (0.1)
	Stage 1	7.3 (0.1)	8.0 (0.1)
	Stage 2	6.9 (0.1)	7.2 (0.1)
	Stage 3	6.5 (0.1)	6.5 (0.1)

The analysis of Table 2.6 shows that, in general, the thermodynamic parameters of the two proteins are comparable. This is expected considering their amino acid sequence identity (80%), as well as the conservation of the heme core and heme axial coordinations. Interestingly, in both proteins, the strongest redox-Bohr interactions occur with heme IV. The carboxylate group of heme IV propionate 13 (P_{13}^{IV}) was suggested to be the redox-Bohr center of PpcA from G.

sulfurreducens [5]. Considering the high homology between both cytochromes, the conservation of the heme IV architecture [19], as well as the equivalent magnitude of the redox-Bohr interactions, this propionate is most likely the acid-base center of the PpcA from G. metallireducens, as well.

Despite this, the variation of the heme reduction potentials values, which reflect local changes in the surrounding environments of hemes I and III, leads to a different order of oxidation at pH 7: IV-I-III for PpcA from G. metallireducens and I-IV-III for PpcA from G. sulfurreducens. This also has an impact in the dominant microstates at each oxidation stage (Figure 2.25).

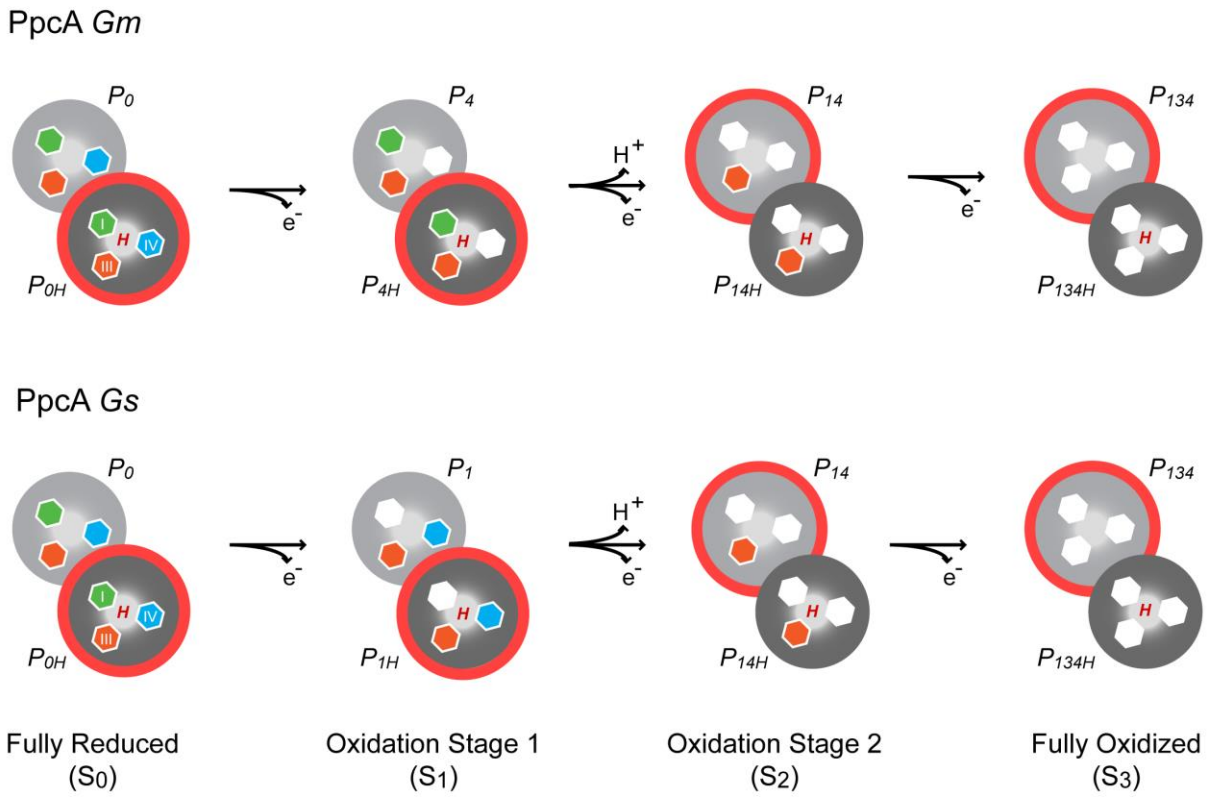

Figure 2.25 – Preferential electron/proton coupled transfer pathways in the homologous PpcA cytochromes from G. metallireducens (Gm) and G. sulfurreducens (Gs) at physiological pH (pH 7) – The figure is represented with the same features of Figure 2.17, with the only difference being the highlighted (red circles) dominant microstates that are part of the preferential electron/proton transfer pathways of both cytochromes.

It is important to note that despite the differences observed in the order of oxidation of the hemes, both cytochromes display a preferential electron/proton pathway and, therefore, contribute to e^-/H^+ energy transduction processes at physiological pH. The comparison between the preferential pathways of electron transfer in G. metallireducens ($P_{0H} \rightarrow P_{4H} \rightarrow P_{14} \rightarrow P_{134}$) and G. sulfurreducens ($P_{0H} \rightarrow P_{1H} \rightarrow P_{14} \rightarrow P_{134}$ [96]) also shows that the proteins are designed

to assure a directional electron transfer to acceptors, involving the same dominant microstates, except those of the first oxidation stage (P_{4H} and P_{1H} for G. metallireducens and G. sulfurreducens, respectively), as result of the change in the reduction potential values of heme I.

The ability of these cytochromes to transfer H^+ may represent additional mechanisms contributing to the proton electrochemical potential gradient across the periplasmic membrane that drives ATP synthesis, as previously suggested [96]. In fact, it has been proven that the use of extracellular electron acceptors (instead of the usual soluble electron acceptors, such as fumarate) by Geobacter bacteria leads to a decrease in biomass production, due to the dissipation of the membrane potential by cytoplasm acidification [97]. In contrast, the cytoplasmic H^+ produced from acetate oxidation are consumed in the cytoplasm when fumarate is the terminal electron acceptor. Through metabolic simulation studies, Mahadevan and co-workers [97] showed that cellular growth in the presence of insoluble electron acceptors is only possible when additional e^-/H^+ coupling mechanisms are present (when compared with the number of mechanisms existing in cellular growth with fumarate respiration). These additional mechanisms most likely involve the coupling of electron transfer to periplasmic cytochromes with proton translocation, leading to additional membrane potential and consequent ATP production by ATP synthase. Although there are no studies that show how G. metallireducens metabolically behaves outside the physiological pH, one may infer that the bacterium is going to have a similar behavior to G. sulfurreducens. In a study involving the PpcA and PpcD cytochromes from G. sulfurreducens [96], it was suggested that G. sulfurreducens probably becomes metabolically inactive at pH 6 or lower because of the insufficient proton translocation across the IM at those conditions, which is related with the fact that those periplasmic cytochromes only perform e^-/H^+ at pH values between 7-8 [94, 98-100]. This hypothesis further supports the importance of the PpcA cytochrome in the metabolic regulation of G. metallireducens.

2.3 – Conclusions

In this Chapter, NMR and visible spectroscopic data were used to probe the functional properties of the triheme cytochrome PpcA from G. metallireducens. In order to achieve this, the assignment of the heme methyl NMR signals was carried out for the fully reduced and oxidized states. These assignments constituted the starting points for the thermodynamic studies, performed by probing the heme methyl chemical shift variation during the protein oxidation at different pH values. These data, together with data obtained from visible redox titrations, were fitted with the thermodynamic model that allowed the determination of the heme reduction potentials, the heme interactions and the properties of the redox-Bohr center.

The results obtained showed that the heme reduction potentials of the cytochrome PpcA are modulated by heme-heme interactions and by interactions with the redox-Bohr center, located in the vicinity of heme IV (probably the carboxylate group of the P_{13}^{IV}). The order of oxidation of the hemes is pH independent, however, the cytochrome is designed to perform e^-/H^+ within the cellular optimal pH range for growth, reinforcing the physiological significance of the redox-Bohr effect observed.

A comparative analysis with the PpcA from G. sulfurreducens demonstrated that the homologous cytochromes may have similar functions, participating in electron transfer and contributing to additional membrane potential and consequent ATP production. However, the homologous cytochromes possess some different functional features that would be interesting to explore, considering the high sequence identity between the two cytochromes (80%). This would lead to a better understanding of how the polypeptide chain of closely related proteins uniquely modulates the properties of their cofactors to assure effectiveness in their respective metabolic pathways. In fact, the data obtained suggests that although the G. sulfurreducens and G. metallireducens bacteria are very similar, the last one is optimized to probably function at less negative redox potential windows. Since previous studies on G. sulfurreducens biofilms have shown that the electrochemical responses are mainly driven by the highly abundant periplasmic cytochromes (such as PpcA) [101-103], one can conclude that the higher reduction potential values of the cytochrome PpcA from G. metallireducens also suggest that in this bacterium, the electron transfer from cytoplasmic electron donors towards periplasmic cytochromes is accomplished with higher driving force, conferring extracellular electron transfer directionality.

2.4 – References

[1] Y.H. Ding, K.K. Hixson, C.S. Giometti, A. Stanley, A. Esteve-Núñez, T. Khare, S.L. Tollaksen, W. Zhu, J.N. Adkins, M.S. Lipton, R.D. Smith, T. Mester, D.R. Lovley, The proteome of dissimilatory metal-reducing microorganism Geobacter sulfurreducens under various growth conditions, Biochim. Biophys. Acta, 1764 (2006) 1198-1206.

[2] J.R. Lloyd, C. Leang, A.L. Hodges Myerson, M.V. Coppi, S. Cuifo, B. Methe, S.J. Sandler, D.R. Lovley, Biochemical and genetic characterization of PpcA, a periplasmic c-type cytochrome in Geobacter sulfurreducens, Biochem. J., 369 (2003) 153-161.

[3] J.M. Dantas, L. Morgado, M. Aklujkar, M. Bruix, Y.Y. Londer, M. Schiffer, P.R. Pokkuluri, C.A. Salgueiro, Rational engineering of Geobacter sulfurreducens electron transfer components: A foundation for building improved Geobacter-based bioelectrochemical technologies, Front. Microbiol., 6 (2015) 752.

[4] L. Morgado, M. Bruix, Y.Y. Londer, P.R. Pokkuluri, M. Schiffer, C.A. Salgueiro, Redox-linked conformational changes of a multiheme cytochrome from Geobacter sulfurreducens, Biochem. Bioph. Res. Co., 360 (2007) 194-198.

[5] L. Morgado, M. Bruix, V. Orshonsky, Y.Y. Londer, N.E. Duke, X. Yang, P.R. Pokkuluri, M. Schiffer, C.A. Salgueiro, Structural insights into the modulation of the redox properties of two Geobacter sulfurreducens homologous triheme cytochromes, Biochim. Biophys. Acta, 1777 (2008) 1157-1165.

[6] L. Morgado, M. Bruix, M. Pessanha, Y.Y. Londer, C.A. Salgueiro, Thermodynamic characterization of a triheme cytochrome family from Geobacter sulfurreducens reveals mechanistic and functional diversity, Biophys. J., 99 (2010) 293-301.

[7] L. Morgado, M. Bruix, P.R. Pokkuluri, C.A. Salgueiro, D.L. Turner, Redox- and pH-linked conformational changes in triheme cytochrome PpcA from Geobacter sulfurreducens, Biochem. J., 474 (2017) 231-246.

[8] L. Morgado, J.M. Dantas, T. Simões, Y.Y. Londer, P.R. Pokkuluri, C.A. Salgueiro, Role of Met^{58} in the regulation of electron/proton transfer in trihaem cytochrome PpcA from Geobacter sulfurreducens, Bioscience Rep., 33 (2013).

[9] L. Morgado, S. Lourenço, Y.Y. Londer, M. Schiffer, P.R. Pokkuluri, C.A. Salgueiro, Dissecting the functional role of key residues in triheme cytochrome PpcA: A path to rational design of G. sulfurreducens strains with enhanced electron transfer capabilities, PLoS One, 9 (2014) e105566.

[10] L. Morgado, V.B. Paixão, M. Schiffer, P.R. Pokkuluri, M. Bruix, C.A. Salgueiro, Revealing the structural origin of the redox-Bohr effect: The first solution structure of a cytochrome from Geobacter sulfurreducens, Biochem. J., 441 (2012) 179-187.

[11] L. Morgado, I.H. Saraiva, R.O. Louro, C.A. Salgueiro, Orientation of the axial ligands and magnetic properties of the hemes in the triheme ferricytochrome PpcA from G. sulfurreducens determined by paramagnetic NMR, FEBS Lett., 584 (2010) 3442-3445.

[12] M. Pessanha, Y.Y. Londer, W.C. Long, J. Erickson, P.R. Pokkuluri, M. Schiffer, C.A. Salgueiro, Redox characterization of Geobacter sulfurreducens cytochrome c_7: Physiological relevance of the conserved residue F15 probed by site-specific mutagenesis, Biochemistry, 43 (2004) 9909-9917.

[13] M. Pessanha, L. Morgado, R.O. Louro, Y.Y. Londer, P.R. Pokkuluri, M. Schiffer, C.A. Salgueiro, Thermodynamic characterization of triheme cytochrome PpcA from Geobacter sulfurreducens: Evidence for a role played in e^-/H^+ energy transduction, Biochemistry, 45 (2006) 13910-13917.

[14] E. Afkar, Y. Fukumori, Purification and characterization of triheme cytochrome c_7 from the metal-reducing bacterium, Geobacter metallireducens, FEMS Microbiol. Lett., 175 (1999) 205-210.

[15] J.E. Champine, B. Underhill, J.M. Johnston, W.W. Lilly, S. Goodwin, Electron transfer in the dissimilatory iron-reducing bacterium Geobacter metallireducens, Anaerobe, 6 (2000) 187-196.

[16] The UniProt Consortium, UniProt: The universal protein knowledgebase, Nucleic Acids Res., 45 (2017) D158-D169.

[17] J.M. Dantas, L. Morgado, A.C. Marques, C.A. Salgueiro, Probing the effect of ionic strength on the functional robustness of the triheme cytochrome PpcA from Geobacter sulfurreducens: A contribution for optimizing biofuel cell's power density, J. Phys. Chem. B, 118 (2014) 12416-12425.

[18] N. Ponomarenko, J. Niklas, P.R. Pokkuluri, O. Poluektov, D.M. Tiede, Electron paramagnetic resonance characterization of the triheme cytochrome from Geobacter sulfurreducens, Biochemistry, 57 (2018) 1722-1732.

[19] P.C. Portela, T.M. Fernandes, J.M. Dantas, M.R. Ferreira, C.A. Salgueiro, Biochemical and functional insights on the triheme cytochrome PpcA from Geobacter metallireducens, Arch. Biochem. Biophys., 644 (2018) 8-16.

[20] B. Jacobson, W.A. Anderson, J.T. Arnold, A proton magnetic resonance study of the hydration of deoxyribonucleic acid, Nature, 173 (1954) 772.

[21] M. Saunders, A. Wishnia, J.G. Kirkwood, The nuclear magnetic resonance spectrum of ribonuclease 1, J. Am. Chem. Soc., 79 (1957) 3289-3290.

[22] M.P. Williamson, T.F. Havel, K. Wüthrich, Solution conformation of proteinase inhibitor IIA from bull seminal plasma by ^{1}H nuclear magnetic resonance and distance geometry, J. Mol. Biol., 182 (1985) 295-315.

[23] G.S. Rule, T.K. Hitchens, Fundamentals of protein NMR spectroscopy, First edition, Springer, Netherlands, 2006.

[24] J. Larmor, LXIII. On the theory of the magnetic influence on spectra and on the radiation from moving ions, Lond. Edinb. Dubl. Phil. Mag. J. Sci., 44 (1897) 503-512.

[25] R.J. Abraham, M. Mobli, Modelling ^{1}H NMR spectra of organic compounds: Theory, applications and NMR prediction software, First edition, Wiley-VCH, West Sussex, 2008.

[26] V. Kanelis, J.D. Forman-Kay, L.E. Kay, Multidimensional NMR methods for protein structure determination, IUBMB Life, 52 (2008) 291-302.
[27] S. Grzesiek, H.-J. Sass, From biomolecular structure to functional understanding: New NMR developments narrow the gap, Curr. Opin. Struc. Biol., 19 (2009) 585-595.
[28] K.R. Keshari, D.M. Wilson, Chemistry and biochemistry of ^{13}C hyperpolarized magnetic resonance using dynamic nuclear polarization, Chem. Soc. Rev., 43 (2014) 1627-1659.
[29] J. Jeener, B.H. Meier, P. Bachmann, R.R. Ernst, Investigation of exchange processes by two-dimensional NMR spectroscopy, J. Chem. Phys., 71 (1979) 4546-4553.
[30] H.C. Gaede, NMR exchange spectroscopy, Modern NMR spectroscopy in education, Am. Chem. Soc., 2007, 176-189.
[31] G. Fischer, E. Kleinpeter, Application of 2D EXSY NMR spectroscopy to the study of the dynamic behaviour of aroylcyanoketene-S,S-dimethylacetals, Magn. Reson. Chem., 29 (1991) 204-206.
[32] C.L. Perrin, T.J. Dwyer, Application of two-dimensional NMR to kinetics of chemical exchange, Chem. Rev., 90 (1990) 935-967.
[33] C.A. Salgueiro, J.M. Dantas, Multiheme cytochromes, Protein folding and structure, Springer-Verlag Berlin Heidelberg, 2017.
[34] K. Ono, K. Kimura, T. Yagi, H. Inokuchi, Mössbauer study of cytochrome c_3, J. Chem. Phys., 63 (1975) 1640-1642.
[35] H. Drucker, L.L. Campbell, R.W. Woody, Optical rotatory properties of the cytochromes c_3 from three species of Desulfovibrio, Biochemistry, 9 (1970) 1519-1527.
[36] G.R. Bell, J.-P. Lee, H.D. Peck, J. Le Gall, Reactivity of Desulfovibrio gigas hydrogenase toward artificial and natural electron donors or acceptors, Biochimie, 60 (1978) 315-320.
[37] D.V. DerVartanian, J. Le Gall, A monomolecular electron transfer chain: Structure and function of cytochrome c_3, Biochim. Biophys. Acta - Rev. Bioenergetics, 346 (1974) 79-99.
[38] J. Le Gall, M. Bruschi-Heriaud, D.V. DerVartanian, Electron paramagnetic resonance and light absorption studies on c-type cytochromes of the anaerobic sulfate reducer Desulfovibrio, Biochim. Biophys. Acta, 234 (1971) 499-512.
[39] A.V. Xavier, J.J.G. Moura, J. Le Gall, D.V. Dervartanian, Oxidation-reduction potentials of the hemes in cytochrome c_3 from Desulfovibrio gigas in the presence and absence of ferredoxin by EPR spectroscopy, Biochimie, 61 (1979) 689-695.
[40] C.M. Dobson, N.J. Hoyle, C.F. Geraldes, M. Bruschi, J. Le Gall, P.E. Wright, R.J. Williams, Outline structure of cytochrome c_3 and consideration of its properties, Nature, 249 (1974) 425-429.
[41] S. Forsén, R.A. Hoffman, Study of moderately rapid chemical exchange reactions by means of nuclear magnetic double resonance, J. Chem. Phys., 39 (1963) 2892-2901.
[42] C.C. McDonald, W.D. Phillips, J. Le Gall, Proton magnetic resonance studies of Desulfovibrio cytochromes c_3, Biochemistry, 13 (1974) 1952-1959.

[43] J.J.G. Moura, H. Santos, I. Moura, G.J. Le, G.R. Moore, R.J. Williams, A.V. Xavier, NMR redox studies of Desrulfovibrio vulgaris cytochrome c_3, Eur. J. Biochem., 127 (1982) 151-155.

[44] A.V. Xavier, J.J.G. Moura, NMR studies of electron carrier proteins from sulphate reducing bacteria, Biochimie, 60 (1978) 327-338.

[45] P. Bianco, J. Haladjian, Study of cytochromes c_3 from Desulfovibrio vulgaris (Hildenborough) and Desulfovibrio desulfuricans (Norway) by differential pulse polarography and spectroelectrochemical method, Biochim. Biophys. Acta - Bioenergetics, 545 (1979) 86-93.

[46] P. Bianco, J. Haladjian, Current-potential responses for a tetrahemic protein: A method of determining the individual half-wave potentials of cytochrome c_3 from Desulfovibrio desulfuricans strain Norway, Electrochim. Acta, 26 (1981) 1001-1004.

[47] M.J. Eddowes, H. Elzanowska, H.A.O. Hill, Electrochemistry of cytochrome c_3 from Desulfovibrio desulphuricans (Norway), Biochem. Soc. T., 7 (1979) 735.

[48] K. Niki, T. Yagi, H. Inokuchi, K. Kimura, Electrochemical behavior of cytochrome c_3 of Desulfovibrio vulgaris, strain Miyazaki, on the mercury electrode, J. Am. Chem. Soc., 101 (1979) 3335-3340.

[49] W.F. Sokol, D.H. Evans, K. Niki, T. Yagi, Reversible voltammetric response for a molecule containing four non-equivalent redox sites with application to cytochrome c_3 of Desulfovibrio vulgaris, strain Miyazaki, J. Electroanal. Chem. Interfacial Electrochem., 108 (1980) 107-115.

[50] J.W. van Leeuwen, C. van Dijk, H.J. Grande, C. Veeger, A pulse-radiolysis study of cytochrome c_3, Eur. J. Biochem., 127 (1982) 631-638.

[51] H. Santos, D.L. Turner, A.V. Xavier, J. Le Gall, Two-dimensional NMR studies of electron transfer in cytochrome c_3, J. Magn. Reson., 59 (1984) 177-180.

[52] J.M. Dantas, L. Morgado, Y.Y. Londer, A.P. Fernandes, R.O. Louro, P.R. Pokkuluri, M. Schiffer, C.A. Salgueiro, Pivotal role of the strictly conserved aromatic residue F15 in the cytochrome c_7 family, J. Biol. Inorg. Chem., 17 (2012) 11-24.

[53] J.M. Dantas, T. Simões, L. Morgado, C. Caciones, A.P. Fernandes, M.A. Silva, M. Bruix, P.R. Pokkuluri, C.A. Salgueiro, Unveiling the structural basis that regulates the energy transduction properties within a family of triheme cytochromes from Geobacter sulfurreducens, J. Phys. Chem. B, 120 (2016) 10221-10233.

[54] A.S. Alves, N.L. Costa, M. Tien, R.O. Louro, C.M. Paquete, Modulation of the reactivity of multiheme cytochromes by site-directed mutagenesis: Moving towards the optimization of microbial electrochemical technologies, J. Biol. Inorg. Chem., 22 (2017) 87-97.

[55] B.M. Fonseca, I.H. Saraiva, C.M. Paquete, C.M. Soares, I. Pacheco, C.A. Salgueiro, R.O. Louro, The tetraheme cytochrome from Shewanella oneidensis MR-1 shows thermodynamic bias for functional specificity of the hemes, J. Biol. Inorg. Chem., 14 (2009) 375-385.

[56] C.M. Paquete, R.O. Louro, Molecular details of multielectron transfer: The case of multiheme cytochromes from metal respiring organisms, Dalton T., 39 (2010) 4259-4266.

[57] M. Pessanha, R.O. Louro, I.J. Correia, E.L. Rothery, K.L. Pankhurst, G.A. Reid, S.K. Chapman, D.L. Turner, C.A. Salgueiro, Thermodynamic characterization of a tetrahaem cytochrome isolated from a facultative aerobic bacterium, Shewanella frigidimarina: A putative redox model for flavocytochrome c_3, Biochem. J., 370 (2003) 489-495.

[58] M. Pessanha, E.L. Rothery, R.O. Louro, D.L. Turner, C.S. Miles, G.A. Reid, S.K. Chapman, A.V. Xavier, C.A. Salgueiro, Redox behaviour of the haem domain of flavocytochrome c_3 from Shewanella frigidimarina probed by NMR, FEBS Lett., 578 (2004) 185-190.

[59] M. Pessanha, E.L. Rothery, C.S. Miles, G.A. Reid, S.K. Chapman, R.O. Louro, D.L. Turner, C.A. Salgueiro, A.V. Xavier, Tuning of functional heme reduction potentials in Shewanella fumarate reductases, Biochim. Biophys. Acta, 1787 (2009) 113-120.

[60] I.J. Correia, C.M. Paquete, R.O. Louro, T. Catarino, D.L. Turner, A.V. Xavier, Thermodynamic and kinetic characterization of trihaem cytochrome c_3 from Desulfuromonas acetoxidans, Eur. J. Biochem., 269 (2002) 5722-5730.

[61] I.J. Correia, C.M. Paquete, A. Coelho, C.C. Almeida, T. Catarino, R.O. Louro, C. Frazão, L.M. Saraiva, M.A. Carrondo, D.L. Turner, A.V. Xavier, Proton-assisted two-electron transfer in natural variants of tetraheme cytochromes from Desulfomicrobium sp., J. Biol. Chem., 279 (2004) 52227-52237.

[62] E. Lebrun, C. Simenel, F. Guerlesquin, M. Delepierre, ^{1}H NMR study of the Fe_4S_4 center in ferredoxin I from Desulfovibrio desulfuricans Norway: Sequence-specific assignment of the cluster-ligated cysteines, Magn. Reson. Chem., 34 (1996) 873-880.

[63] R.O. Louro, T. Catarino, J. Le Gall, D.L. Turner, A.V. Xavier, Cooperativity between electrons and protons in a monomeric cytochrome c_3: The importance of mechano-chemical coupling for energy transduction, Chembiochem, 2 (2001) 831-837.

[64] M. Ogata, N. Kiuchi, T. Yagi, Characterization and redox properties of high molecular mass cytochrome c_3 (Hmc) isolated from Desulfovibrio vulgaris Miyazaki, Biochimie, 75 (1993) 977-983.

[65] C.M. Paquete, P.M. Pereira, T. Catarino, D.L. Turner, R.O. Louro, A.V. Xavier, Functional properties of type I and type II cytochromes c_3 from Desulfovibrio africanus, Biochim. Biophys. Acta, 1767 (2007) 178-188.

[66] C.M. Paquete, D.L. Turner, R.O. Louro, A.V. Xavier, T. Catarino, Thermodynamic and kinetic characterisation of individual haems in multicentre cytochromes c_3, Biochim. Biophys. Acta, 1767 (2007) 1169-1179.

[67] J.S. Park, K. Kano, Y. Morimoto, Y. Higuchi, N. Yasuoka, M. Ogata, K. Niki, H. Akutsu, ^{1}H NMR studies on ferricytochrome c_3 from Desulfovibrio vulgaris Miyazaki F and its interaction with ferredoxin I, J. Biomol. NMR, 1 (1991) 271-282.

[68] J.S. Park, T. Ohmura, K. Kano, T. Sagara, K. Niki, Y. Kyogoku, H. Akutsu, Regulation of the redox order of four hemes by pH in cytochrome c_3 from D. vulgaris Miyazaki F, Biochim. Biophys. Acta, 1293 (1996) 45-54.

[69] P.O. Quintas, M.S. Oliveira, T. Catarino, D.L. Turner, Electron transfer between multihaem cytochromes c_3 from Desulfovibrio africanus, Biochim. Biophys. Acta, 1827 (2013) 502-506.

[70] H. Santos, J.J. Moura, I. Moura, J. Le Gall, A.V. Xavier, NMR studies of electron transfer mechanisms in a protein with interacting redox centres: Desulfovibrio gigas cytochrome c_3, Eur. J. Biochem., 141 (1984) 283-296.

[71] D.L. Turner, C.A. Salgueiro, T. Catarino, J. Le Gall, A.V. Xavier, NMR studies of cooperativity in the tetrahaem cytochrome c_3 from Desulfovibrio vulgaris, Eur. J. Biochem, 241 (1996) 723-731.

[72] J.A.N.F. Gomes, R.B. Mallion, Aromaticity and ring currents, Chem. Rev., 101 (2001) 1349-1384.

[73] C.E. Johnson, F.A. Bovey, Calculation of nuclear magnetic resonance spectra of aromatic hydrocarbons, J. Chem. Phys., 29 (1958) 1012-1014.

[74] R.E. Mayo, J.H. Goldstein, A proton magnetic resonance investigation of biphenyl, Mol. Phys., 10 (1966) 301-307.

[75] R. McWeeny, Ring currents and proton magnetic resonance in aromatic molecules, Mol. Phys., 1 (1958) 311-321.

[76] G. Merino, T. Heine, G. Seifert, The induced magnetic field in cyclic molecules, Chem. Eur. J., 10 (2004) 4367-4371.

[77] C.S. Wannere, P.v.R. Schleyer, How do ring currents affect ^{1}H NMR chemical shifts?, Org. Lett., 5 (2003) 605-608.

[78] G.P. Moss, Nomenclature of tetrapyrroles. Recommendations 1986 IUPAC-IUB joint commission on biochemical nomenclature (JCBN), Eur. J. Biochem, 178 (1988) 277-328.

[79] R.M. Keller, K. Wüthrich, Assignment of the heme c resonances in the 360 MHz ^{1}H NMR spectra of cytochrome c, Biochim. Biophys. Acta - Protein Struct., 533 (1978) 195-208.

[80] D.L. Turner, C.A. Salgueiro, J. Le Gall, A.V. Xavier, Structural studies of Desulfovibrio vulgaris ferrocytochrome c_3 by two-dimensional NMR, Eur. J. Biochem., 210 (1992) 931-936.

[81] C.A. Salgueiro, D.L. Turner, A.V. Xavier, Use of paramagnetic NMR probes for structural analysis in cytochrome c_3 from Desulfovibrio vulgaris, Eur. J. Biochem., 244 (1997) 721-734.

[82] J.R. Bolton, G.K. Fraenkel, Electron spin resonance study of the pairing theorem for alternant hydrocarbons: ^{13}C splittings in the anthracene positive and negative ions, J. Chem. Phys., 40 (1964) 3307-3320.

[83] L. Morgado, A.P. Fernandes, Y.Y. Londer, M. Bruix, C.A. Salgueiro, One simple step in the identification of the cofactors signals, one giant leap for the solution structure

determination of multiheme proteins, Biochem. Biophys. Res. Commun., 393 (2010) 466-470.

[84] D.L. Turner, C.A. Salgueiro, P. Schenkels, J. Le Gall, A.V. Xavier, Carbon-13 NMR studies of the influence of axial ligand orientation on haem electronic structure, Biochim. Biophys. Acta, 1246 (1995) 24-28.

[85] J.D. Bernal, The relation of microscopic structure to molecular structure, Q. Rev. Biophys., 1 (1968) 81-87.

[86] R.O. Louro, T. Catarino, D.L. Turner, M.A. Picarra-Pereira, I. Pacheco, J. LeGall, A.V. Xavier, Functional and mechanistic studies of cytochrome c_3 from Desulfovibrio gigas: Thermodynamics of a "proton thruster", Biochemistry, 37 (1998) 15808-15815.

[87] S. Papa, Proton translocation reactions in the respiratory chains, Biochim. Biophys. Acta - Rev. Bioenergetics, 456 (1976) 39-84.

[88] A.V. Xavier, Thermodynamic and choreographic constraints for energy transduction by cytochrome c oxidase, Biochim. Biophys. Acta - Bioenergetics, 1658 (2004) 23-30.

[89] C.A. Salgueiro, D.L. Turner, H. Santos, J. Le Gall, A.V. Xavier, Assignment of the redox potentials to the four haems in Desulfovibrio vulgaris cytochrome c_3 by 2D-NMR, FEBS Lett., 314 (1992) 155-158.

[90] D.W. Marquardt, An algorithm for least-squares estimation of nonlinear parameters, J. Soc. Ind. Appl. Math., 11 (1963) 431-441.

[91] L. Morgado, A.P. Fernandes, Y.Y. Londer, P.R. Pokkuluri, M. Schiffer, C.A. Salgueiro, Thermodynamic characterization of the redox centres in a representative domain of a novel c-type multihaem cytochrome, Biochem. J., 420 (2009) 485-492.

[92] D. Sun, A. Wang, S. Cheng, M. Yates, B.E. Logan, Geobacter anodireducens sp. nov., an exoelectrogenic microbe in bioelectrochemical systems, Int. J. Syst. Evol. Microbiol., 64 (2014) 3485-3491.

[93] J. Sun, B. Sayyar, J.E. Butler, P. Pharkya, T.R. Fahland, I. Famili, C.H. Schilling, D.R. Lovley, R. Mahadevan, Genome-scale constraint-based modeling of Geobacter metallireducens, BMC Syst. Biol., 3 (2009) 15.

[94] A.E. Franks, K.P. Nevin, H. Jia, M. Izallalen, T.L. Woodard, D.R. Lovley, Novel strategy for three-dimensional real-time imaging of microbial fuel cell communities: Monitoring the inhibitory effects of proton accumulation within the anode biofilm, Energ. Environ. Sci., 2 (2009) 113-119.

[95] J.C. Wilks, J.L. Slonczewski, pH of the cytoplasm and periplasm of Escherichia coli: Rapid measurement by green fluorescent protein fluorimetry, J. Bacteriol., 189 (2007) 5601-5607.

[96] L. Morgado, J.M. Dantas, M. Bruix, Y.Y. Londer, C.A. Salgueiro, Fine tuning of redox networks on multiheme cytochromes from Geobacter sulfurreducens drives physiological electron/proton energy transduction, Bioinorg. Chem. Appl., 2012 (2012) 298739.

[97] R. Mahadevan, D.R. Bond, J.E. Butler, A. Esteve-Núñez, M.V. Coppi, B.O. Palsson, C.H. Schilling, D.R. Lovley, Characterization of metabolism in the Fe(III)-reducing organism

Geobacter sulfurreducens by constraint-based modeling, Appl. Environ. Microbiol., 72 (2006) 1558-1568.

[98] J.T. Babauta, H.D. Nguyen, T.D. Harrington, R. Renslow, H. Beyenal, pH, redox potential and local biofilm potential microenvironments within Geobacter sulfurreducens biofilms and their roles in electron transfer, Biotechnol. Bioeng., 109 (2012) 2651-2662.

[99] C.I. Torres, A. Kato Marcus, B.E. Rittmann, Proton transport inside the biofilm limits electrical current generation by anode-respiring bacteria, Biotechnol. Bioeng., 100 (2008) 872-881.

[100] C.I. Torres, H.-S. Lee, B.E. Rittmann, Carbonate species as OH^- carriers for decreasing the pH gradient between cathode and anode in biological fuel cells, Envir. Sci. Tech., 42 (2008) 8773-8777.

[101] Y. Liu, H. Kim, R.R. Franklin, D.R. Bond, Linking spectral and electrochemical analysis to monitor c-type cytochrome redox status in living Geobacter sulfurreducens biofilms, Chemphyschem, 12 (2011) 2235-2241.

[102] E. Marsili, J.B. Rollefson, D.B. Baron, R.M. Hozalski, D.R. Bond, Microbial biofilm voltammetry: Direct electrochemical characterization of catalytic electrode-attached biofilms, Appl. Environ. Microbiol., 74 (2008) 7329-7337.

[103] S. Srikanth, E. Marsili, M.C. Flickinger, D.R. Bond, Electrochemical characterization of Geobacter sulfurreducens cells immobilized on graphite paper electrodes, Biotechnol. Bioeng., 99 (2008) 1065-1073.

3

Expression, purification and biochemical characterization of GSU0105

"*If you can't explain it simply, you don't understand well enough.*"

Albert Einstein

3 – Expression, purification and biochemical characterization of GSU0105

In 2006, Ding and co-workers [1] highlighted a group of three cytochromes (GSU0105, GSU0701 and GSU2515) that are highly expressed in Fe(III) reducing conditions, but are not expressed at all in cultures grown on fumarate, linking them directly with EET networks. GSU0105 has three CXXCH heme binding motifs and by analyzing its amino acid sequence with a protein subcellular localization prediction software (LocTree 3 [2]), it was concluded that the cytochrome is most probably located on the periplasm. GSU0701 (also designated as OmcJ), on the other hand, is predicted to be located in the OM of G. sulfurreducens, having six CXXCH heme binding motifs [3]. Finally, GSU2515 is a monoheme cytochrome [1], predicted to be located either on the periplasm or in the OM of the bacterium [4].

Taking advantage of the expression and purification protocols developed for the periplasmic cytochromes from G. sulfurreducens [5, 6], GSU0105 was thought as the best candidate for initial expression and purification tests. By analyzing GSU0105 amino acid sequence, it is possible to infer that the heme axial coordination is necessarily different from the cytochromes belonging to the PpcA-family (Figure 3.1), which all have His-His c-type heme groups [7].

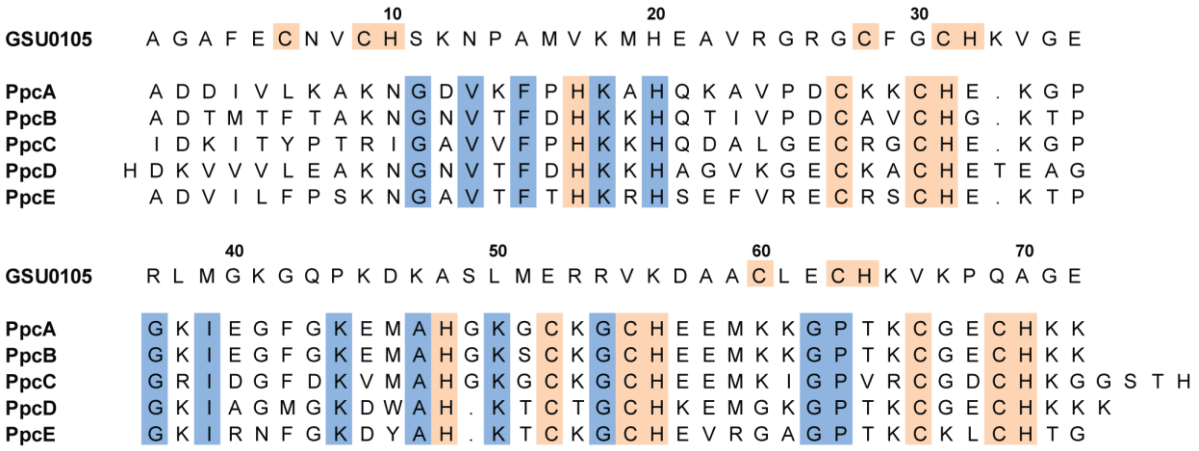

Figure 3.1 – Amino acid alignment of the PpcA-family cytochromes (PpcA, PpcB, PpcC, PpcD and PpcE) with the periplasmic cytochrome GSU0105 – The conserved residues in the PpcA-family are highlighted with blue boxes. The heme-attached residues (from the CXXCH heme binding motif, plus the distal histidines of each heme confirmed for the PpcA-family cytochromes) are highlighted in orange boxes.

Besides the three histidine residues included on the CXXCH binding motifs, there is only one free histidine residue (His^{20}), meaning that only one of the GSU0105 heme groups can have a His-His coordination. As described in Chapter 1, c-type hemes can be distally coordinated by

methionine, histidine, asparagine, tyrosine, lysine residues and/or have the distal position of the heme transiently vacant. Therefore, there are many possible scenarios for the axial coordination of two out of the three hemes of GSU0105, making this cytochrome a very interesting target for biochemical, biophysical and structural studies.

The analysis of Figure 3.1 shows that GSU0105 has very low sequence identity with all the cytochromes of the PpcA-family. Surprisingly, the main biochemical features of concern for its purification are remarkably similar with those cytochromes (Table 3.1). GSU0105 is biochemically similar to all the PpcA-family cytochromes in terms of isoelectric point and molecular weight.

Table 3.1 – Biochemical characteristics of periplasmic cytochromes from G. sulfurreducens – The presented molecular weights are approximated. The isoelectric points were all theoretically predicted using the Compute pI/MW tool, from ExPASy – Swiss Institute of Bioinformatics (https://www.expasy.org).

Protein	Gene	Residues	Molecular weight (kDa)	Isoelectric point
GSU0105	GSU0105	72	9.7	9.2
PpcA	GSU0612	71	9.6	9.2
PpcB	GSU0364	71	9.6	9.0
PpcC	GSU0365	75	9.6	8.8
PpcD	GSU1024	71	9.6	9.0
PpcE	GSU1760	70	9.7	9.5

By the time this Thesis started, GSU0105 was already cloned into the vector pVA203 [7, 8] with the sequence presented in Figure 3.1. In this Chapter, the work developed in the optimization of the expression and purification protocols of this cytochrome is discussed and a preliminary biochemical and functional characterization is presented.

3.1 – Materials and methods

3.1.1 – Expression and purification

The expression of GSU0105 was performed in different E. coli strains (BL21 (DE3), JM109 and SF110) containing the plasmid pEC86. These cells were transformed with the plasmid pGSU0105 (containing the gene GSU0105, encoding for GSU0105 cytochrome, an ampicillin resistance gene, a lac promoter and an OmpA leader sequence [9]) and grown in 2xYT media supplemented with 34 μg/mL chloramphenicol and 100 μg/mL ampicillin, to an OD_{600} of approximately 1.5 at 30 ºC. Then, protein expression was induced either with 10 or 100 μM of IPTG and the cultures were left growing at 24 or 30 ºC overnight.

After overnight incubation, cells were harvested by centrifugation at 6400 xg for 20 minutes, at 4 ºC. The cell pellet was gently resuspended in 30 mL of lysis buffer (20% sucrose, 100 mM Tris-HCl pH 8, 0.5 mM EDTA, containing 0.5 mg/mL of lysozyme), per liter of initial cell culture. After 15 minutes of incubation at room temperature, 30 mL of pre-cooled water were added to the cell suspension, which was then left incubating on ice for 15 minutes. Following that step, the suspension was centrifugated at 14700 xg for 20 minutes, at 4 ºC. The supernatant constituted the periplasmic fraction, which was ultracentrifugated at 150000 xg for 1 hour, at 4 ºC. The final supernatant was dialyzed against 2 x 4.5 L of 10 mM Tris-HCl pH 8, using a Spectra/Por dialysis membrane (MWCO: 3.5 kDa), and then loaded onto either 2 x 5 mL Bio-Scale™ Mini UNOsphere™ S cartridges (Bio-Rad) or 2 x 5 mL HiTrap SP HP cartridges (GE Healthcare), equilibrated with the same buffer. The protein was eluted with a sodium chloride gradient (0-300 mM). The obtained fractions were evaluated by SDS-PAGE (15% acrylamide/bis-acrylamide), stained either for hemes (TMBZ staining) or with BlueSafe (see protocol for both types of staining in section 6.2). The fractions containing the protein were concentrated to 1 mL in Amicon Ultra centrifugal filter units (Ultra-4, MWCO 3 kDa) and equilibrated with 100 mM sodium phosphate buffer pH 8, before being injected in a XK 16/70 Superdex 75 molecular exclusion column, equilibrated with the same buffer. Both chromatography steps were performed on an ÄKTA Pure system and the final protein purity was evaluated by SDS-PAGE. The concentration of the cytochrome was determined by measuring the absorbance of the reduced form at 552 nm, using the extinction coefficient of 97.5 mM^{-1} cm^{-1}, determined for PpcA from G. sulfurreducens. The UV-visible absorption spectra of GSU0105 were acquired in the oxidized and reduced (achieved with addition of sodium dithionite) states in a Thermo Scientific Evolution 201 spectrophotometer. The measurements were made with a quartz cuvette (Helma), with 1 cm path length, at room temperature.

3.1.2 – NMR studies

3.1.2.1 – Sample preparation

Protein samples were prepared with approximately 350 μM concentration, in 32 mM phosphate buffer, pH 8, with NaCl (100 mM of final ionic strength). The buffer was prepared either in pure $^{2}H_2O$ (CIL isotopes) or in 90% H_2O/10% $^{2}H_2O$. In the first case, the protein samples were prepared after liophylization. The pH values of the samples were measured with a glass micro electrode and were not corrected for isotope effects. For sample reduction, the NMR tubes were sealed with a gas-tight serum cap and the air was flushed out from the sample with argon (Gasin). Then, two different approaches were used: (i) the samples were reduced directly in the NMR tube with gaseous hydrogen (Air Liquide) in the presence of catalytic amounts of hydrogenase from Desulfovibrio vulgaris (Hildenborough); or (ii) the samples were reduced with direct addition of sodium dithionite in small aliquots from a degassed stock solution, prepared in the sample buffer (in $^{2}H_2O$). These additions were made either by using an Hamilton syringe or by direct addition inside an anaerobic glove box (MBraun) with O_2 levels kept under 0.5 ppm, with argon circulation.

3.1.2.2 – NMR experiments

All the NMR experiments were acquired in a Bruker Avance III 600 MHz spectrometer equipped with a triple-resonance cryoprobe (TCI) and processed using TopSpin3.5.7™ (Bruker BioSpin, Karlsruhe, Germany). The ^{1}H chemical shifts were calibrated using the water signal as internal reference.

3.1.2.2.1 – Reduced state experiments

1D ^{1}H-NMR spectra were acquired in a partial reduced state (see section 3.2.2), at 298 K. The spectra were acquired with 32k data points, a spectral width of 30 kHz, with a total of 1024 transients and water pre-saturation.

3.1.2.2.2 – Oxidized state experiments

1D ^{1}H-NMR spectra were acquired in the oxidized state, at 298 K. The spectra were acquired with 32k data points, a spectral width of 96 kHz, with a total of 8192 transients and water pre-saturation.

3.1.3 – Electrochemistry

3.1.3.1 – Fundamentals

Electrochemistry is a dynamic science, whose beginnings date back to the 18th century, when the Italian physician Luigi Galvani described the connection between chemical reactions and electricity in the manuscript "De Viribus Electricitatis in Motu Musculari Commentarius" [10]. Electrochemistry may be defined as the study of chemical reactions used to produce electric power or, alternatively, the use of electricity to affect chemical processes or systems [11]. Hence, electrochemistry can be seen as the relationship between electricity and chemistry, namely the measurements of electric quantities, such as current, potential, charge and their relationship to several chemical parameters. These chemical reactions, involving the transfer of electrons to and from molecules or ions, are often referred to as redox (reduction/oxidation) reactions [12].

In electrochemistry, unlike other techniques of chemical measurements that involve homogenous bulk solutions, reactions are heterogeneous in nature, as they take place at interfaces, usually electrode-solution boundaries. The electrode creates a phase boundary that differentiates otherwise identical solute molecules in (i) those at a distance from the electrode and (ii) those close enough to the surface of the electrode in order to participate in the electron transfer process [11].

Electrochemical responses or signals are divided in two main types: (i) faradaic or redox signals, which are caused by changes in the redox state of the analyte and that obey the Faraday Law and (ii) tensametric or "non-faradaic" signals, which are caused by changes in the differential capacitance of the electrode double layer, due to the adsorption, desorption or reorientation of the sample on the electrode surface [12].

There are several electrochemical methods to detect these types of signals, namely controlled-potential and controlled-current ones [11]. Voltammetric methods (controlled-potential methods) are based on the monitorization of the changes in current of the sample, depending on the applied potential (against the potential of the reference electrode) at the working electrode. The potential versus time apparatus defines the voltammetric mode. Basic voltammetric methods are linear sweep voltammetry, cyclic voltammetry (CV), differential pulse voltammetry, square wave voltammetry and alternating current voltammetry. Controlled-current (galvanostatic) methods are based on the application of a current on the working electrode, while the differences in potential are monitored in a time dependent manner [13].

In this Thesis, the method used was CV. This technique is the most widely used for approaching qualitative information about electrochemical reactions (thermodynamics of redox processes, coupled chemical reactions and adsorption processes). CV consists of scanning linearly the potential of a stationary working electrode, using a triangular potential waveform (Figure 3.2) [12].

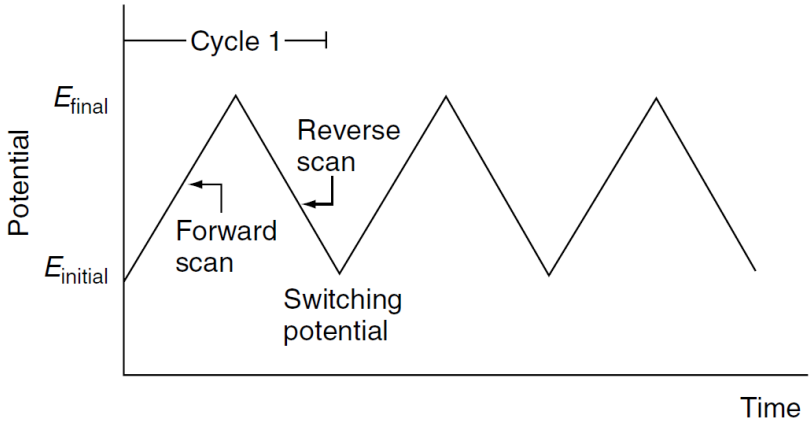

Figure 3.2 – Potential-time excitation signal in a cyclic voltammetric experiment – Every cycle in a CV experiment is composed of a forward scan and a reverse scan. In the forward and reverse scans, reduction and oxidation reactions occur, respectively. This image was taken from [12].

Depending on the information sought, single or multiple cycles can be used. During the potential sweep, the potentiostat measures the current resulting from the applied potential. The resulting current-potential plot is termed a cyclic voltammogram. The cyclic voltammogram is a complicated, time-dependent function of a large number of physical and chemical parameters [12]. In Figure 3.3, it is possible to see the expected response of a reversible redox couple during a single potential cycle. It is assumed that only the oxidized form «O» is present initially. Thus, a negative-going potential scan is chosen for the first half-cycle, starting from a value where no reduction occurs.

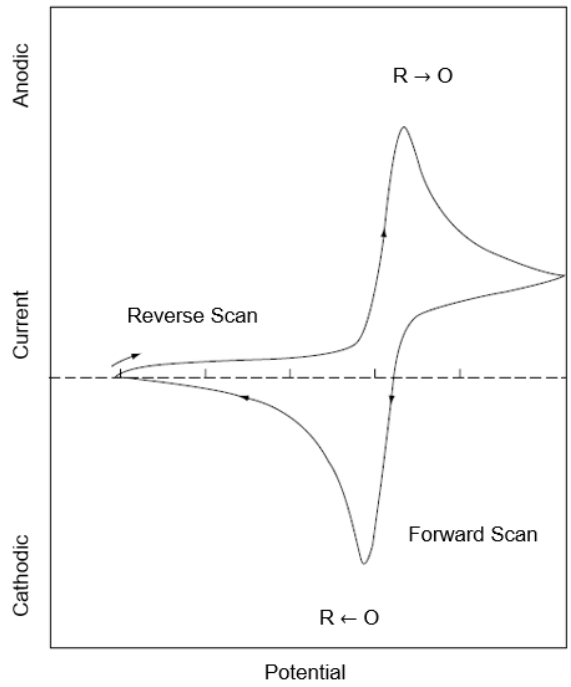

Figure 3.3 – Typical cyclic voltammogram for a reversible redox couple, during a single potential cycle – In the presented voltammogram, "O" and "R" represent the oxidized and reduced species of the redox pair, respectively. In cyclic voltammetry, the anodic peaks (resulting from oxidation reactions) are positive and the cathodic peaks (resulting from reduction reactions) are negative. This figure was adapted from [12].

As the applied potential approaches the characteristic E^0 (standard reduction potential) for the redox process, a cathodic current begins to increase, until a peak is reached. After traversing the potential region in which the reduction process takes place, the direction of the potential sweep is reversed. During the reverse scan, reduced "R" molecules (generated in the forward half-cycle and accumulated near the surface) are reoxidized back to "O", resulting in an anodic peak.

3.1.3.2 – Protein electrochemistry

The several advantages of electrochemical methods (low cost, rapidity and sensitivity) make them very promising in the growing fields of proteomics and biomedicine. Electrochemistry of proteins is based on (i) the investigation of the redox properties of non-protein particles conjugated to protein molecules, (ii) the application of various labels attached to the protein molecule and on (iii) label-free investigation of non-conjugated proteins, which is related only on their intrinsic electroactivity [14].

Protein electrochemistry experiments are usually carried out using a potentiostat in conjunction with electrochemical cells, where the different electrodes, sample and electrolyte are placed. Electrochemical cells are vessels in which electrochemical measurements are performed. Depending on the experimental requirements, these cells can be of various types and have different compartments. The most common type of cells are the ones with three-electrode systems, which consist of (i) the working electrode, on which the electrochemical reaction occurs, (ii) the reference electrode, which is not affected by changes in current during the electrochemical reaction and (iii) the auxiliary electrode, which is used to ensure a flowing current to close the circuit. These cells usually contain stirring systems and argon inlet entrances, for pressing out oxygen and allow experiments to be run in low oxygen environments [12].

There are many types of working electrodes, with the most common ones being metal and carbon-based electrodes [12, 15-21]. An ideal working electrode needs to have the following characteristics: (i) technical stability, (ii) chemical inertness, (iii) homogeneity, (iv) large hydrogen overpotential, (v) capability of chemical modification in service of specific analyte investigation, (vi) non-toxicity, (vii) durability, (ix) low cost maintenance and (x) appropriate surface properties. Every working electrode has its advantages and disadvantages and in some electrochemical experiments, it is useful to combine various types of working electrodes, in order to overcome and compensate those individual disadvantages. The type(s) of working electrode(s) depends on the nature of the investigated analyte [12].

The potential of the reference electrodes is constant, known and independent of the investigated sample conditions. The most commonly used reference electrodes are the silver chloride (Ag/AgCl, 3M KCl) and the saturated calomel (Hg/Hg_2Cl_2, saturated KCl) electrodes [12]. Furthermore, the auxiliary electrodes are usually made of well-conductive and inert materials, such as platinum [12]. The potentiostat controls the potential difference between the working electrode and the reference electrode. Usually, in these experiments, it is important to include in the cell solution a large quantity of inert "supporting electrolyte", which usually has inert salt concentrations three orders of magnitude higher than the concentration of the active species in study [22]. In protein electrochemistry, it is very common to use pyrolytic graphite (PG) electrodes, since they have been proved to be especially useful for probing redox-active proteins [23]. Rather than measuring the electrochemical response associated with a transient adsorption event, proteins can be immobilized, often irreversibly, on the electrode surface. The proteins on PG usually maintain their native function after immobilization, possibly due to the diversity of aromatic and oxo species present in the surface and their similarity to the protein's natural environment [14, 23, 24]. Furthermore, the immobilization removes macromolecular

diffusion from electrochemical measurements, which greatly simplifies the interpretation of protein voltammetry data and allows analyses to be carried out until sub-picomole amounts of protein sample [25, 26].

CV was used to study the intrinsically electroactive protein GSU0105, in order to get initial insights on the redox potentials of the different hemes.

3.1.3.3 – Electrochemical studies

The electrochemical assays for GSU0105 were performed using a μAUTOLAB type III potentiostat, in a single compartment electrochemical cell (Metrohm) with a three electrodes configuration, inside a Faraday cage. PG disk was used as working electrode (3 mm diameter). A platinum wire and a Ag/AgCl (3M, KCl) were the counter and reference electrodes, respectively. The working electrode was polished with alumina of different grades (0.3 and 1 μm, from Buehler), then immersed in Millipore water in an ultra-sound bath and, finally, thoroughly rinsed with Millipore water. A small amount of protein (5 μL, 200 μM) was let to evaporate at room temperature, until it reached approximately half of the initial volume (solvent casting technique). Then, the protein sample was immobilized on the electrode using a cellulose membrane (Spectra/Por) with a 3500 Da cut-off, that was fitted to the electrode with an O-ring, forming a uniform thin layer. The control assays were performed using Bovine Serum Albumin (BSA (NZYTech), 5 μL, 200 μM). The supporting electrolyte (50 mL) used for the studies was 32 mM phosphate buffer, 0.1 M NaCl, pH 7. The cyclic voltammetry (CV) assays were carried out at 293 ± 1 K, using different scan rates (5, 10, 20, 35, 50, 75, 100, 150, 200, 500, 1000, 2000 and 5000 mV s^{-1}). The experiments were performed in triplicates. Before the electrochemical experiments, the electrolyte was degassed for 25 minutes using a continuous flow of high purity argon (Gasin). The assays were performed with positive argon pressure on the electrochemical cell headspace. The potential values were converted and are presented in reference to NHE.

3.2 – Results and discussion

3.2.1 – Optimization of the expression and purification of GSU0105

3.2.1.1 – Optimization of the strains and protein expression induction

The GSU0105 cytochrome was initially expressed as previously described for the PpcA-family cytochromes of G. sulfurreducens, using E. coli BL21 (DE3) cells [6]. The first purification step encompassed a cation exchange chromatography (performed with 2 x 5 mL Bio-Scale™ Mini UNOsphere™ S cartridges) and the results are presented in Figure 3.4.

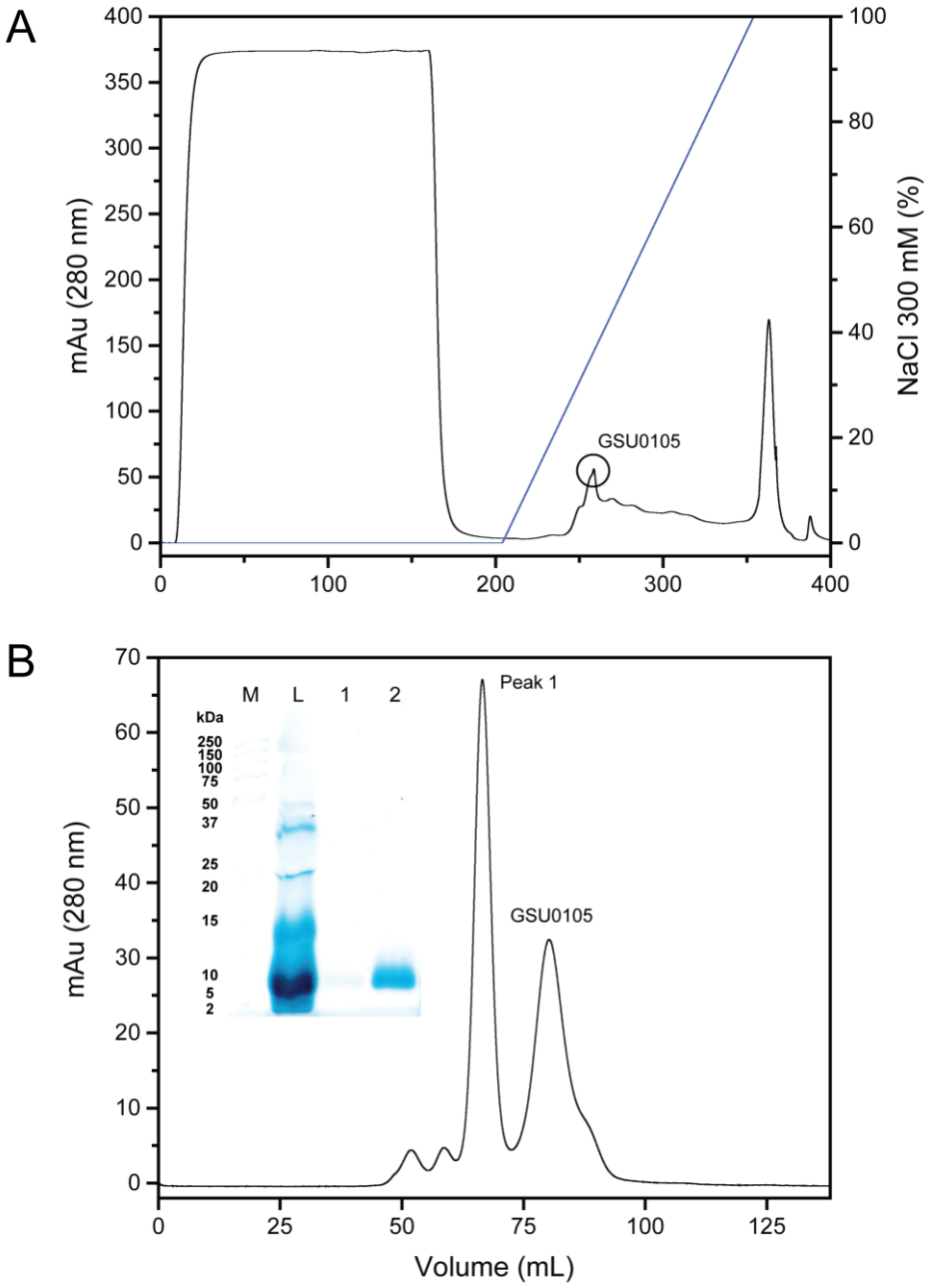

Figure 3.4 – Purification of GSU0105 – (A) Cation exchange chromatography of GSU0105 – The primary and secondary y-axis report the variation of absorbance at 280 nm (black line) and the NaCl gradient profile (blue line), respectively. (B) Size exclusion chromatography of GSU0105 – The inset shows the SDS-PAGE analysis of the fraction resulted from the cation exchange chromatography step (lane L), as well as the fractions of peaks 1 (lane 1) and GSU0105 (lane 2). Lane M corresponds to the molecular weight marker (Protein Plus Protein™ Dual Xtra Standards, from Bio-Rad). The gel was stained with TMBZ.

In the cation exchange chromatography step (Figure 3.4A), the eluted fractions were analyzed by SDS-PAGE (data not shown). The fractions containing GSU0105 were concentrated to 1 mL before being injected in the size exclusion chromatography column. The final fractions, resulting

from this final purification step (Figure 3.4B), were also analyzed by TMBZ stained SDS-PAGE, as shown on the inset of Figure 3.4B. The obtained protein was quantified and 0.0125 mg of GSU0105 per liter of cell culture were obtained. Considering this low yield, the expression and purification protocols were further optimized.

In order to gather some insights on which possible changes could be made in the different protocol steps, an analysis of the expression and purification protocols, together with the results obtained, was performed. The low yields obtained in the first protein expression and purification test can be due to different factors, namely low levels of expression as a result of unoptimized experimental conditions in the expression and purification processes (competent cell strain, temperature of incubation, buffer, elution methods, columns used, among others).

The first parameter to optimize regarded the amount of IPTG used in protein expression. Therefore, protein expression was induced with a higher concentration of IPTG (100 μM). In a second round of expression and purification of GSU0105, protein expression was performed in the same conditions, with the only difference being the IPTG concentration for protein expression induction. The higher IPTG concentration did not affect the intensity of the periplasmic fraction color, which was an initial indicator that the protein yield did not increase. The size exclusion elution profile (Figure 3.5) of the concentrated fractions resulting from the cation exchange chromatography step presents a band with lower intensity for GSU0105, thus confirming that the use of a higher IPTG concentration did not increase the protein expression. In fact, it can be said that the use higher IPTG concentrations results in lower GSU0105 expression yields.

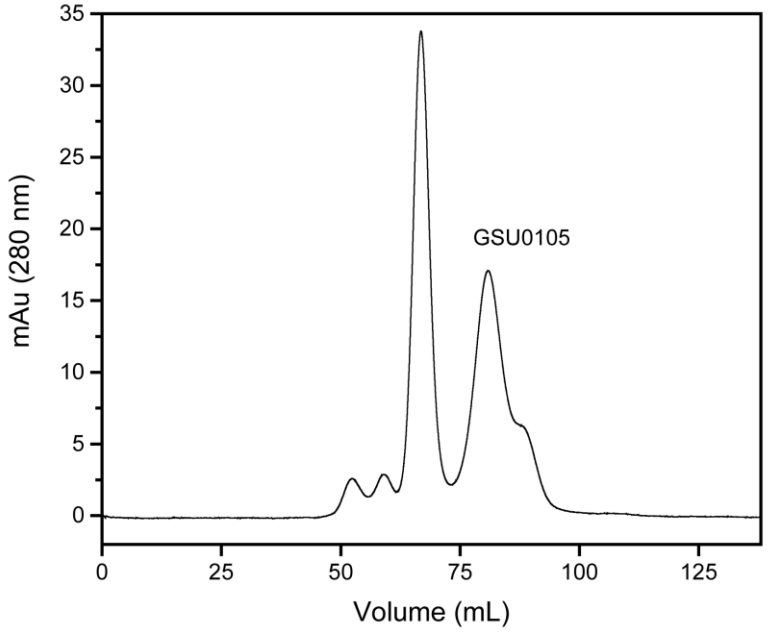

Figure 3.5 – Size exclusion chromatography elution profile of GSU0105 – The peak corresponding to GSU0105 is indicated.

The second parameter to optimize regarded the temperatures of cell growth after protein induction. In another trial, protein expression was performed at 24 ^{o}C (also with more time of incubation after induction), since many works have proven that expressing proteins with complex post-translational modifications works better at lower temperatures [27-29]. In the case of GSU0105, the expression of the apo-protein has to occur sufficiently slow to allow the cells to produce the heme cofactor and incorporate it in the polypeptide chain. This fact may also be related with the results obtained with higher IPTG concentrations, since the protein expression could have increased, but the cell was not capable to produce the heme cofactor at a sufficient rate to perform the necessary post-translational incorporations efficiently and correctly. By comparing the results obtained with the different incubation temperatures after protein expression induction (Figure 3.6), it is clear that the protein expression is very similar at 24 ^{o}C and 30 ^{o}C.

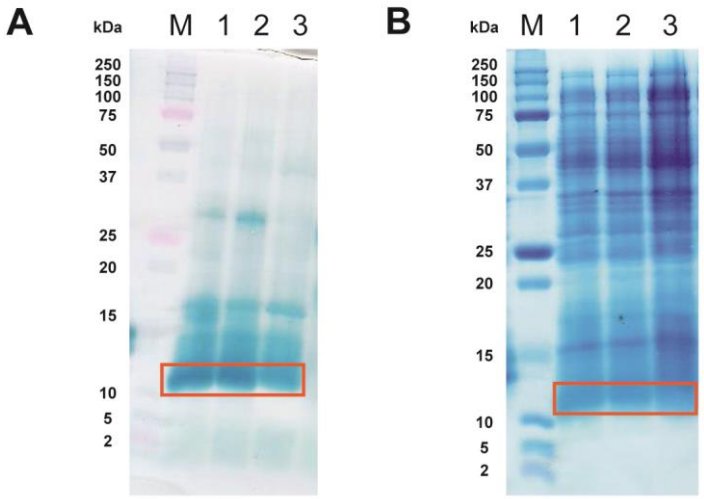

Figure 3.6 – SDS-PAGE analysis of the GSU0105 protein expression induction temperature dependence – (A) TMBZ staining. (B) BlueSafe staining. On both cases (A and B), the molecular weight marker (lane M) used was the Protein Plus Protein™ Dual Xtra Standards. Lane 1 corresponds to the protein content of the cells after protein induction and growth at 24 ºC. Lane 2 corresponds to the protein content of the cells after protein induction and growth at 30 ºC. Lane 3 corresponds to the protein content of the cells before protein induction (up until this point, the cells were grown at 30 ºC).

Finally, the expression of GSU0105 was tested out in the E. coli strains JM109 and SF110, that were previously used with success for the expression of other Geobacter cytochromes [30, 31]. Considering so, the commonly used calcium chloride competent cells preparation protocol [32] was used to prepare competent cells of the JM109 and SF110 E.coli strains, containing the pEC86 plasmid [33, 34]. The protein expression was performed according to the previous conclusions (10 μM IPTG, followed by an overnight incubation at 30 ºC) and after the cation exchange step, it was clear that the JM109 strain had the most promising results compared to the SF110 strain (Figure 3.7).

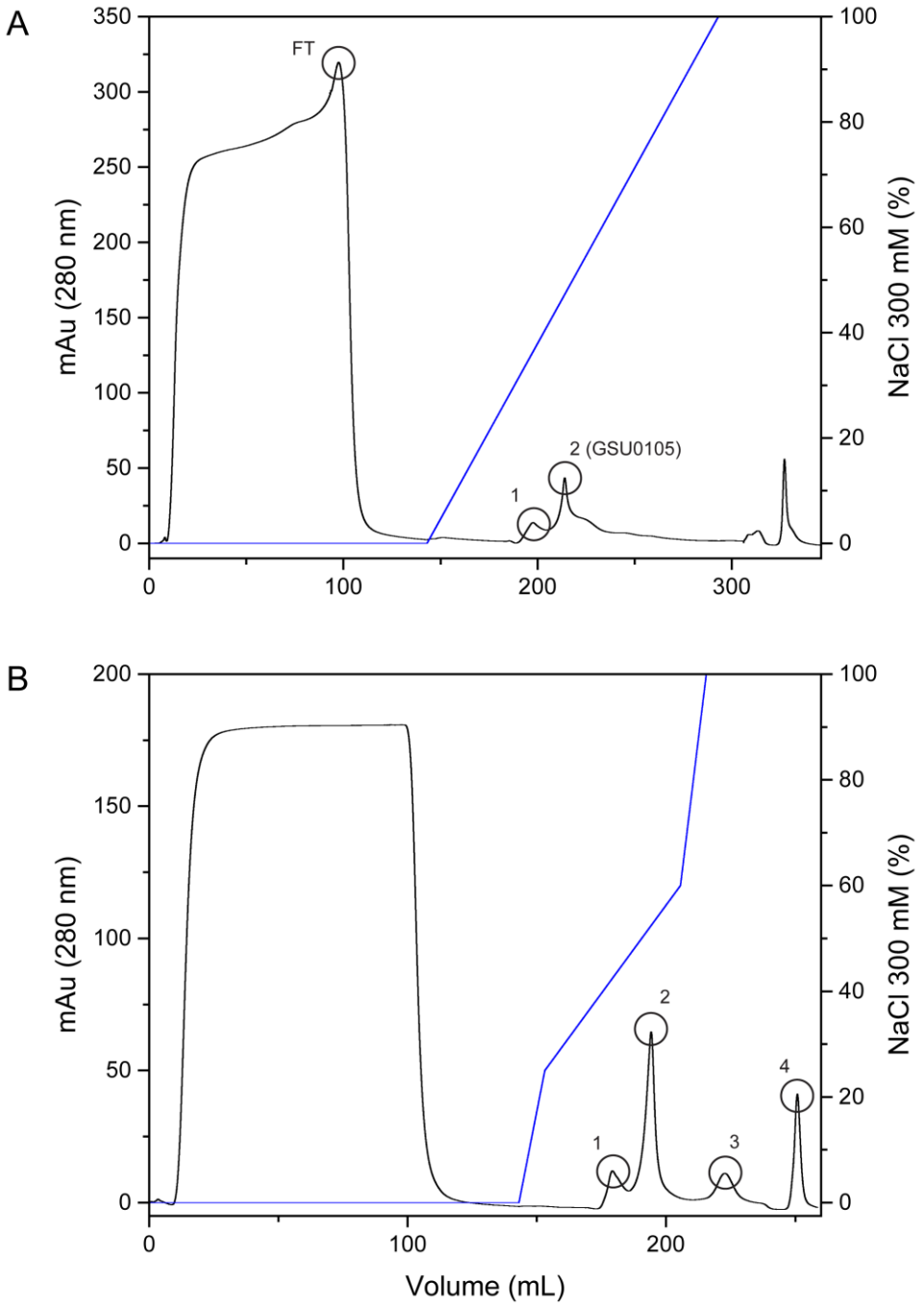

Figure 3.7 – Cation exchange chromatography elution profiles of the periplasmic fractions of E.coli JM109 and E. coli SF110 cells – The chromatograms obtained for the (A) JM109 and (B) SF110 strains are represented. In both chromatograms, the primary and secondary y-axis report the variation of absorbance at 280 nm (black line) and the NaCl gradient profile (blue line), respectively. The peaks analyzed by SDS-PAGE (Figure 3.8) are marked.

The fractions obtained were further analyzed by SDS-PAGE and the results demonstrated that a peak for GSU0105 was only found in one of the fractions resulting from the cation

exchange chromatography performed on the periplasmic fraction of the E. coli JM109 cells (Figure 3.8).

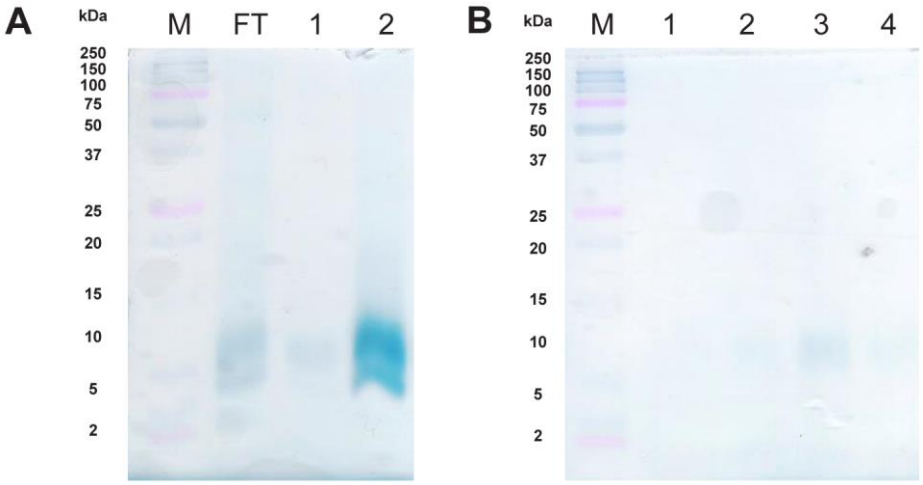

Figure 3.8 – Protein expression of JM109 and SF110 E. coli strains – SDS-PAGE of different fractions eluted during the cation exchange chromatography step of the periplasmic fractions of (A) JM109 and (B) SF110 cells. The molecular weight marker (lane M) used was the Protein Plus Protein™ Dual Xtra Standards. The remaining lanes are identified according to the labels presented in Figure 3.7.

After protein expression and purification, it was clear that the E. coli strain JM109 is more adequate for the expression of GSU0105, since the yields increased considerably when compared with the BL21 (DE3) strain, as discussed in section 3.2.1.3.

3.2.1.2 – Optimization of the purification

Since a considerable amount of protein did not bind to the column in the first cation exchange purification, an attempt to optimize the process was tested. GSU0105 is a very basic protein (predicted isoelectric point of 9.2) and at the experimental conditions used (10 mM Tris-HCl pH 8), it should strongly bind to the cation exchange column used. There were a few possible reasons why the protein was not binding to the cation exchange column, namely the capacity of ion-exchange of the resin [35]. Therefore, a different set of columns (2 x 5 mL HiTrap SP HP cartridges) was used in the second purification process. The peak corresponding to GSU0105 (Figure 3.9) was eluted with the same percentage of 300 mM NaCl and had a similar intensity, meaning that the columns from GE Healthcare did not have an effect on the cation exchange chromatography step.

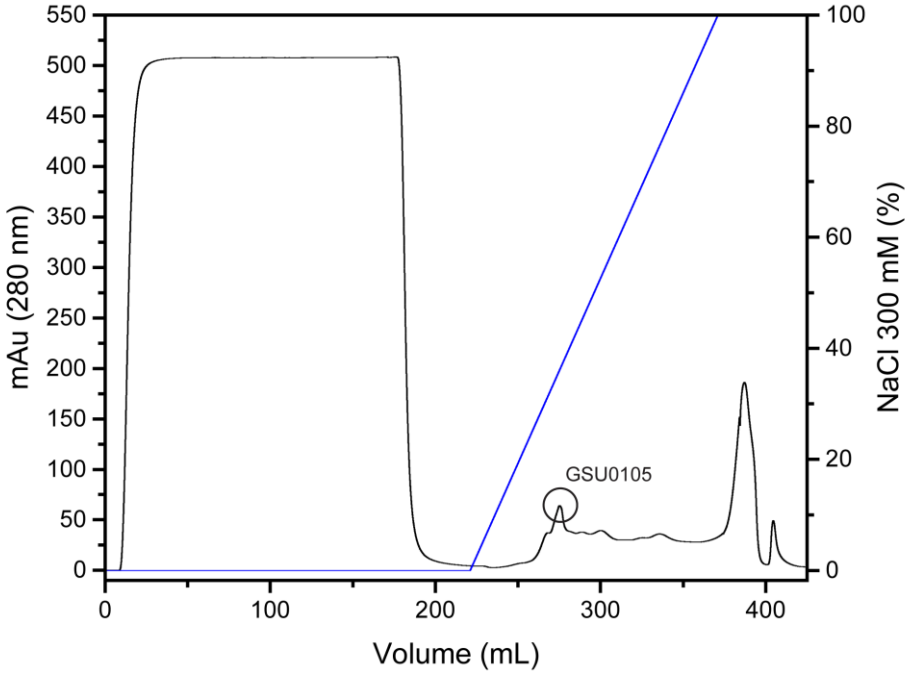

Figure 3.9 – Cation exchange chromatography elution profile of GSU0105 – The primary and secondary y-axis report the variation of absorbance at 280 nm (black line) and the NaCl gradient profile (blue line), respectively. The peak corresponding to GSU0105 is indicated.

3.2.1.3 – Final conclusions

Combining the data obtained with all the different expression and purification tests, the protocol of expression and purification of GSU0105 was reassessed and it was concluded that the E. coli JM109 strain was the most adequate host for protein expression, which should be induced with 10 μM IPTG, followed by overnight incubation at 30 °C. By gathering the above conditions, an increase of 13-fold in the total protein yield was achieved (0.165 mg/liter of cell culture).

3.2.2 – Preliminary spectroscopic characterization of GSU0105

UV-visible and NMR spectroscopies were used to probe the protein's heme spin-state and the nature of the heme axial ligands of the cytochrome GSU0105.

3.2.2.1 – UV-visible features of GSU0105

The optical absorption spectrum of the oxidized cytochrome (Figure 3.10) has maxima at 354, 408 and 527 nm.

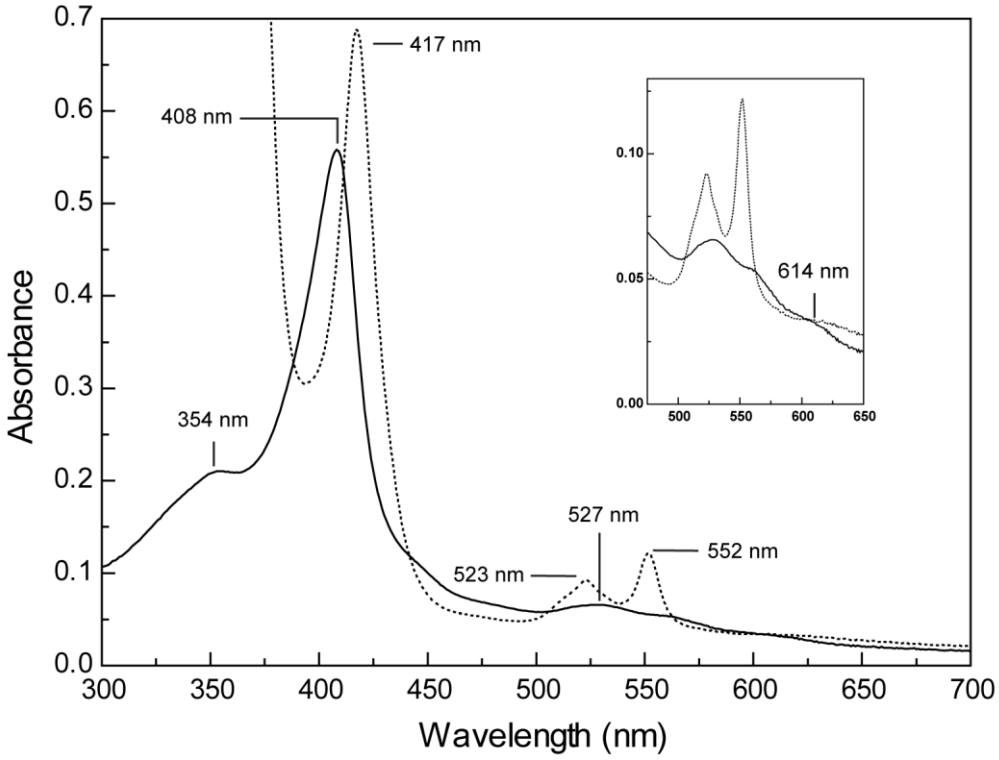

Figure 3.10 - UV-visible spectra features of cytochrome GSU0105 in the oxidized and reduced states – The maxima of the UV-visible spectra of the cytochrome in the oxidized (solid line) and reduced states (dashed line) are labeled. The inset shows a close in of the region containing the CT band (see below), in the oxidized state, indicative of high-spin character. The spectra were acquired with approximately 1 μM of protein.

Upon reduction, the protein shows the Soret, β and α bands at 417, 523 and 552 nm, respectively. At first look, the spectral patterns are similar with those presented by low-spin hexacoordinated hemes [36], in both states.

According to Moore and Pettigrew [36], cytochromes can have multiple arrangements of spin-states between the ferrihemochrome (Fe^{3+}) and ferrohemochrome (Fe^{2+}) forms. The UV-visible spectrum of the reduced cytochrome is typical of a low-spin cytochrome, but the spectrum of the oxidized form seems to present a pattern with a mixture of low- and high-spin signatures. High-spin cytochromes (in this case, S = 5/2, Fe(III)) usually present a charge-transfer (CT) absorbance band between 600-640 nm [36], which results from a weakening of the Met-Fe bond. This band is present (although subtle and really broad) in the UV-visible spectrum of the oxidized GSU0105 (see inset of Figure 3.10), with a maximum at 614 nm.

The spin-state of most cytochromes c does not change with an alteration in the oxidation state. An example of two exceptions are the periplasmic heme-containing sensor proteins

GSU0582 and GSU0935 from G. sulfurreducens [37]. These cytochromes c possess one heme with His-Met coordination in the reduced state. The change in the redox state of these sensor proteins is coupled to a heme spin-state/coordination alteration, as a consequence of the detachment of the methionine residue at the heme distal position in the reduced form [37, 38]. Therefore, these cytochromes are high- (S = 5/2) and low-spin (S = 0) in the oxidized and reduced forms, respectively. The UV-visible spectra of these cytochromes in the oxidized state both present a CT band with maximum at 623 nm [37].

Considering the above mentioned, one hypothesis that explains the spectral pattern (Figure 3.10) of GSU0105 is that one of its hemes is His-Met coordinated in the low-spin reduced state, which becomes high-spin in the oxidized state, probably due to the detachment of the axial methionine. Furthermore, there are reports in the literature that match the proposed hypothesis for GSU0105. In fact, the cytochrome c from Wolinella succinogenes has a low-spin state in the reduced form (with histidine and methionine axial ligation, just as hypothesized for at least one of the hemes of GSU0105) and a mixture of high- and low-spin states in the oxidized form [39]. This would mean that GSU0105 possesses a His-Met coordinated heme in the reduced state, which then is in an equilibrium between an hexacoordinated (His-Met, low-spin) and a pentacoordinated (His-vacant, high-spin) form, in the oxidized state. All these evidences have to be tested by EPR and NMR experiments, as previously described [37, 39].

On the other hand, since it is expected that the axial ligand from at least one of the hemes is a methionine residue, a 695 nm band should be visible in the UV-visible spectrum of the oxidized form. Theorell and Åkesson [40, 41] first observed a weak 695 nm absorbance band in a ferricytochrome c. Further studies confirmed that this band is sensitive to pH and to the conformational state of the protein [42-45]. The fact that the displacement of the methionine ligand is coincident with the loss of the 695 band, together with the observation that most cytochromes possessing a 695 nm band contain a methionine ligand, has led to the view that the 695 nm band is diagnostic of methionine coordination [46-49]. However, its absence does not mean Met is not a ligand, as proved by Ångström and co-workers [50] in 1982, using NMR spectroscopy. Furthermore, the ionization of the axial His to histidinate causes a shift of the 695 nm band to shorter wavelengths, to a point where it may not be resolved from the α/β bands in the optical spectrum [36, 47].

Thus, the absence of a band at 695 nm in the UV-visible spectra does not mean that GSU0105 has no hemes coordinated with methionine residues. Further UV-visible spectroscopy assays need to be performed at higher protein concentrations, since this band is not very intense and is usually observed at much higher concentrations than the ones used in the assays performed [51].

3.2.2.2 – NMR features of GSU0105

NMR is a very powerful technique to identify the spin-state of heme groups in proteins, since NMR signals appear in quite distinct spectral regions, depending if the hemes are high- or low-spin. In the paramagnetic oxidized state, the 1D ^{1}H-NMR spectra of high-spin cytochromes display extremely broad signals and some frequencies above 40 ppm (usually belonging to heme methyl substituents). Low-spin cytochromes, on the other end, present narrower spectral windows, with the main heme substituents frequencies ranging from 8 to 35 ppm. In the diamagnetic reduced state, 1D ^{1}H-NMR spectra are also quite distinct for high- and low-spin cytochromes. In fact, high-spin hemes present wider spectral regions (ranging from -15 up to 30 ppm) than low-spin ones (ranging from -5 up to 10 ppm).

The 1D ^{1}H-NMR signals of GSU0105 in the oxidized state are very broad and cover a wide spectral region, namely from –10 ppm to above 65 ppm (Figure 3.11A). Therefore, the cytochrome is paramagnetic in the oxidized state, with at least one high-spin heme (Fe(III), S = 5/2), as hypothesized with the analysis of the UV-visible spectra previously presented. The broad signals (due to the strong paramagnetic contribution of the high- and low-spin heme(s)) make it very difficult to analyze other spectral features of the cytochrome in the paramagnetic state.

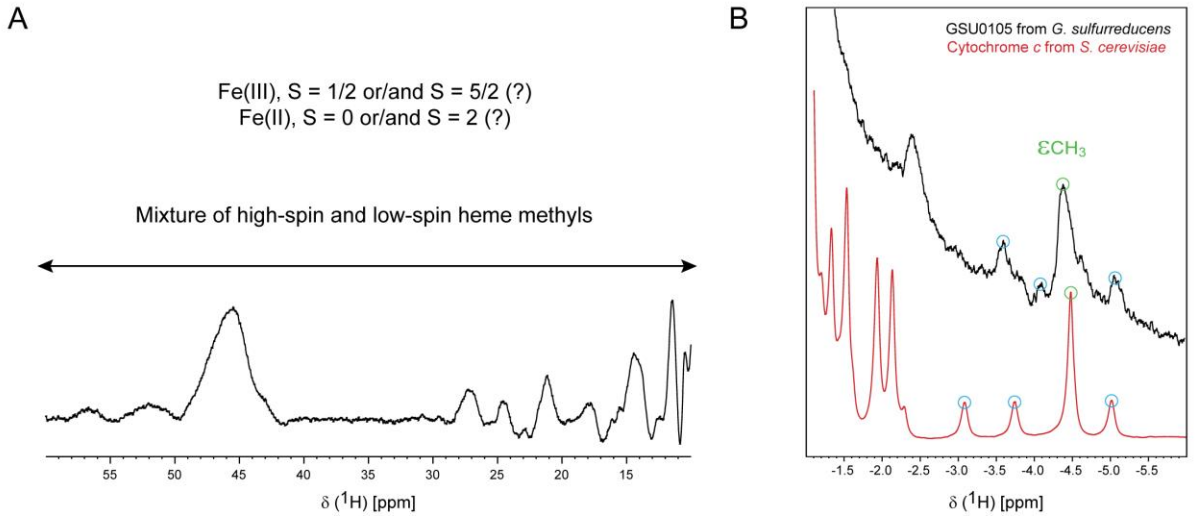

Figure 3.11 – Expansion of the 1D ^{1}H-NMR spectra of GSU0105, in 32 mM sodium phosphate, pH 8 (100 mM ionic strength), at 298 K – (A) NMR spectrum of GSU0105 in the oxidized state. The heme methyl signals are spread over the entire spectral width, due to the paramagnetic effect of multiple unpaired electrons. The possible spin-states of the hemes irons are indicated for the oxidized (Fe(III)) and reduced (Fe(II)) states. The spectrum was obtained with a 350 μM sample. (B) Low-frequency regions of the spectra of GSU0105 from G. sulfurreducens (black) and cytochrome c from Saccharomyces cerevisiae (red), in the reduced state. The three-proton intensity peak (εCH_3) and the three resolved one-proton intensity peaks, typical of methionine distal coordination, are highlighted by green and blue circles, respectively. The spectrum was obtained with a 20 μM sample.

An initial straightforward partial reduction of the sample was achieved with direct addition of sodium dithionite powder to the NMR tube containing GSU0105 (around 20 μM). The spectrum obtained (Figure 3.11B) displays the typical signal pattern of a distal coordinated methionine, which includes a three-proton intensity peak at approximately -3 ppm and up to four resolved one proton intensity peaks in the low-frequency region of the spectrum due to the heme ring-current effects [36]. However, the low-resolution of the spectrum, together with the fact that sodium dithionite was added in an uncontrolled manner, led to the necessity of improving the experimental reduction protocol. Furthermore, the signal widths were still large and the sample was possibly not completely reduced. Therefore, a more concentrated sample (350 μM) was prepared and a catalytical reduction was attempted by using hydrogenase from Desulfovibrio vulgaris (Hildenborough). However, after several cycles of hydrogen saturation, no differences in sample color were observed. Since the spectroscopic features of the heme groups usually allow for a naked eye distinction between the oxidized (brown) and reduced (pink) states, this indicated that no reduction occurred. Indeed, NMR experiments supported this hypothesis (data not shown).

After the unsuccessful sample reduction with hydrogenase, a different approach was used. Sodium dithionite is a powerful reducing agent ($E^{o'}$ = -0.66 V vs NHE, at pH 7 [52]) and is commonly used in redox experiments. In the commercially available form (powder), sodium dithionite may have different levels of activity (depending on the company, batch, age and conservation conditions), meaning that only a percentage is active. Therefore, proper solutions were prepared according to the procedure described in section 6.7, in order to guarantee that the additions to the protein sample followed a stoichiometry of one electron per heme group. After the solutions of sodium dithionite were prepared and degassed with argon, direct additions were performed in the NMR tube, either by using an Hamilton syringe or by direct addition, inside an anaerobic glove box. The sample redox state was confirmed after each addition by 1D ^{1}H-NMR, and not even with stoichiometries well above the 1:1 (electron:heme) sample reduction was achieved.

From the above, no confident conclusions can be taken about the spin-state of the cytochrome in the reduced state. In fact, only for the low concentrated sample of GSU0105 (20 μM), typical signals for a heme distal coordinated Met were observed (Figure 3.11B). Overall, the data obtained suggested that at least one heme group is His-Met axially coordinated, which further supports the statements made upon the UV-visible analysis.

Further insights are needed in order to understand why the protein is not reduced with the addition of sodium dithionite. Partial reduction seems to be occurring (since visually, changes in color were observed with the addition of the reducing agent), but not to a full extent that leads the protein to a stable fully reduced state. The hemes redox potentials may be very different from each other and/or very negative, factors that further complicate the reduction process. In order to probe this, an electrochemistry study was carried out.

3.2.3 – Electrochemical characterization of GSU0105

The voltammograms obtained for cytochrome GSU0105 at different scan rates are presented in Figures 3.12 and 3.13. The voltammograms are represented in two sets, for simplicity, since at higher scan rates the peak intensities become too intense and would mask the initial scans if represented together.

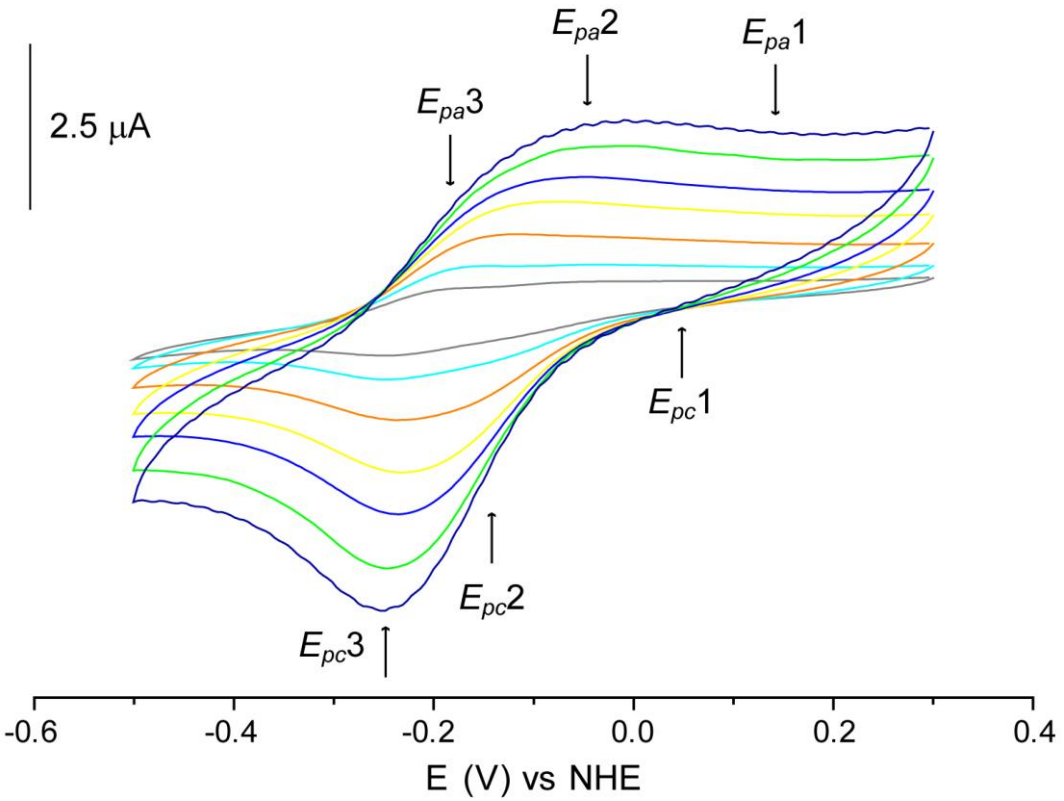

Figure 3.12 – CV assays of 200 μM GSU0105 in phosphate buffer with NaCl (170 mM final ionic strength), at pH 7 – The voltammograms were recorded at different scan rates: 5 (gray), 10 (cyan), 20 (orange), 35 (yellow), 50 (blue), 75 (green) and 100 (dark blue) mV s^{-1}. The peak intensity scale is presented in μA. The anodic and cathodic peaks corresponding to each redox center are marked (also see Figure 6.10).

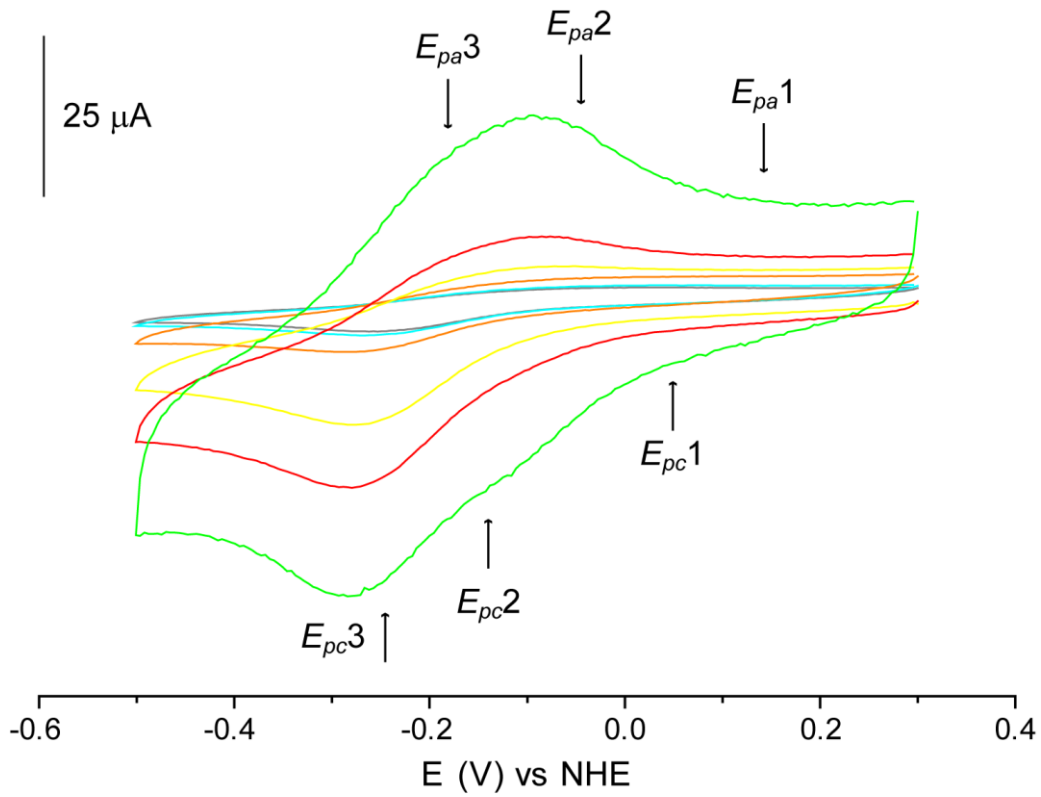

Figure 3.13 – CV assays of 200 μM GSU0105 in phosphate buffer with NaCl (170 mM final ionic strength), at pH 7 – The voltammograms were recorded at different scan rates: 150 (gray), 200 (cyan), 500 (orange), 1000 (yellow), 2000 (red) and 5000 (green) mV s^{-1}. The peak intensity scale is presented in μA. The anodic and cathodic peaks corresponding to each redox center are marked.

By analyzing the voltammograms obtained, it is possibly to verify that the protein has 3 redox pairs, which is in agreement with the number of predicted redox centers for GSU0105. This was further confirmed with the analysis of the voltammogram of the control assay performed with BSA, at the same experimental conditions (see section 6.8), which confirmed that the peaks observed at the cytochrome's voltammogram are not related with the electrolyte neither with surface processes associated with the electrode material. Therefore, they are the result of intrinsic mechanisms of the protein.

The unequivocally identification of the different anodic and cathodic peaks (as depicted in Figures 3.12 and 3.13) was achieved by obtaining voltammograms at specific potential intervals: (i) 0.3 to 0.1 V vs NHE, (ii) 0.3 to 0.0 V vs NHE, (iii) 0.3 to -0.05 V vs NHE, (iv) 0.3 to -0.15 V vs NHE, (v) 0.3 to -0.25 V vs NHE, (vi) 0.3 to -0.4 V vs NHE and (vii) 0.3 to -0.5 V vs NHE. These different voltammograms, which are represented in Figure 3.14, allowed the indexation of the different anodic and cathodic peaks.

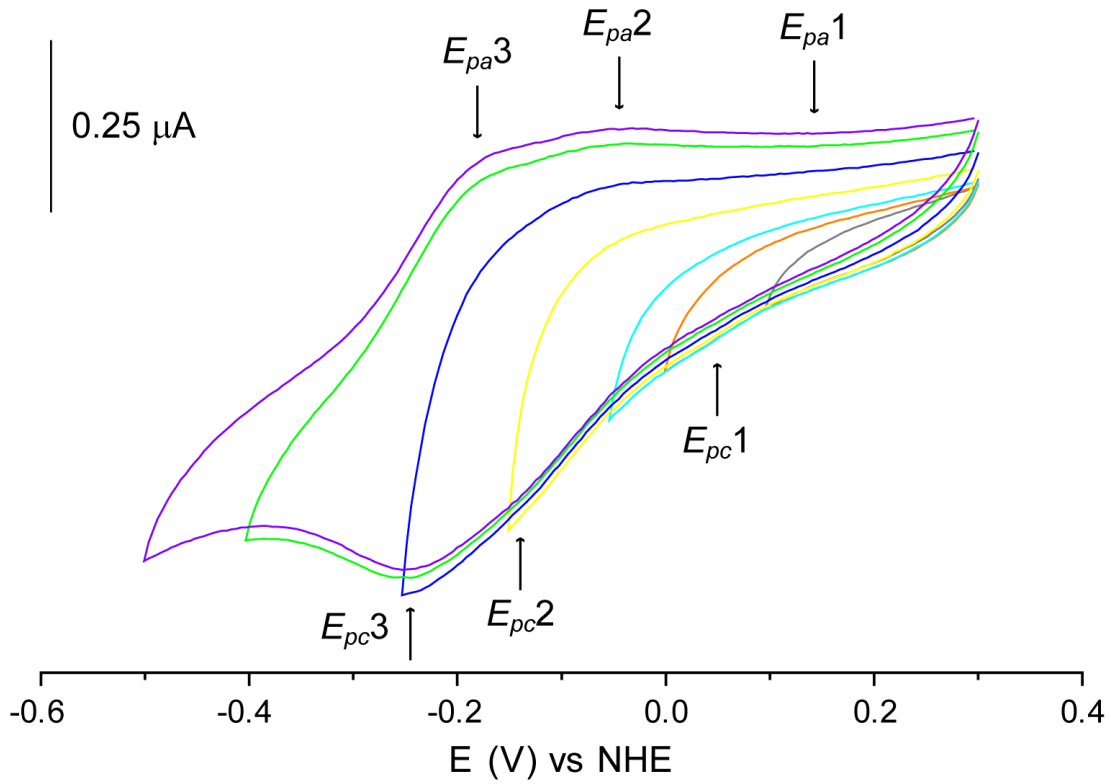

Figure 3.14 – Indexation of the anodic and cathodic peaks of GSU0105 – The CV assays were performed with 200 μM GSU0105 in phosphate buffer with NaCl (170 mM final ionic strength), at pH 7. The voltammograms were recorded with a scan rate of 10 mV s^{-1}, with different potential windows: 0.3 to 0.1 V vs NHE (gray), 0.3 to 0.0 V vs NHE (orange), 0.3 to -0.05 V vs NHE (cyan), 0.3 to -0.15 V vs NHE (yellow), 0.3 to -0.25 V vs NHE (dark blue), 0.3 to -0.4 V vs NHE (green) and 0.3 to -0.5 V vs NHE (purple). The peak intensity scale is presented in μA. The anodic and cathodic peaks corresponding to each redox center are marked.

The anodic and cathodic current peaks of the redox centers were observed approximately at the following average values: (i) for the first redox center, 131 and 51 mV vs NHE, respectively, (ii) for the second redox center, -54 and -146 mV vs NHE, respectively and (iii) for the third redox center, -205 and -218 mV vs NHE, respectively. These values correspond to formal potentials of 91 ± 16, -100 ± 23 and -212 ± 26 mV vs NHE, for the first, second and third redox centers. These formal potentials ($E^{0'}$) were calculated according to Equation 15, where E_{pa} and E_{pc} correspond to the anodic and cathodic potentials of the respective peaks.

$$E^{0\prime} = (E_{pa} + E_{pc})/2 \quad (15)$$

Although is not possible to directly assign the redox centers observed in the electrochemical experiments, one can infer, together with the data obtained in the previous sections, that the redox center with the most positive formal potential is probably the His-Met coordinated heme

observed in the NMR experiments, since c-type heme groups with this type of coordination usually present more positive redox potentials when compared to bis-histidinyl coordinated hemes [43, 53-60]. This is directly related with the fact of the side chain methionine sulfur being a good electron acceptor, which favors the electron-rich reduced state of the heme, resulting in more positive redox potentials compared to bis-histidinyl coordinated heme groups [43, 53]. However, there are exceptions to these observations, namely on the domain C of the dodecaheme GSU1996 [61] and on the cytochrome subunit of the photosynthetic reaction center from Rhodopseudomonas viridis [62, 63].

Many studies have been made in order to explain these exceptions [64-66], which are probably related with the tuning of the hemes potential by electrostatic interactions between the heme cofactor and protein surroundings (both polypeptide chain and neighboring hemes). Further experiments and techniques need to be used in order to confirm the hypothesis of the redox center with more positive formal potentials being the one coordinated by His and Met residues.

Further conclusions can be taken about this more positive redox center. It is observed that with slower scan rates, the anodic and cathodic peaks corresponding to this center are more intense and resolved. On the other way, with faster scan rates, the peaks are less intense and more difficult to observe. This means that the heterogeneous electron transfer constant (k_{sh}) of this center is relatively slow, since it can be observed more clearly at lower scan rates. This constant reflects the ease of electron transfer between the working electrode and the protein. Moreover, with higher scan rates, the anodic peak of the redox center is almost completely flat and unobservable, which is probably a consequence of intramolecular electron transfer. This phenomenon leads to a decrease in the populations of oxidized molecules and to a consequent lack of signal (absence of anodic peak). During the oxidation process, the more positive redox center transfers electrons to the other redox centers before the electrode is capable of reaching the potential values at which the anodic peak is usually resolved. The remaining redox centers have close formal potentials and are more easily distinguished and resolved at higher scan rates. For that reason, and compared to the other redox center, these centers possess faster electron transfer rates with the electrode, with the redox center number 2 being, apparently, the fastest one. Therefore, the electron transfer rates in GSU0105 are k_{sh} (redox center 2) > k_{sh} (redox center 3) > k_{sh} (redox center 1).

Comparing the formal potentials of the redox centers of GSU0105 (91, -100 and -212 mV vs NHE) with other triheme cytochromes (Table 3.2), it is possible to verify that the redox centers

1 (91 mV) and 3 (-212 mV) are the most positive and the most negative hemes found in all triheme cytochromes studied to date.

Table 3.2 – Heme reduction potentials of triheme cytochromes from G. metallireducens (Gm), G. sulfurreducens (Gs) and Desulfuromonas acetoxidans (Da) at pH 7 and 293 K – The values presented (vs NHE) were calculated using the values published in the indicated references.

Cytochrome	Heme reduction potentials (mV)		
	Heme I	Heme III	Heme IV
GmPpcA (this Thesis)	-82	-18	-121
GsPpcA [67]	-148	-106	-114
GsPpcB [67]	-147	-155	-122
GsPpcD [67]	-150	-98	-152
GsPpcE [67]	-155	-160	-97
GSU1996 (Domain C) [61]	-70	-146	-109
Dac_7 [68]	-193	-186	-123

The redox center 2 (-100 mV vs NHE), on the other side, has a reduction potential with values relatively similar to the ones presented by other triheme cytochromes, especially with the hemes III of PpcA and PpcD from G. sulfurreducens and with the hemes IV of PpcE and Domain C of GSU1996 from G. sulfurreducens, as well. This value is still, however, considerably more positive when compared with most of the heme groups of the PpcA-family of triheme cytochromes. These comparisons are, however, preliminary and superficial, considering the (i) necessity of performing more assays in order to have a consistent statistical meaning, (ii) values of errors obtained, that if considered, slightly change the interpretations made.

The main goal of the electrochemical studies was to get initial insights on the hemes redox potentials and eventually relate those results with the fact that sodium dithionite does not lead to total GSU0105 reduction. The formal potentials of all the redox centers are more positive than the formal potential of sodium dithionite ($E^{0'}$ = -0.66 V vs NHE, at pH 7 [52]), meaning that the reduction of the hemes is thermodynamically favorable, if looking to the redox potentials of the components involved in the reaction (sodium dithionite as the reducing agent and the redox centers of GSU0105 as the oxidizing agents). The absence of reduction of GSU0105 in the presence of sodium dithionite is then most probably related with the kinetics of the electron transfer process. This subject needs to be further investigated.

3.3 – Conclusions

In this Chapter, the expression and purification protocols for GSU0105 cytochrome of G. sulfurreducens were optimized. Initially, the cytochrome was heterologously expressed in E. coli BL21 (DE3) cells, but it was concluded that higher yields are obtained in E. coli JM109 cells. Other factors that may affect protein expression were tested, namely IPTG concentration and cell growth temperatures after protein induction. The best expression conditions for GSU0105 were obtained with 10 μM IPTG and cell growth at 30 ^{o}C. The final optimized yield was 0.165 mg per liter of cell culture.

Furthermore, preliminary spectroscopic insights were obtained for the GSU0105 cytochrome. The UV-visible spectra of GSU0105 display features of c-type cytochromes containing low-spin hemes in the reduced state and a mixture of low- and high-spin hemes in the oxidized state. This mixture probably includes a high-spin heme (which undergoes a redox-linked spin-state change, caused by the detachment of the axial methionine of one of the heme groups) and two low-spin hemes.

The 1D ^{1}H-NMR spectra of GSU0105 revealed that the cytochrome is paramagnetic and diamagnetic in the oxidized and reduced states, respectively. Furthermore, the large spectral width of the 1D ^{1}H-NMR spectrum of GSU0105 in the oxidized state suggests the presence of at least one high-spin heme (Fe(III), S = 5/2). The remaining heme-spin states need to be accessed with different techniques, namely EPR. In the reduced state, the 1D ^{1}H-NMR spectrum of GSU0105 shows a typical pattern of methionine axial coordination, which together with the data from UV-visible experiments, further supports the hypothesis of a redox-linked spin-state change, due to the detachment of the axial methionine of one of the heme groups. Considering the spectroscopic data, it is plausible to affirm that the cytochrome GSU0105 has three low-spin hemes (S = 0) in the reduced state (one His-His, one His-Met and one unknown) and a mixture of low- and high-spin characters in the oxidized state (S = 1/2 and S = 5/2, Fe(III)), with one His-His heme (low-spin), one His-vacant heme (high-spin) and one heme with unknown coordination. There are examples of cytochromes that contain heme groups with different types of axial coordination, such as GSU1996 [69] (see Chapter 1). However, GSU1996 is low-spin in both oxidation stages.

Electrochemical studies were performed using CV, in order to access the reduction potential values of the heme groups. The values measured for the three redox centers were 91 ± 16, -100 ± 23 and -212 ± 26 mV. The reduction potential values of all the redox centers are more positive

than that of sodium dithionite ($E^{0'}$ = -0.66 V vs NHE, at pH 7 [52]), meaning that the reduction of the hemes is thermodynamically favorable. Therefore, the absence of reduction of GSU0105 in the presence of sodium dithionite is most probably related with the kinetics of the electron transfer process.

The heme with the more positive redox potential was hypothesized as being His-Met coordinated, although further experiments need to be performed to confirm this hypothesis. By analysis of the voltammograms at different scan rates, it was concluded that the heterogeneous electron transfer constants of the redox centers are different.

3.4 – References

[1] Y.H. Ding, K.K. Hixson, C.S. Giometti, A. Stanley, A. Esteve-Núñez, T. Khare, S.L. Tollaksen, W. Zhu, J.N. Adkins, M.S. Lipton, R.D. Smith, T. Mester, D.R. Lovley, The proteome of dissimilatory metal-reducing microorganism Geobacter sulfurreducens under various growth conditions, Biochim. Biophys. Acta, 1764 (2006) 1198-1206.

[2] T. Goldberg, M. Hecht, T. Hamp, T. Karl, G. Yachdav, N. Ahmed, U. Altermann, P. Angerer, S. Ansorge, K. Balasz, M. Bernhofer, A. Betz, L. Cizmadija, K.T. Do, J. Gerke, R. Greil, V. Joerdens, M. Hastreiter, K. Hembach, M. Herzog, M. Kalemanov, M. Kluge, A. Meier, H. Nasir, U. Neumaier, V. Prade, J. Reeb, A. Sorokoumov, I. Troshani, S. Vorberg, S. Waldraff, J. Zierer, H. Nielsen, B. Rost, LocTree3 prediction of localization, Nucleic Acids Res., 42 (2014) 350-355.

[3] M. Aklujkar, M.V. Coppi, C. Leang, B.C. Kim, M.A. Chavan, L.A. Perpetua, L. Giloteaux, A. Liu, D.E. Holmes, Proteins involved in electron transfer to Fe(III) and Mn(IV) oxides by Geobacter sulfurreducens and Geobacter uraniireducens, Microbiology, 159 (2013) 515-535.

[4] S.M. Strycharz, R.H. Glaven, M.V. Coppi, S.M. Gannon, L.A. Perpetua, A. Liu, K.P. Nevin, D.R. Lovley, Gene expression and deletion analysis of mechanisms for electron transfer from electrodes to Geobacter sulfurreducens, Bioelectrochemistry, 80 (2011) 142-150.

[5] J.M. Dantas, L. Morgado, M. Aklujkar, M. Bruix, Y.Y. Londer, M. Schiffer, P.R. Pokkuluri, C.A. Salgueiro, Rational engineering of Geobacter sulfurreducens electron transfer components: A foundation for building improved Geobacter-based bioelectrochemical technologies, Front. Microbiol., 6 (2015) 752.

[6] A.P. Fernandes, I. Couto, L. Morgado, Y.Y. Londer, C.A. Salgueiro, Isotopic labeling of c-type multiheme cytochromes overexpressed in E. coli, Prot. Expr. Purif., 59 (2008) 182-188.

[7] P.R. Pokkuluri, Y.Y. Londer, X. Yang, N.E. Duke, J. Erickson, V. Orshonsky, G. Johnson, M. Schiffer, Structural characterization of a family of cytochromes c_7 involved in Fe(III) respiration by Geobacter sulfurreducens, Biochim. Biophys. Acta, 1797 (2010) 222-232.

[8] P.R. Pokkuluri, Y.Y. Londer, N.E. Duke, J. Erickson, M. Pessanha, C.A. Salgueiro, M. Schiffer, Structure of a novel c_7-type three-heme cytochrome domain from a multidomain cytochrome c polymer, Protein Sci., 13 (2004) 1684-1692.

[9] Y.Y. Londer, P.R. Pokkuluri, D.M. Tiede, M. Schiffer, Production and preliminary characterization of a recombinant triheme cytochrome c_7 from Geobacter sulfurreducens in Escherichia coli, Biochim. Biophys. Acta, 1554 (2002) 202-211.

[10] L. Galvani, De viribus electricitatis in motu musculari commentarius, Academy of Arts and Sciences of the Bologna Institute, Bologna, 1791.

[11] A. Kaifer, M. Gómez-Kaifer, Supramolecular electrochemistry, Wiley-VCH, New York, 1999.

[12] J. Wang, Analytical electrochemistry, VCH Publishers Inc., New York, 1994.
[13] P.T. Kissinger, W.R. Heineman, Laboratory techniques in electroanalytical chemistry, Second edition, Dekker: Monticello Inc., New York, 1996.
[14] C.F. Blanford, The birth of protein electrochemistry, Chem. Commun., 49 (2013) 11130-11132.
[15] G. Billon, C.M.G. van den Berg, Gold and silver micro-wire electrodes for trace analysis of metals, Electroanal., 16 (2004) 1583-1591.
[16] V. Brabec, 314 - Electrochemical oxidation of nucleic acids and proteins at graphite electrode. Qualitative aspects, Bioelectroch. Bioener., 7 (1980) 69-82.
[17] J. Heyrovský, J. Babička, Polarographic studies with the dropping mercury kathode. Part XIII. The effect of albumins, Collect. Czech. Chem. C., 2 (1930) 370-379.
[18] M. Heyrovský, Early polarographic studies on proteins, Electroanal., 16 (2004) 1067-1073.
[19] U. Oesch, J. Janata, Electrochemical study of gold electrodes with anodic oxide films - II. Inhibition of electrochemical redox reactions by monolayers of surface oxides, Electrochim. Acta, 28 (1983) 1247-1253.
[20] J.A. Reynaud, B. Malfoy, A. Bere, The electrochemical oxidation of three proteins: RNAase A, bovine serum albumin and concanavalin A at solid electrodes, J. Electroanal. Chem. Interfacial Electrochem., 116 (1980) 595-606.
[21] M. Sluyters-Rehbach, Impedances of electrochemical systems: Terminology, nomenclature and representation - Part I: Cells with metal electrodes and liquid solutions (IUPAC Recommendations 1994), Pure Appl. Chem., 66 (1994) 1831-1891.
[22] V. Fourmond, C. Léger, Protein Electrochemistry: Questions and answers, Biophotoelectrochemistry: From bioelectrochemistry to biophotovoltaics, Springer International Publishing, Cham, 2016, 1-41.
[23] H.A.O. Hill, Bio-electrochemistry, Pure Appl. Chem., 59 (1987) 743-748.
[24] C.F. Blanford, F.A. Armstrong, The pyrolytic graphite surface as an enzyme substrate: Microscopic and spectroscopic studies, J. Solid State Electr., 10 (2006) 826-832.
[25] C. Léger, P. Bertrand, Direct electrochemistry of redox enzymes as a tool for mechanistic studies, Chem. Rev., 108 (2008) 2379-2438.
[26] C. Léger, S.J. Elliott, K.R. Hoke, L.J.C. Jeuken, A.K. Jones, F.A. Armstrong, Enzyme electrokinetics: Using protein film voltammetry to investigate redox enzymes and their mechanisms, Biochemistry, 42 (2003) 8653-8662.
[27] M. Ferrer, T.N. Chernikova, M.M. Yakimov, P.N. Golyshin, K.N. Timmis, Chaperonins govern growth of Escherichia coli at low temperatures, Nat. Biotechnol., 21 (2003) 1266-1267.
[28] T. San-Miguel, P. Perez-Bermudez, I. Gavidia, Production of soluble eukaryotic recombinant proteins in E. coli is favoured in early log-phase cultures induced at low temperature, Springerplus, 2 (2013) 89.

[29] A. Vera, N. Gonzalez-Montalban, A. Aris, A. Villaverde, The conformational quality of insoluble recombinant proteins is enhanced at low growth temperatures, Biotechnol. Bioeng., 96 (2007) 1101-1106.
[30] M.N. Alves, A.P. Fernandes, C.A. Salgueiro, C.M. Paquete, Unraveling the electron transfer processes of a nanowire protein from Geobacter sulfurreducens, Biochim. Biophys. Acta - Bioenergetics, 1857 (2016) 7-13.
[31] M.A. Silva, R.C. Valente, P.R. Pokkuluri, D.L. Turner, C.A. Salgueiro, T. Catarino, Thermodynamic and kinetic characterization of two methyl-accepting chemotaxis heme sensors from Geobacter sulfurreducens reveals the structural origin of their functional difference, Biochim. Biophys. Acta, 1837 (2014) 920-928.
[32] J. Sambrook, D.W. Russell, Preparation and transformation of competent E. coli using calcium chloride, C. S. H. Protoc., 2006 (2006) 3932.
[33] L. Thöny-Meyer, Biogenesis of respiratory cytochromes in bacteria, Microbiol. Mol. Biol. Rev., 61 (1997) 337-376.
[34] L. Thöny-Meyer, F. Fischer, P. Kunzler, D. Ritz, H. Hennecke, Escherichia coli genes required for cytochrome c maturation, J. Bacteriol., 177 (1995) 4321-4326.
[35] A. Williams, V. Frasca, Ion-exchange chromatography, Current Protocols in Protein Science, 15 (1999) 8.2.1-8.2.30.
[36] G.R. Moore, G.W. Pettigrew, Cytochromes c: Evolutionary, structural and physicochemical aspects, Molecular Biology, Springer-Verlag Heidelberg, Berlin, 1990.
[37] P.R. Pokkuluri, M. Pessanha, Y.Y. Londer, S.J. Wood, N.E.C. Duke, R. Wilton, T. Catarino, C.A. Salgueiro, M. Schiffer, Structures and solution properties of two novel periplasmic sensor domains with c-type heme from chemotaxis proteins of Geobacter sulfurreducens: Implications for signal transduction, J. Mol. Biol., 377 (2008) 1498-1517.
[38] T. Catarino, M. Pessanha, A.G. De Candia, Z. Gouveia, A.P. Fernandes, P.R. Pokkuluri, D. Murgida, M.A. Marti, S. Todorovic, C.A. Salgueiro, Probing the chemotaxis periplasmic sensor domains from Geobacter sulfurreducens by combined resonance raman and molecular dynamic approaches: NO and CO sensing, J. Phys. Chem. B, 114 (2010) 11251-11260.
[39] I. Moura, M.Y. Liu, C. Costa, M.C. Liu, G. Pai, A.V. Xavier, J. LeGall, W.J. Payne, J.J. Moura, Spectroscopic characterization of a high-potential monohaem cytochrome from Wolinella succinogenes, a nitrate-respiring organism. Redox and spin equilibria studies, Eur. J. Biochem., 177 (1988) 673-682.
[40] H. Theorell, Å. Åkesson, Studies on cytochrome c. I. Electrophoretic purification of cytochrome c and its amino acid composition, J. Am. Chem. Soc., 63 (1941) 1804-1811.
[41] H. Theorell, Å. Åkesson, Studies on cytochrome c. II. The optical properties of pure cytochrome c and some of its derivatives, J. Am. Chem. Soc., 63 (1941) 1812-1818.
[42] B. Chance, C.P. Lee, L. Mela, D.F. Wilson, Some properties of the 695 nm band of cytochrome c, Structure and function of cytochromes, Univ. Park Press, Baltimore, 1968, 353-356.

[43] G.W. Pettigrew, G.R. Moore, Cytochromes c: Biological aspects, London, 1987.
[44] A. Schejter, P. George, The 695 mμ band of ferricytochrome c and its relationship to protein conformation, Biochemistry, 3 (1964) 1045-1049.
[45] E. Shechter, P. Saludjian, Conformation of ferricytochrome c. IV. Relationship between optical absorption and protein conformation, Biopolymers, 5 (1967) 788-790.
[46] G.R. Moore, G.J. McClune, N.J. Clayden, R.J. Williams, B.M. Alsaadi, J. Angstrom, R.P. Ambler, J. van Beeumen, P. Tempst, R.G. Bartsch, T.E. Meyer, M.D. Kamen, Metal coordination centres of class II cytochromes c, Eur. J. Biochem., 123 (1982) 73-80.
[47] G.R. Moore, R.J. Williams, J. Peterson, A.J. Thomson, F.S. Mathews, A spectroscopic investigation of the structure and redox properties of Escherichia coli cytochrome b-562, Biochim. Biophys. Acta, 829 (1985) 83-96.
[48] Y.P. Myer, P.A. Bullock, Cytochrome b_{562} from Escherichia coli: Conformational, configurational, and spin-state characterization, Biochemistry, 17 (1978) 3723-3729.
[49] C. Van den Branden, J. Van Beeumen, J. De Ley, A. Van de Mieroop, Purification and properties of cytochrome c-556 from Agrobacterium tumefaciens B2a, H-S. Z. Physiol. Chem., 356 (1975) 1251-1258.
[50] J. Ångström, G.R. Moore, R.J.P. Williams, The magnetic susceptibility of ferricytochrome c, Biochim. Biophys. Acta - Protein Struct., 703 (1982) 87-94.
[51] J.M. Dantas, Characterization of extracellular electron transfer networks in Geobacter sulfurreducens, a key bacterium for bioremediation and bioenergy applications, PhD Thesis, Chemistry Department, FCT-UNL, Monte da Caparica, 2017.
[52] S.G. Mayhew, The redox potential of dithionite and SO^{-2} from equilibrium reactions with flavodoxins, methyl viologen and hydrogen plus hydrogenase, Eur. J. Biochem., 85 (1978) 535-547.
[53] L. Banci, I. Bertini, A. Rosato, G. Varani, Mitochondrial cytochromes c: A comparative analysis, J. Biol. Inorg. Chem., 4 (1999) 824-837.
[54] G. Battistuzzi, M. Borsari, J.A. Cowan, A. Ranieri, M. Sola, Control of cytochrome c redox potential: Axial ligation and protein environment effects, J. Am. Chem. Soc., 124 (2002) 5315-5324.
[55] A. Dolla, L. Florens, P. Bianco, J. Haladjian, G. Voordouw, E. Forest, J. Wall, F. Guerlesquin, M. Bruschi, Characterization and oxidoreduction properties of cytochrome c_3 after heme axial ligand replacements, J. Biol. Chem., 269 (1994) 6340-6346.
[56] S. Hay, T. Wydrzynski, Conversion of the Escherichia coli cytochrome b_{562} to an archetype cytochrome b: A mutant with bis-histidine ligation of heme iron, Biochemistry, 44 (2005) 431-439.
[57] P. Hosseinzadeh, Y. Lu, Design and fine-tuning redox potentials of metalloproteins involved in electron transfer in bioenergetics, Biochim. Biophys. Acta, 1857 (2016) 557-581.

[58] G.T. Miller, B. Zhang, J.K. Hardman, R. Timkovich, Converting a c-type to a b-type cytochrome: Met61 to His61 mutant of Pseudomonas cytochrome c-551, Biochemistry, 39 (2000) 9010-9017.

[59] A.L. Raphael, H.B. Gray, Axial ligand replacement in horse heart cytochrome c by semisynthesis, Proteins, 6 (1989) 338-340.

[60] F.A. Tezcan, J.R. Winkler, H.B. Gray, Effects of ligation and folding on reduction potentials of heme proteins, J. Am. Chem. Soc., 120 (1998) 13383-13388.

[61] L. Morgado, A.P. Fernandes, Y.Y. Londer, P.R. Pokkuluri, M. Schiffer, C.A. Salgueiro, Thermodynamic characterization of the redox centres in a representative domain of a novel c-type multihaem cytochrome, Biochem. J., 420 (2009) 485-492.

[62] S.M. Dracheva, L.A. Drachev, A.A. Konstantinov, A.Y. Semenov, V.P. Skulachev, A.M. Arutjunjan, V.A. Shuvalov, S.M. Zaberezhnaya, Electrogenic steps in the redox reactions catalyzed by photosynthetic reaction-centre complex from Rhodopseudomonas viridis, Eur. J. Biochem., 171 (1988) 253-264.

[63] G. Fritzsch, S. Buchanan, H. Michel, Assignment of cytochrome hemes in crystallized reaction centers from Rhodopseudomonas viridis, Biochim. Biophys. Acta - Bioenergetics, 977 (1989) 157-162.

[64] Y. Takayama, N.D. Werbeck, H. Komori, K. Morita, K. Ozawa, Y. Higuchi, H. Akutsu, Strategic roles of axial histidines in structure formation and redox regulation of tetraheme cytochrome c_3, Biochemistry, 47 (2008) 9405-9415.

[65] P. Voigt, E.-W. Knapp, Tuning heme redox potentials in the cytochrome c subunit of photosynthetic reaction centers, J. Biol. Chem., 278 (2003) 51993-52001.

[66] Z. Zheng, M.R. Gunner, Analysis of the electrochemistry of hemes with E_ms spanning 800 mV, Proteins, 75 (2009) 719-734.

[67] L. Morgado, M. Bruix, M. Pessanha, Y.Y. Londer, C.A. Salgueiro, Thermodynamic characterization of a triheme cytochrome family from Geobacter sulfurreducens reveals mechanistic and functional diversity, Biophys. J., 99 (2010) 293-301.

[68] I.J. Correia, C.M. Paquete, R.O. Louro, T. Catarino, D.L. Turner, A.V. Xavier, Thermodynamic and kinetic characterization of trihaem cytochrome c_3 from Desulfuromonas acetoxidans, Eur. J. Biochem., 269 (2002) 5722-5730.

[69] P.R. Pokkuluri, Y.Y. Londer, N.E. Duke, M. Pessanha, X. Yang, V. Orshonsky, L. Orshonsky, J. Erickson, Y. Zagyansky, C.A. Salgueiro, M. Schiffer, Structure of a novel dodecaheme cytochrome c from Geobacter sulfurreducens reveals an extended 12 nm protein with interacting hemes, J. Struct. Biol., 174 (2011) 223-233.

4

Exploring membrane proteins from Geobacter sulfurreducens

"An expert is a person who has made all the
mistakes that can be made in a very narrow field."

Niels Bohr

4 – Exploring membrane proteins of Geobacter sulfurreducens

Over the years, membrane proteins have been gathering attention from the scientific community, since they play a fundamental role in many critical biological processes. Membrane proteins are essential components of biological processes such as ions, metabolites or water transport, signal transduction, sensing cell environment and control of cell-cell contact [1]. Although it is crucial to understand the functional mechanisms behind all these processes, the study of membrane proteins has only recently started to be developed. In fact, membrane protein structural biology is still a largely unconquered area, given that approximately 25% of all proteins are membrane proteins and only about 800 unique structures are available [2, 3]. These proteins are difficult to study owing to their partially hydrophobic surfaces, flexibility and lack of stability. Thanks to the development of high-throughput techniques in structural biology and methods that are emerging for effective expression, solubilization, purification and crystallization of membrane proteins, a rapid increase in the rate at which membrane protein structures and biochemical data are published is expected.

Membrane proteins can be classified into two broad categories – integral (intrinsic) and peripheral (extrinsic) – based on the nature of the membrane-protein interactions (Figure 4.1).

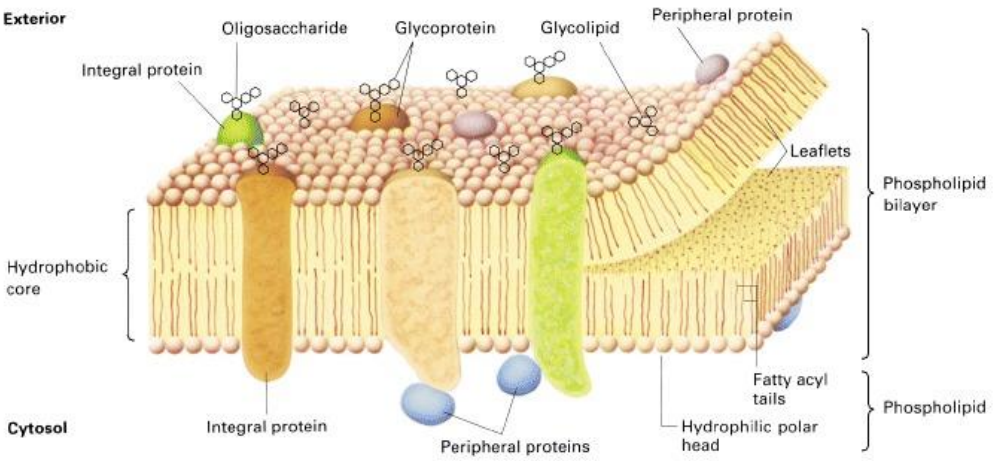

Figure 4.1 – Schematic diagram of typical membrane proteins in a biological membrane – The phospholipid bilayer, the basic structure of all cellular membranes, consists of two leaflets of phospholipid molecules whose fatty acyl tails form the hydrophobic interior of the bilayer. Their polar, hydrophilic head groups line both surfaces. Most integral proteins span the bilayer as shown. A few of them are tethered to one leaflet by a covalently attached lipid anchor group. Peripheral proteins are primarily associated with the membrane by specific protein-protein interactions. Oligosaccharides bind mainly to membrane proteins, however, some bind to lipids, forming glycolipids. This image was taken from [4].

Integral membrane proteins have one or more segments that are embedded in the phospholipid bilayer. Most integral proteins contain residues with hydrophobic side chains that interact with fatty acyl groups of the membrane phospholipids, thus anchoring the protein to the membrane. On the other hand, peripheral membrane proteins do not interact with the hydrophobic core of the phospholipid bilayer. Instead, these proteins usually bind to the membrane indirectly by interactions with integral membrane proteins or directly by interactions with lipid polar head groups.

Geobacter are Gram-negative bacteria and as in all the bacteria of this type, the OM plays pivotal roles in bacterial survival in a wide range of environments, serving as a protective barrier and allowing the uptake of nutrients [5, 6]. OM proteins are major components of the OM and include anchoring lipoproteins and transmembrane β-barrel proteins, such as porins, substrate-specific transporters and active transporters [5]. The transmembrane β-barrel proteins are characterized by the number of anti-parallel β-strands, ranging in number from eight to twenty-four [7]. Porins are the most abundant and important transmembrane β-barrel proteins of the OM, comprising up to 2% of the entire protein content of the cell [6]. They serve as water-filled open channels allowing the passive penetration of hydrophilic molecules, which are discriminated depending on their overall physicochemical properties (size, hydrophobicity and charge) [8].

These OM porin-like proteins can form trans-OM conductive porin-cytochrome (Pcc) complexes, by getting together with OM and periplasmic cytochromes c, in order to transfer electrons from the periplasmic space and across the OM to the extracellular electron acceptors [9-12]. Examples of this kind of complexes include the well-characterized S. oneidensis MtrA-MtrB-MtrC complex [13], as well as OmaB-OmbB-OmcB and OmaC-OmbC-OmcC complexes of G. sulfurreducens [11], which are represented in Figure 4.2 together with other similar complexes.

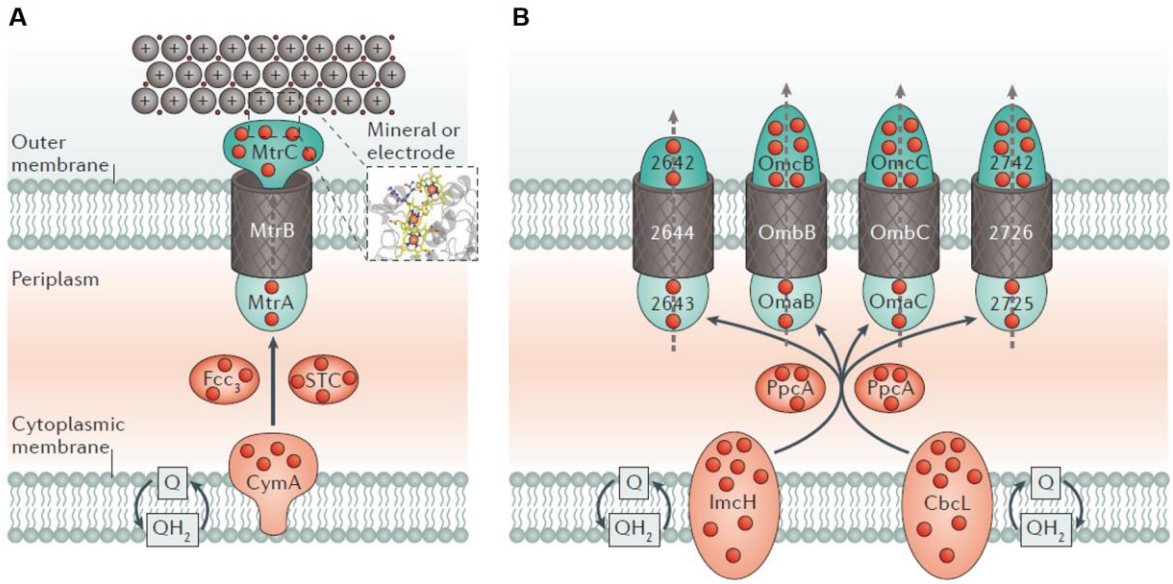

Figure 4.2 – The proposed Mtr and Pcc extracellular electron transfer pathways – In the (A) metal-reducing (Mtr) pathways of S. oneidensis MR-1 and (B) in the porin-cytochrome (Pcc) pathways of G. sulfurreducens, electrons are transferred from quinol (QH_2) in the cytoplasmic membrane, through the periplasm, and across the OM to the bacterial surface. In S. oneidensis, MtrC then transfers electrons to surface iron atoms directly through its solvent-exposed heme iron atom (inset of (A) – brown sphere, based on Edwards and co-workers [14]). This mechanism is likely similar in G. sulfurreducens. This figure was taken from [11].

Several models have been presented for explaining how electrons are conducted from inside of the cell to the extracellular environment in Gram-negative bacteria. These models are based on studies performed with EET components of S. oneidensis [15]. However, it is unknown how the electrons are transferred once outside the cell. There are three main theories regarding this subject: the electrons are transferred (i) directly from OM cytochromes to insoluble electron sinks (as presented in Figure 4.2), (ii) by assemblies of cytochromes, perhaps associated with extracellular appendages, sometimes referred to as nanowires or (iii) via electron shuttles (Figure 4.3) [15].

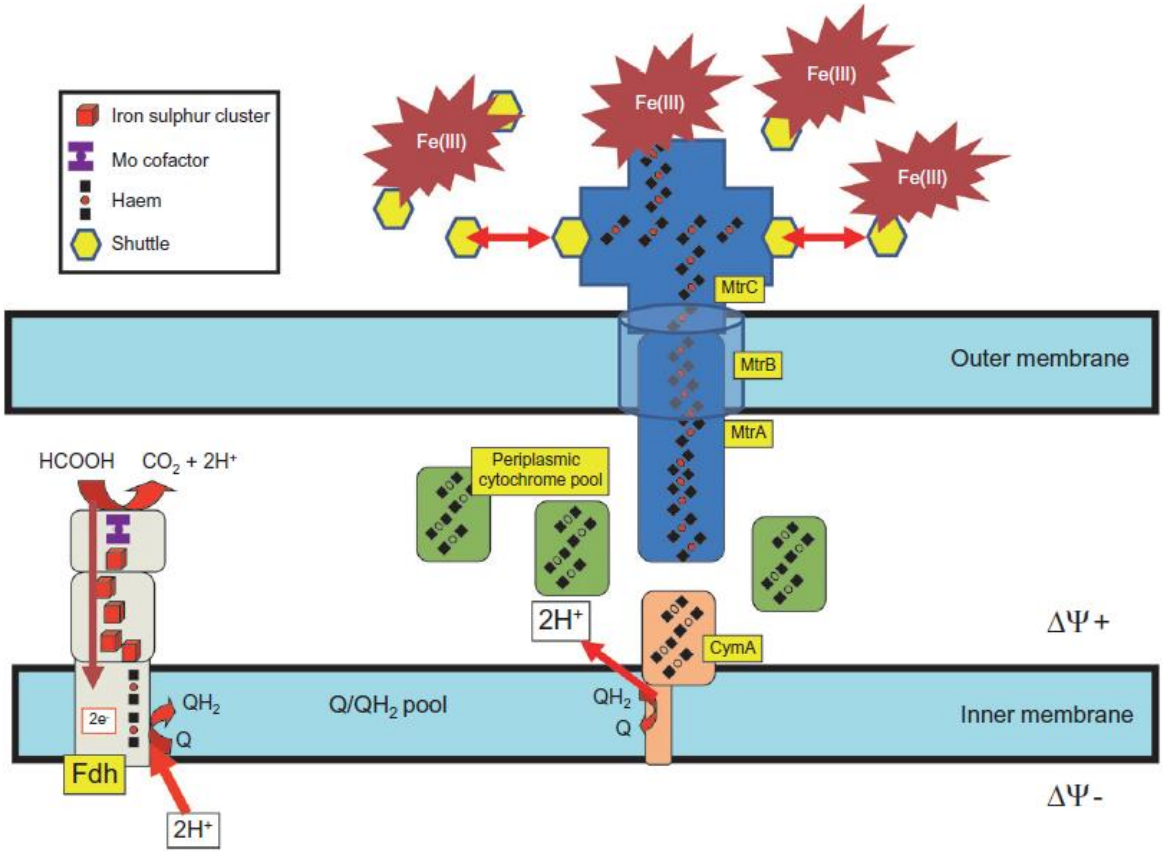

Figure 4.3 – Scheme for electron transfer from the inner cytoplasmic membrane to the extracellular environment in S. oneidensis – The scheme is illustrated with formate as electron donor. The formate dehydrogenase (Fdh)-CymA redox loop couples the net movement of two positive charges from the membrane potential-negative ($\Delta\Psi-$) to the membrane potential-positive ($\Delta\Psi+$) side of the membrane, per two electrons transferred in one Q/QH_2 cycle. The electrons are then transferred from the periplasmic components to the MtrA-MtrB-MtrC complex and once they reach the cell exterior, different mechanisms of electron transfer are activated. This figure was taken from [15].

Considering the above mentioned, it would be interesting to further confirm the theories presented for electron transfer in Gram-negative bacteria by using other bacteria models (such as Geobacter) and further contribute for the general understanding of how electron transfer is carried out to final insoluble acceptors in the extracellular environment, in these bacteria.

As previously said, the G. sulfurreducens genome contains more than 100 genes predicted to encode cytochromes c [16]. However, only a limited number of OM cytochromes has been characterized with some detail [9, 10, 12, 17-20]. Considering the above mentioned, there is the need to functionally and structurally characterize these proteins, in order to further understand how the EET routes are organized in Geobacter.

Recently, other OM complexes, OmaW(GSU2643)-OmbW(GSU2644)-OmcW(GSU2642) and OmaV(GSU2725)-OmbV(GSU2726)-OmcV(GSU2724), were shown to be involved in EET

to Fe(III) and Mn(IV) oxides [21, 22]. OmaW and OmaV are predicted to be periplasmic peripheral membrane proteins, bonded indirectly to the membrane by interactions with the integral membrane proteins OmbW and OmbV, respectively.

Considering that peripheral membrane proteins can be dissociated using relatively mild techniques that break the electrostatic or hydrogen bonds between the peripheral proteins and the membrane, without total membrane disruption, OmaW and OmaV proteins were chosen as the cytochromes of choice for initial expression and purification tests. These cytochromes have a theoretical molecular weight of around 18.5 kDa and are both predicted to have 5 heme groups, according to the number of CXXCH motifs present in their sequences (Figure 4.4).

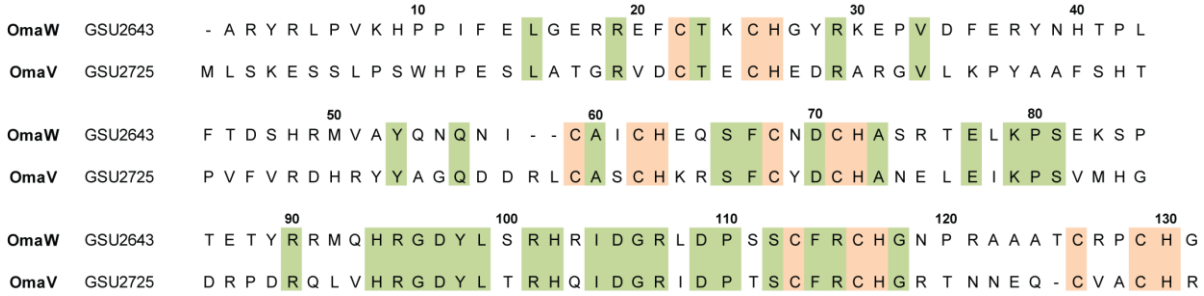

Figure 4.4 – Amino acid sequence alignment of OmaW and OmaV from G. sulfurreducens – The heme binding motifs and the conserved residues are highlighted in orange and green, respectively.

The pentaheme cytochromes share 49% amino acid sequence identity and 58 conserved residues, including the Cys and His residues included on the CXXCH binding motifs. Their main biochemical features are presented in Table 4.1.

Table 4.1 – Biochemical characteristics of OM cytochromes from G. sulfurreducens – The presented molecular weights are approximated. The isoelectric points were all theoretically predicted using the Compute pI/MW tool, from ExPASy – Swiss Institute of Bioinformatics (https://www.expasy.org).

Protein	Gene	Residues	Molecular weight (kDa)	Isoelectric point
OmaW	GSU2643	131	18.5	9.0
OmaV	GSU2725	133	18.4	7.7

By the time this Thesis started, OmaW and OmaV were already cloned into the vector pVA203 [23, 24]. In this Chapter, several biochemical and molecular biology techniques were used to improve the purification protocols of these cytochromes. The results obtained and the improvements achieved are presented and discussed.

4.1 – Materials and methods

4.1.1 – Insertion of His-tag on the pGSU2643 (OmaW) plasmid

In order to facilitate the process of purification of the OmaW cytochrome, the plasmid pGSU2643, containing the gene encoding for the referred cytochrome, was modified to contain an His-tag, a cleavage site for the TEV (Tobacco Etch Virus) protease and two pairs of Gly-Ser linker sequences. These linker sequences are quite flexible, due to the small and simple structure of the two amino acids that compose them. These linkers are often used in fusion proteins design [25]. The cleavage site for the TEV protease was added so the tag can be further removed, after the purification processes [26].

The desired sequence (Table 4.2) was inserted into the pGSU2643 vector (using a strategy based on the Q5® Site-Directed Mutagenesis kit, from New England Biolabs) at the 5' end of the sequence encoding for the OmaW cytochrome (N-terminal of the protein). The primers used in the procedure were produced by Invitrogen and are presented in Table 4.2.

Table 4.2 – Sequences of the DNA insert and primers used to produce the pGSU2643H plasmid, encoding for the N-terminal His-tagged OmaW cytochrome – The melting temperatures (T_m) for each primer were calculated from the Thermo Scientific web tool (https://www.thermofisher.com). The annealing temperature calculated for the pair of primers was 72 °C, using the same tool. The Gly-Ser linkers, the His residues composing the His-tag and the cleavage site for TEV protease are highlighted in blue, orange and green, respectively. In the primers, the sequences complementary to the pGSU2643 plasmid are highlighted in red.

	DNA sequence	T_m (°C)
His-tag insert	5' GGCAGCCATCATCATCATCATCACAG CGGCGAAAACCTGTATTTTCAGTCT 3'	–
Primer forward	5' CTGTGATGATGATGATGATGGCT GCCGGCGGCCGCAACGGTAGC 3'	81.0
Primer reverse	5' CGGCGAAAACCTGTATTTTCA GTCTGCGCGCTATCGGCTGCCC 3'	79.1

The Q5® Site-Directed Mutagenesis kit is designed for rapid and efficient incorporation of insertions, deletions and substitutions into double stranded plasmid DNA. The first step of the protocol is an exponential amplification using standard primers and a master mix formulation of the Q5 Hot Start High-Fidelity DNA Polymerase (Figure 4.5).

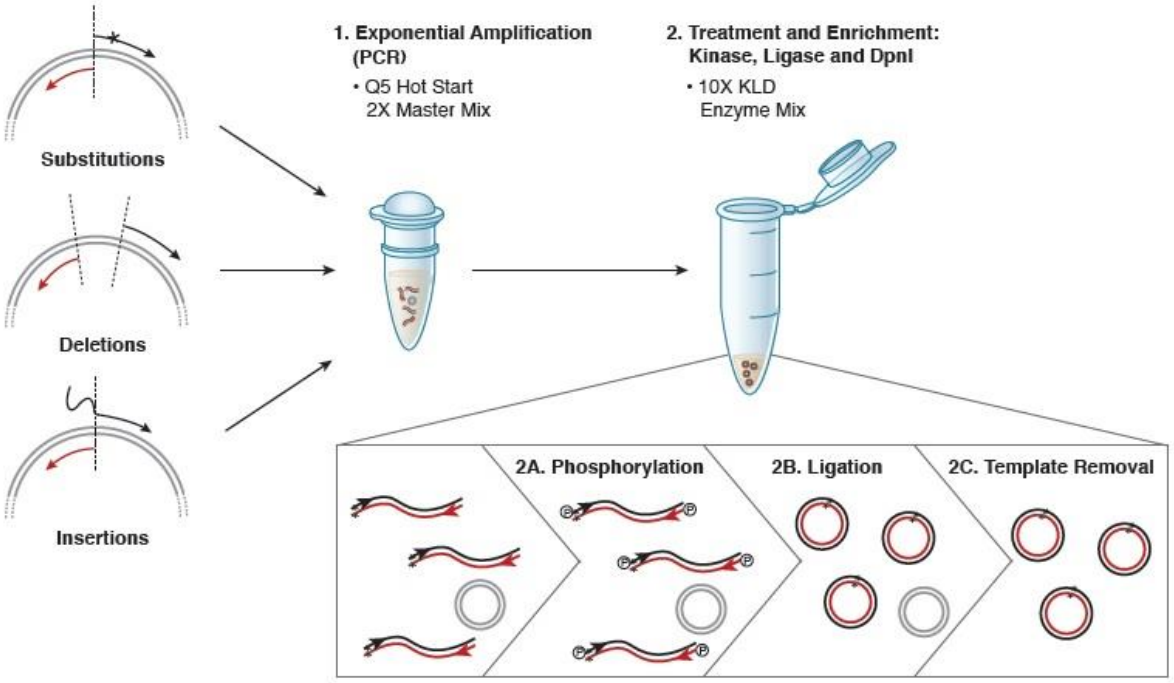

Figure 4.5 – Overview of the Q5® Site-Directed Mutagenesis kit from New England Biolabs – This figure was adapted from the Instructions Manual of the kit.

The second step involves incubation with a unique enzyme mix containing a kinase, a ligase and DpnI (Figure 4.5). Together, these enzymes allow for rapid circularization of the PCR product and removal of the template DNA. The final step involves a transformation in competent cells for final plasmid maturation.

The experiments were performed following the kit's protocol to prepare the His-tagged OmaW. The first step (exponential amplification, with insertion of the target sequence) was performed by Polymerase Chain Reaction (PCR). PCR is a widely used technique in molecular biology for exponentially amplify a single copy or a few copies of a specific segment of DNA to generate thousands to millions of copies of a particular DNA sequence [27].

The PCR samples were prepared with the conditions presented in Table 4.3. PCR cycling conditions used for the insertion of the target sequence are indicated in Table 4.4.

Table 4.3 – Composition of the final PCR mix (reaction volume = 50 μL).

PCR reaction mix components	Final concentration
Phusion GC/HF buffer	1x
Phusion High-Fidelity DNA polymerase	1 U*[1]
Deoxynucleotides (dNTPs)	0.2 mM
Primer forward	0.5 μM
Primer reverse	0.5 μM
DNA template (pGSU2643)	0.2 or 0.5 ng/μL

* The Phusion DNA polymerase, the Phusion GC/HF buffers and the dNTPs are all from Thermo Scientific. *[1]1 U = amount of enzyme necessary to catalize the conversion of 1 μmole of substrate per minute.

Table 4.4 – PCR cycling conditions – The annealing/extension time was calculated according to the manufacturer's indication of 15-30 seconds/kb.

PCR step		Temperature (°C)	Time (seconds)
Initial denaturation		98	30
Denaturation	25x	98	8
Annealing/extension		72	100
Final extension		72	600
Final hold		16	–

The annealing and extension steps are represented as a single one because in this case the temperature of primer annealing is equivalent to the optimal temperature of activity (72 °C) for the polymerase used in the assays (Phusion High-Fidelity DNA polymerase). Negative controls were carried out for the PCR reaction and the results were analyzed by 1% agarose gel electrophoresis, stained with GreenSafe Premium (NZYTech). The protocol of the agarose gel electrophoresis step is presented in section 6.3. After this step, the PCR products were purified using the NZYMiniprep kit (NZYTech) and quantified in the Nanodrop (Thermo Fischer Scientific).

In molecular biology, vectors and inserts digested by restriction enzymes contain the necessary terminal modifications in the 5' phosphate and 3' hydroxyl groups in order to be further hybridized, once inside competent cells. Fragments created by PCR, however, do not possess these necessary modifications, unless the amplification process is performed with previously phosphorylated primers. In this type of fragments, the 5' ends of the amplicon are non-phosphorylated and need to be treated by a kinase to introduce the 5' phosphate. Therefore,

since the primers used in this experiment were not previously phosphorylated, kinase was used in the second step of the mutagenesis protocol.

Furthermore, this step also included the use of the DNA ligase and DpnI enzymes. DNA ligase is added to catalyze the formation of the phosphodiester bonds crucial to bind the DNA strands of the PCR product. The addition of DpnI is related with the necessity of eliminating the DNA template (pGSU2643). This enzyme is specific for methylated and hemimethylated DNA. Since DNA isolated from most E. coli strains is methylated, it is susceptible to DpnI digestion. Hence, DpnI is frequently used after a PCR reaction to digest the methylated parental DNA template and select for the newly synthesized DNA containing mutations. Taking into account these considerations, a protocol was developed for the sample incubation with the different enzymes.

The PCR products were incubated with 1 U (in this case, one unit is defined as the amount of DpnI required to digest completely 1 μg of plasmid DNA in 50 μL of the reaction mixture at 37 °C for one hour) of DpnI (NZYTech) at 37 °C for 2 hours (optimal activity temperature of the enzyme) and then left at 80 °C for 20 minutes (DpnI inactivation). The reaction mix was prepared according to the enzymes manufacturer's indications. Then, the samples were submitted to a single step which comprised the enzymatic reactions of both the T4 polynucleotide kinase (NZYTech) and the T4 DNA ligase (Thermo Scientific). The samples were prepared with the conditions presented in Table 4.5 (which included a specific buffer with the necessary substrates for both enzymatic reactions) and then left incubating at 37 °C for 1 hour (optimal activity temperature of the enzymes) and 65 °C for 10 minutes (enzyme activity inactivation).

Table 4.5 – Composition of the final enzymatic mix – The T4 DNA ligase buffer (1x) from Thermo Scientific contains 10 mM $MgCl_2$, 10 mM dithiothreitol (DTT) and 0.5 mM ATP.

Enzymatic mix components	Final concentration
T4 DNA ligase buffer (Thermo Scientific)	1x
T4 polynucleotide kinase	1 U*
T4 DNA ligase	1 U*
PCR product	64 ng

*1 U = amount of enzyme necessary to catalize the conversion of 1 μmole of substrate per minute.

After the enzyme treatment, the constructed vectors were transformed in E. coli DH5α competent cells and plated for selection in Luria-Bertani (LB) medium supplemented with

ampicillin (100 μM/mL). Proper controls were performed. The resulting colonies were screened by colony PCR [28, 29] (with primers complementary to the pVA203 plasmid) and analyzed by 1.3% agarose gel electrophoresis. The colonies with PCR products of the correct size were grown in liquid LB supplemented with ampicillin for plasmid extraction and purification, using the NZYMiniprep kit. Finally, the presence of the desired insertion was confirmed by DNA sequencing performed by STAB Vida.

4.1.2 – Expression of OmaW and OmaV of Geobacter sulfurreducens

The OmaW and OmaV cytochromes were expressed as previously described for other cytochromes of G. sulfurreducens [23, 30]. The expression was performed in E. coli BL21 (DE3) cells, containing the plasmid pEC86 [31, 32]. These cells were transformed with the plasmids pGSU2643H/pGSU2643 or pGSU2725 (containing the genes GSU2643 (with and without an His-tag) and GSU2725, respectively, an ampicillin resistance gene, a lac promoter and an OmpA leader sequence [30]) and grown in 2xYT media supplemented with 34 μg/mL chloramphenicol and 100 μg/mL ampicillin, to an OD_{600} of approximately 1.5 at 30 ^{o}C. Then, protein expression was induced with 100 μM of IPTG and the cultures were left at 30 ^{o}C for overnight growth.

4.1.3 – Purification of OmaW and OmaV of Geobacter sulfurreducens

After overnight incubation, cells were harvested by centrifugation at 6400 xg for 20 minutes, at 4 ^{o}C. The cell pellet was gently resuspended in 10 mM Tris-HCl pH 8.1 (containing 0.5 mg/mL of lysozyme, 0.5 mM EDTA, DNase (Sigma-Aldrich) and protease inhibitors – 1 mM of phenylmethylsulphonyl fluoride (PMSF, Sigma-Aldrich) and 2 mM of benzamidine-HCl (Sigma-Aldrich)) and disrupted by three passages through a French Press (Thermo Scientific IEC), at a pressure of 1400 psi (1 psi = 6.9 kPa). The cell lysates were then centrifugated at 30000 xg for 30 minutes at 4 ^{o}C, and the resultant pellets and supernatants analyzed by SDS-PAGE (15% acrylamide/bis-acrylamide), stained either for hemes (TMBZ staining) or with BlueSafe (see protocol for both types of staining in section 6.2). The soluble and insoluble fractions containing the target proteins were further purified by chromatographic techniques (see below) or resuspended in various conditions, respectively.

Throughout the optimization of the purification protocol, different approaches were used for protein solubilization, based either on (i) mild techniques that detach the target proteins from the membrane and (ii) total membrane disruption with the use of detergents. The solutions used based on the first and second approaches are presented in Tables 4.6 and 4.7 (detergents and glycerol), respectively.

Table 4.6 – Solutions used for mild solubilization of OmaW and OmaV cytochromes.

10 mM Tris-HCl pH 8.1 + 300 mM NaCl	10 mM Tris-HCl pH 7.5 + 6 M GuHCl*
10 mM Tris-HCl pH 8.1 + 1 M NaCl	100 mM sodium phosphate pH 7 + 2 M NaCl
10 mM Tris-HCl pH 8.1 + 8 M urea	100 mM Na_2CO_3 pH 10.6
10 mM Tris-HCl pH 7.5 + 8 M urea	100 mM Na_2CO_3 pH 10.6 + 2 M NaCl

*GuHCl stands for guanidine hydrochloride.

Table 4.7 – Solutions used for total membrane disruption and/or solubilization of the OmaV and OmaW cytochromes – The buffers used are indicated in parenthesis.

2% (w/v) SDS (1x PBS* pH 7.5)	0.1% (w/v) LDAO (10 mM Tris-HCl pH 7.5 + 150 mM NaCl)
2% (w/v) SDS (1x PBS* pH 7.5 + 500 mM NaCl)	0.2% (w/v) LDAO (10 mM Tris-HCl pH 7.5 + 300 mM NaCl)
2% (v/v) Triton X-100 (1x PBS* pH 7.5)	0.5% (w/v) CHAPS (10 mM Tris-HCl pH 7.5 + 150 mM NaCl)
5% (v/v) Triton X-100 (10 mM Tris-HCl pH 7.5 + 300 mM NaCl)	10% (v/v) glycerol (10 mM Tris-HCl pH 7.5 + 150 mM NaCl)

*PBS stands for phosphate-buffered saline.

Although glycerol is not a detergent and does not lead to membrane disruption, it is known to increase protein stability and solubility [33, 34]. In fact, Shi and co-workers [35] previously suggested a purification protocol for multiheme c-type cytochromes using 10% glycerol. Therefore, assays using glycerol as a solubilization agent were also performed. The assays performed using the conditions indicated in Table 4.7 were all performed with OmaW.

In either case, after homogenization of the cell pellets (achieved either by mechanical stirring or with a homogenizer), the mixtures were maintained at 4 ^{o}C for 30 minutes, with gentle stirring, before being ultracentrifugated at 100000 xg for 60 minutes at 4 ^{o}C. This procedure followed a protocol previously presented by Smith [36]. To check for protein solubilization, the resultant pellets and supernatants were analyzed by SDS-PAGE.

OmaW and OmaV were partially solubilized with 10 mM Tris-HCl pH 7.5 + 8 M urea. The samples were then dialyzed against sodium acetate pH 5.85 + 8 M urea and only OmaV was kept in solution in these conditions, while OmaW precipitated. OmaV was then loaded onto 2 x 5 mL HiTrap SP HP cartridges (GE Healthcare), equilibrated with the same buffer of the dialysis process. The protein was eluted with a sodium chloride step gradient (0.5 and 1 M) and

the obtained fractions were analyzed by SDS-PAGE. This chromatographic step was performed on a ÄKTA Prime (GE Healthcare) system.

4.1.4 – Purification of His-tagged OmaW

After overnight incubation, cells were lysed as described in the previous section, with the same buffer (at pH 7.5). The cell lysates were then separated and supplemented with other components (see below) and the protein was purified by affinity chromatography (Ni-NTA affinity purification), using either an ÄKTA Pure system or gravity flow columns.

On the first approach, the cell lysates were mixed with 10 mM Tris-HCl pH 7.5 + 300 mM NaCl + 20 mM imidazole. Cell debris were then removed by centrifugation at 30000 xg for 30 minutes at 4 ^{o}C and the resultant supernatant was ultracentrifugated at 100000 xg for 1 hour, at 4 ^{o}C, before being loaded onto a 5 mL HisTrap FF Crude cartridge (GE Healthcare), equilibrated with the same buffer. The protein was eluted with an imidazole gradient (0-500 mM) and the obtained fractions were analyzed by SDS-PAGE and UV-visible spectroscopy. The UV-visible absorption spectrum for one of the fractions was acquired in the oxidized state, between 300-750 nm, in a Thermo Scientific Evolution 201 spectrophotometer. The measurement was made with a quartz cuvette (Helma), with 1 cm path length, at room temperature.

On the second approach, the cell lysates were mixed either with 10 mM Tris-HCl pH 7.5 + 150 mM NaCl + 20 mM imidazole or with 10 mM Tris-HCl pH 7.5 + 0.5% CHAPS + 20 mM imidazole. The mixtures were then directly loaded onto gravity flow columns (from G-Biosciences, containing a 3 mm hydrophobic polyethylene layer, with 30 μm pores), prepared with Ni^{2+}-beads (5 mL of HisPur™ Ni-NTA resin (Thermo Scientific)), previously equilibrated with the equivalent buffers (either with 150 mM NaCl or 0.5% CHAPS) and incubated for 1 hour under continuous shaking. The protein was eluted with an imidazole step gradient (100, 250 and 500 mM), containing either 150 mM NaCl or 0.5% CHAPS, and the obtained fractions were analyzed by SDS-PAGE.

4.2 – Results and discussion

4.2.1 – Optimization of the expression and purification protocols

The optimization of expression and purification protocols for membrane proteins is very demanding, since modifications in each step of the protocol, such as vector design, culture conditions, expression strategies, protein extraction, choice of detergents and buffer conditions, can have a significant impact on the final yield and sample quality [37]. Some central factors that could determine the yield, integrity, activity and stability of the expressed proteins are the availability of highly processive transcription and translation machineries, suitable folding environments, the lipid composition of cellular membranes, the presence of efficient targeting systems and appropriate pathways for post-translational modifications [37].

The membrane proteins that were studied on this Thesis have special requirements, since they possess complex post-translational modifications (the incorporation of the hemes cofactors). To date, the most efficient strain used in the expression of multiheme cytochromes of G. sulfurreducens has been E. coli BL21 (DE3), containing the pEC86 plasmid that codes for all the machinery required for the hemes incorporation [31, 32]. Therefore, the protein expression was performed in this E. coli strain and the growth conditions were kept according to the protocols previously optimized for the PpcA-family cytochromes [38]. As demonstrated in the next sections, both OmaW and OmaV presented acceptable expression levels and, therefore, the main concern regarded the protein purification protocols, which were tested and optimized.

4.2.1.1 – Purification of OmaW and OmaV using mild techniques

In the first protein expression and purification test, the periplasmic fractions were isolated using the protocol presented in the previous Chapters. However, the results obtained after the first centrifugation clearly indicated that the majority of the cytochrome c content was in the pellets (Figure 4.6).

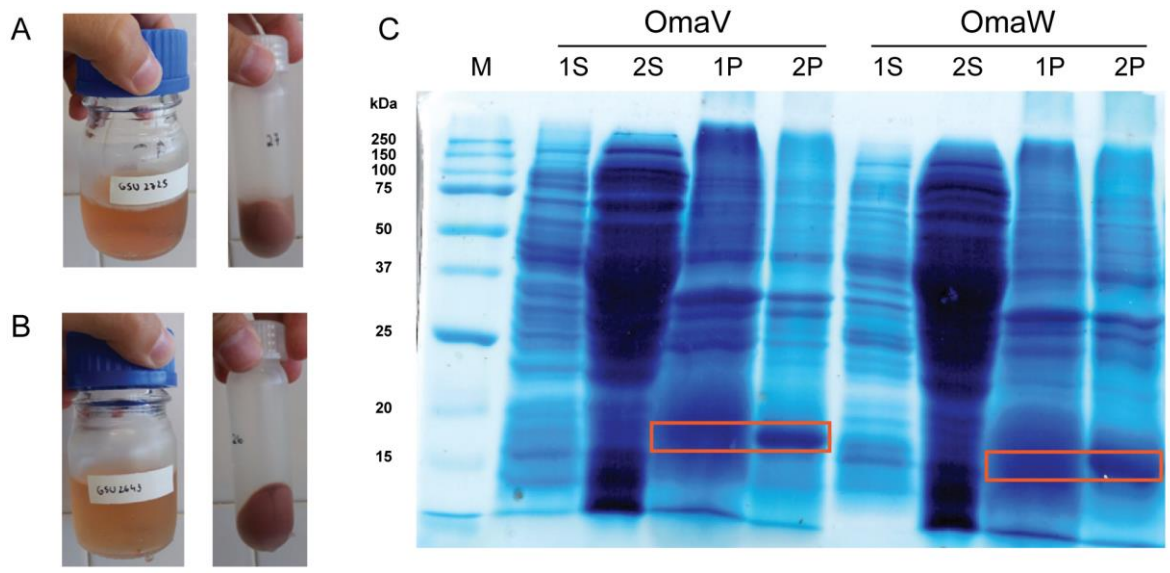

Figure 4.6 – SDS-PAGE of OmaV and OmaW supernatants and pellets after periplasmic fraction isolation and mechanical lysis with the French-press – Supernatants and pellets of the (A) OmaV (GSU2725) and (B) OmaW (GSU2643) cytochromes. (C) SDS-PAGE analysis of different pellets (P) and supernatants (S) of OmaV and OmaW. The different numbers correspond to different conditions: 1 – samples after periplasmic fraction isolation; 2 – samples after mechanical lysis with the French-press. Lane M corresponds to the molecular weight marker (Protein Plus Protein™ Dual Xtra Standards). The bands corresponding to either OmaV or OmaW are highlighted with orange boxes.

The red color of the pellets and the strong protein bands at the correct molecular weigths for both OmaW and OmaV (Figure 4.6) were indicative of a high cytochrome c content, which for initial trials of expression and purification was reflected as an acceptable yield. Therefore, no further modifications were made in the expression protocol of the OmaW and OmaV cytochromes. However, in the future, improvements may be necessary in the expression protocol, after a convenient and efficient purification protocol is developed.

Considering that OmaW and OmaV cytochromes were in the pellets, they were resuspended and further lysed mechanically, using the French-Press. After the centrifugation cycle, the resultant pellets and supernatants presented red and yellow colors, respectively. The protein location was further confirmed by SDS-PAGE (Figure 4.6C). Since the mechanical lysis did not lead to total membrane disruption and consequent protein detachment, the resultant pellets were resuspended in various conditions, as an attempt to solubilize the proteins. As previously said, peripheral membrane proteins can be dissociated using relatively mild techniques that break the electrostatic or hydrogen bonds between the peripheral proteins and the membrane, without total membrane disruption. There are commonly used reagents that work for the extraction of peripheral membrane proteins (Table 4.8).

Table 4.8 – Treatments for the extraction of peripheral membrane proteins – The details presented are general indications for the protocols of extraction. This table was adapted from [36].

Extraction type	Extraction details
Acidic buffers	Buffer with pH 3.0-5.0
Alkaline buffers	Buffer with pH 8.0-12.0
Chaotropic ions	I^-, ClO_4^-, SCN^-
Denaturing agents	8 M urea or 6 M GuHCl
Metal chelators	10 mM EDTA or EGTA
Salt solutions (high ionic strength)	1 M NaCl or KCl

Peripheral proteins extraction from the membrane is often accomplished with (i) buffers containing high salt concentrations, as the presence of salt decreases the electrostatic interactions between proteins and charged residues [39]; (ii) chaotropic ions, which disrupt hydrophobic bonds present in the membrane surface and promote the transfer of hydrophobic groups from the non-polar environment of the membrane to the aqueous phase [39]; (iii) alkaline or acid buffers, since extreme pH values result in disruption of sealed membrane structures, without denaturing the lipid bilayer and disrupting integral membrane proteins [40, 41]; (iv) chelating agents, due to the fact that some peripheral membrane proteins are attached to the membrane via specific ions (such as Ca^{2+}) that can be further chelated [42]; and (v) denaturing agents, that totally disrupt the protein structure and detach it from any biological surface [36].

Hence, the pellets were resuspended in different buffers, following the indications of Table 4.8. After the resuspension and homogenization of each pellet, cell suspensions were placed in eight different conditions, as indicated in Table 4.2. After proper incubation time and centrifugation, the resultant pellets and supernatants for the different conditions were analyzed by SDS-PAGE (Figures 4.7 and 4.8).

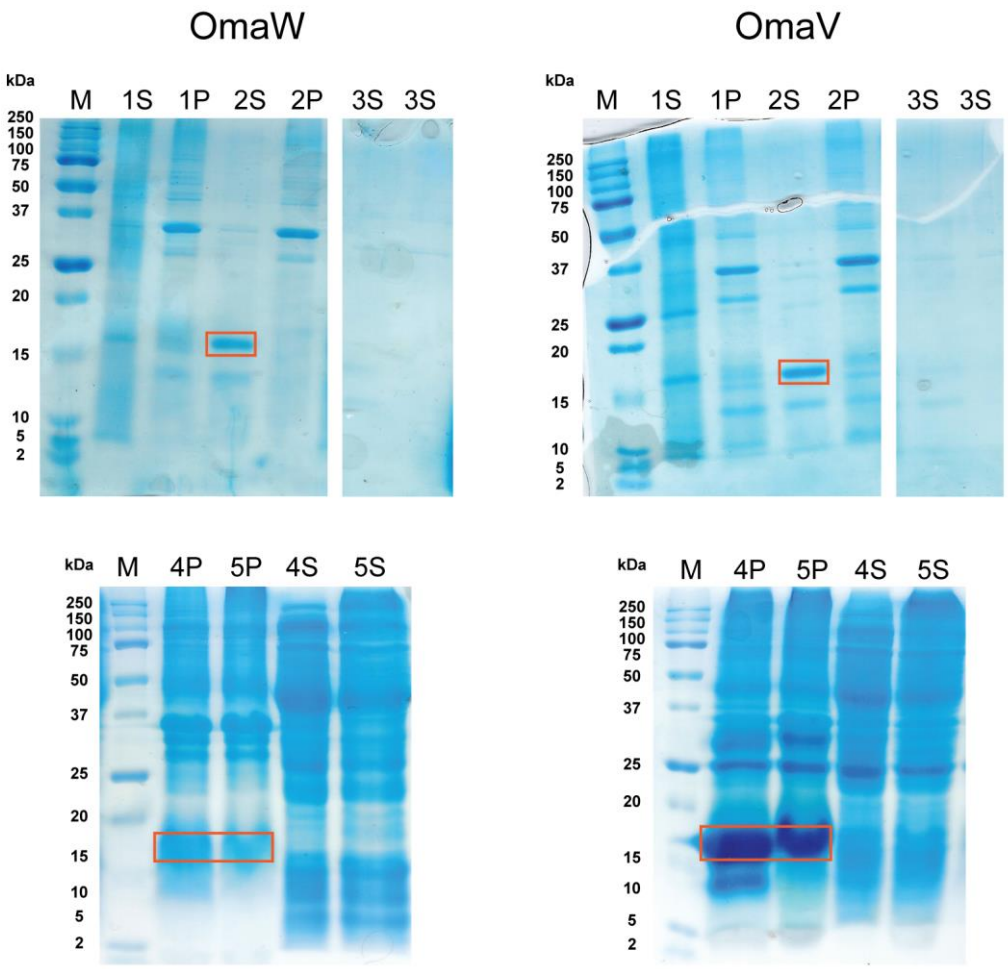

Figure 4.7 – SDS-PAGE analysis of the different mild solubilization techniques (Part 1) – The left and right panels correspond to OmaW and OmaV cytochromes, respectively. S and P correspond to supernatant and pellet, respectively. The different numbers correspond to different conditions: 1 – 10 mM Tris-HCl pH 8.1 + 8 M urea; 2 – 100 mM Na_2CO_3 pH 10.6; 3 – Tris-HCl pH 8.1 + 300 mM NaCl; 4 and 5 – 10 mM Tris-HCl pH 8.1, without and with 1 M NaCl, respectively. In all the gels, lane M corresponds to the molecular weight marker (Protein Plus Protein™ Dual Xtra Standards). The bands corresponding to either OmaV or OmaW are highlighted with orange boxes.

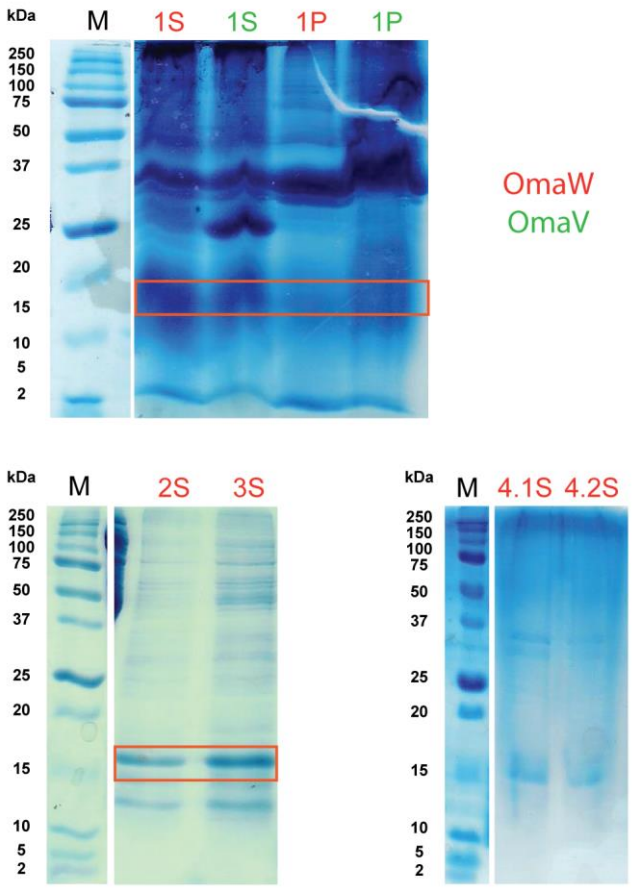

Figure 4.8 – SDS-PAGE analysis of the different mild solubilization techniques (Part 2) – In all the gels, S and P correspond to supernatant and pellet, respectively. The lanes identified either in red or green correspond to OmaW or OmaV cytochromes, respectively. The different numbers correspond to different conditions: 1 – 10 mM Tris-HCl pH 7.5 + 8 M urea; 2 – 100 mM Na_2CO_3 pH 10.6 + 2 M NaCl; 3 – 100 mM sodium phosphate pH 7 + 2 M NaCl; 4.1 and 4.2 – 10 mM Tris-HCl pH 7.5 + 6 M GuHCl, before and after a centrifugation step at 100000 xg, respectively. In all the gels, lane M corresponds to the molecular weight marker (Protein Plus Protein™ Dual Xtra Standards). The bands corresponding to either OmaV or OmaW are highlighted with orange boxes.

By analyzing Figures 4.7 and 4.8, it is possible to verify that some solubilization occurred using three conditions: (i) 100 mM Na_2CO_3 pH 10.6 (with and without 2 M NaCl), (ii) 100 mM phosphate buffer pH 7 + 2 M NaCl and (iii) 10 mM Tris-HCl pH 7.5 + 8 M urea. The solubilization achieved with the two first conditions occurred in insignificant amounts since the supernatants presented a yellow color and the pellets were dark red. The third solubilization condition resulted in light pink supernatants and red pellets. Therefore, the supernatant of the OmaV cytochrome was submitted to a cation exchange chromatography in the presence of urea. During the preparation of the OmaW supernatant for the chromatography step, the protein precipitated and it was not possible to perform the cation exchange on that cytochrome.

Concentrated solutions of urea are usually used to denature proteins in a reversible way [43, 44]. Urea can affect protein structure by both direct and indirect mechanisms. In the indirect mechanism, urea is presumed to disrupt the structure of water, thus making hydrophobic groups more readily solvated [45-50]. In the direct mechanism, urea interacts either directly with the protein backbone (via hydrogen bonds and other electrostatic interactions with charged and polar side chains) or with amino acids through more favorable van der Waals attractions as compared with water [51, 52].

There are many studies which have analyzed the effects of urea on cytochromes, as well as the ability of these types of proteins to refold after urea denaturation [53-58]. In most cytochromes c, that are evidences that indicate that the addition of urea to the protein solution results in uncoupling of the polypeptide chain from close proximity to the heme(s) group(s), without detachment of the cofactors [55, 59], meaning that a complete renaturation is viable in most cases. However, one of the studies also demonstrates that in some cases, there is disruption of the protein-heme bonds (possibly by replacement of the intrinsic ligands by an urea molecule) [55], which further complicates the process of correct refolding.

Furthermore, there are a few works published on multiheme cytochromes whose purification steps involve the use of urea, with protein renaturation [60, 61]. The cation exchange chromatography of OmaV was performed in denaturation conditions and the resulted fractions were analyzed by SDS-PAGE (Figure 4.9).

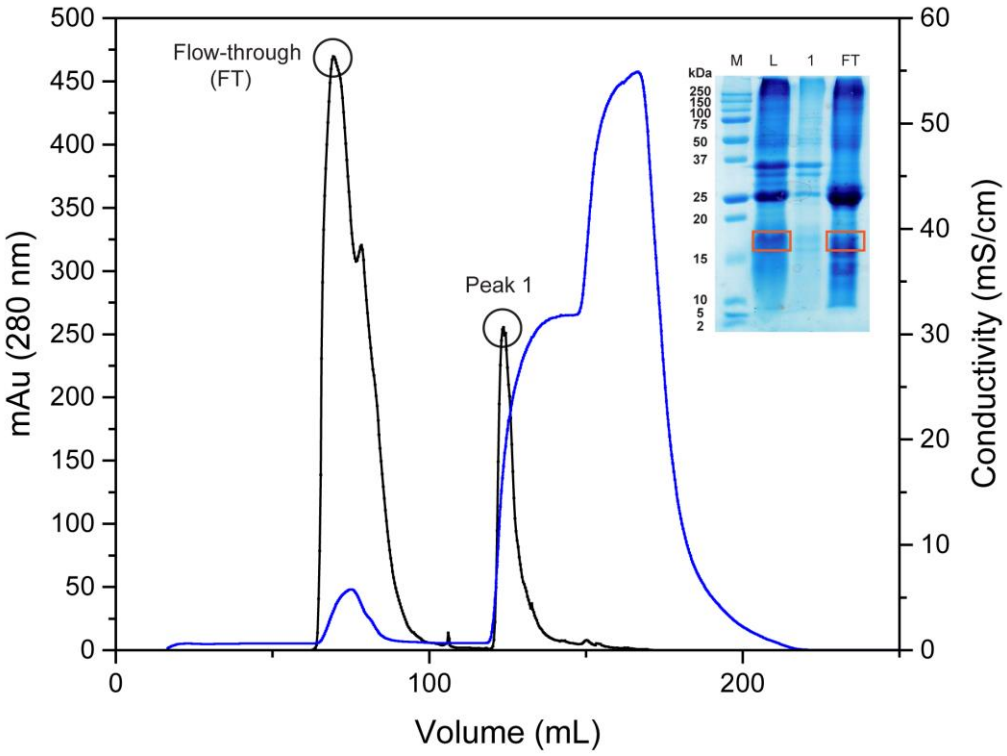

Figure 4.9 – Cation exchange chromatography of OmaV in the denaturated state – The primary and secondary y-axis report the variation of absorbance at 280 nm (black line) and the conductivity (blue line), respectively. The NaCl step gradient (0.5 and 1 M) is not represented. The inset shows the SDS-PAGE analysis of the chromatographic step. Lane M corresponds to the molecular weight marker (Protein Plus Protein™ Dual Xtra Standards). Lane L corresponds to the initial sample, before loading. Lane FT corresponds to the flow-through. Lane 1 corresponds to peak 1. The bands corresponding to OmaV are highlighted with orange boxes. The gel was stained with BlueSafe.

The fractions obtained after the application of the NaCl gradient did not contain OmaV. The protein did not bind to the column and other experimental conditions regarding the cation exchange chromatography should be reconsidered in next experimental trials.

4.2.1.2 – Purification of OmaW and OmaV using detergents

As seen in the previous section, the mild techniques of solubilization applied did not result in significant protein solubilization and considering the gathered results, it was inferred that the OmaW and OmaV cytochromes are more embedded in the OM than expected. Considering that OmaW and OmaV are interacting with the integral membrane proteins OmbW and OmbV, there are at least two reasons why these proteins are not solubilizing with the mild techniques used – the pentaheme cytochromes may be (i) stability-dependent on the anchoring of these proteins to the integral membrane components of the complexes, meaning that the consequent detachment of the OmaW and OmaV cytochromes destabilizes their structure and results in

protein denaturation and consequent precipitation or (ii) attached to the membrane with stronger interactions, that are not disrupted with mild techniques. Therefore, detergents were used in the next approaches of protein solubilization. The use of detergents is directly related with the fact that the solubilization of integral membrane proteins is only achieved with disruption of the lipid bilayer, which can be accomplished with several types of detergents.

Detergents are amphipathic molecules that contain both hydrophobic and hydrophilic moieties and form micelles in water. Micelles are clusters of detergent molecules in which the hydrophilic head moieties face outwards. Detergents solubilize proteins by binding to the hydrophobic parts of the protein on one side and interacting with the aqueous parts on the other side. Helenius and Simons [62] classify detergents by their overall chemical structure as type A and type B, which are further subdivided according to their electric charge as nonionic, ionic or zwitterionic detergents (see below). Type A detergents exhibit flexible hydrophobic tails and hydrophilic head groups, whereas type B detergents are more rigid and are cholesterol-based structures, with amphiphilic properties (Table 4.9).

Table 4.9 – Classification of detergents, according to Helenius and Simons [62] – The presented detergents are commonly employed in the solubilization of biological membranes.

Global charge	Chemical structure	
	Type A	Type B
Nonionic	Triton X-100 Octylglucoside Lubrol PX	Digitonin
Zwitterionic	Zwittergent 3-14	CHAPS
Ionic	–	Sodium cholate

In ionic detergents, the polar head group contains either a positive (cationic) or negative (anionic) charge. Anionic detergents typically have negatively-charged sulfate groups as the hydrophilic head, whereas cationic detergents usually contain a positively-charged ammonium group. The polar head groups of zwitterionic detergents contain both negatively and positively charged atomic groups, having an overall neutral charge. These compounds share characteristics of both ionic and nonionic detergents but are typically more efficient at breaking protein-protein bonds without affecting the proteins involved in the process, since they effectively break the protein bonds while maintaining the native state and charge of the individual proteins. Finally, nonionic detergents contain molecules with head groups that are uncharged.

The selection of a particular detergent depends on the properties of the protein of interest and on the given aims of the subsequent experiments involving that protein. It is also important to be aware of the unique critical micelle concentration (CMC), which is the concentration of free detergent at which the transition from disperse detergent molecules to a micellar structure occurs. Since solubilization corresponds to the removal of the protein from the membrane into the detergent micelle, the CMC is the minimal concentration of detergent necessary to form the required micellar structure for protein extraction. CMC values vary between detergents (some are indicated in Table 4.10).

Table 4.10 – Critical micelle concentration (CMC) for detergents commonly used in integral membrane proteins extraction – This table was adapted from [36]. The values presented are averaged or presented in intervals commonly reported by detergent manufacturers.

Global charge	Detergent name	CMC (mM)
Nonionic	Big Chap	3.4
	$C_{12}E_8$	< 0.1
	Triton X-100	0.3
	Triton X-114	0.2
Zwitterionic	CHAPS	3 – 10
	CHAPSO	4 – 8
	LDAO	1
Ionic	CTAB	1
	Sodium cholate	10
	Sodium deoxycholate	2
	SDS	6 – 8

Considering the above mentioned, different trials with detergents were performed in the pellets of the OmaW cytochrome, using the conditions presented in Table 4.3. The trials were performed with concentrations above the CMC values of the utilized detergents, to guarantee formation of the required micellar structures for protein extraction.

According to Ohlendieck [40], retention of a membrane protein in the supernatant following a centrifugation for 60 minutes at 100000 xg (after a solubilization protocol) defines the protein as soluble. Therefore, the supernatants which resulted from the solubilization protocol with the different detergents (and subsequent centrifugation) were analyzed by SDS-PAGE (Figure 4.10).

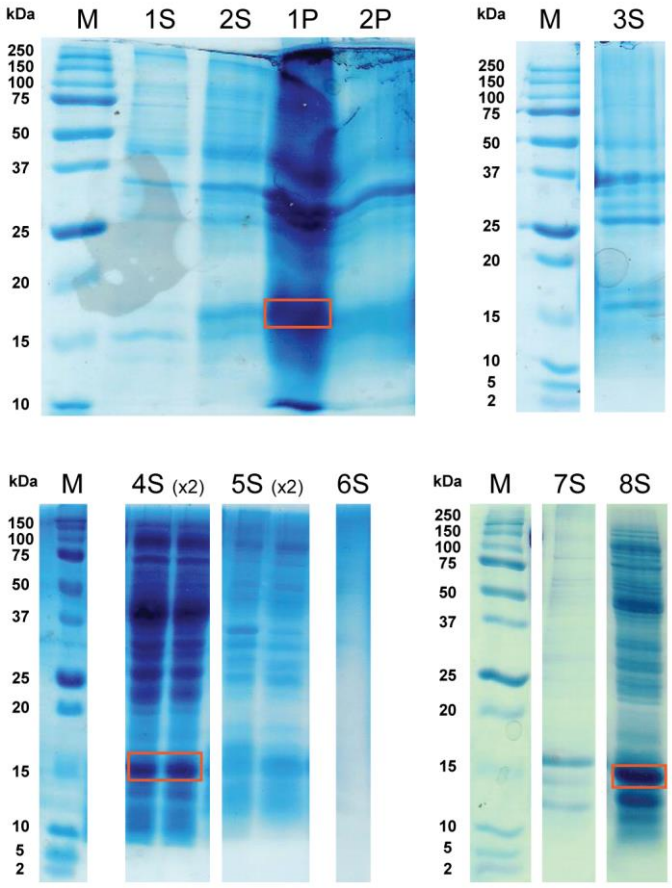

Figure 4.10 – SDS-PAGE analysis of the different detergent or glycerol based solubilization techniques – In all the gels, S and P correspond to supernatant and pellet, respectively. The different numbers correspond to different conditions: 1 – 2% Triton X-100 (1x PBS pH 7.5); 2 – 2% SDS (1x PBS pH 7.5); 3 – 2% SDS (1x PBS pH 7.5 + 500 mM NaCl); 4 – 0.5% CHAPS (10 mM Tris-HCl pH 7.5 + 150 mM NaCl); 5 – 0.1% LDAO (10 mM Tris-HCl pH 7.5 + 150 mM NaCl); 6 – 10% glycerol (10 mM Tris-HCl pH 7.5 + 150 mM NaCl); 7 – 5% Triton X-100 (10 mM Tris-HCl pH 7.5 + 300 mM NaCl); 8 – 0.2% LDAO (10 mM Tris-HCl pH 7.5 + 300 mM NaCl). In all the gels, lane M corresponds to the molecular weight marker (Protein Plus Protein™ Dual Xtra Standards). The bands corresponding to OmaW are highlighted with orange boxes.

By analyzing Figure 4.10, it is possible to verify that protein solubilization occurred using two conditions: (i) 0.2% LDAO (10 mM Tris-HCl pH 7.5 + 300 mM NaCl) and (ii) 0.5% CHAPS (10 mM Tris-HCl pH 7.5 + 150 mM NaCl). Out of the two conditions, it was decided that the following trials (purification of His-tagged OmaW, using affinity chromatography) would be performed using the zwitterionic detergent CHAPS as the membrane disruption agent. This choice was related with the existence of other works in the literature which have used CHAPS to solubilize membrane multiheme cytochromes [13, 63, 64].

4.2.1.3 – Purification of His-tagged OmaW

The use of affinity tags has been implemented in the purification of complex protein systems [65], namely on the purification of membrane proteins. In fact, some protocols have been reported for the purification of mono- and multiheme cytochromes, using this type of strategies [30, 35, 61, 66-70]. Considering the several unsuccessful conditions tested for the purification of OmaV and OmaW presented, the insertion of an His-tag in the expression vectors of these cytochromes was thought as a solution to further simplify the purification protocols of these proteins. This procedure was only performed on the OmaW cytochrome.

As described in section 4.1.1, the insertion of the His-tag involved an initial PCR step, for which experimental conditions were optimized. Four different conditions were tested: (i) 0.2 ng/μL of DNA template with Phusion GC buffer, (ii) 0.2 ng/μL of DNA template with Phusion HF buffer, (iii) 0.5 ng/μL DNA template with Phusion GC buffer and (iv) 0.2 ng/μL DNA template with Phusion HF buffer. The error rate of Phusion DNA polymerase in HF buffer is lower than that in GC buffer. Therefore, the HF buffer should be used as the default buffer for high-fidelity amplification. However, GC buffer can improve the performance of Phusion DNA polymerase on some difficult or long templates, such as GC-rich or those with complex secondary structures. For those reasons, PCR assays were performed with both buffers. The final results were analyzed by 1% agarose gel electrophoresis (Figure 4.11).

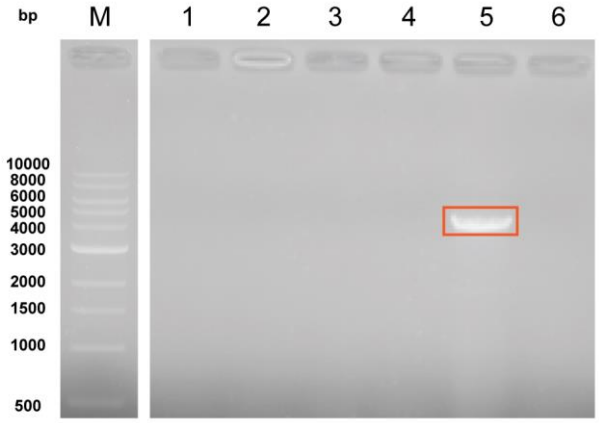

Figure 4.11 – Gel electrophoresis of PCR products in 1% agarose gel, 1x TAE (Tris-acetate-EDTA) buffer – Lane M corresponds to the 1 kb DNA ladder, from New England Biolabs. The remaining lanes are as follows: 1 – negative control of Phusion GC buffer; 2 – Phusion GC buffer with 0.2 ng/μL DNA template; 3 – Phusion GC buffer with 0.5 ng/μL DNA template; 4 – negative control of Phusion HF buffer; 5 – Phusion HF buffer with 0.2 ng/μL DNA template; 6 – Phusion HF buffer with 0.5 ng/μL DNA template. The DNA band corresponding to the PCR product (expected size of 4750 bp) is highlighted by an orange box.

By analyzing the results, it is clear that lane 5 contains the desired PCR product, which was further treated with DpnI, kinase and ligase enzymes. The resulting colonies were screened by colony PCR and analyzed by agarose gel electrophoresis. The plasmids of the colonies with PCR products of the correct size were purified and analyzed by DNA sequencing. The mature protein sequence, encoded by this plasmid, is presented in Figure 4.12.

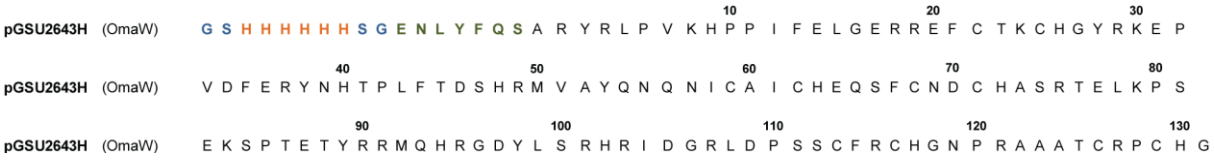

Figure 4.12 – Final sequence of the His-tagged OmaW – The Gly-Ser linkers, the His residues composing the His-tag and the cleavage site for TEV protease are highlighted in blue, orange and green, respectively.

After the insertion of the His-tag, initial purification procedures were tested. In the first procedure, after mechanical lysis with the French-press, the cell lysates buffer was adjusted to 10 mM Tris-HCl pH 7.5 + 300 mM NaCl + 20 mM imidazole and loaded onto HisTrap FF Crude cartridge (GE Healthcare), equilibrated with the same buffer. The elution profile is presented in Figure 4.13, together with the SDS-PAGE analysis of the different fractions.

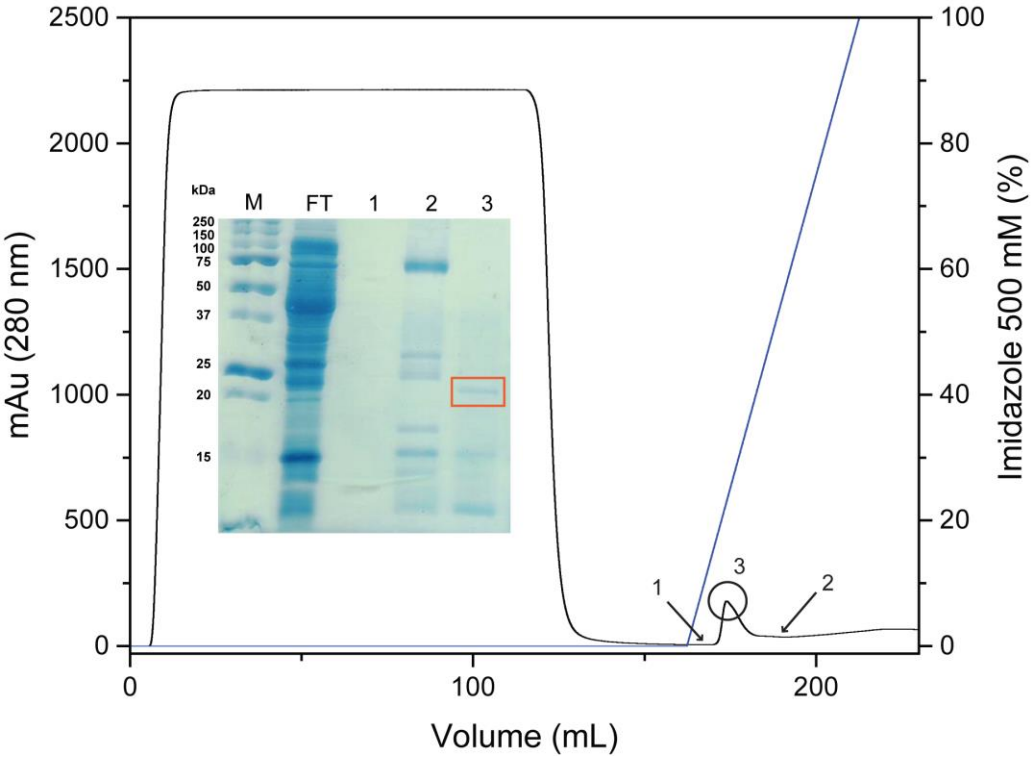

Figure 4.13 – Affinity chromatography of OmaW – The primary and secondary y-axis report the variation of absorbance at 280 nm (black line) and the imidazole gradient profile (blue line), respectively. The inset shows the SDS-PAGE analysis of the chromatographic step. Lane M corresponds to the molecular weight marker (Protein Plus Protein™ Dual Xtra Standards). Lane FT corresponds to the flow-through. Lanes 1-3 correspond to different fractions, highlighted in the chromatogram. In lane 3, a band containing the expected molecular weight for the His-tagged OmaW (around 20 kDa) is highlighted by an orange box. The gel was stained with BlueSafe.

One of the fractions (eluted at 23% of imidazole gradient) contained a band with the molecular weight expected for OmaW. This fraction was further analyzed by UV-visible spectroscopy and the spectrum presented typical patterns of cytochromes c [71], as shown in Figure 4.14.

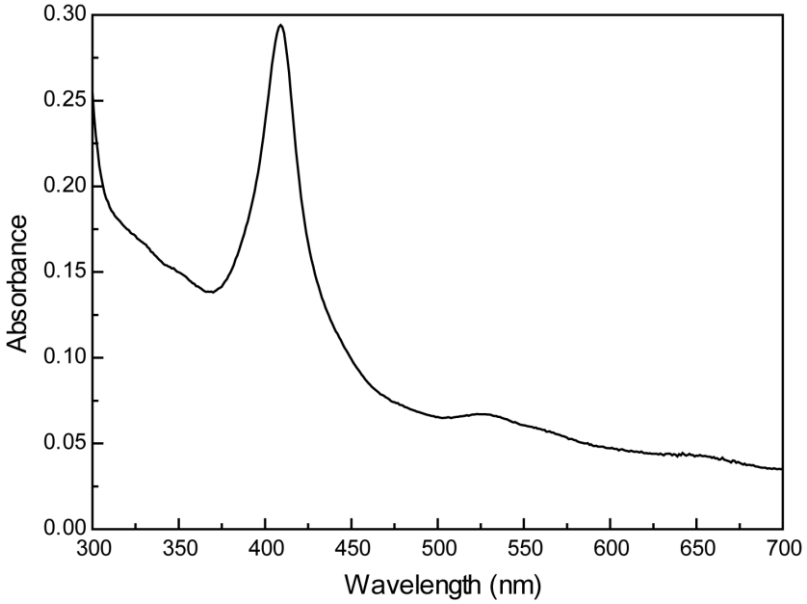

Figure 4.14 – UV-visible spectrum of the fraction containing OmaW in the oxidized state – The spectrum presents the Soret band at 409 nm, typical of cytochromes c [71]. The remaining bands may also be correlated with the presence of OmaW in the analyzed fraction, but there are too many contaminations to take valid conclusions.

On the second purification procedure, the same cell lysates buffer was adjusted to 10 mM Tris-HCl pH 7.5 + 150 mM NaCl + 20 mM imidazole or to 10 mM Tris-HCl pH 7.5 + 0.5% CHAPS + 20 mM imidazole and directly loaded onto Ni-NTA beads equilibrated with the same buffer. The fractions resulted from those two chromatographic steps were then analyzed by SDS-PAGE (Figure 4.15).

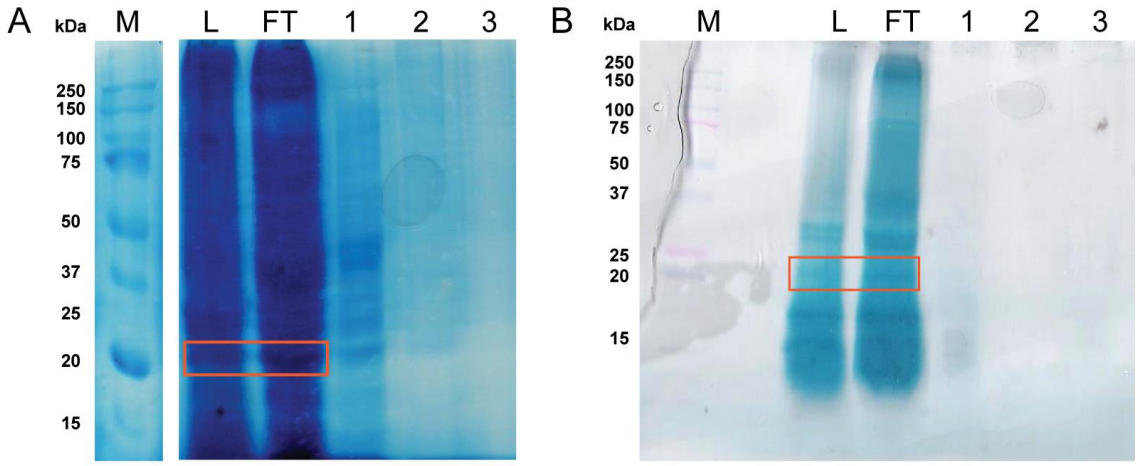

Figure 4.15 – SDS-PAGE analysis of the affinity chromatographies performed in Ni^{2+} beads – The (A) and (B) electrophoresis gels refer to the chromatographies performed with 0.5% CHAPS and 150 mM NaCl, respectively. In both gels, lane L corresponds to the mixtures before loading on the columns; lane FT corresponds to the flow-through and lanes 1, 2 and 3 correspond to the fractions eluted with 100, 250 and 500 mM imidazole, respectively. Lane M corresponds to the molecular weight marker (Protein Plus Protein™ Dual Xtra Standards). The gel bands containing the His-tagged OmaW are highlighted by orange boxes. The (A) and (B) gels were stained with BlueSafe and TMBZ, respectively.

By analyzing the results, no fractions containing OmaW were obtained after the affinity chromatography, either with 100, 250 or 500 mM imidazole. Further conditions need to be tested out in order to find a suitable purification protocol.

4.3 – Conclusions

In this Chapter, the membrane cytochromes OmaW (GSU2643) and OmaV (GSU2725) were expressed in E. coli BL21 (DE3) cells. Several purification protocols were tested, using either mild solubilization techniques or detergents for total membrane disruption. In total, 16 different solubilization conditions were tested and only 4 resulted in protein solubilization: (i) 100 mM Na_2CO_3 pH 10.6 (with and without 2 M NaCl), (ii) 10 mM Tris-HCl pH 7.5 + 8 M urea, (iii) 0.2% LDAO (10 mM Tris-HCl pH 7.5 + 300 mM NaCl) and (iv) 0.5% CHAPS (10 mM Tris-HCl pH 7.5 + 150 mM NaCl). These conditions can be utilized in future purification processes and some of them were already used during the chromatographic processes presented.

In the presence of 10 mM Tris-HCl pH 7.5 + 8 M urea, the cell lysates containing OmaV were partially solubilized and submitted to a cation exchange chromatography step. However, pure protein could not be obtained and purification conditions need to be further optimized.

In order to facilitate the process of purification of the OmaV and OmaW, an His-tag was inserted into the pGSU2643 plasmid (expressing the OmaW cytochrome). This approach can be further applied in other expression vectors, namely on the pGSU2725 plasmid.

Taking advantage of some of the solubilization conditions with positive results and of the His-tag inserted into the pGSU2643 plasmid (OmaW), different affinity chromatographies were tested. Promising results were obtained using 10 mM Tris-HCl pH 7.5 + 300 mM NaCl + 20 mM imidazole, immediately after French-press mechanical lysis.

The overall work described in this Chapter did not lead to an effective purification protocol, but it will hopefully stand as a major building block for the development of definitive and appropriate purification strategies for membrane-associated multiheme cytochromes from Geobacter bacteria.

4.4 – References

[1] J.-J. Lacapere, Membrane protein structure and function characterization: Methods and protocols, First edition, Humana Press, Paris, 2017.

[2] E.P. Carpenter, K. Beis, A.D. Cameron, S. Iwata, Overcoming the challenges of membrane protein crystallography, Curr. Opin. Struc. Biol., 18 (2008) 581-586.

[3] I. Moraes, The next generation in membrane protein structure determination, First edition, Springer International Publishing, London, 2016.

[4] H. Lodish, A. Berk, L. Zipursky, P. Matsudaira, D. Baltimore, J. Darnell, Molecular cell biology, Fourth edition, Media Connected, New York, 2000.

[5] H. Nikaido, Molecular basis of bacterial outer membrane permeability revisited, Microbiol. Mol. Biol. R., 67 (2003) 593-656.

[6] K. Zeth, M. Thein, Porins in prokaryotes and eukaryotes: Common themes and variations, Biochem. J., 431 (2010) 13.

[7] J.W. Fairman, N. Noinaj, S.K. Buchanan, The structural biology of β-barrel membrane proteins: A summary of recent reports, Curr. Opin. Struc. Biol., 21 (2011) 523-531.

[8] R. Koebnik, P. Locher Kaspar, P. Van Gelder, Structure and function of bacterial outer membrane proteins: Barrels in a nutshell, Mol. Microbiol., 37 (2002) 239-253.

[9] Y. Liu, J.K. Fredrickson, J.M. Zachara, L. Shi, Direct involvement of ombB, omaB, and omcB genes in extracellular reduction of Fe(III) by Geobacter sulfurreducens PCA, Front. Microbiol., 6 (2015) 1075.

[10] Y. Liu, Z. Wang, J. Liu, C. Levar, M.J. Edwards, J.T. Babauta, D.W. Kennedy, Z. Shi, H. Beyenal, D.R. Bond, T.A. Clarke, J.N. Butt, D.J. Richardson, K.M. Rosso, J.M. Zachara, J.K. Fredrickson, L. Shi, A trans-outer membrane porin-cytochrome protein complex for extracellular electron transfer by Geobacter sulfurreducens PCA, Environ. Microbiol. Rep., 6 (2014) 776-785.

[11] L. Shi, H. Dong, G. Reguera, H. Beyenal, A. Lu, J. Liu, H.-Q. Yu, J.K. Fredrickson, Extracellular electron transfer mechanisms between microorganisms and minerals, Nat. Rev. Microbiol., 14 (2016) 651.

[12] L. Shi, J.K. Fredrickson, J.M. Zachara, Genomic analyses of bacterial porin-cytochrome gene clusters, Front. Microbiol., 5 (2014) 657.

[13] R.S. Hartshorne, C.L. Reardon, D. Ross, J. Nuester, T.A. Clarke, A.J. Gates, P.C. Mills, J.K. Fredrickson, J.M. Zachara, L. Shi, A.S. Beliaev, M.J. Marshall, M. Tien, S. Brantley, J.N. Butt, D.J. Richardson, Characterization of an electron conduit between bacteria and the extracellular environment, P. Natl. Acad. Sci. USA, 106 (2009) 22169.

[14] M.J. Edwards, N.A. Baiden, A. Johs, S.J. Tomanicek, L. Liang, L. Shi, J.K. Fredrickson, J.M. Zachara, A.J. Gates, J.N. Butt, D.J. Richardson, T.A. Clarke, The X-ray crystal structure of Shewanella oneidensis OmcA reveals new insight at the microbe–mineral interface, FEBS Lett., 588 (2014) 1886-1890.

[15] D.J. Richardson, J.N. Butt, J.K. Fredrickson, J.M. Zachara, L. Shi, M.J. Edwards, G. White, N. Baiden, A.J. Gates, S.J. Marritt, T.A. Clarke, The 'porin–cytochrome' model for microbe-to-mineral electron transfer, Mol. Microbiol., 85 (2012) 201-212.

[16] B.A. Methé, K.E. Nelson, J.A. Eisen, I.T. Paulsen, W. Nelson, J.F. Heidelberg, D. Wu, M. Wu, N. Ward, M.J. Beanan, R.J. Dodson, R. Madupu, L.M. Brinkac, S.C. Daugherty, R.T. DeBoy, A.S. Durkin, M. Gwinn, J.F. Kolonay, S.A. Sullivan, D.H. Haft, J. Selengut, T.M. Davidsen, N. Zafar, O. White, B. Tran, C. Romero, H.A. Forberger, J. Weidman, H. Khouri, T.V. Feldblyum, T.R. Utterback, S.E. Van Aken, D.R. Lovley, C.M. Fraser, Genome of Geobacter sulfurreducens: Metal reduction in subsurface environments, Science, 302 (2003) 1967-1969.

[17] J.M. Dantas, M.A. Silva, D. Pantoja-Uceda, D.L. Turner, M. Bruix, C.A. Salgueiro, Solution structure and dynamics of the outer membrane cytochrome OmcF from Geobacter sulfurreducens, Biochim. Biophys. Acta, 1858 (2017) 733-741.

[18] K. Inoue, X. Qian, L. Morgado, B.C. Kim, T. Mester, M. Izallalen, C.A. Salgueiro, D.R. Lovley, Purification and characterization of OmcZ, an outer-surface, octaheme c-type cytochrome essential for optimal current production by Geobacter sulfurreducens, Appl. Environ. Microbiol., 76 (2010) 3999-4007.

[19] X. Qian, T. Mester, L. Morgado, T. Arakawa, M.L. Sharma, K. Inoue, C. Joseph, C.A. Salgueiro, M.J. Maroney, D.R. Lovley, Biochemical characterization of purified OmcS, a c-type cytochrome required for insoluble Fe(III) reduction in Geobacter sulfurreducens, Biochim. Biophys. Acta, 1807 (2011) 404-412.

[20] L.R. Teixeira, J.M. Dantas, C.A. Salgueiro, C.M. Cordas, Thermodynamic and kinetic properties of the outer membrane cytochrome OmcF, a key protein for extracellular electron transfer in Geobacter sulfurreducens, Biochim. Biophys. Acta - Bioenergetics, 1859 (2018) 1132-1137.

[21] M. Aklujkar, M.V. Coppi, C. Leang, B.C. Kim, M.A. Chavan, L.A. Perpetua, L. Giloteaux, A. Liu, D.E. Holmes, Proteins involved in electron transfer to Fe(III) and Mn(IV) oxides by Geobacter sulfurreducens and Geobacter uraniireducens, Microbiology, 159 (2013) 515-535.

[22] F. Jiménez Otero, C.H. Chan, D.R. Bond, Identification of different putative outer membrane electron conduits necessary for Fe(III) citrate, Fe(III) oxide, Mn(IV) oxide, or electrode reduction by Geobacter sulfurreducens, J. Bacteriol., 200 (2018) e00347-00318.

[23] P.R. Pokkuluri, Y.Y. Londer, N.E. Duke, J. Erickson, M. Pessanha, C.A. Salgueiro, M. Schiffer, Structure of a novel c_7-type three-heme cytochrome domain from a multidomain cytochrome c polymer, Protein Sci., 13 (2004) 1684-1692.

[24] P.R. Pokkuluri, Y.Y. Londer, X. Yang, N.E. Duke, J. Erickson, V. Orshonsky, G. Johnson, M. Schiffer, Structural characterization of a family of cytochromes c_7 involved in Fe(III) respiration by Geobacter sulfurreducens, Biochim. Biophys. Acta, 1797 (2010) 222-232.

[25] M. van Rosmalen, M. Krom, M. Merkx, Tuning the flexibility of glycine-serine linkers to allow rational design of multidomain proteins, Biochemistry, 56 (2017) 6565-6574.
[26] S. Raran-Kurussi, S. Cherry, D. Zhang, D.S. Waugh, Removal of affinity tags with TEV protease, Heterologous gene expression in E.coli: Methods and protocols, Springer New York, New York, NY, 2017, 221-230.
[27] K. Mullis, F. Faloona, S. Scharf, R. Saiki, G. Horn, H. Erlich, Specific enzymatic amplification of DNA in vitro: The polymerase chain reaction, Cold Spring Harb. Symp. Quant. Biol., 51 - Part 1 (1986) 263-273.
[28] K. Ohno, M. Tanaka, H. Ino, H. Suzuki, M. Tashiro, T. Ibi, K. Sahashi, A. Takahashi, T. Ozawa, Direct DNA sequencing from colony: Analysis of multiple deletions of mitochondrial genome, Biochim. Biophys. Acta, 1090 (1991) 9-16.
[29] L.I. Zon, D.M. Dorfman, S.H. Orkin, The polymerase chain reaction colony miniprep, Biotechniques, 7 (1989) 696-698.
[30] Y.Y. Londer, P.R. Pokkuluri, D.M. Tiede, M. Schiffer, Production and preliminary characterization of a recombinant triheme cytochrome c_7 from Geobacter sulfurreducens in Escherichia coli, Biochim. Biophys. Acta, 1554 (2002) 202-211.
[31] L. Thöny-Meyer, Biogenesis of respiratory cytochromes in bacteria, Microbiol. Mol. Biol. Rev., 61 (1997) 337-376.
[32] L. Thöny-Meyer, F. Fischer, P. Kunzler, D. Ritz, H. Hennecke, Escherichia coli genes required for cytochrome c maturation, J. Bacteriol., 177 (1995) 4321-4326.
[33] K. Gekko, S.N. Timasheff, Mechanism of protein stabilization by glycerol: Preferential hydration in glycerol-water mixtures, Biochemistry, 20 (1981) 4667-4676.
[34] V. Vagenende, M.G.S. Yap, B.L. Trout, Mechanisms of protein stabilization and prevention of protein aggregation by glycerol, Biochemistry, 48 (2009) 11084-11096.
[35] L. Shi, J.T. Lin, L.M. Markillie, T.C. Squier, B.S. Hooker, Overexpression of multi-heme c-type cytochromes, Biotechniques, 38 (2005) 297-299.
[36] S.M. Smith, Strategies for the purification of membrane proteins, Protein chromatography - Methods and protocols, Humana Press, New York, 2016.
[37] F. Junge, B. Schneider, S. Reckel, D. Schwarz, V. Dötsch, F. Bernhard, Large-scale production of functional membrane proteins, Cell. Mol. Life Sci., 65 (2008) 1729-1755.
[38] A.P. Fernandes, I. Couto, L. Morgado, Y.Y. Londer, C.A. Salgueiro, Isotopic labeling of c-type multiheme cytochromes overexpressed in E. coli, Prot. Expr. Purif., 59 (2008) 182-188.
[39] H. Ahmed, Principles and reactions of protein extraction, purification and characterization, First edition, CRC Press, Boca Raton, 2004.
[40] K. Ohlendieck, Extraction of membrane proteins, Protein purification protocols, Springer, New Jersey, 1996.
[41] I.M. Rosenberg, Membrane proteins, Protein analysis and purification, Springer, Boston, 2005.

[42] W. Stillwell, Chapter 6 - Membrane proteins, An introduction to biological membranes (Second Edition), Elsevier, 2016, 89-110.
[43] D.V. Beauregard, R.E. Barrett, Ultrasonics and water structure in urea solutions, J. Chem. Phys., 49 (1968) 5241-5244.
[44] A.K. Soper, E.W. Castner, A. Luzar, Impact of urea on water structure: A clue to its properties as a denaturant?, Biophys. Chem., 105 (2003) 649-666.
[45] G. Barone, E. Rizzo, V. Vitagliano, Opposite effect of urea and some of its derivatives on water structure, J. Phys. Chem., 74 (1970) 2230-2232.
[46] B.J. Bennion, V. Daggett, The molecular basis for the chemical denaturation of proteins by urea, P. Natl. Acad. Sci. USA, 100 (2003) 5142-5147.
[47] E.G. Finer, F. Franks, M.J. Tait, Nuclear magnetic resonance studies of aqueous urea solutions, J. Am. Chem. Soc., 94 (1972) 4424-4429.
[48] H.S. Frank, F. Franks, Structural approach to the solvent power of water for hydrocarbons: Urea as a structure breaker, J. Chem. Phys., 48 (1968) 4746-4757.
[49] G.G. Hammes, P.R. Schimmel, An investigation of water-urea and water-urea-polyethylene glycol interactions, J. Am. Chem. Soc., 89 (1967) 442-446.
[50] D.B. Watlaufer, S.K. Malik, L. Stoller, R.L. Coffin, Nonpolar group participation in the denaturation of proteins by urea and guanidinium salts: Model compound studies, J. Am. Chem. Soc., 86 (1964) 508-514.
[51] D.R. Robinson, W.P. Jencks, The effect of compounds of the urea-guanidinium class on the activity coefficient of acetyltetraglycine ethyl ester and related compounds, J. Am. Chem. Soc., 87 (1965) 2462-2470.
[52] A. Wallqvist, D.G. Covell, D. Thirumalai, Hydrophobic interactions in aqueous urea solutions with implications for the mechanism of protein denaturation, J. Am. Chem. Soc., 120 (1998) 427-428.
[53] M. Fedurco, J. Augustynski, C. Indiani, G. Smulevich, M. Antalík, M. Bánó, E. Sedlák, M.C. Glascock, J.H. Dawson, Electrochemistry of unfolded cytochrome c in neutral and acidic urea solutions, J. Am. Chem. Soc., 127 (2005) 7638-7646.
[54] K. Mukhopadhyay, J.T.J. Lecomte, A relationship between heme binding and protein stability in cytochrome b_5, Biochemistry, 43 (2004) 12227-12236.
[55] Y.P. Myer, Conformation of cytochromes. III. Effect of urea, temperature, extrinsic ligands, and pH variation on the conformation of horse heart ferricytochrome c, Biochemistry, 7 (1968) 765-776.
[56] R. Patel, M.U.H. Mir, U.K. Singh, I. Beg, A. Islam, A.B. Khan, Refolding of urea denatured cytochrome c: Role of hydrophobic tail of the cationic gemini surfactants, J. Colloid Interf. Sci., 484 (2016) 205-212.
[57] R. Varhač, Urea-induced modification of cytochrome c flexibility as probed by cyanide binding, Biochimi. Biophys. Acta - Proteins Proteom., 1834 (2013) 739-744.

[58] Y. Yamamori, R. Ishizuka, Y. Karino, S. Sakuraba, N. Matubayasi, Interaction-component analysis of the hydration and urea effects on cytochrome c, J. Chem. Phys., 144 (2016) 085102.

[59] S.-R. Yeh, S. Han, D.L. Rousseau, Cytochrome c folding and unfolding: A biphasic mechanism, Accounts Chem. Res., 31 (1998) 727-736.

[60] H.K. Carlson, A.T. Iavarone, A. Gorur, B.S. Yeo, R. Tran, R.A. Melnyk, R.A. Mathies, M. Auer, J.D. Coates, Surface multiheme c-type cytochromes from Thermincola potens and implications for respiratory metal reduction by Gram-positive bacteria, P. Natl. Acad. Sci. USA, 109 (2012) 1702-1707.

[61] C.S. Stephen, E.V. LaBelle, S.L. Brantley, D.R. Bond, Abundance of the multiheme c-type cytochrome OmcB increases in outer biofilm layers of electrode-grown Geobacter sulfurreducens, PLoS One, 9 (2014) e104336.

[62] A. Helenius, K. Simons, Solubilization of membranes by detergents, Biochim. Biophys. Acta - Rev. Biomembranes, 415 (1975) 29-79.

[63] T.A. Clarke, M.J. Edwards, A.J. Gates, A. Hall, G.F. White, J. Bradley, C.L. Reardon, L. Shi, A.S. Beliaev, M.J. Marshall, Z. Wang, N.J. Watmough, J.K. Fredrickson, J.M. Zachara, J.N. Butt, D.J. Richardson, Structure of a bacterial cell surface decaheme electron conduit, P. Natl. Acad. Sci. USA, 108 (2011) 9384.

[64] R.S. Hartshorne, B.N. Jepson, T.A. Clarke, S.J. Field, J. Fredrickson, J. Zachara, L. Shi, J.N. Butt, D.J. Richardson, Characterization of Shewanella oneidensis MtrC: A cell-surface decaheme cytochrome involved in respiratory electron transport to extracellular electron acceptors, JBIC Journal of Biological Inorganic Chemistry, 12 (2007) 1083-1094.

[65] M.E. Kimple, A.L. Brill, R.L. Pasker, Overview of affinity tags for protein purification, Current Protocols in Protein Science, 73 (2018) 9.9.1-9.9.23.

[66] B.-C. Kim, X. Qian, C. Leang, M.V. Coppi, D.R. Lovley, Two putative c-type multiheme cytochromes required for the expression of OmcB, an outer membrane protein essential for optimal Fe(III) reduction in Geobacter sulfurreducens, J. Bacteriol., 188 (2006) 3138.

[67] Y.Y. Londer, Expression of recombinant cytochromes c in E. coli, Heterologous gene expression in E.coli: Methods and protocols, Humana Press, Totowa, NJ, 2011, 123-150.

[68] C. Reyes, F. Qian, A. Zhang, S. Bondarev, A. Welch, M.P. Thelen, C.W. Saltikov, Characterization of axial and proximal histidine mutations of the decaheme cytochrome MtrA from Shewanella sp. strain ANA-3 and implications for the electron transport system, J. Bacteriol., 194 (2012) 5840-5847.

[69] J.N. Rumbley, L. Hoang, S.W. Englander, Recombinant equine cytochrome c in Escherichia coli: High-level expression, characterization, and folding and assembly mutants, Biochemistry, 41 (2002) 13894-13901.

[70] L.A. Zacharoff, D.J. Morrone, D.R. Bond, Geobacter sulfurreducens extracellular multiheme cytochrome PgcA facilitates respiration to Fe(III) oxides but not electrodes, Front. Microbiol., 8 (2017) 2481.

[71] G.R. Moore, G.W. Pettigrew, Cytochromes c: Evolutionary, structural and physicochemical aspects, Molecular Biology, Springer-Verlag Heidelberg, Berlin, 1990.

5

Future perspectives

"*Success is walking from failure to failure with no loss of enthusiasm.*"

Winston Churchill

5 – Future perspectives

The work developed in this Thesis will stand as a contribution for the general understanding of the Geobacter bacteria EET pathways and assist the development of rationally designed mutant strains, with higher current density production in MFCs and optimized bioremediation capabilities.

The thermodynamic and functional differences between the homologous PpcA cytochromes from G. metallireducens and G. sulfurreducens discussed in this Thesis will be further explored together with the determination of the solution structure of PpcA from G. metallireducens. The assignment of the backbone, side chain and heme substituents in the reduced state (BMRB accession number 27363) was already accomplished and the structure calculation is already in progress. The diamagnetic structure to be obtained will then be compared with the one already available for PpcA from G. sulfurreducens (PDB ID: 2LDO [1]). Structure-function relationships will be established in order to explain how the non-conserved residues near hemes I and III modulate the properties of these redox centers and concomitant thermodynamic and functional properties.

In order to probe redox-linked conformational changes, the structure of PpcA from G. metallireducens will also be determined in the oxidized state. The experiments necessary for the assignment of the NMR backbone and side chain signals were already obtained. The structure determination of low-spin paramagnetic cytochromes in solution requires the use of paramagnetic constraints to achieve good precision and accuracy [2, 3]. The quality of these constraints depends on the correct placement of the magnetic axes that define the magnetic susceptibility tensor of the unpaired electrons. These axes can be defined from paramagnetic NMR chemical shifts of the substituents at the heme periphery (α-substituents). The assignment of most of the heme substituents was accomplished in this Thesis and will serve as a starting point for the assignment of the remaining substituents, following strategies previously described [4, 5].

Furthermore, in order to elucidate the physiological function and mechanistic influence of individual key residues in PpcA from G. metallireducens, different mutants of the cytochrome will be designed and prepared by site-directed mutagenesis. The thermodynamic and functional features of the mutants will be compared with the data obtained in this Thesis for the wild-type protein.

The preliminary results obtained for the GSU0105 cytochrome suggest that the cytochrome has three low-spin hemes in the reduced state and a mixture of low- and high-spin characters in the oxidized state. These evidences will be further confirmed by EPR. The results also point out the existence of a combination of His-Met, His-His and His-unknown coordinations, that need to be accessed. The coordinations of the heme groups will be confirmed by NMR or X-ray crystallography. The determination of the paramagnetic solution structure and/or any studies performed in the oxidized state will always be challenging, considering the high-spin character of the cytochrome.

UV-visible redox-titrations and electrochemical assays will be performed on the cytochrome GSU0105 at different experimental conditions, in order to get more insights on the heme reduction potentials and overall thermodynamic properties of the cytochrome. Finally, gathering the structure determination with these parameters, structure-function relationships will be accessed, as well as comparative studies with other triheme cytochromes, namely the PpcA-family cytochromes.

The development of proper expression and purification protocols for OM cytochromes is still in a preliminary stage. In the future, improvements may be necessary in the protein expression protocol, either to guarantee higher expression yields or to increase protein solubility, by varying different expression conditions. Further purification steps for the OmaW and OmaV cytochromes will be tested using the solubilization conditions summarized in Chapter 4, as well as others. The implementation of the protocol for insertion of affinity tags in expression vectors, also presented in Chapter 4, will be further applied in other OM expression vectors. The hypothesis that the peripheral membrane proteins OmaW and OmaV are not stable in the absence the remaining components of the complex (OmbW/OmcW for OmaW and OmbV/OmcV for OmaV) needs to be taken into consideration and in the future, these proteins may be co-expressed together with the remaining components of the OM complexes. Furthermore, some OM proteins from G. sulfurreducens have been recently cloned into the pVA203 [6, 7] or pET-28a(+) (Novagen) plasmids using RF cloning (Restriction-Free cloning) [8]. The cloned proteins are indicated in Table 5.1.

Table 5.1 – Features of the recently cloned OM proteins – The presented molecular weight (MW) values are approximated. TM stands for transmembrane.

Protein	Gene	Residues	MW (kDa)	CXXCH motifs	TM motifs
OmbW	GSU2644	394	44.2	–	20
OmcW	GSU2642	205	26.2	6	–
OmcV	GSU2724	661	75.6	13	–
OmcB	GSU2737	722	82.3	12	–
OmcC	GSU2731	746	85.7	12	–

Initial expression tests will be performed for these cytochromes taking advantage of the work carried out on OmaV and OmaW proteins.

Finally, and as an ultimate goal, the main future objective would be to interconnect the work performed in the different chapters and find physiological partners for the different cytochromes. This could be accomplished with the complementary use of different disciplines, namely microbiology, electrochemistry and, structural and functional biochemistry.

5.1 – References

[1] L. Morgado, V.B. Paixão, M. Schiffer, P.R. Pokkuluri, M. Bruix, C.A. Salgueiro, Revealing the structural origin of the redox-Bohr effect: The first solution structure of a cytochrome from Geobacter sulfurreducens, Biochem. J., 441 (2012) 179-187.

[2] M. Assfalg, L. Banci, I. Bertini, M. Bruschi, P. Turano, 800 MHz ^{1}H NMR solution structure refinement of oxidized cytochrome c_7 from Desulfuromonas acetoxidans, Eur. J. Biochem., 256 (2001) 261-270.

[3] A.C. Messias, D.H. Kastrau, H.S. Costa, J. LeGall, D.L. Turner, H. Santos, A.V. Xavier, Solution structure of Desulfovibrio vulgaris (Hildenborough) ferrocytochrome c_3: Structural basis for functional cooperativity, J. Mol. Biol., 281 (1998) 719-739.

[4] L. Morgado, A.P. Fernandes, Y.Y. Londer, M. Bruix, C.A. Salgueiro, One simple step in the identification of the cofactors signals, one giant leap for the solution structure determination of multiheme proteins, Biochem. Biophys. Res. Commun., 393 (2010) 466-470.

[5] L. Morgado, I.H. Saraiva, R.O. Louro, C.A. Salgueiro, Orientation of the axial ligands and magnetic properties of the hemes in the triheme ferricytochrome PpcA from G. sulfurreducens determined by paramagnetic NMR, FEBS Lett., 584 (2010) 3442-3445.

[6] P.R. Pokkuluri, Y.Y. Londer, N.E. Duke, M. Pessanha, X. Yang, V. Orshonsky, L. Orshonsky, J. Erickson, Y. Zagyansky, C.A. Salgueiro, M. Schiffer, Structure of a novel dodecaheme cytochrome c from Geobacter sulfurreducens reveals an extended 12 nm protein with interacting hemes, J. Struct. Biol., 174 (2011) 223-233.

[7] P.R. Pokkuluri, Y.Y. Londer, X. Yang, N.E. Duke, J. Erickson, V. Orshonsky, G. Johnson, M. Schiffer, Structural characterization of a family of cytochromes c_7 involved in Fe(III) respiration by Geobacter sulfurreducens, Biochim. Biophys. Acta, 1797 (2010) 222-232.

[8] S.R. Bond, C.C. Naus, RF-Cloning.org: An online tool for the design of restriction-free cloning projects, Nucleic Acids Res., 40 (2012) 209-213.

6 Appendix

"Big things have small beginnings."

T. E. Lawrence

6 – Appendix

6.1 – Reagents

Table 6.1 – List of the reagents used in this Thesis – The name of the reagents and their respective chemical formula, CAS number and supplier are indicated.

Reagent	Chemical formula	CAS number	Supplier
Acetic acid	CH_3COOH	64-19-7	Sigma-Aldrich
Acrylamide/bis-acrylamide	–	79-06-1	NZYTech
Agar	–	9002-18-0	VWR
Agarose	$C_{24}H_{38}O_{19}$	9012-36-6	NZYTech
Ammonia persulfate (PSA)	$(NH_4)_2S_2O_8$	7727-54-0	Riedel-de Haën
Ampicillin	$C_{16}H_{18}N_3O_4SNa$	69-52-3	NZYTech
Benzamidine-HCl	$C_7H_9N_2Cl$	1670-14-0	Sigma-Aldrich
BlueSafe	–	–	NZYTech
Bromophenol blue	$C_{19}H_{10}Br_4O_5S$	115-39-9	Sigma-Aldrich
Calcium chloride	$CaCl_2$	10043-52-4	Sigma-Aldrich
Casein peptone	–	91079-40-2	VWR
CHAPS	$C_{32}H_{58}N_2O_7S$	75621-03-3	Carl Roth
Chloramphenicol	$C_{11}H_{12}Cl_2N_2O_5$	56-75-7	NZYTech
Deuterium chloride	^2HCl	7698-05-7	Sigma-Aldrich
Deuterium oxide	^2H_2O	7789-20-0	CIL Isotopes
Disodium phosphate	Na_2HPO_4	10028-24-7	VWR
DNase	–	–	Sigma-Aldrich
Ethanol	C_2H_6O	64-17-5	Sigma-Aldrich
EDTA	$C_{10}H_{16}N_2O_8$	60-00-4	Amresco
Glycerol	$C_3H_8O_3$	56-81-5	Fluka
Glycine	$C_2H_5NO_2$	56-40-6	NZYTech
GreenSafe	–	–	NZYTech
Guanidine hydrochloride	CH_6ClN_3	50-01-1	Fluka
Hydrochloric acid	HCl	7647-01-0	Carlo Erba
Hydrogen peroxide	H_2O_2	7722-84-1	Sigma-Aldrich
Imidazole	$C_3H_4N_2$	288-32-4	Sigma-Aldrich
IPTG	$C_9H_{18}O_5S$	367-93-1	NZYTech
LDAO	$C_{14}H_{31}NO$	1643-20-5	Glycon
Lysozyme	–	12650-88-3	Sigma-Aldrich
Methanol	CH_3OH	67-56-1	Fisher Chemical
Monopotassium phosphate	KH_2PO_4	7778-77-0	Carlo Erba
Monosodium phosphate	NaH_2PO_4	10049-21-5	Merck

Table 6.1 (continued)

Reagent	Chemical formula	CAS number	Supplier
PMSF	$C_7H_7FO_2S$	329-98-6	Sigma-Aldrich
Potassium chloride	KCl	7447-40-7	Panreac
Propanol	C_3H_8O	67-63-0	VWR
Pyridine	C_5H_5N	110-86-1	Fisher Chemical
SDS	$CH_3(CH_2)_{11}SO_4Na$	151-21-3	VWR
Sodium acetate	CH_3COONa	127-09-3	Sigma-Aldrich
Sodium carbonate	Na_2CO_3	5968-11-6	Sigma-Aldrich
Sodium chloride	NaCl	7647-14-5	NZYTech
Sodium deuteroxide	NaO^2H	14014-06-3	Sigma-Aldrich
Sodium dithionite	$Na_2S_2O_4$	7775-14-6	Fisher Chemical
Sodium hydroxide	NaOH	1310-73-2	Pronalab
Sucrose	$C_{12}H_{22}O_{11}$	57-50-1	Fisher Chemical
TEMED	–	110-18-8	Fluka
TMBZ	$C_{16}H_{20}N_2$	54827-17-7	Acros Organics
Tris	$C_4H_{11}NO_3$	77-86-1	NZYTech
Triton X-100	–	9002-93-1	Sigma-Aldrich
Urea	$(NH_2)_2CO$	57-13-6	Sigma-Aldrich
Yeast extract	–	8013-01-2	NZYTech

6.2 – SDS-PAGE electrophoresis

Throughout this Thesis, protein purity was evaluated by SDS-PAGE, using a Mini-Protean® Electrophoresis System (Bio-Rad). The SDS-PAGE gel recipe (5% stacking gel and 15% running gel) is presented in Table 6.3.

Table 6.2 – SDS-PAGE gel recipe for 5% stacking gel + 15% running gel.

Stock solutions	Stacking gel (μL)	Running gel (μL)
1.5 M Tris-HCl pH 8.8	–	750
0.5 M Tris-HCl pH 6.8	450	–
40% acrylamide/bis-acrylamide (37.5:1)	225	1880
10% SDS	18	50
H_2O	1107	2280
10% PSA	13.5	38
TEMED	2	2.5

All the samples were loaded with the same loading buffer (2% SDS, 5% glycerol, 0.01% bromophenol blue, in 62.5 mM Tris-HCl pH 6.8), after an incubation time of 5 minutes at 95 ^{o}C. The electrophoresis were run in 1x SDS running buffer (25 mM Tris, 192 mM glycine, 1% SDS), at 120 V during 90 minutes. The molecular weight marker used was the Precision Plus Protein™ Dual Xtra Standards (Bio-Rad, Figure 6.1).

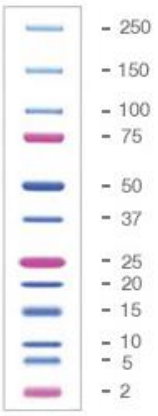

Figure 6.1 – Protein molecular weight marker Precision Plus Protein™ Dual Xtra Standards (Bio-Rad) – The numbers on the right refer to the molecular weight of each band, in kDa.

Finally, the electrophoresis gels were stained either with TMBZ or with BlueSafe (see below).

6.2.1 – Heme staining of SDS-PAGE electrophoresis gels

The heme staining of SDS-PAGE electrophoresis gels is based on the peroxidase activity of the heme group. The heme group of any cytochrome is capable of using H_2O_2 has an electron acceptor and catalyze an oxidative reaction until the formation of H_2O. Based on this, in the heme staining of SDS-PAGE gels, tetramethylbenzidine (TMBZ, from Acros Organics) is used as a chromogenic electron donor (TMBZ forms a blue precipitate when oxidized, leading to light blue bands in the SDS-PAGE gel) and H_2O_2 as an electron acceptor [1, 2]. In order for this staining technique to work, the heme(s) group(s) have to be in the oxidized state and so, the loading-buffer used does not contain β-mercaptoethanol.

After running the SDS-PAGE electrophoresis, the gel is placed in a solution containing TMBZ (Solution C) for 30 minutes. The gel must be incubated while stirring with no light exposure. Then, 300 μL of 30% H_2O_2 are directly added, followed by another 30 minutes of incubation. Finally, the gel is washed twice with a sodium acetate/propanol solution (Solution D). The necessary solutions for this staining method are indicated in Table 6.4.

Table 6.3 – Solutions for heme staining.

Solution	Composition/Name	Preparation
A	4.17 mM TMBZ	30 mg of TMBZ in 30 mL of methanol
B	0.25 M sodium acetate	17.01 g of sodium acetate trihydrate in 500 mL (pH 5 – adjusted with acetic acid)
C	Coloring solution	30 mL solution A + 70 mL solution B
D	Washing solution	70 mL solution B + 30 mL propanol

6.2.2 – BlueSafe staining of SDS-PAGE electrophoresis gels

BlueSafe is a NZYTech protein stain which consists of a safer alternative (it does not contain methanol or acetic acid) to the traditional Coomassie Blue staining for detecting proteins in SDS-PAGE [3]. BlueSafe does not require the use of a destaining solution and is capable of detecting low concentration proteins (60 ng within 10-15 minutes, and down to 10 ng within 30-60 minutes) [3]. For staining the gels presented in this Thesis, about 25 mL of BlueSafe solution were added to the gel and incubated for 60 minutes with gentle agitation before removing the excess. BlueSafe was reused 2-3 times, when conserved at 4 ^{o}C.

It is important to note that BlueSafe staining is not efficient in protein bands that were previously strongly stained with heme staining. Therefore, a protein band that was strongly stained with heme staining may not have the same relative intensity with BlueSafe.

6.3 – Agarose gel electrophoresis

Throughout this Thesis, the purity of the PCR products was evaluated by agarose gel electrophoresis, using a kuroGel Midi 13 Horizontal Electrophoresis System (VWR). The agarose gels were prepared by adding either 1 or 1.3 g of agarose (for 1 and 1.3% agarose gels, respectively) to 100 mL of 1x TAE buffer (40 mM Tris, 20 mM acetic acid and 1 mM EDTA) and 1 μL of GreenSafe Premium (NZYTech).

GreenSafe Premium is a new nucleic acid stain, introduced by NZYTech, that can be used as a safer alternative to the traditional ethidium bromide for detecting nuclei acids in agarose gels. It is as sensitive as ethidium bromide and can be used exactly in the same way in agarose gel electrophoresis. This stain emits green fluorescence when bound to DNA or RNA, having two secondary fluorescence excitation peaks (around 270 and 290 nm) and one strong excitation peak centered at 530 nm.

All the samples were loaded with the same loading buffer (1x DNA gel loading dye, from Fermentas). The electrophoresis were run in 1x TAE running buffer, at 90 V during 60 minutes. The DNA ladder used was the 1 kb DNA ladder, from New England Biolabs (Figure 6.2).

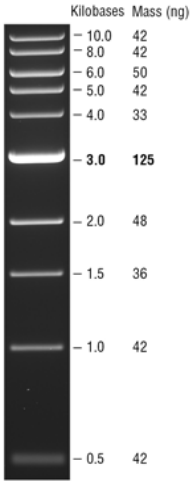

Figure 6.2 – 1 kb DNA ladder from New England Biolabs – The numbers on the right refer to the number of kilobases and mass (in ng) of each band.

Finally, the bands were observed under UV light (VWR UV transilluminator).

6.4 – NMR signal assignments

The experiments used to perform the different assignments were acquired in a Bruker Avance III 600 MHz spectrometer. The heme substituents are named in agreement with the IUPAC-IUB nomenclature for tetrapyrroles [4].

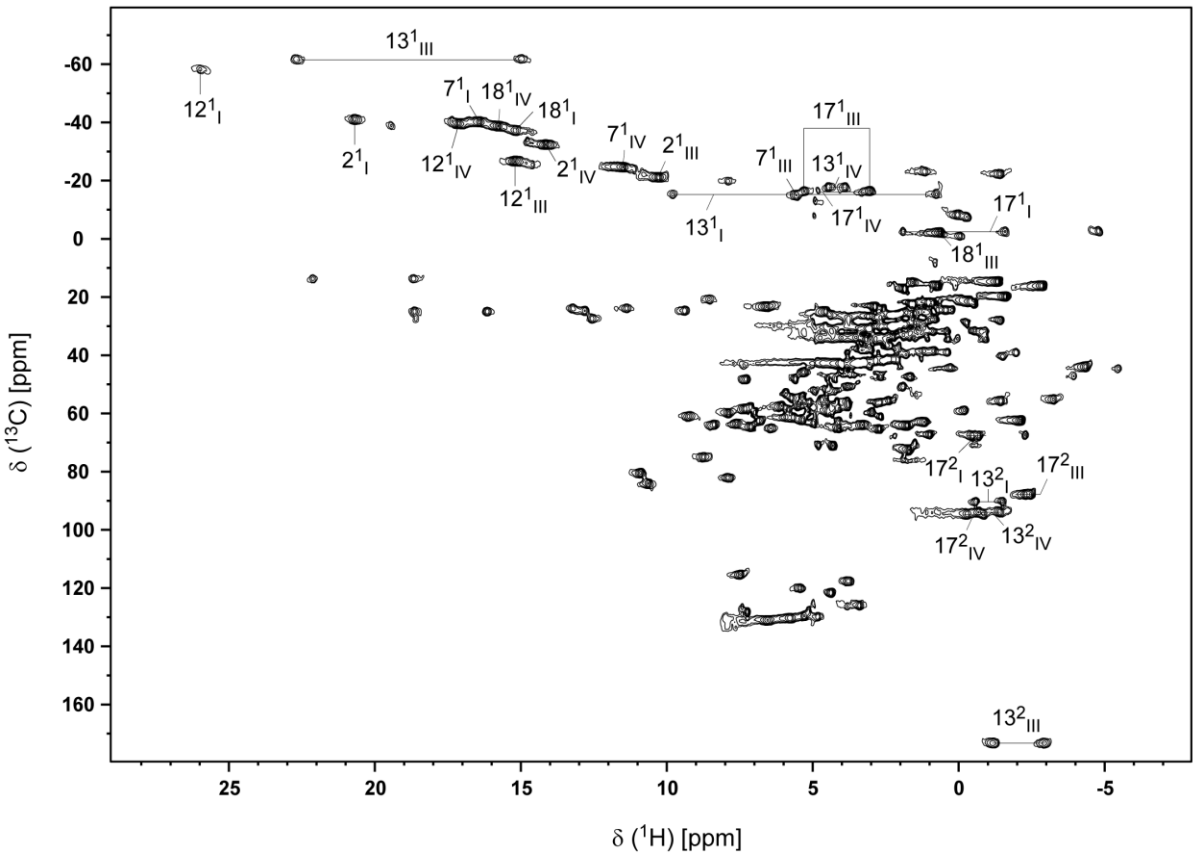

Figure 6.3 – $^{1}H,^{13}C$-HMQC spectrum of PpcA from G. metallireducens, at pH 8.1, 288 K – The heme methyls and propionates signals are identified in the spectrum. The peaks of the protons connected to the same carbon atoms (CH_2 groups) are linked by a straight line. The detailed assignment is presented in Table 6.5.

Table 6.4 – Heme methyls and propionates assignment (^{1}H and ^{13}C) of PpcA from G. metallireducens in the oxidized state, at 250 mM ionic strength, pH 8.1, 288 K.

Heme substituent	Heme I		Heme III		Heme IV	
	^{13}C	^{1}H	^{13}C	^{1}H	^{13}C	^{1}H
2^{1}	-41.77	20.69	-21.81	10.28	-33.11	14.14
7^{1}	-40.97	16.43	-15.60	5.57	-25.29	11.50
12^{1}	-59.09	25.98	-27.40	15.20	-40.26	17.12
13^{1}	-15.89	0.77 9.79	-62.60	14.97 22.69	-18.47	3.90 4.46
13^{2}	93.88	-1.41 -0.68	173.60	-2.94 -1.16	90.19	-1.48 -0.59
17^{1}	-3.07	-1.59 1.91	-17.02	3.06 5.29	-17.21	3.06 4.82
17^{2}	67.38	-0.69 -0.47	87.65	-2.47 -2.30	94.45	-0.84 -0.29
18^{1}	-37.98	15.20	-2.74	0.64	-39.48	15.77

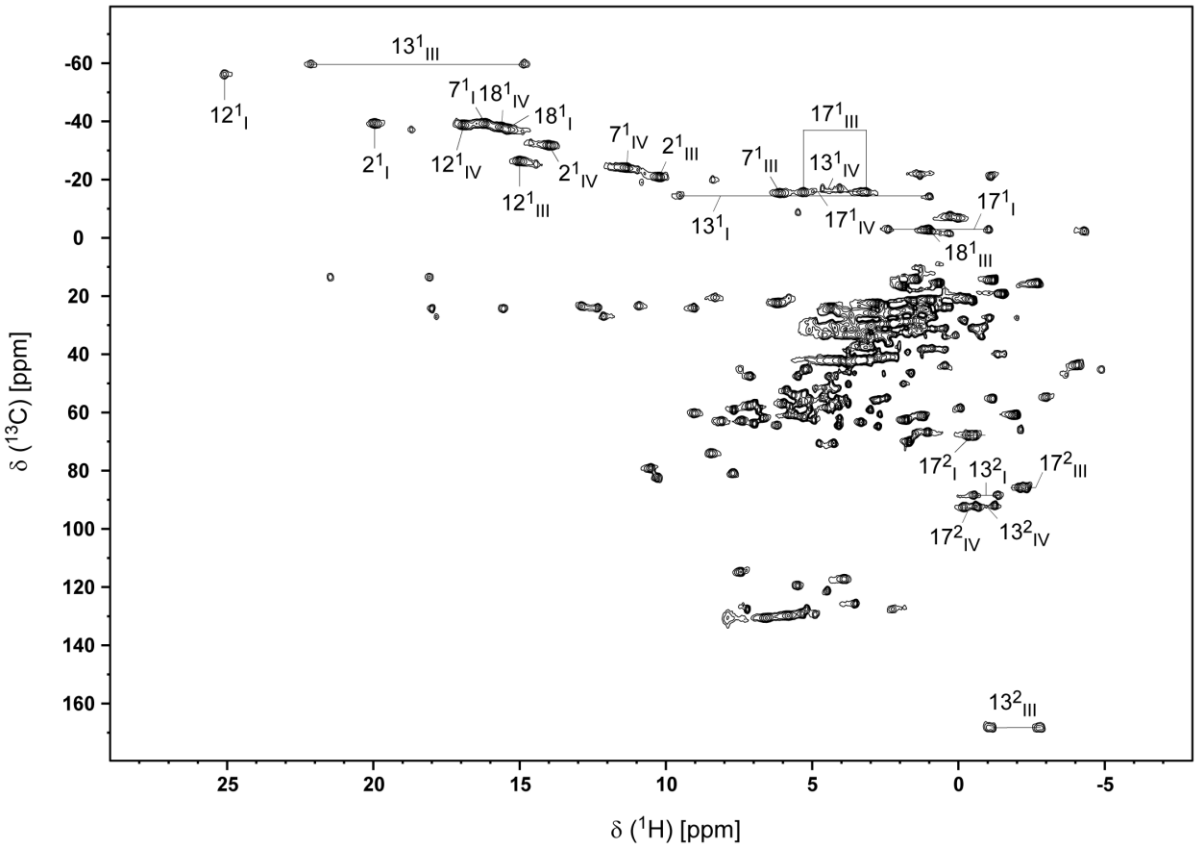

Figure 6.4 – ^{1}H,^{13}C-HMQC spectrum of PpcA from G. metallireducens, at pH 8.1, 298 K – The heme methyls and propionates signals are identified in the spectrum. The peaks of the protons connected to the same carbon atoms (CH_2 groups) are linked by a straight line. The detailed assignment is presented in Table 6.6.

Table 6.5 – Heme methyls and propionates assignment (^{1}H and ^{13}C) of PpcA from G. metallireducens in the oxidized state, at 250 mM ionic strength, pH 8.1, 298 K.

Heme substituent	Heme I		Heme III		Heme IV	
	^{13}C	^{1}H	^{13}C	^{1}H	^{13}C	^{1}H
2^{1}	-39.52	19.96	-21.03	10.22	-31.95	13.99
7^{1}	-39.50	16.17	-15.53	6.09	-24.24	11.34
12^{1}	-56.44	25.08	-26.55	14.99	-38.96	16.91
13^{1}	-14.55	0.98 9.52	-60.06	14.84 22.14	-17.14	4.05 4.64
13^{2}	88.57	-1.36 -0.55	168.70	-2.82 -1.11	92.11	-1.26 -0.60
17^{1}	-3.03	-1.05 2.39	-15.89	3.15 5.29	-16.08	3.31 4.98
17^{2}	68.02	-0.58 -0.36	86.09	-2.34 -2.13	92.78	-0.68 -0.19
18^{1}	-37.48	15.42	-2.93	1.01	-38.22	15.62

Table 6.6 – Heme methyls and propionates assignment (^{1}H and ^{13}C) of PpcA from G. metallireducens in the oxidized state, at 250 mM ionic strength, pH 5.8, 288 K.

Heme substituent	Heme I		Heme III		Heme IV	
	^{13}C	^{1}H	^{13}C	^{1}H	^{13}C	^{1}H
2^1	-41.28	20.68	-21.88	10.29	-33.79	14.48
7^1	-40.95	16.52	5.68	5.68	-24.67	11.27
12^1	-58.91	25.91	-27.13	15.19	-38.18	15.67
13^1	-14.72	0.79 9.30	-62.65	14.89 22.88	-18.76	2.89 5.02
13^2	89.05	-1.32 -0.57	174.60	-2.89 -1.14	95.03	-0.88 -0.30
17^1	-2.90	-1.85 2.76	-17.07	2.98 5.29	-17.95	3.83 4.55
17^2	67.95	-0.35 0.05	87.77	-2.44 -2.17	96.49	-0.89 -0.21
18^1	-38.67	15.95	-2.57	0.59	-38.66	15.59

Table 6.7 – Chemical shifts of the heme methyl protons of PpcA from G. metallireducens in the reduced and oxidized (values in parenthesis) states, at pH 5.8 and 288 K – The paramagnetic contribution (δ_{ox} - δ_{red}) of the observed chemical shifts at the oxidized state is indicated for each heme methyl proton.

Heme substituents	Chemical shift (ppm)			δ_{ox} - δ_{red}		
	I	III	IV	I	III	IV
2^1CH_3	3.55 (20.68)	4.50 (10.29)	3.64 (14.48)	17.13	5.79	10.84
7^1CH_3	3.55 (16.52)	3.99 (5.68)	3.08 (11.27)	12.97	1.69	8.19
12^1CH_3	2.88 (25.91)	3.51 (15.19)	3.84 (15.67)	23.03	11.68	11.83
18^1CH_3	3.34 (15.95)	3.96 (0.59)	3.37 (15.59)	12.61	-3.37	12.22

6.5 – NMR pH titration of PpcA from G. metallireducens

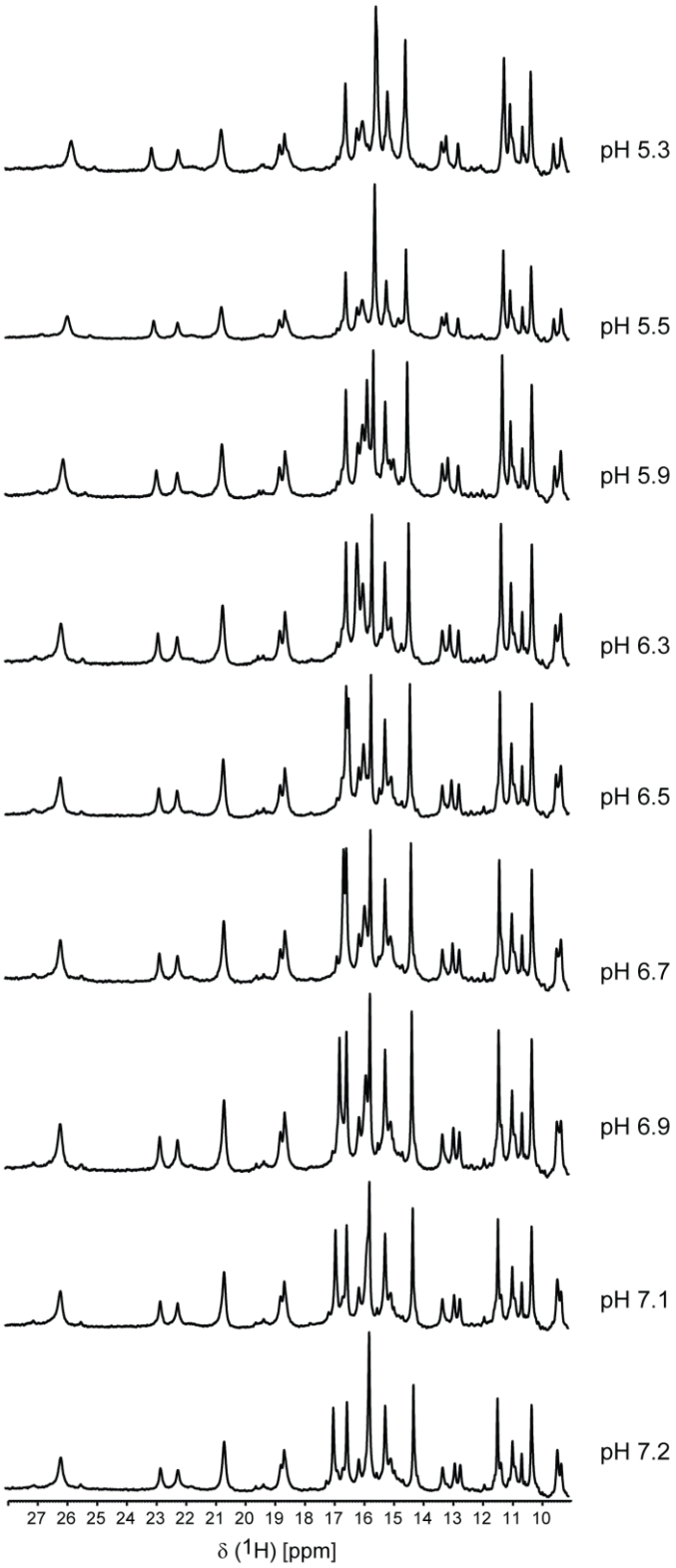

Figure 6.5 – 1D ^{1}H-NMR pH titration of PpcA from G. metallireducens in the oxidized state, at 288 K (pH 5.3 – 7.2) – The ^{1}H chemical shift changes of the heme methyls were followed at different pH values. Samples were prepared in 80 mM phosphate buffer, 250 mM final ionic strength.

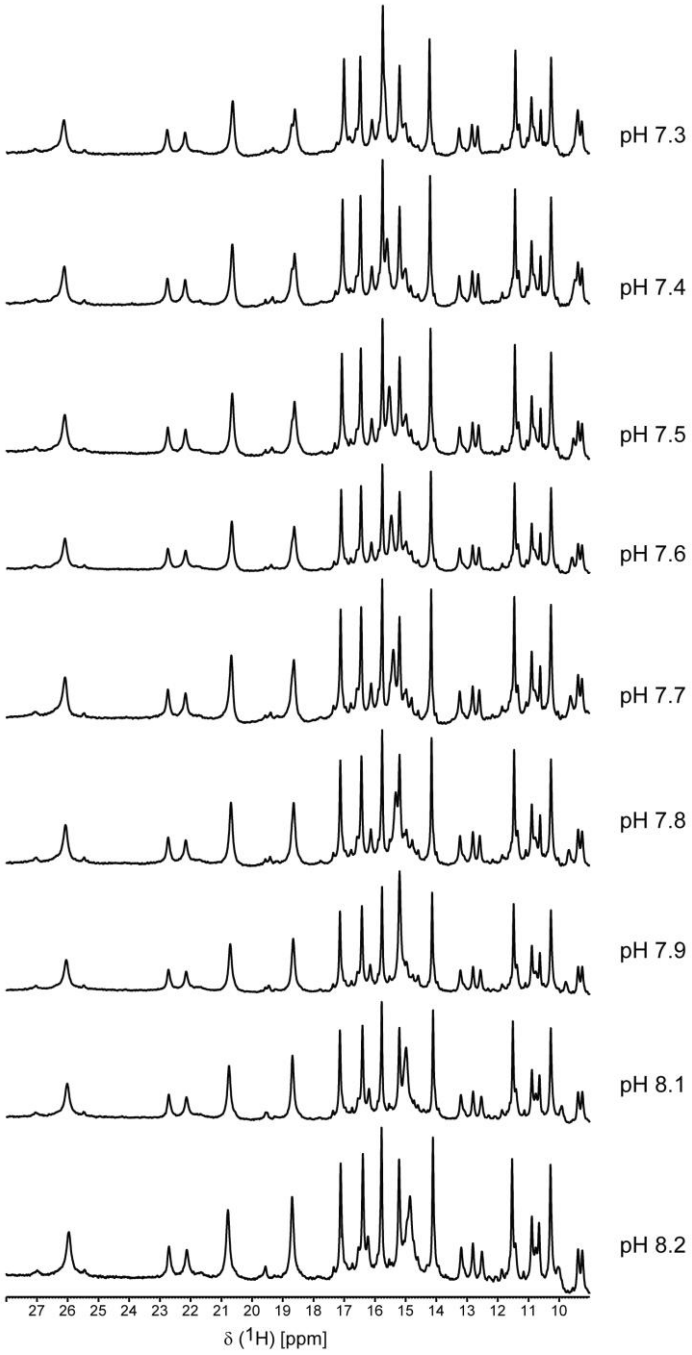

Figure 6.6 – 1D ^{1}H-NMR pH titration of PpcA from G. metallireducens in the oxidized state, at 288 K (pH 7.3 – 8.2) – The ^{1}H chemical shift changes of the heme methyls were followed at different pH values. Samples were prepared in 80 mM phosphate buffer, 250 mM final ionic strength.

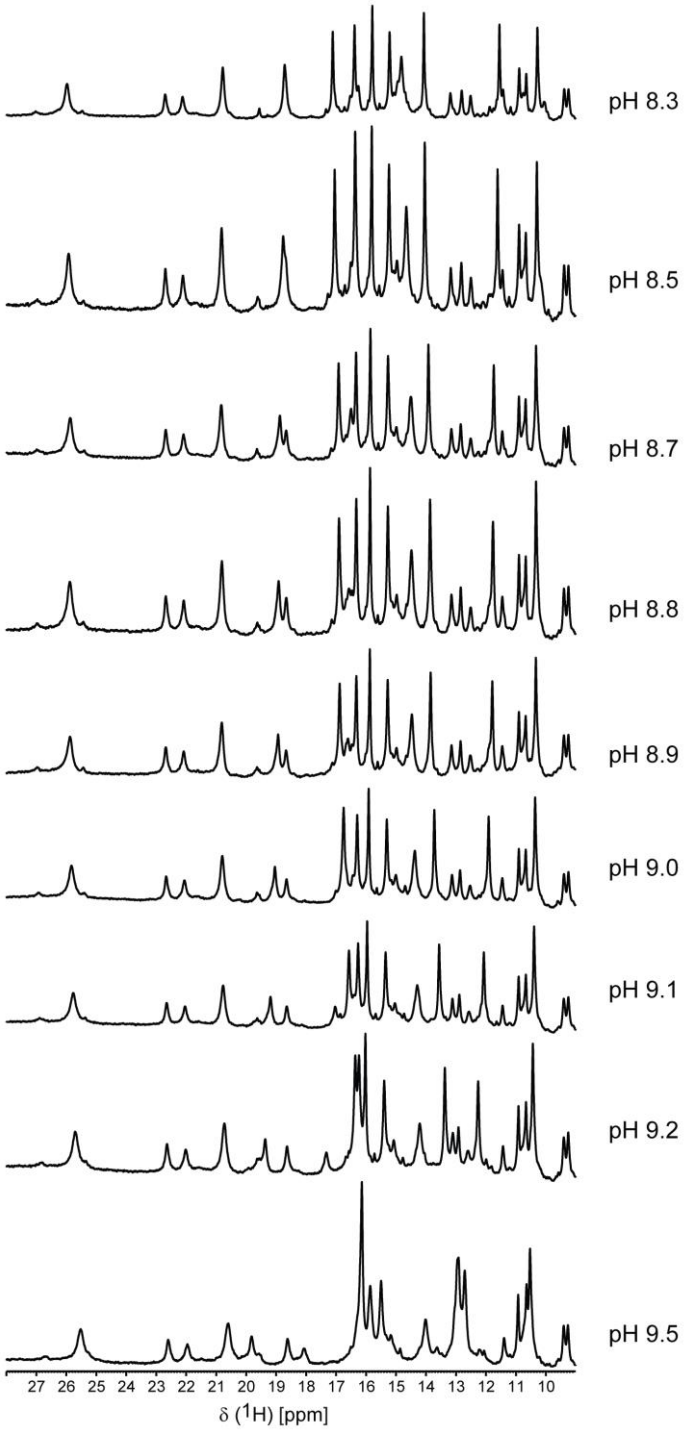

Figure 6.7 – 1D ^{1}H-NMR pH titration of PpcA from G. metallireducens in the oxidized state, at 288 K (pH 8.3 – 9.5) – The ^{1}H chemical shift changes of the heme methyls were followed at different pH values. Samples were prepared in 80 mM phosphate buffer, 250 mM final ionic strength.

6.6 – NMR redox titrations of PpcA from G. metallireducens

Table 6.8 – Heme methyl chemical shifts of PpcA from G. metallireducens at different stages of oxidation (pH 5.8 – 8.9) – The heme oxidation fractions (x_i), in each stage of oxidation, were calculated according to the equation $x_i = (\delta_i-\delta_0)/(\delta_3-\delta_0)$, where δ_i, δ_0 and δ_3 are the observed chemical shifts of the heme methyl in stage i, 0 (fully reduced) and 3 (fully oxidized), respectively. The values indicated in parenthesis were obtained from the fitting of the thermodynamic model.

pH 5.8	Chemical shift (ppm)			x_i			
Oxidation stage	I	III	IV	I	III	IV	$\sum x_i$
0	3.55	3.51	3.64	0.00	0.00	0.00	0.00
1	6.91	(4.83)	11.02	0.20	0.11	0.68	0.99
2	17.77	5.34	13.76	0.83	0.16	0.94	1.93
3	20.70	15.18	14.45	1.00	1.00	1.00	3.00
pH 6.3	Chemical shift (ppm)			x_i			
Oxidation stage	I	III	IV	I	III	IV	$\sum x_i$
0	3.55	3.51	3.64	0.00	0.00	0.00	0.00
1	6.77	(4.87)	11.03	0.19	0.12	0.68	0.99
2	17.95	5.24	13.76	0.84	0.15	0.94	1.93
3	20.69	15.19	14.43	1.00	1.00	1.00	3.00
pH 6.9	Chemical shift (ppm)			x_i			
Oxidation stage	I	III	IV	I	III	IV	$\sum x_i$
0	3.55	3.51	3.64	0.00	0.00	0.00	0.00
1	5.95	(4.72)	11.70	0.14	0.10	0.76	1.00
2	17.80	5.23	13.67	0.83	0.15	0.94	1.92
3	20.63	15.20	14.27	1.00	1.00	1.00	3.00
pH 7.6	Chemical shift (ppm)			x_i			
Oxidation stage	I	III	IV	I	III	IV	$\sum x_i$
0	3.55	3.51	3.64	0.00	0.00	0.00	0.00
1	5.20	(4.43)	12.19	0.10	0.08	0.81	0.99
2	17.83	5.31	13.62	0.83	0.15	0.95	1.93
3	20.67	15.19	14.14	1.00	1.00	1.00	3.00

Table 6.8 (continued)

pH 8.3	Chemical shift (ppm)			x_i			
Oxidation stage	I	III	IV	I	III	IV	$\sum x_i$
0	3.55	3.51	3.64	0.00	0.00	0.00	0.00
1	5.02	(4.22)	12.27	0.09	0.06	0.82	0.97
2	18.07	5.13	13.53	0.84	0.14	0.94	1.92
3	20.80	15.21	14.11	1.00	1.00	1.00	3.00
pH 8.9	Chemical shift (ppm)			x_i			
Oxidation stage	I	III	IV	I	III	IV	$\sum x_i$
0	3.55	3.51	3.64	0.00	0.00	0.00	0.00
1	(4.96)	(4.17)	12.14	0.08	0.06	0.83	0.97
2	18.19	5.14	13.35	0.85	0.14	0.94	1.93
3	20.84	15.30	13.92	1.00	1.00	1.00	3.00

6.7 – Preparation of sodium dithionite solutions

Sodium dithionite solutions were prepared according to the procedure described below.

The sample used for the NMR experiments was prepared with a concentration of 380 μM. Considering that GSU0105 has 3 hemes, this means that there is a total concentration of 1.14 mM hemes in solution. Sodium dithionite transfers 2 electrons when oxidized, meaning that there is the need of having at least 570 μM of active sodium dithionite in solution in order to respect the intended ratio of 1:1 (electron:heme).

Initially, a 10.3 mM solution of sodium dithionite was prepared in 32 mM phosphate buffer, pH 8, with NaCl (100 mM of final ionic strength). The UV-visible spectrum of sodium dithionite has a local maximum absorbance peak at 315 nm, for which the molar extinction coefficient was previously determined (ε_{315nm} = 8000 M^{-1} cm^{-1}) [5, 6]. Therefore, the concentration of active sodium dithionite in solution was determined from the absorbance at 315 nm, with the use of the respective molar extinction coefficient. A spectrum was obtained between 200-375 nm and the result is presented below (Figure 6.8).

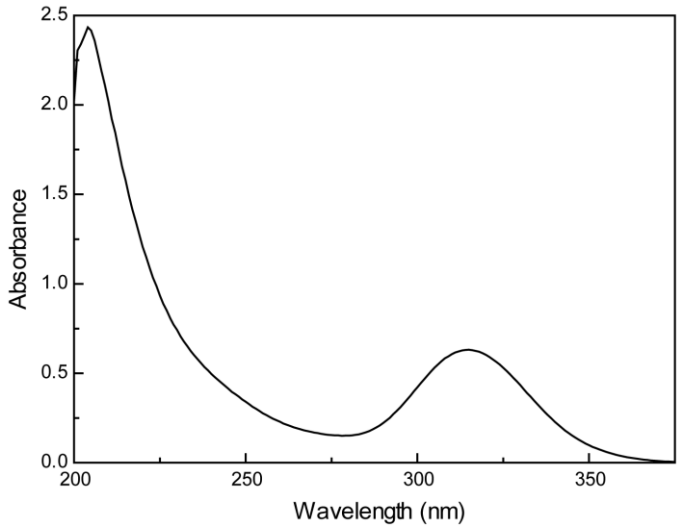

Figure 6.8 – UV-visible spectrum of sodium dithionite – The spectrum was obtained with a 0.5 mM sodium dithionite solution, in a 1 cm path length quartz cell (Helma), at room temperature.

The observed absorbance at 315 nm was 0.631, meaning that there was 0.0789 mM active sodium dithionite in solution. The sample analyzed by UV-visible spectroscopy was prepared from the 10.3 mM sodium dithionite solution and then diluted 1:20. Therefore, about 16% of the total sodium dithionite in solution was active. This value was taken into account in the preparation of the following solutions, in order to respect the 1:1 (electron:heme) ratio when adding sodium dithionite to GSU0105.

6.8 – Electrochemistry data

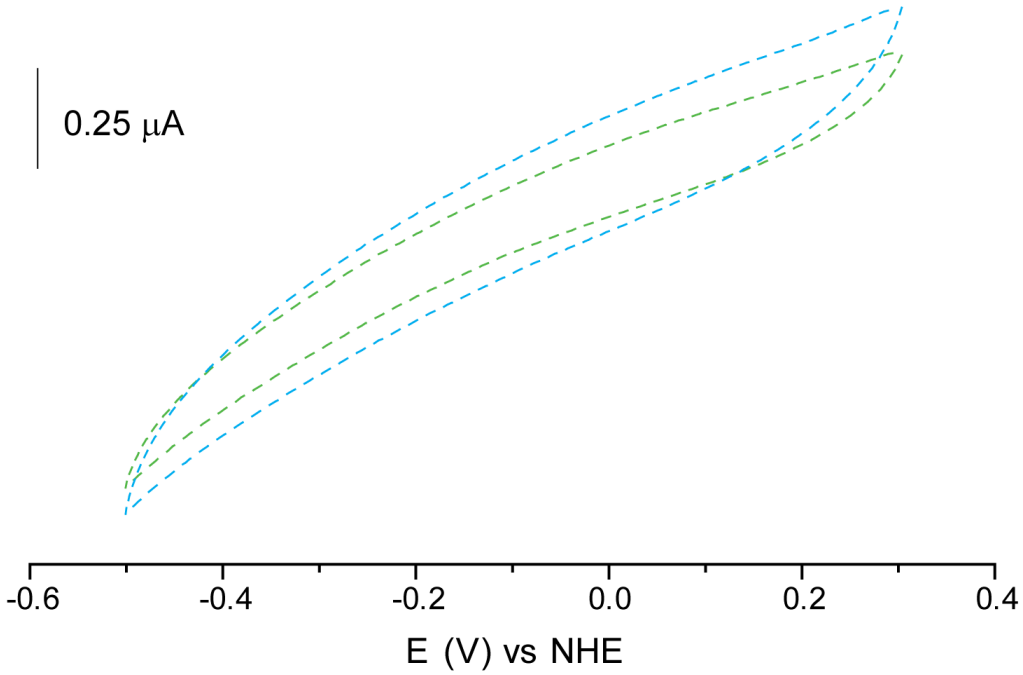

Figure 6.9 – Cyclic voltammetry control assays with 200 μM BSA in phosphate buffer with NaCl (170 mM final ionic strength), at pH 7 – The voltammograms were recorded at two different scan rates: 10 (green) and 20 (blue) mV s^{-1}. The peak intensity scale is presented in μA.

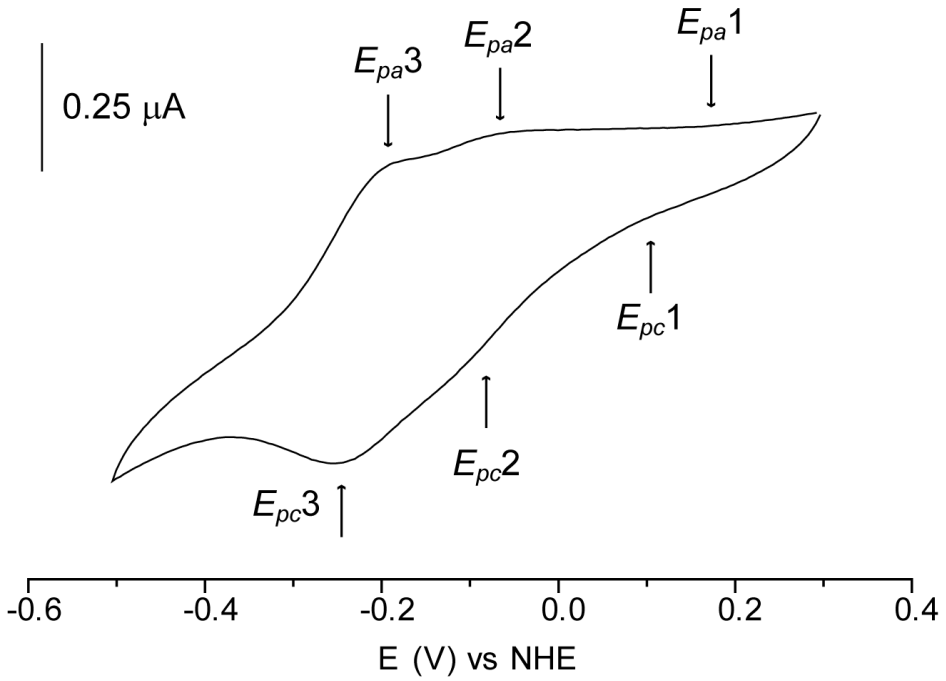

Figure 6.10 – Anodic and cathodic peaks of GSU0105 redox centers at 5 mV s^{-1}. The voltammogram presented was plotted from Figure 3.12. The peak intensity scale is presented in μA.

Table 6.9 – Electrochemical parameters of the first redox center (I) of GSU0105 – The different parameters are presented with the respective errors.

Redox center	Scan speed (mV s^{-1})	E_{pa} (mV)	E_{pc} (mV)	I_{pa} (μA)	I_{pc} (μA)
I	5	138 ± 15	49 ± 13	0.0008 ± 0.0002	0.0008 ± 0.0002
	10	133 ± 21	32 ± 19	0.0008 ± 0.0001	0.0008 ± 0.0006
	20	98 ± 27	32 ± 12	0.0010 ± 0.0005	0.0009 ± 0.0002
	35	107 ± 20	30 ± 9	0.0015 ± 0.0009	0.0011 ± 0.0006
	50	94 ± 27	41 ± 6	0.0018 ± 0.0012	0.0011 ± 0.0008
	75	151 ± 19	52 ± 4	0.0031 ± 0.0016	0.0020 ± 0.0005
	100	144 ± 16	58 ± 2	0.0103 ± 0.0065	0.0097 ± 0.0026
	150	133 ± 14	76 ± 6	0.0117 ± 0.0075	0.0104 ± 0.0034
	200	165 ± 22	65 ± 4	0.0194 ± 0.0052	0.0122 ± 0.0039
	500	153 ± 3	54 ± 19	0.0267 ± 0.0112	0.0188 ± 0.0063
	1000	133 ± 18	69 ± 10	0.0275 ± 0.0131	0.0190 ± 0.0056
	2000	120 ± 1	38 ± 16	0.1013 ± 0.0108	0.0617 ± 0.0084
	5000	140 ± 13	71 ± 13	0.3750 ± 0.0009	0.3520 ± 0.0401

Table 6.10 – Electrochemical parameters of the second redox center (II) of GSU0105 – The different parameters are presented with the respective errors.

Redox center	Scan speed (mV s^{-1})	E_{pa} (mV)	E_{pc} (mV)	I_{pa} (μA)	I_{pc} (μA)
II	5	-55 ± 3	-139 ± 28	0.0011 ± 0.0003	0.0008 ± 0.0004
	10	-73 ± 15	-181 ± 31	0.0012 ± 0.0003	0.0013 ± 0.0006
	20	-113 ± 30	-136 ± 22	0.0012 ± 0.0004	0.0017 ± 0.0003
	35	-62 ± 6	-91 ± 17	0.0022 ± 0.0008	0.0017 ± 0.0001
	50	-97 ± 25	-95 ± 15	0.0024 ± 0.0007	0.0026 ± 0.0011
	75	-57 ± 5	-166 ± 4	0.0026 ± 0.0003	0.0039 ± 0.0002
	100	-33 ± 28	-181 ± 13	0.0139 ± 0.0027	0.0150 ± 0.0038
	150	-22 ± 46	-168 ± 19	0.0167 ± 0.0021	0.0173 ± 0.0042
	200	-33 ± 22	-146 ± 23	0.0183 ± 0.0018	0.0208 ± 0.0076
	500	-42 ± 4	-157 ± 27	0.0287 ± 0.0050	0.0346 ± 0.0021
	1000	-46 ± 16	-150 ± 24	0.0341 ± 0.0129	0.0499 ± 0.0145
	2000	-48 ± 15	-137 ± 25	0.1025 ± 0.0061	0.1283 ± 0.0375
	5000	-42 ± 9	-148 ± 21	0.2822 ± 0.0266	0.5067 ± 0.0624

Table 6.11 – Electrochemical parameters of the third redox center (III) of GSU0105 – The different parameters are presented with the respective errors.

Redox center	Scan speed (mV s^{-1})	E_{pa} (mV)	E_{pc} (mV)	I_{pa} (μA)	I_{pc} (μA)
III	5	-208 ± 15	-254 ± 16	0.0015 ± 0.0006	0.0042 ± 0.0005
	10	-195 ± 6	-259 ± 22	0.0023 ± 0.0008	0.0052 ± 0.0007
	20	-203 ± 12	-243 ± 6	0.0028 ± 0.0004	0.0055 ± 0.0014
	35	-252 ± 30	-232 ± 9	0.0029 ± 0.0006	0.0061 ± 0.0022
	50	-261 ± 41	-236 ± 3	0.0032 ± 0.0004	0.0077 ± 0.0020
	75	-177 ± 19	-250 ± 4	0.0039 ± 0.0013	0.0077 ± 0.0011
	100	-199 ± 4	-245 ± 16	0.0119 ± 0.0024	0.0209 ± 0.0058
	150	-188 ± 28	-261 ± 19	0.0179 ± 0.0033	0.0260 ± 0.0048
	200	-181 ± 6	-263 ± 16	0.0227 ± 0.0021	0.0414 ± 0.0098
	500	-197 ± 4	-258 ± 16	0.0335 ± 0.0054	0.0573 ± 0.0126
	1000	-203 ± 13	-250 ± 16	0.0487 ± 0.0023	0.0826 ± 0.0203
	2000	-208 ± 6	-263 ± 16	0.0943 ± 0.0089	0.1800 ± 0.0462
	5000	-201 ± 14	-256 ± 25	0.4422 ± 0.0153	0.4584 ± 0.1218

6.9 – Redox and pH dependence of paramagnetic chemical shifts

The observed chemical shift (δ_{obs}) of a certain nucleus in a paramagnetic protein is a result of the diamagnetic (δ_d or $\delta^{i,0}$) and paramagnetic (δ_p) contributions.

$$\delta_{obs} = \delta_d + \delta_p \tag{16}$$

The paramagnetic shift of a certain heme methyl (δ_p), not the total chemical shift (δ_{obs}), is proportional to the degree of oxidation of that particular heme methyl, meaning that it can be used to monitor the oxidation of each heme throughout a redox titration.

In the experimental conditions used for the redox titration followed by NMR, the intramolecular electron exchange is fast and, therefore, the observed chemical shift of a heme methyl group (i, j or k) in each oxidation stage (S) depends on the ratio between the populations of the microstates which have that particular heme oxidized and the sum of the populations of all microstates of that oxidation stage. The observed chemical shift of a certain methyl group i ($\delta_{obs}^{i,S}$) can be calculated in stages 1 to 3, according to the equations presented below:

$$\delta_{obs}^{i,1} - \delta^{i,0} = (\delta^{i,3} - \delta^{i,0})\frac{p_{i,1}}{p_{i,1}+p_{i,1}^{H}} + (\delta_H^{i,3} - \delta^{i,0})\frac{p_{i,1}^{H}}{p_{i,1}+p_{i,1}^{H}} \tag{17}$$

$$\delta_{obs}^{i,2} - \delta^{i,0} = (\delta^{i,3} - \delta^{i,0})\frac{p_{ij,2}+p_{ik,2}}{p_{ij,2}+p_{ik,2}+p_{ij,2}^{H}+p_{ik,2}^{H}} + (\delta_H^{i,3} - \delta^{i,0})\frac{p_{ij,2}^{H}-p_{ik,2}^{H}}{p_{ij,2}+p_{ik,2}+p_{ij,2}^{H}+p_{ik,2}^{H}} \tag{18}$$

$$\delta_{obs}^{i,3} - \delta^{i,0} = (\delta^{i,3} - \delta^{i,0})\frac{p_{ijk,3}}{p_{ijk,3}+p_{ijk,3}^{H}} + (\delta_H^{i,3} - \delta^{i,0})\frac{p_{ijk,3}^{H}}{p_{ijk,3}+p_{ijk,3}^{H}} \tag{19}$$

In these equations, $\delta^{i,0}$ is the observed chemical shift of the heme methyl i in the fully reduced protein and $\delta^{i,3}$ and $\delta_H^{i,3}$ are those observed in the fully oxidized deprotonated and protonated protein, respectively. The chemical shift of the heme methyl in the fully reduced form is assumed to be independent of pH. Then, $p_{i,S}$ and $p_{i,S}^{H}$ are the sums over all the populations with heme i oxidized in stage S, with the redox-Bohr center being deprotonated and protonated, respectively; $p_{ij,S}$ and $p_{ij,S}^{H}$ are the sums over all the populations with hemes i and j oxidized in stage S, with the redox-Bohr center being deprotonated and protonated, respectively; $p_{ik,S}$ and $p_{ik,S}^{H}$ are the sums over all the populations with hemes i and k oxidized in stage S, with the redox-Bohr center being deprotonated and protonated, respectively; and $p_{ijk,S}$ and $p_{ijk,S}^{H}$ are the sums over all the

populations with hemes i, j and k oxidized in stage S, with the redox-Bohr center being deprotonated and protonated, respectively.

6.10 – References

[1] C.F. Goodhew, K.R. Brown, G.W. Pettigrew, Haem staining in gels, a useful tool in the study of bacterial c-type cytochromes, Biochim. Biophys. Acta - Bioenergetics, 852 (1986) 288-294.

[2] P.E. Thomas, D. Ryan, W. Levin, An improved staining procedure for the detection of the peroxidase activity of cytochrome P-450 on sodium dodecyl sulfate polyacrylamide gels, Anal. Biochem., 75 (1976) 168-176.

[3] I.M. Luís, B.M. Alexandre, M.M. Oliveira, I.A. Abreu, Selection of an appropriate protein extraction method to study the phosphoproteome of maize photosynthetic tissue, PLoS One, 11 (2016) e0164387.

[4] G.P. Moss, Nomenclature of tetrapyrroles. Recommendations 1986 IUPAC-IUB joint commission on biochemical nomenclature (JCBN), Eur. J. Biochem, 178 (1988) 277-328.

[5] M. Dixon, The acceptor specificity of flavins and flavoproteins. I. Techniques for anaerobic spectrophotometry, Biochim. Biophys. Acta - Bioenergetics, 226 (1971) 241-258.

[6] S.G. Mayhew, The redox potential of dithionite and SO^{-2} from equilibrium reactions with flavodoxins, methyl viologen and hydrogen plus hydrogenase, Eur. J. Biochem., 85 (1978) 535-547.